Development of a lung-liver in vitro coculture model for the risk assessment of inhaled xenobiotics

Sabrina Madiedo-Podvršan

Par **Sabrina MADIEDO-PODVRŠAN**

Development of a lung-liver in vitro coculture model for the risk assessment of inhaled xenobiotics

Thèse présentée
pour l'obtention du grade
de Docteur de l'UTC

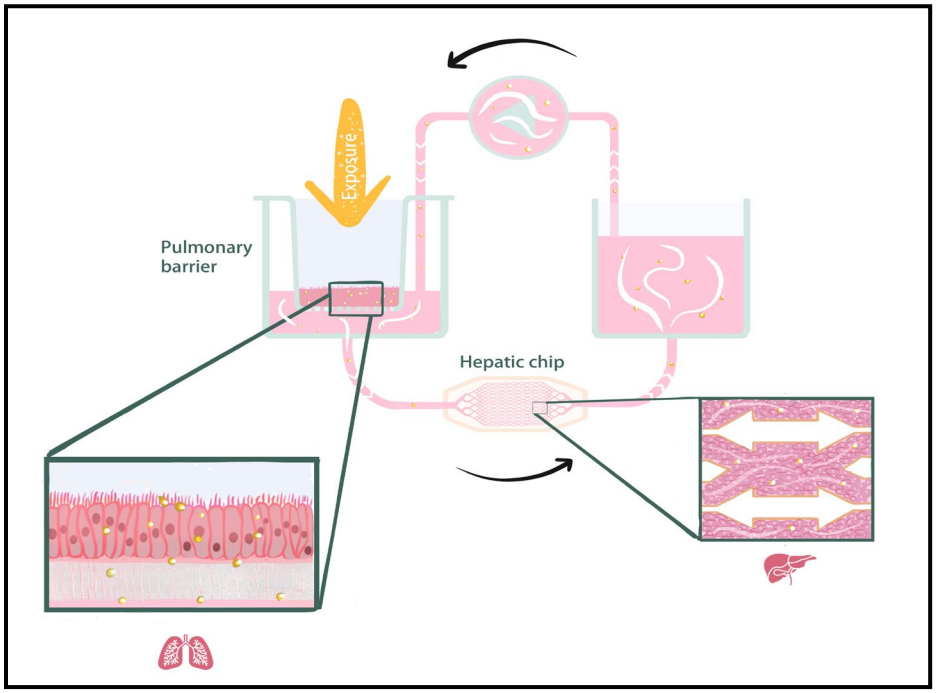

Soutenue le 7 novembre 2022
Spécialité : Bioingénierie : Unité de Recherche en Biomécanique et Bioingénierie (UMR-7338)
D2703

THÈSE DE DOCTORAT

Ecole doctorale 71 : Sciences pour l'ingénieur

Spécialité : Bioingénierie

Development of a lung-liver *in vitro* coculture model for the risk assessment of inhaled xenobiotics

---

Présentée par

Sabrina MADIEDO-PODVRŠAN

le 7 novembre 2022

Pour l'obtention du grade de docteur de
UNIVERSITÉ DE TECHNOLOGIE DE COMPIÈGNE

Directrices de thèse : Pr. Muriel VAYSSADE, Dr. Ghislaine LACROIX

Laboratoire de Biomécanique et Bioingénierie (BMBI)
Equipe Cellules Biomatériaux et Bioréacteurs (CBB)
CNRS UMR 7338

Jury :

Samy Gobaa	Ingénieur de recherche HDR, Institut Pasteur	Rapporteur
Jérémie Pourchez	DR INSERM, UMR INSERM U1059, Mines Saint-Etienne	Rapporteur
Stéphanie Descroix	DR INSERM, UMR 168, Institut Curie	Examinatrice
Cécile Legallais	DR CNRS, UMR CNRS 7338, UTC	Examinatrice
Fabrice Soncin	DR INSERM, CNRS IRL 2820, LIMMS	Examinateur
Muriel Vayssade	Professeur, UMR CNRS 7338, UTC	Directrice de thèse
Ghislaine Lacroix	Ingénieur de recherche, INERIS	Directrice de thèse
Rachid Jellali	Ingénieur de recherche, UMR CNRS 7338, UTC	Membre invité

Funding

This thesis was funded by the European Regional Development Fund (ERDF) 2014/2020 and the national research program Environnement-Santé-Travail (PNR EST) of the French National Food Safety Agency (Anses).

The doctoral grant relative to the project LuLi is part-funded by the European Regional Development Fund (ERDF).

Abstract

Urbanization and globalization are prevailing social phenomena that multiply and complexify the sources of modern pollution. Amongst others, air pollution has been recognized as an omnipresent life-threatening hazard, comprising a wide range of toxic airborne xenobiotics that expose man to acute and chronic threats. The defense mechanisms involved in hazardous exposure responses are complex and comprise local and systemic biological pathways. Due to this complexity, animal models are considered prime study models. However, in light of animal experimentation reduction (3Rs), we developed and investigated an alternative *in vitro* method to study systemic-like responses to inhalation-like exposures. In this context, a coculture platform was established to emulate inter-organ crosstalks between the pulmonary barrier, which constitutes the route of entry of inhaled compounds, and the liver, which plays a major role in xenobiotic metabolism. Both compartments respectively comprised a Calu-3 insert and a HepG2/C3A biochip which were jointly cultured in a dynamically-stimulated environment for 72 hours. The present model was characterized using acetaminophen (APAP), a well-documented hepatotoxicant, to visibly assess the passage and circulation of a xenobiotic through the device. Two kinds of models were developed: (1) the developmental model allowed for the technical setup of the coculture, and (2) the physiological-like model better approximates a *vivo* environment. Based on viability, and functionality parameters the developmental model showed that the Calu-3 bronchial barrier and the HepG2/C3A biochip can successfully be maintained viable and function in a dynamic coculture setting for 3 days. In a stress-induced environment, present results reported that the coculture model emulated active and functional *in vitro* crosstalk that seemingly was responsive to high (1.5 and 3 mM) and low (12 and 24 μM) xenobiotic exposure doses. Lung/liver crosstalk induced modulation of stress response dynamics, delaying cytotoxicity, proving that APAP fate, biological behaviors and cellular stress responses were modulated in a broader systemic-like environment.

Keywords: bioengineering, organ-on-a-chip, toxicology, coculture

Résumé

L'urbanisation et la mondialisation sont des phénomènes de société qui multiplient et complexifient les sources de pollution. Parmi elles, la pollution atmosphérique impacte notablement la santé humaine à l'échelle mondiale de par son caractère transfrontière [1]–[3]. L'appareil respiratoire est une voie d'absorption de nombreux xénobiotiques, sous forme de gaz, d'aérosols ou de nanoparticules. Une fois dans les voies respiratoires, les substances inhalées sont susceptibles d'interagir avec les cellules pulmonaires. Les mécanismes par lesquels des xénobiotiques inhalés induisent des dommages pulmonaires sont complexes, notamment en raison de l'hétérogénéité cellulaire des poumons. En raison de cette complexité, les modèles animaux constituent un outil de référence pour les études toxicologiques prédictives, cependant, dans le contexte européen de réduction de l'expérimentation animale (REACH, et les règles 3R), le développement de méthodes alternatives fiables est devenu une nécessité. Les modèles *in vitro* sont de bons candidats car plus simple et moins couteux à mettre en œuvre que les modèles *vivo* et permettent de travailler avec des cellules ou des tissus d'origine humaine ce qui contribue à améliorer la pertinence des résultats. Cependant, l'extrapolation limitée du *vitro* au *vivo* est souvent liée à un manque de complexité des modèles, notamment en raison de l'absence de communication inter-organes. Les technologies des multi-organes sur puce cherchent à surmonter ces limitations en connectant plusieurs organoïdes métaboliquement actifs au sein d'un même circuit de culture afin de reproduire des interactions de type systémiques. Dans ce contexte, nous décrivons un modèle permettant de connecter *in vitro*, par le biais de la microfluidique, une barrière pulmonaire (voie d'entrée des xénobiotiques inhalés) à un organe détoxifiant tel que le foie, afin d'évaluer la toxicité liée à un stress inhalatoire de façon plus systémique. Cette approche permet de considérer la biotransformation des composés inhalés et l'interaction inter-organes comme possible modulateurs de la toxicité.
Le projet étant dans les premières phase de développement, la robustesse expérimentale était au cœur du projet. L'objectif principal était de prouver qu'une substance modèle était capable de transiter dans le dispositif, au travers des deux compartiments tissulaires, afin de pouvoir étudier la dynamique inter-organes poumon/foie en condition de stress xénobiotique. Le projet a été articulé en trois phases expérimentales :

- Caractérisation des réponses biologiques spécifiques aux tissus pulmonaire et hépatique en réponse à un stress. La viabilité, la fonctionnalité et les activités métaboliques des monocultures ont été évaluées après exposition à une substance modèle.

- Adaptation et préparation des monocultures aux conditions de co-culture (milieu

de co-culture, effet du flux sur le développement tissulaire pulmonaire) afin de préserver la viabilité et la fonctionnalité des tissus.

- Les compartiments pulmonaire et hépatique ont été réunis et cultivés jointement dans un circuit de culture microfluidique fermé. La co-culture a été exposée à une substance modèle à travers la barrière pulmonaire afin d'imiter un mode d'exposition inhalatoire. Les paramètres de viabilité et de fonctionnalité des tissus ont été évalué post-culture afin de mettre en évidence quelconque phénomène d'interaction inter-organe.

Le modèle développé étant destiné à être utilisé pour étudier les risques liés à l'exposition à la pollution atmosphérique, inhalée par les voies respiratoires, le compartiment pulmonaire est la cible principale de l'étude. La caractérisation du modèle de co-culture a été réalisé grâce à l'exposition d'un agent hépatotoxique de référence, largement étudié dans la littérature : l'acétaminophène aussi connu sous le nom de paracétamol (APAP). L'exposition à la barrière pulmonaire n'est pas physiologique mais permet d'observer quantitativement le passage et la circulation du xénobiotique à travers le dispositif car l'APAP interfère avec la viabilité et les performances métaboliques hépatique, permettant ainsi de vérifier que le compartiment hépatique peut avoir accès à l'exposition effectuée à travers la barrière pulmonaire.
Deux types de modèles de co-culture ont été développé :

- Un modèle de développement a permis la mise en place technique de la plateforme de co-culture. Cette configuration comprend un tissu pulmonaire Calu-3, cultivé en condition submergé, connecté à une biopuce hépatique HepG2/C3A. Les concentrations d'exposition choisies pour ce modèle reposent sur des seuils d'hépatotoxicité connus, 1,5 mM et 3 mM, afin de permettre une meilleure quantification des réponses biologiques. Ces concentrations correspondent à des concentrations dites " systémiques ", auxquelles le compartiment hépatique aura accès par le flux, après dilution dans le milieu circulant. Les concentrations d'APAP déposées localement en amont sur la barrière Calu-3 tiennent compte de la dilution du milieu total qui suit. Pour atteindre des valeurs systémiques de 1,5 mM et 3 mM, les expositions locales ont été fixées à 7,5 mM et 15 mM du côté pulmonaire respectivement.

- Un modèle plus physiologique se rapprochant davantage d'une exposition *vivo*. Le tissu Calu-3 est soumis à une brève période de différentiation à l'interface air-liquide (ALI) et le mode d'exposition repose sur un volume d'exposition faible (200 μL) qui impose localement une concentration d'exposition de 0,5 et 1 mM d'APAP sur la barrière Calu-3 qui se diluera ensuite à respectivement 12 et 24 μM dans le milieu systémique.

Évaluation du profil cytotoxique des monocultures pulmonaire et hépatique en réponse à l'exposition d'une substance modèle : étude du cas de l'acétaminophène

Étude de la réponse au stress d'une biopuce HepG2/C3A métaboliquement active

Le tissu hépatique a été reconstruit en condition de culture dynamique au sein d'une biopuce microstructurée en PDMS développée et caractérisée précédemment [4]–[10]. Ce mode de culture a déjà été utilisé pour la culture de cellules HepG2/C3A et a permis l'amélioration de la fonctionnalité hépatique *in vitro*, notamment du métabolisme xénobiotique [8]–[11]. Nos observations morphologiques et les données métaboliques coïncident avec la littérature, et indiquent dans l'ensemble que les biopuces de cellules HepG2/C3A utilisées sont différenciées et métaboliquement actives, et qu'elles sont capable de percevoir et répondre à l'exposition d'APAP. Les réponses biologiques à l'exposition d'APAP ont déjà été étudiées, mais à des doses plus faibles, ne dépassant pas 1 mM [5], [8]. Les environnements de culture cellulaire testés à 1,5 et 3 mM d'APAP ont induit une cytotoxicité importante. L'hépatotoxicité de l'APAP est liée à la production du métabolite réactif N-acetyl-p-benzoquinone imine (NAPQI), via les cytochromes P450 (CYP) [12]. Le NAPQI peut être conjugué au glutathion (GSH) via les GST pour produire un métabolite APAP-glutathion (APAP-GSH) non toxique, cependant, en condition de production excessive de NAPQI les stocks de GSH peuvent s'épuiser, ce qui bloque la détoxification du NAPQI et entraîne son accumulation. Conformément à Prot et al. le suivi de l'activité CYP1A des cellules HepG2/C3A, par le biais du test EROD, permet de suivre la production de NAPQI toxique [13]. Nos résultats indiquent que l'APAP induit une augmentation de l'activité métabolique du CYP1A dès 3 mM d'exposition, et peut-être même dès 1,5 mM puisque le métabolisme tend à être déjà plus élevé que l'activité basale, impliquant que la production de NAPQI serait accrue. Une quantification des conjugués APAP-GSH permettrait de suivre le processus de détoxification des NAPQI [14]. Cependant, une détoxification des NAPQI produit serait peu probable étant donné qu'une augmentation importante de la mortalité cellulaire a été constaté. Malgré l'apparente cytotoxicité provoquait par les expositions, les niveaux d'albumine mesurés indiquent que la différenciation des cellules HepG2/C3A n'a pas été affectée.
Il semblerait donc que les biopuces de cellules HepG2/C3A perçoivent l'APAP, à des concentrations hépatotoxiques, et sont capable de répondre à ce stress. L'APAP provoque une cytotoxicité apparente à partir de 1,5 mM, qui s'intensifie à 3 mM, mais qui ne provoque malgré tout aucune dédifférenciation cellulaire.

Analyse des effets de l'APAP sur la barrière pulmonaire Calu-3

Les cellules Calu-3 ont été choisies pour modéliser le compartiment pulmonaire. Elles forment un tissu cohésif de cellules sécrétrices et ciliés. Même si les cellules sont immortalisées, elles possèdent des propriétés semblables à celles des cellules primaires (TEER,

perméabilité tissulaire), notamment en matière de métabolisme xénobiotique. En effet, la littérature rapporte la présence de métabolisme de phase I (CYP1A1, 2B6, 2E1), II (UGTs) et des transporteurs de phase III (MRP1, P-gp) actifs [15]–[19].
Les tissus Calu-3 cultivés en condition submergé ont bénéficié d'un volume de milieu apical suffisant pour atteindre des concentrations d'exposition élevées, la solubilité de l'APAP étant un facteur critique. Les observations morphologiques et de viabilité cellulaire ont montré que les expositions de 7,5 et 15 mM d'APAP induisent une cytotoxicité apparente non dose-dépendante. Les cellules présentaient notamment une morphologie anormalement agrandie, pouvant être corrélée, d'après la littérature, à des cellules sénescentes. L'augmentation de la taille des cellules entraînerait une augmentation du rapport cytoplasme/ADN, qui contribuerait à l'arrêt du cycle cellulaire [20]. L'APAP a également affecté le métabolisme mitochondrial des cellules Calu-3, l'activité ayant diminué de près de moitié. Cela pourrait être dû à l'accumulation de NAPQI étant donné que la littérature rapporte que les mitochondries sont les principales cibles des NAPQI [21]. Ce phénomène se traduisant par un stress oxydatif mitochondrial dans le foie [22], des mesures des espèces réactives de l'oxygène (ROS) pourrait être réalisées afin d'étudier si la réduction de l'activité mitochondriale chez les cellules Calu-3 pourrait aussi être liée à un stress oxydatif et donc possiblement à l'accumulation de NAPQI. Cette perte de viabilité expliquerait alors l'impact que les expositions ont eu sur la cohésion tissulaire, s'étant notamment traduit par la perte de fonction barrière. Les résulats ont rapporté une baisse de TEER, qui selon la classification établie dans la littérature ont fait passer les tissus Calu-3 de "serré", avec des valeurs supérieures à 2000 $\Omega.cm^2$, à "intermédiaire" tendant plutôt vers "fuyant" puisque les valeurs se situent aux alentours de 300 $\Omega.cm^2$ [23]. L'intégrité de la barrière dépend de l'architecture des jonctions intercellulaires [24]. Les immunomarquages des jonctions d'adhérence E-Cadherin et des jonctions serrées Claudin-1 ont révélé que l'APAP perturbait le réseau de Claudin-1. Les jonctions serrées sont impliquées dans la régulation de la perméabilité macromoléculaire et ionique, en contrôlant l'accès aux espaces paracellulaires [25], ce qui expliquerait l'augmentation de la perméabilité tissulaire mesurée par le test de Lucifer Yellow. La perte de la fonction barrière s'est également traduit par la diminution du taux de mucines MUC5AC détectées à la surface des tissus Calu-3. Alors que la littérature rapporte qu'*in vivo* les agressions extérieures activent la production de mucine des voies aériennes [26], la baisse du taux de mucines de surface pourrait donc indiquer que l'APAP interfèrerait avec la production de mucine. Cela pourrait être dû au fait que les cellules sont déjà trop endommagées par l'exposition pour maintenir un métabolisme actif. Il semblerait donc que les tissus Calu-3 perçoivent et répondent au stress causé par l'exposition d'APAP à fortes concentrations d'exposition.

Complexification du modèle pulmonaire vers des conditions de culture et d'exposition plus physiologiques

Le protocole de reconstruction comprend 24 heures de différentiation à l'interface air-liquide, un volume (200 μL) et des concentrations (0,5 and 1 mM) d'exposition plus

faibles. Ce mode de différentiation a largement été étudié et souligné pour les avantages fonctionnels qu'il confère aux tissus pulmonaires [27]. En ce qui concerne les tissus Calu-3, les équipes de Forbes et Kristan ont documenté la façon dont l'ALI a permis une différentiation tissulaire semblables aux épithéliums des voies respiratoires *in vivo*, notamment par l'amélioration de la production de mucus couvrant la surface cellulaire et la pseudostratification du tissu [28], [29]. Ces caractéristiques morphologiques et fonctionnelles se sont également manifestées dans nos tissus Calu-3 semi-ALI.
Les valeurs de TEER et de perméabilité des tissus différenciées à l'ALI excèdent habituellement ceux des tissus cultivés en condition submergé, or ce constat ne se s'est pas traduit dans nos expériences, probablement dû au fait que les tissus n'ont pas bénéficié d'assez de temps pour se réadapter complètement à la culture après le passage à l'ALI, sachant qu'ils subissent un changement abrupt d'approvisionnement en nutriments et en oxygène lorsque le milieu apical est retiré. Cette phase d'adaptation pourrait provoquer une phase de latence momentanée dans la culture. Malgré tout, en raison de l'amélioration globale de la différenciation tissulaire, les échantillons semi-ALI devraient présentés de meilleures propriétés cytoprotectrices, ainsi les effets indésirables liés aux expositions à l'APAP devraient être atténués. Comme il n'y a pas de données sur l'effet de l'exposition directe de l'APAP sur des modèles pulmonaires *in vitro*, les seules données que nous pouvons utiliser sont les effets traditionnellement documentés sur cellules hépatiques. Alors que Prot et al. rapportent que l'acétaminophène a entraîné une EC50 à 1 mM d'exposition pendant 72 heures de contact avec les biopuces HepG2/C3A [8], la viabilité et la fonctionnalité des tissus Calu-3 sont restées stables à une exposition de 0,5 et 1 mM. L'absence d'effets pourrait être due à l'amélioration de la production de mucus qui pourrait moduler la toxicité de l'APAP [29]. L'APAP étant hydrophobe, le mucus peut le retenir momentanément et partiellement. Par conséquent, réduire ou au moins retarder le contact de l'APAP avec les cellules Calu-3 pourrait réduire la toxicité observée. Cependant, il semblerait qu'une toxicité a commencé à se dégager de façon dose-dépendante, entraînant des changements subtils des activités mitochondriales et des TEER.

En conclusion, l'utilisation de lignées cellulaires a permis de générer des données robustes et reproductibles rendant l'interprétation des données plus claire. Le fait que les tissus bronchiques et hépatiques aient été reconstruits respectivement sur des inserts de culture et des biopuces, facilite leur manipulation et leur observation (silicone transparent pour la biopuce, membrane semi-opaque pour l'insert). Dans l'ensemble, les données actuelles montrent que les reconstructions pulmonaire et hépatique ont généré des tissus assez différenciés pour répondre métaboliquement à une exposition xénobiotique tout en restant viables.

Transition de la monoculture à la co-culture

Avant de réunir les deux tissus en culture, quelques tests et ajustements ont été effectués pour veiller à ce que les conditions de co-culture permettent de maintenir la viabilité et

les fonctionnalités tissulaires des deux compartiments précédemment établis. La mise en co-culture implique un espace de culture commun où un milieu commun circule en continu grâce à une perfusion microfluidique. Dans le cadre du projet, et dans le temps qui nous a été imparti, nous avons choisi d'étudier les principaux paramètres suivants pour suivre l'évolution et l'adaptation des tissus au nouveau mode de culture :

- Choix d'un milieu de co-culture commun : sachant que le modèle de co-culture en était aux premiers stades de développement et que le choix du milieu de culture est une étude à part entière, l'optimisation de la composition du milieu de co-culture n'était pas encore une priorité. Ce type d'étude correspond à des étapes plus avancées de l'optimisation du modèle. Néanmoins, comme le modèle de co-culture est destiné à étudier l'interaction entre les deux tissus, le milieu commun ne doit interférer que très peu avec les caractéristiques de viabilité et de différenciation des tissus. Nous avons caractérisé l'effet du milieu à base de RPMI 1640 (milieu de culture des cellules Calu-3) sur les cellules HepG2/C3A. Le milieu RPMI 1640 ne semble par induire de perturbation cellulaire, les cellules ne perçoivent ni de cytotoxicité ou de stress cellulaire. Cependant, la sécrétion d'albumine hépatique est réduite, ce qui pourrait indiquer que la différenciation des cellules HepG2/C3A a été affectée par le changement de milieu. Néanmoins, globalement le comportement des cellules HepG2/C3A cultivés en milieu RPMI 1640 est resté le même que dans leur milieu de prédilection, c'est-à-dire qu'elles sont sensibles à l'exposition d'APAP et qu'elles répondent au stress de la même façon.

- Effet de la perfusion microfluidique sur le développement de la barrière bronchique : dans le contexte de notre projet, la stimulation mécanique du compartiment pulmonaire est mineure, en condition de co-culture les inserts Calu-3 sont intégrés dans un circuit microfluidisé, donc la contrainte de cisaillement générée ne concerne que la région basale de la membrane, imposant des forces de friction indirectes. Les résultats ont montré que les tissus cultivés en condition submergés et semi-ALI réagissent différemment au flux, et que globalement la culture dynamique semble favoriser un meilleur développement des tissus.

- Potentiel d'absorption passive des équipements de culture cellulaire : Les résultats de quantification ont révélé que le matériel de culture n'absorbe pas l'APAP et donc que la biodisponibilité reste la même que les concentrations d'exposition initiales. Les effets biologiques expérimentaux observés peuvent donc être corrélés aux concentrations d'exposition théoriques.

- Recirculation du milieu dans le circuit fermé durant la période de culture : La quantification de la perméabilité basale des tissus indique qu'une réexposition à l'APAP par le côté baso-latéral est plausible étant donné que les mesures indiquent que la perméabilité basale des tissus est supérieure à la perméabilité apicale.

Analyse de la dynamique de co-culture hépato-pulmonaire en réponse à l'exposition à l'acétaminophène

Mise en évidence de l'impact de la co-culture sur la modulation de la réponse au stress grâce au modèle de développement

Dans l'ensemble, les résultats montrent que les compartiments pulmonaire et hépatique peuvent être cultivés ensemble pendant 72 heures, étant donné qu'ils présentent des comportements cellulaires stables et fonctionnels, similaires à ceux de la monoculture, bien que la co-culture ait entraîné une réorganisation de l'architecture tissulaire du tissu Calu-3. La perte du marquage de la Claudine-1 aurait dû entraîner une augmentation de la perméabilité de la barrière, puisqu'ils sont responsables de la régulation de l'accès aux espaces paracellulaires [25], or ce n'était pas le cas. La compréhension de l'implication des cellules HepG2/C3A dans le maintien de la perméabilité des tissus Calu-3 malgré la perte de l'intégrité tissulaire nécessiterait une étude plus approfondie. Comme les poumons et le foie n'interagissent pas directement *in vivo*, ces effets n'ont pas été observés ou étudiés dans la littérature.

Les conditions de co-culture ont permis le passage de l'APAP à travers la barrière Calu-3 et dans le système circulatoire. En effet, l'APAP a été détecté dans le milieu circulant et a probablement atteint le compartiment hépatique, l'homéostasie ayant été altérée. Dans l'ensemble, les expositions à l'APAP ont suscité des comportements cellulaires similaires à ceux de la monoculture, à savoir que la présence d'APAP entraînait une cytotoxicité apparente, mais l'intensité des effets étaient réduits et les réponses tissulaires suivaient une cinétique différente dans le cadre de la co-culture. Alors que les CYP1A étaient à peine induits dans les biopuces monocultivées exposées à 3 mM d'APAP, les mesures d'activité des biopuces HepG2/C3A cocultivées révèlent une induction plus précoce et 5 fois plus intense, probablement associée à une production accrue de NAPQI toxique, cependant, les effets cytotoxiques associés ne sont pas proportionnels, ce qui signifierait qu'une détoxification de NAPQI aurait lieu. De plus, étant donné que la littérature rapporte que les NAPQI ciblent les mitochondriales [21], sa possible détoxification expliquerait pourquoi le métabolisme mitochondrial des cellules Calu-3 cocultivées a été mieux préservé qu'en monoculture.

Le renforcement des possibles mécanismes de détoxification entraînant une cytotoxicité retardée en condition de co-culture, met en évidence une interaction active et fonctionnelle entre les deux compartiments du modèle. Des observations similaires ont été évaluées dans d'autres modèles poumon/foie récemment développés où une induction retardée de la toxicité a également été observée après des expositions à l'aflatoxine B1 [30], [31].

Mise en évidence de la sensibilité du modèle de co-culture à de faibles doses d'exposition

Le modèle de reconstruction pulmonaire plus physiologique, comprenant une période de différentiation à l'ALI du tissu Calu-3, n'a pas perturbé l'homéostasie de la co-culture poumon/foie. De la même façon que pour le modèle de développement précédemment décrit, la présence de la biopuce HepG2/C3A a perturbé la pseudostratification du tissu pulmonaire Calu-3 ainsi que son réseau de jonctions adherens E-Cadherin. Néanmoins, l'APAP a pu traverser la barrière semi-ALI du modèle et rejoindre le milieu circulant commun, et même à de faibles concentrations d'exposition, l'APAP semble encore pouvoir atteindre le compartiment hépatique, comme en témoignent de légers changements dans la synthèse de l'albumine hépatique. Les comportements cellulaires de la co-culture semi-ALI en réponse aux traitements à l'APAP sont similaires à ceux observés en monoculture, c'est-à-dire qu'aucune interférence n'a été observé en matière de viabilité ou de fonctionnalité hépatique ou bronchique. Le modèle de co-culture semi-ALI est suffisamment métaboliquement compétent pour répondre à de faibles doses d'exposition, étant donné que les métabolites APAP-glucuronide et APAP-sulfate ont été fortement détectés dans les milieux post-culture.

Dans l'ensemble, le modèle méritera probablement d'être amélioré pour optimiser le mode d'exposition à l'ALI et pour complexifier les reconstructions pulmonaires et hépatiques afin d'obtenir une meilleure représentation du *vivo*. La présente co-culture poumon/foie présente un potentiel prometteur pour permettre l'amélioration des prédictions des risques et des dangers liés à la toxicité par inhalation.

Acknowledgments

Je remercie le Fonds européen de développement régional (FEDER) 2014/2020 et à l'Agence Nationale Sécurité Sanitaire Alimentaire Nationale (Anses) pour le cofinancement de ce travail.
J'exprime ma sincère reconnaissance à l'ensemble des membres du jury pour avoir accepté d'évaluer mon travail. Je souhaite tout particulièrement remercier le Dr. Samy Gobaa et le Pr. Jérémie Pourchez pour avoir accepté de juger mon travail de thèse en qualité de rapporteurs. Je vous suis reconnaissante pour le temps que vous avez consacré à la lecture et à l'évaluation de mon manuscrit. Je remercie le Dr. Stéphanie Descroix, le Dr. Cécile Legallais et le Dr. Fabrice Soncin qui m'ont fait l'honneur de participer à mon jury de thèse.
Je tiens à adresser mes remerciements à mes directrices de thèse, Pr. Muriel Vayssade et Dr. Ghislaine Lacroix, pour m'avoir donné l'opportunité et la confiance pour mener ce projet à bien. Votre accompagnement et votre disponibilité ont su enrichir et inspirer mes travaux de thèse. J'aimerais également témoigner ma reconnaissance au Dr. Rachid Jellali pour son accompagnement tout au long de cette thèse, tant bien du point de vue expérimentale que scientifique. Ton implication et ton soutien ont contribué au bon déroulement de ma thèse.
Je remercie le Dr. Anne Riu et le Dr. Cécile Legallais d'avoir fait partie de mon comité de suivi de thèse. Le temps dédié à l'évaluation de l'avancement de mon travail et vos conseils avisés ont été précieux.
Les années de thèse au sein du laboratoire de Biomécanique et Bioingénierie (BMBI) et plus particulièrement dans l'équipe Cellules Biomatériaux Bioréacteurs (CBB), en collaboration avec l'INERIS, ont été riche en rebondissements et en challenges, rendant cette expérience professionnelle d'autant plus épanouissante.
Je remercie tous les membres de l'équipe CBB pour leur accueil chaleureux, leur sympathie et leur bienveillance qui m'ont permis de réaliser ma thèse dans un environnement de confiance. Une pensée aussi aux anciens, Felix, Mégane, Augustin, Lilandra, et Mattia pour l'intégration que vous m'avez réservé.
Mathilde, l'aventure n'aurait pas été la même sans toi. Partenaire de galère, de réussite, de doutes du premier au dernier jour. Heureuse d'avoir pu partager cette aventure avec toi. Nathália, notre rayon de soleil brésilien, quelle chance que nos chemins se soient croisés. Manon, Claire et Antoine, merci pour votre soutien sans faille. Je mesure la chance de vous avoir eu à mes côtés.
And of course, a special thought to my family; Mami for never doubting me, Ati for empowering me, Natasha for inspiring me and Romain for your wise words. Léo, petit

monstre, through thick and thin, you've been there since the beginning, thank you for your patience and unconditional support (and thank you for taking care of my 100+ LaTeX errors, your contribution to my thesis was therefore significant). Thank you for being my cheerleaders, you are my rock, your love powers me through.

Contents

List of Figures

List of Tables

Abbreviation

ADME: absorption, distribution, metabolism, and excretion
AEC: alveolar epithelial cells
AECI: type I alveolar epithelial cells
AECII: type II alveolar epithelial cells
ALI: air-liquid interface
ANOVA: one-way analysis of variance APAP: N-acetyl-para-aminophenol, acetaminophen, paracetamol
APAP-GLU: APAP glucuronide
APAP-GSH: APAP glutathione
APAP-SULF: APAP sulfate
ATCC: American Type Culture Collection
BSA: bovine serum albumin
CYP: cytochrome
CYP450: cytochrome P450
COPD: chronic obstructive pulmonary disease
DAPI: 4,6-diamidino-2-phenylindole
DME: drug-metabolizing enzymes
EDTA: ethylenediaminetetraacetic acid
ELISA: enzyme-linked immuno assay
ECM: extra cellular matrix
EROD: ethoxyresorufin-O- deethylase
FBS: fetal bovine serum
FMO: flavin-containing monooxygenases
GST: glutathione s-transferases
HBSS: Hanks' Balanced Salt solution
HEPES: N-2-hydroxyethylpiperazine-N-2-ethane sulfonic acid
HSCs: hepatic stellate cells
IDCCM: Integrated Dynamic Cell Culture in Microsystems
IIDMP: Integrated Insert in a Dynamic Microfluidic Platform
iPSCs: Induced pluripotent stem cells
L-L: liquid-liquid interface
LSEC: liver sinusoidal endothelial cells
LY: Lucifer Yellow
MUC: mucins
MRP2: multidrug resistance-associated protein 2

NAPQI: N-acetyl-p-benzoquinone imine
Papp : apparent permeability coefficient ($cm.s^{-1}$)
PAS: Periodic acid-Schiff
PBS: Phosphate Buffer Saline
PDMS: polydimethylsiloxane
PFA: paraformaldehyde
PHH: primary human hepatocytes
PM: particulate matter
RPMI 1640: Roswell Park Memorial Institute 1640
SD: standard deviation
SULT: sulfotransferases
TEER: transepithelial electrical resistance
UGT: UDP-glucuronosyltransferases
VOCs: volatile organic compounds
WHO: World Health Organization
2D: two-dimensional
3D: three-dimensional

Chapter 1

General research context

1.1 Airborne hazards

Air, more precisely oxygen, is one of the vital components that enabled and sustains life on Earth. The quality of ambient air is closely linked to climate and ecosystems both of which are regulated by the coexistence of the biotic (living organisms) and the abiotic (hydrosphere, lithosphere, and atmosphere) realms. Typically composed of 78% nitrogen, 21% oxygen, and 1% a combination of carbon, helium, methane, argon, and hydrogen, the natural state of air has been challenged by human presence on Earth. Indeed, anthropogenic air pollution has been referred to as one of the biggest public health hazards of modern society. The World Health Organization (WHO) reports that 99% of the global population breathes highly polluted air and estimated at least 7 million related deaths each year [32]. Sources of air pollution are multiple, context-specific, and increasingly threaten human health [33]–[35].

1.1.1 Genesis and evolution through time

Air pollution is defined as any physical, chemical, or biological hazard released in ambient air. Human activity has dictated the way air pollution has evolved since the dawn of civilization. Exposure to polluted air has fundamentally been influenced by lifestyle. Indeed, adverse effects can be traced back to ancient societies where indoor fires were used for domestic use (e.g. heating). Dwellings were poorly ventilated and smoke probably engulfed small villages which surely impacted human health. Egyptian and Peruvian mummified lungs of that period displayed blackened tissues, a sign of anthracosis [36], [37]. Meanwhile, cities continued rising faster than urban planning could develop which multiplied pollution sources. For instance, bathrooms remained rare, chamber pots were emptied into streets, and city ditches were used as latrines. Therefore, airborne hazards were various and omnipresent in public spaces. Localized exposures globalized when industrial activities flourished especially when smelting and mining appeared. Evolution of human activities towards lead and copper production, and then coal mining [38], endangered air quality on a further global scale. Coal was at the heart of the Industrial Revolution, and global production increased by almost 80% in the span of a century, from the 1800s to the 1900s. Coal was essential to the rise of industrial civilization until fossil energies offered higher profit opportunities [39]. The fast-growing pace of the industrial

era was enabled by the globalization of exchanges. Improved transport infrastructures allowed to respond to the increasing demand for energy by supplying faster and in bigger quantities to industries and households. Although the Industrial Revolution allowed for unprecedented technological, and societal progress, it introduced humanity to a new pollution era. Economic growth encouraged the urbanization of cities which often went hand in hand with the destruction of surrounding nature. For instance, early 1900s German official reports linked damage to cropland and forests to increasing rates of air pollution on a regional scale in the Ruhr area [40]. The rapid increase of industrial cities has not been inconsequential, as it led to ecological catastrophes such as 1952's Great London Smog. Heavy loaded atmospheric pollution in the capital for 5 consecutive days not only killed over 4,000 people but affected the life expectancy of English people several months after this episode as death rates remained unusually high [41]. This episode highlighted the relationship between air pollution and human health. Air pollution is a complex mix of naturally occurring or man-made gases and particles in the atmosphere. Pollutants stem from two types of sources:

- Geogenic and biogenic emissions are emitted naturally respectively by non-living and living sources (e.g. volcanic eruptions, volatile organic compound emissions from forests).
- Anthropogenic sources engineered by human activities and resulting in the release of airborne compounds into the atmosphere

Since the Industrial Revolution, the atmospheric concentration of greenhouse gases has increased enough to contribute to historically high global temperatures [42]. The planet's average temperature rose by $0.8°C$ since 1880, and predictions estimate that this trend could intensify and peak towards an additional $1.8°C$ to $5.8°C$ by the end of the twenty-first century. Regulations, such as the 1970 Clean Air Act Amendments, and working groups, such as the Environmental Protection Agency in the United States, have emerged around the globe to work towards air pollution regulations (National Ambient Air Quality Standards) to protect human and environmental health.

1.1.2 Exposure categories

An individual's exposome varies throughout life according to exposure sources, patterns, and intensity. When it comes to atmospheric exposome, pollutants have taken a considerable share in modern societies. They can be classified based on where they originated:

- Primary pollutants are emitted directly from a source into the atmosphere. Amongst them, carbon monoxide (CO), volatile organic compounds (VOCs), nitrogen oxides (NO_x), sulfur dioxides (SO_2), and particulate matter (PM) are well known for inducing highly hazardous atmospheric conditions.
- Secondary pollutants are stable compounds formed in the atmosphere as a result of chemical reactions between primary pollutants and atmospheric compounds.

Ground-level ozone (O_3) for example is one of the most widely known secondary pollutants. It is formed between oxides of nitrogen and VOCs. It composes the characteristic smog of urban areas, and has been described as causing adverse effects on human health [43].

They can also be found under different shapes [44]:

- Gaseous air pollutants can be carbon- (CO, CO_2, CH_4), nitrogen- (NO, N_2O, NH_3), sulfur- (SO_4), or halogen-based [45]. Ground-level ozone (O_3) for instance is a major gaseous air pollutant.
- Particulate matter or aerosols are small liquid droplets, loaded with microscopic solid particles, suspended in the air. They are categorized according to their size: particles less than 100 microns (PM_{100}), 10 microns (PM_{10}), 4 microns (PM_4), 2.5 microns ($PM_{2.5}$), or 0.1 microns ($PM_{0.1}$). Particulate pollution is made up of a variety of components, including acids (nitrates and sulfates), organic chemicals, metals, soil or dust particles, and allergens [46].

All these different airborne elements can diffuse in the atmosphere in various ways. They can be emitted by a direct source or stagnate and compose the ambient air as immissions.

1.1.2.1 Natural sources

Natural pollution sources of air are part of the environment's natural equilibrium. However, the danger of their occurrence resides in the intensity of associated manifestations which can considerably disrupt air quality and threaten human health. For example, the important forest fires that broke out this summer in the Gironde department in France, destroying more than 7,000 hectares of forest in the space of a few weeks, caused severe air pollution episodes where the alert threshold for suspended particles (PM_{10}) was exceeded (50 $\mu g/m^3$) [47]. The threat relating to these events is also complexified by their transborder nature, as they can easily be carried out through air streams and travel long distances, affecting global atmospheric composition [48].
Categories of natural pollutants are diverse and ubiquitous in ambient environments. Depending on their nature, their presence is conveyed or triggered in different ways.
Biological agents constitute a source of natural air pollution, and airborne allergens are the most common; they are antigens capable of eliciting an allergic immune response with accompanying clinical symptoms (e.g. rhinitis, asthma) [49], [50]. Primary sources include occupational dust emanating from plants (pollens), and fungi (spores). Their solubility, stability, and molecular properties influence their entry route into the body and the organ(s) they can reach and in which they can induce an immune response. In ambient air, they disperse via air movements, mainly according to meteorological factors, and settle based on their aerodynamic phenotype. Their spreading can also be facilitated by attaching to living organisms (humans, animals). Their allergenic potential can reportedly be aggravated by their ability to attach air pollutants to their surface [51].

The potency of natural pollution has been increased by anthropological activities, particularly greenhouse gas emissions. Indeed, they contribute to the premature warming of the atmosphere which induces weather pattern fluctuations that are important factors in natural pollution instability. Heat waves, wind, and rain streams have been disrupted and exacerbated by climate change, and their impact on air quality has increased global mortality and morbidity rates [52], [53]. For instance, maximum atmospheric ozone concentrations, reported as health hazardous, have been documented to be prolonged and aggravated by higher temperatures [54]. Another study showed that for every $1°C$ temperature increase during the 2006 heat wave in Porto (Portugal), global mortality increased by 2.7%, and chronic obstructive pulmonary disease (COPD) patient morbidity increased by 5.4% [55]. What progressively turns cities into urban heat islands increases natural sources of air pollutant emissions by accelerating, amplifying, or provoking natural disasters (e.g. hurricanes, flooding, soil erosion). As climate models suggest that a $1°C$ increase can induce a two to sixfold risk of wildfire occurrence in the western United States [56]. Not only do they generate great amounts of air toxics but these types of events favor the movement of populations. These changes can accelerate disease spreading [57] in particular air traveling pathogens (e.g. mycotoxins, bacteria, viruses). Coughing and sneezing are bodily functions that generate aerosols which are particle and often pathogen-loaded [58], [59]. Airborne transmissions are greatly facilitated and accelerated when the human density in a given area is high, especially in small enclosed areas [60], [61]. Highly contagious episodes can present threats on a global scale. The pandemic linked to COVID-19 is a recent example of the socio-economic repercussions of such a health disaster [62], [63].

1.1.2.2 Anthropogenic sources

Anthropogenic pollution of the atmosphere is categorized in two different groups: stationary and mobile sources. Population growth is associated to an increasingly energy intensive system. To satisfy this need, globalization and urbanization were pre-industrial drivers that significantly enabled productivity [64], up to this day. The energy sector is one of the most potent of our time, the emissions discharged by manufacturing processes such as energy production (e.g. power plants, heat production), extraction, and distribution (e.g. oil, coal, gas) contributes to the concerning rise of air pollution and more specifically heat-trapping greenhouse gases. The two main associated greenhouse gases are carbon dioxide (CO_2) and methane (CH_4). Ground-level ozone (O_3) in smog also accounts for a significant share of the pollution emanating from industries. Nowadays, industrial activities account for the second-largest source of air pollution. The industrial sector is the most demanding in terms of energy consumption, and consequently accounts for almost 43% of energy-related carbon dioxide release.
Agriculture is a large source of anthropogenic pollution. This sector is a major producer of nitrous oxides, ammonia (byproducts of fertilizer) and methane (livestock) and releases considerable amounts of pesticides [65]–[68]. Fertilizers and mechanization of practices have been implemented to intensify agricultural yields to keep up with the

growing demand. Agricultural practices vary according to local laws and customs, however the Fifth Assessment Report of the Intergovernmental Panel on Climate Change reported that they accounted for at least one third of the global anthropogenic greenhouse gas emissions [69].
The sector of transportation is also a big consumer of energy, on average 22% of global primary energy are utilized by transports. The predominant fuels are diesel and gasoline, and their combustion emits high levels of particulate matter ($PM_{2.5}$ and PM_{10}) and nitrogen oxides (precursor of O_3 and smog) [70] which reportedly threaten human health by provoking chronic disorders such as asthma, or even death [71]–[73]. Transport-related pollution defies all social barriers, as adverse effects are not only concentrated in disadvantageous populations but impact both developed and developing regions worldwide. The sources of industrial pollution mentioned above are among the most recognized but represent only a part of those existing and involved in the deterioration of the current air quality. Many of these emissions generate heat, change temperature and therefore influence global climate which impacts worldwide health.

1.1.3 Socio-sanitary concerns related to increasing levels of air pollution

The greatest threat posed by air pollution is its ubiquity in the air. It not only dominates outdoor spaces but also settles indoors. Therefore, exposure has become inevitable and constant. Schools, bars, the inside of transport vehicles, and houses are daily places that display poor air quality. Indoor pollution originates from different sources:

- Outdoor pollution circulates and invades indoor spaces
- Surrounding facilities (e.g. paint, insulation)
- Domestic activities such as cooking, heating, or cleaning habits

A lot of those vary according to local laws and customs. In developing countries, for instance, households still use to this day biomass or coal to heat and cook [74]–[76]. Due to the stagnation of indoor air, airborne pollutants are present in higher concentrations in enclosed spaces rather than outdoors [77]. Fine particles, nitrogen dioxide, carbon monoxide, VOCs, and biological allergens are among the indoor pollutants of utmost concern to human health. Because air pollution is ubiquitous in the environment and exposures can be acute, chronic, or both, quantifying the associated health hazards is challenging, however the WHO estimates that deaths attributable to air pollution exposure account for 11% of lung cancer deaths, 23% of COPD deaths, and 12% of ischaemic heart disease [74]. As we reportedly spend 90% of our time indoors [78], improving our knowledge of inhalation toxicology is crucial to predicting and preventing the risks and hazards associated with air pollution.
Overall, air pollution is currently impacting all levels of our society. On a global scale, it disturbs our biosphere, global warming has repercussions on ecosystems, and ecological disasters, such as the extinction of fauna and flora, are increasingly frequent and threaten

the socio-economic stability of our societies, as well as the individual well-being of worldwide populations [79]. Studies show that exposure is also linked to the development of respiratory, cardiovascular, mental, and perinatal disorders [80] as well as the development of severe mental illnesses [81]. Private and governmental entities and authorities are working towards the management of air pollution to reduce rates to acceptable levels or possible elimination [82]. For this purpose, guidelines and air quality standards were issued as a tool to monitor risk through limit values [83]. In Europe, they exist under the terms of AQLVs (Air Quality Limit Values (AQLVs), and in the USA under the National Ambient Air Quality Standards (NAAQS). While both standards and directives are based on different mechanisms, significant success has been achieved in the reduction of overall emissions and associated health and environmental effects. The European Directive measures levels of pollution and identifies emission sources in specific geographical areas of risk, whereas the USA establish global air quality criterion considering all sources of the pollutants and their precursors [84].

1.2 The respiratory tract: target organ of inhalation-type exposures

1.2.1 Anatomy and physiology of the respiratory apparatus

Internalization of oxygen is vital to ensure bodily functions. Air enters through the respiratory tract which is structurally divided into upper and lower airways. The upper airway begins at the nose and continues along the throat, pharynx, larynx, and trachea, making the way into the lower airway comprising the bronchi leading to the lungs. The lungs are asymmetrically paired organs lodged in the thoracic cavity, surrounded by the rib cage (Fig. 1.1). They are lined by the pleura which is a two-layered serous membrane formed by an outer parietal and an inner visceral layer. Both layers glide over each other to allow pulmonary ventilation movements.

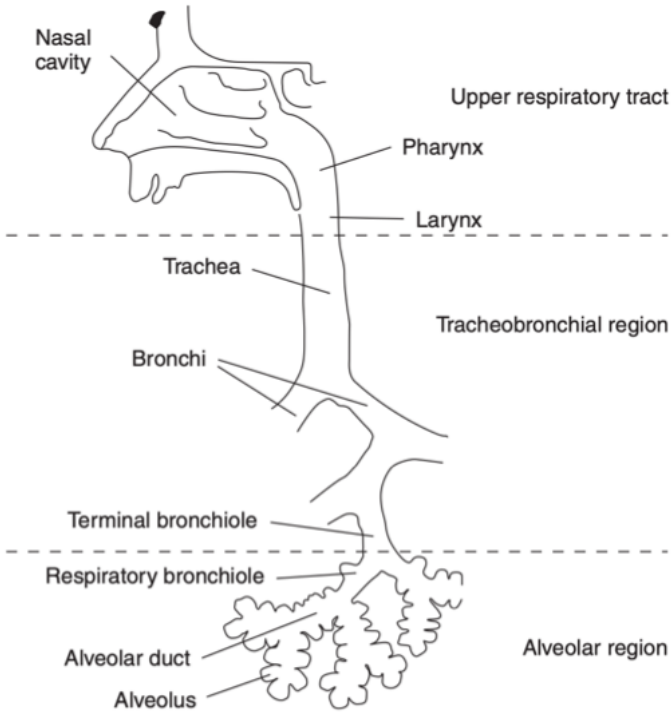

FIGURE 1.1: Diagram of the three physiological regions comprising the human respiratory tract. Reproduced with permission from [85].

The respiratory system is compartmentalized into two functional sections (Fig. 1.3):

- The conduction airways, comprising the trachea, the bronchi, and bronchioles, ensure the transport and filtration of inhaled air. They are made of pseudostratified columnar ciliated epithelia, which protect the distal areas of the lungs from airborne threats. Three key mechanisms work to this end: air humidification, mucus secretion, and clearance. Morphology and function vary along the bronchial tree, and are modulated by the local cellular composition of tissues.

- The acinar airways, also known to be the respiratory division, are in charge of gas exchange, and are composed of respiratory bronchioles, alveolar ducts, alveolar sacs, and alveoli. Fibrous tissue, smooth muscles, vessels, and nerves accompany the air passages. This zone is responsible for oxygen supply and carbon dioxide removal.

The lining of respiratory airways comprises a variety of cells and epithelia structures that carry out vital functions to support pulmonary homeostasis, including fluid balance, metabolism, clearance, and inflammatory response to injury. Overall, epithelia continuously line the internal and external surfaces of the lungs. They are formed by juxtaposed cells joined by intercellular junctions allowing them to coherently function as a unified tissue to serve as a barrier and a surface of exchange. Cellular junctional complexes ensure key functions such as paracellular permeability (tight junctions [86]), intercellular communication (gap junctions [87]), or even cell-cell contact maintaining

tissue integrity (adherens junctions [88]) 1.2. Epithelial cells rest on a dense basement membrane, via hemidesmosomes, that comprises a type IV collagen and laminin-based upper layer, known as the lamina densa, secreted by epithelial cells, and a type III and V collagen and fibronectin based lower layer, the lamina reticularis, synthesized by subepithelial fibroblasts [89]. This membrane acts as cell anchorage, enables cell polarity, and separates the epithelium from the underlying subepithelial compartment [90].

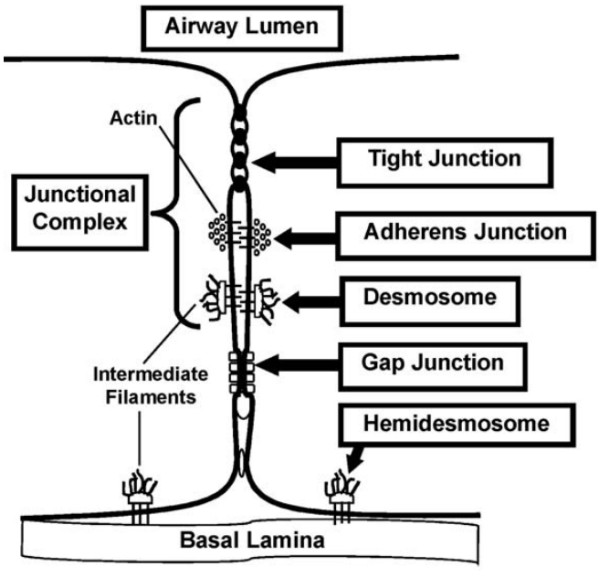

FIGURE 1.2: Schematic diagram of the various epithelial cell junctional complexes. Tight junctions are essential in maintaining the barrier properties of epithelial sheets. Adherens junctions are associated with actin filaments, usually forming an adhesion belt around the cells. Desmosomes form cell–cell contacts and associated with intermediate filaments. Gap junctions allow the passage of small water-soluble ions and molecules. Hemi-desmosomes resemble half a desmosomes and form cell-ECM junctions. Reproduced with permission from [91].

Epithelia structure lining the respiratory airways vary depending on the location in the bronchial tree [92]:

- Pseudostratified columnar epithelium from the trachea to the bronchioles. They are majorly colonized by ciliated, basal, and secretory (goblet) cells.
- Non-stratified cuboidal epithelium line the bronchioles. They are characterized by the presence of Clara cells
- Simple squamous (type I) and cuboidal (type II) pneumocytes (also known as alveolar epithelial cells (AEC)) constitute the alveolar epithelium

According to the respiratory airway section, the epithelium rests on differently composed subepithelial tissues, comprising the lamina propria (connective tissue), cartilage and muscle fibers.
At least eight morphologically distinct epithelial cell types are present in human respiratory epithelium. They can be classified into three categories according to structural,

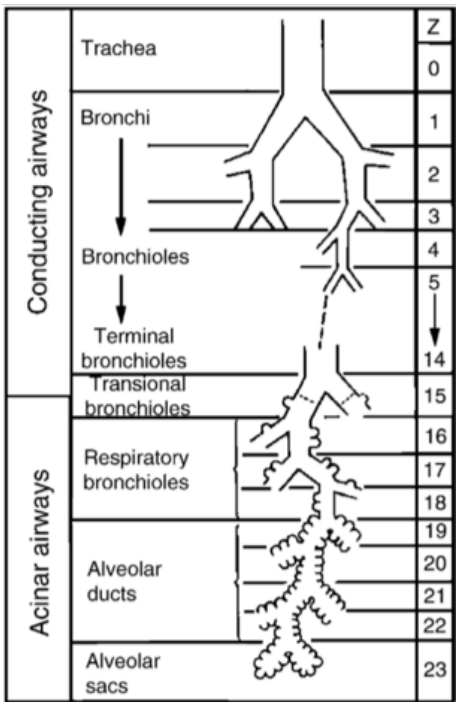

FIGURE 1.3: Model of the human airway tract according to its characteristic hierarchical branching systems from the trachea (generation 0) through the acinar airways (generations 15-23), and ending in alveolar sacs. Reproduced with permission from [93].

functional and biochemical criteria: basal, ciliated and secretory [94]. In addition, immune cells, inflammatory cells and phagocytic cells migrate to and remain within the epithelium or transit through to the lumen.

Basal cells are ubiquitous in the conducting airways, their presence decreases the deeper the airways go [95]. Their attachment to the basement membrane determines their structural role. They also act as progenitors of pulmonary epithelia, i.e. they have the ability to proliferate and differentiate into every other cell type that composes the respiratory system [96], [97].

Club cells, also known as Clara cells, compose bronchial and bronchiolar epithelia [98]. They are filled with secretory granules that upon release line the surface of epithelia with surfactant [99]. They also play a metabolic protective role as they contain high levels of glutathione et de cytochrome P450 (CYP450) capable of biotransforming inhaled xenobiotics [100]. They also contribute to the restoration and the cellular renewal of tissues as they are progenitors capable of differentiating into ciliated and mucus-secreting cells [101], [102]. Columnar ciliated epithelial cells are predominant in the airways, they account for over 50% of all pulmonary epithelial cells [94], [103]. They are characterized by the presence of cilia at their apical pole, typically 300 cilia per cell [104]. Cilia synchronously rotate creating a mucociliary movement enabling the clearance of the epithelium which consists in the evacuation of any foreign body trapped in the mucus lining [105]

Mucous cells, also known as goblet cells, are secretory cells of the airway epithelium

[106]. They produce the mucus that lines the epithelium. The viscoelastic properties of mucus are involved in the proper mucocilary clearance process [107]. Mucus is mainly composed of glycoproteins also known as mucins (MUC) which include different types, the main ones being MUC5AC and MUC5B [108]. Similar to goblet cells, serous cells are secretory cells. They are referred to as "immobile neutrophils" because they contribute to the defense of the respiratory tract by secreting antimicrobial substances [109]. They also serve in the regeneration of the epithelium since they can differentiate into mucous cells [110].

Pulmonary neuroendocrine cells are sparsely found throughout the bronchial tree [111]. They either exist as single cells or in a grouped conformation as innervated cellular clusters known as neuro-epithelial bodies. They are multi-functional epithelial cells which act as interpulmonary sensors and endocrine mediators that trigger biological responses to inhaled compounds [112].

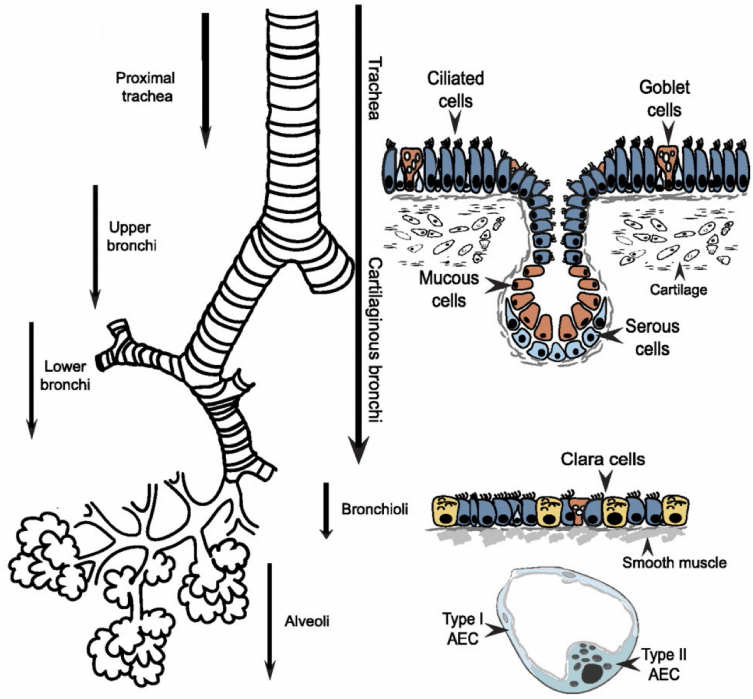

FIGURE 1.4: Schematic illustration of the cellular diversity comprising human lower airways. Adapted from [113].

A respiratory unit is composed of a respiratory bronchiole, alveolar ducts, chambers and alveoli. The alveolus is the functional area of the lung, where gas exchange occurs. Alveoli are the functional unit of the lung. Briefly, oxygen-poor blood rises from the organs to the heart and travels to the lungs, through the pulmonary arteries, where it diffuses into the pulmonary capillaries. Hematosis is the process by which blood is reoxygenated in the lungs. It occurs at the alveolar-capillary barrier, where inhaled oxygen enters the bloodstream and blood carbon dioxide is evacuated into the alveolar space. Human adult lungs comprise on average 300 million alveoli, providing roughly a total exchange surface of 80 to 140 m^2 [114]–[116]. Alveoli are structurally composed by type I and type II AEC.

Type I AEC (AECI) are non-dividing, terminally differentiated cells with a flat squamous morphology, arranged in a monolayer. They cover about 95% of the alveolar surface [117] and provide the majority of the alveoli periphery. They also cover the blood capillaries thus forming the alveolar-capillary barrier, which is where gas exchanges occur. Their cytosol contains few organelles, but numerous pinocytosis vesicles, capable of transporting macromolecules from the alveolar cavity to the interalveolar septum. While type II AEC (AECII) are microvilli-covered spherical cells that insure alveolar tissue renewal thanks to advanced plasticity and self-renewal capacities. AECII are in fact the progenitor cells of AECI [118]. They cover less than 5% of the alveolar surface [119]. They contain intracellular surfactant packed lamellar bodies to ensure surface-regulatory properties of endoalveolar the surface during the breathing cycle. AECII also have immunological properties, such as the synthesis of pro-inflammatory cytokines and chemokines (e.g. TNF-α, IL-1, IL-6, and IL-8) and of antibiotic and anti-oxidant substances [120], [121].
Respiration is an essential function that is mainly protected by muco-ciliary defense mechanisms. Breathing allows for gas exchanges and cellular respiration along with many other vital processes including blood pH regulation, anti-microbial defense and body temperature control [122].

1.2.2 Entry routes and distribution of inhaled particles in the respiratory tract

Breathing is an autonomous function that provides continuous oxygenation to ensure proper bodily functioning. Oxygen is drawn into the lungs from the surrounding air regardless of its composition, exposing the body to all sorts of airborne threats, and therefore represents a major route of exposure to gases, volatile compounds, aerosols and respirable particles. There is a multitude of different airborne matter and various factors influence the way their uptake into the body. Within the framework of my project, the focus is placed on anthropological sources of air pollution.
Inhaled particles are of different sizes and can travel through the air or stagnate according to their physicochemical, and aerodynamical properties. As shown in Fig. 1.5, their size greatly influences their route of entry.

	Percentage of Particles Inhaled and Deposited Particle Aerodynamic Diameter			
Respiratory Tract Region	**0.1 μm**	**1 μm**	**10 μm**	**100 μm**
Head airways	2.1	29	81	50
Tracheobronchial	2.7	2.7	1.5	<0.1
Alveolar	14	12	1.9	<0.1

FIGURE 1.5: Particle deposition along the respiratory tract according to particle diameter [123].

Once the particles have entered the lungs, they can follow three main deposition mechanisms (Fig. 1.6 and 1.4) [124] :

- The distinguishing feature of the respiratory system lays in its architecture. Branching and ramification imposes a shifting geometry that influences the convection

movement linked to inhalation [125], [126]. As a result, the particles contained in the inhaled air are carried by an airstream subject to repeated deviations. Some of them are not able to follow the orientation of this turbulent airflow, and collide on the surface of the tissues. This type of deposition is called impaction and concerns particles over a 5 μm [127].

- Particles settle by gravity on the surface of the surrounding tissue when the inhaled airflow is no longer sufficient to sustain a proper airstream. Gravitational forces regulate this type of deposition, which is known as sedimentation. Shape, dimension and mass density of inhaled particles influence the sedimentation patterns in different airway sites. This kind of mechanism mainly occurs in the lower airways where the airflow is reduced because of increasing pulmonary ramification and size reduction of airways. Sedimentation deposition concerns particles over a 1 μm.

- A random motion known as Brownian motion, which is similar to the motion of gas molecules, is acquired by particles smaller than 0.5 μm. The smaller the particle, the more energetic is the associated Brownian motion. Their deposition is therefore random and can lead to the diffusion of particles into the airway walls, especially in small airways and alveoli, where the airflow is very low. Due to their small size, these particles can cross the epithelial barrier easily and enter the bloodstream [128]. For instance, diffusion mechanisms are involved in the deposition of nanoparticles [129].

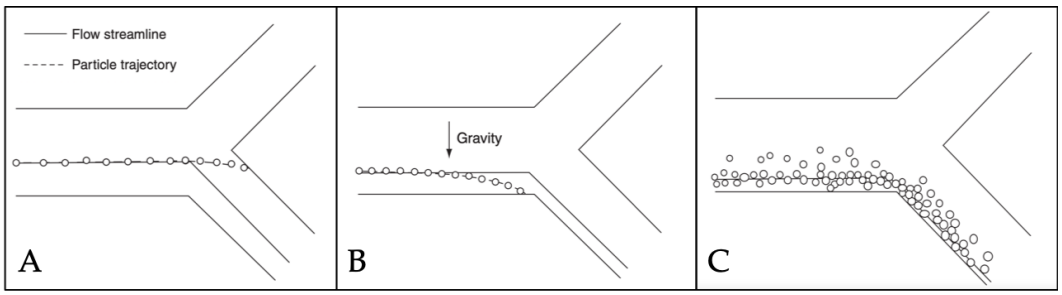

FIGURE 1.6: Particle deposition in the airway by sedimentation (A), by impaction (B), and by diffusion (C). Adapted from [85].

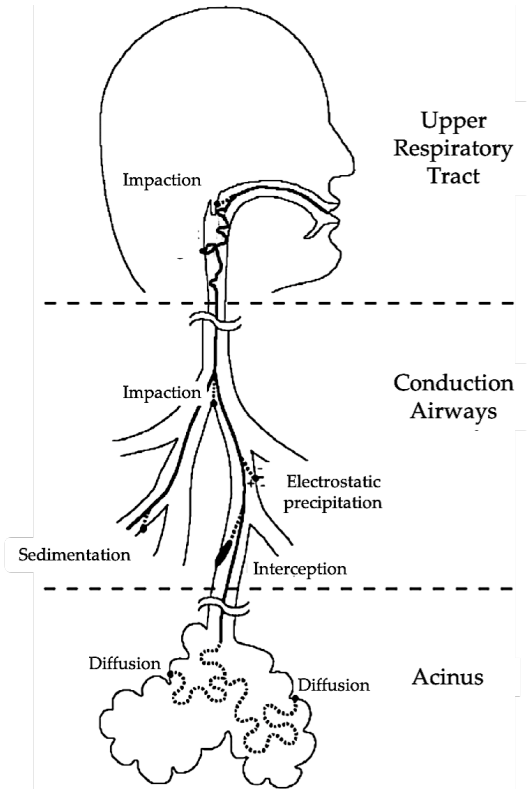

FIGURE 1.7: Diagram of the various deposition mechanisms of inhaled particles that occur along the respiratory tract. Adapted from [130].

Two other deposition mechanisms exist, they represent a small share of the occurring pulmonary depositions:

- Electrostatic precipitation involves the way the charges of inhaled particles interact with the charges of the surrounding airway environment (image forces) or with the charges of other particles present in the airstream (space forces) through repulsion or attraction.
- Interception occurs when a particle is trapped in the airway wall because an edge came close enough and touched its surface. This mechanism mainly concerns long and elongated particles such as fibers [131].

1.2.3 Pulmonary elimination pathways

1.2.3.1 Mechanical clearance

Once particles entered and settled into the walls of the respiratory tract, the organism proceeds to the removal of these particles. Different clearance mechanisms are deployed for this purpose, such those involving mechanical transport:

- Ciliated airways covered with mucus can achieve mucociliary clearance. Particles trapped in the aqueous lining can be moved up, by ciliary movements (mucociliary escalator), to the upper tracheobronchial area and expelled by coughing or swallowing. This kind of mechanical transport works to prevent inhaled hazardous

compounds from reaching the lower airways [105]. Despite the crucial role that mucus and other airway epithelial secretions play in protecting the lungs, chronic mucus hyperproduction often results in impaired mucus clearance which can obstruct the airways and cause infections. These kinds of disorders can lead to high morbidity in asthma, idiopathic pulmonary fibrosis, or cystic fibrosis cases for instance [132].

- Because the alveolar region lacks ciliated cells and mucus lining, alveolar macrophages are essential to the protection of this area. They are cells of the innate immunity, and display a considerable functional plasticity that allows them ensure the homeostasis and the defense of the lower airways. Under normal circumstances they act as sentinel cells and they help orchestrate the activation of the immune cascade through cytokines, and chemokines secretion [133]. By recruiting and differentiating circulating monocytes, thanks to chemokine attraction, their number is increased during the inflammatory response [134]. They engulf the particles or pathogens of interest and head to the interstitium to reach the lymphatic circulation up to the lymph nodes, or carry themselves up to ciliated airways to undergo mucociliary clearance [135]. Though other resident immune cell types, including lymphocytes, neutrophils, and mast cells, are also present, alveolar macrophages constitute the main lineage of innate immunity protection [136].

Besides the mechanical removal of particles by mucociliary or alveolar macrophage clearance, particles can also dissolve into the airway lining and cells (endocytosis). Dissolution also represent an important share of the pulmonary clearing mechanisms as they facilitated the passage into the vascular system. Dissolution rates depend on the pulmonary region, conducting airways are thicker than those of the acinar regions which causes the dissolution to be slower in these areas, and on the physicochemical properties of the particle: higher solubility allows for faster dissolution [137], however the lipid and protein composition of pulmonary lining increases the solubility of lipophilic compounds [138]. Nevertheless, reduced dissolution of inhaled xenobiotics can translate into poor clearance and an accumulation of toxicants. If dissolution processes are inefficient, mechanical clearance intervenes.
Because of morphological and cellular heterogeneity of the respiratory tract, clearance processes vary according to the airway region. The nasal cavities are the first protective barrier of the upper airways. They efficiently trap large compounds are evacuate them by sneezing or blowing [139]. If inhaled particles enter further distal regions, they are rather subject to mechanical clearance processes. Oral coughing and swallowing expel the byproducts of the mucociliary clearance occurring in ciliated and mucus-loaded epithelia. Whereas in alveolar regions, clearance is dependent on the solubility of the deposited particles. Small and hydrophilic compounds diffuse easily through the alveolocapillary barrier into the lymph or the blood [140], which is why bigger or lipophilic toxicants are rather subject to phagocytosis clearance [85].

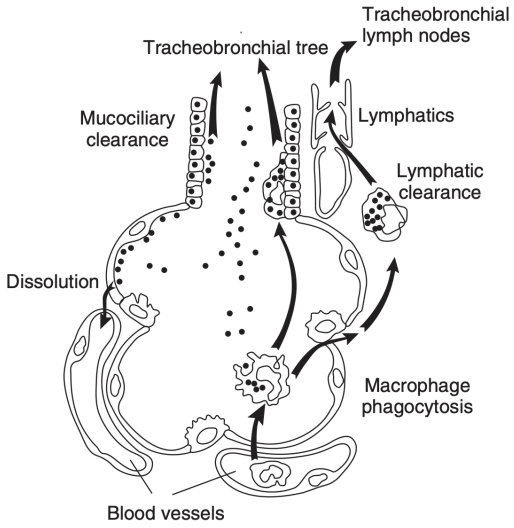

FIGURE 1.8: Schematic of pulmonary clearance mechanisms. Mechanical processes include macrophage phagocytosis and mucociliary clearance. Adapted from [85].

1.2.3.2 Metabolic clearance

1.2.3.2.1 Human xenobiotic transport and metabolism principles

Foreign compounds that enter the body undergo the ADME process, which stands for absorption, distribution, metabolism, and elimination. Associated transport and metabolic pathways ensure the detoxification and excretion of internalized harmful compounds. The toxicity linked to these exogenous substances can be attributed either to their parent form or to their metabolites [141], [142].
Four phases articulate the ADME process:

0. Phase 0 covers the vectorial transcellular uptake of compounds [143]. The family of solute carrier transporters (SLC) is in charge of running this transport [144], [145]. The selective cell entry and intracellular concentration of internalized compounds are determined at this stage.

The metabolic detoxification is ensured by so-called drug-metabolizing enzymes (DME) that biotransform xenobiotics to more hydrophilic forms, to facilitate their extraction [146]. This metabolism comprises phase I and II reactions.

1. Phase I functionalization enzymes are responsible for oxidation, reduction, or hydrolysis reactions to yield polar water-soluble metabolites [147]. Phase I metabolism can lead to xenobiotic inactivation or activation. The CYP450 superfamily largely contributes to the phase I metabolism by primarily catalyzing oxidation reactions. They are membrane-bound isoenzymes [148] present across the body but most abundantly concentrated in the liver [149]. Oxidative reactions require the aid of cofactors such as NADPH-cytochrome P450 reductase [150]:

$$RH + O_2 + NADPH + H^+ \rightarrow ROH + H_2O + NADP^+ \tag{1.1}$$

Apart from CYP450, other key phase I metabolizing enzymes include flavin-containing monooxygenases (FMO), monoamine oxidases, alcohol dehydrogenases, aldehyde dehydrogenases, aldo-keto reductase, NADPH:quinone reductases, and hydrolytic enzymes [147], [151], [152].

2. If phase I is insufficient for excretion, the transferase enzymes of phase II will initiate the conjugation of the metabolites to endogenous hydrophilic groups [153], [154]. Acetylation, methylation, glucuronidation, and sulfation reactions can take place in this manner, as can the addition of glutathione or amino acids. Phase II metabolism usually results in toxicological inactivation or detoxification. Conjugated metabolites are further subject to specific transport machinery, because their hydrophilicity is increased, which facilitates their extraction. Glutathione S-transferases (GST), and UDP-glucuronosyltransferases (UGT) are mainly involved in phase II. Sulfotransferases (SULT), and N-acetyltransferases also contribute to conjugating metabolization.

3. Phase III marks the end of the xenobiotic metabolism pathways and ensures the transport of substrates across the plasma membrane and out of the cell [155]. This elimination is ensured by the ATP-binding cassette transmembrane transporters (ABC) (e.g. e.g. multidrug resistance-associated protein 2 (MRP2), and P-glycoprotein (P-gp)) [156].

1.2.3.2.2 Pulmonary xenobiotic metabolic clearance

Even though the hepatic xenobiotic metabolism predominantly handles foreign compounds that enter the body, the lungs also possess metabolic clearance capacities that play a part in the disposition of intentionally (e.g. drugs) or unintentionally (e.g. airborne pollutants) inhaled compounds [157]. Gene expression and functional data have shown that the characteristic airway substructures, and within them the various cell types, possess different patterns of xenobiotic metabolizing enzymes and therefore the associated enzymatic activities in the lungs depend on the temporal and spatial disposition of substrates. For instance, as alveolar diffusion is rapid, a significant portion of compounds will permeate towards the systemic circulation without being metabolized [158], while compounds trapped in the nasal epithelium will most likely undergo metabolization as the region reportedly displays four-fold higher rates of NADPH-CYP450 reductase than the liver [159]. Most of the xenobiotic metabolizing activities are associated with Clara cells and AECII. In fact, the bronchial region's main source of CY450 comes from Clara cells. Other significantly active xenobiotic-metabolizing cells include basal cells, ciliated cells, AECI, macrophages, and vascular endothelial cells [160], [161]. Because the lungs only have a small fraction of the drug-metabolizing and efflux transporter activity of the gut and liver [162], [163] and they are known to be far more permeable to macromolecules than any other portal of entry in the body [164], even more than the gastrointestinal tract [165], a number of molecules can be delivered very "cleanly" into

the body through the lungs without yielding an array of metabolites. However, for compounds subject to metabolization, several cytochrome (CYP) isoforms are expressed as well as other biotransformation enzymes such SULT, UGT, GST, esterases, peptidases, cyclo-oxygenases, and FMO [160], [164], [166], [167]. For instance, many of the well-characterized CYP450 are expressed primarily in the liver, however, they appear to be present, at low levels, in extrahepatic tissues [168]: human lungs contain most of the hepatic CYP enzymes that are involved in the metabolism of foreign compounds [169]–[171]. Although pulmonary metabolism widely serves detoxification purposes, it is also reportedly involved in biological activation processes leading to reactive metabolites. Indeed, oxidative CYP-catalyzed reactions in the lungs have been documented to lead to the bioactivation of pro-carcinogens and other organic toxicants. This phenomenon affects the parent molecule's bioavailability, toxicodynamics, toxicokinetics, and clearance profile [172]. Because the biggest metabolic activity share goes to phase I metabolism, it is important to note that oxidative CYP-catalyzed reactions within the lungs have been documented to lead to the bioactivation of pro-carcinogens and other organic toxicants [173]. Biotransformation of inhaled xenobiotics into toxic metabolites has been studied in the context of environmental exposure to air pollutants [174] and occupational exposure to anthropogenic aerosols such as pesticides [175]. For instance, human pulmonary CYP1A1 metabolizes benzo(a)-pyrene (a polycyclic aromatic hydrocarbon formed during incomplete diesel combustion) into an an extremely reactive metabolite capable of covalently binding to cellular nucleophiles (e.g. DNA) leading to mutations and eventually altered cell growth and cancer [173].
Previously described mechanical transport clearance mechanisms limit the time available for the metabolic clearance to take place. Gender, age, genetic (e.g. polymorphism), and environmental (e.g. smoking habits) factors also affect the way xenobiotic metabolic clearance unfolds [176], [177].

1.3 Respiratory systemic crosstalk

Organs are interconnected in the body and communicate via the blood and lymphatic circulatory systems to maintain proper local and systemic homeostasis. Given this multi-organ crosstalk setting, the lungs are being studied in a broader systemic framework, especially in the context of disorders and diseases that involve them and other extrapulmonary organs such as kidneys, the gut, the brain, and the heart [178]–[182]. As toxicity is closely linked to hepatic metabolism, pulmonary and hepatic crosstalks have also been investigated and their interaction has mostly been highlighted in pathological contexts [183]. Li and Kim's teams documented the impact of inhaled pollutants (e.g. black carbon emissions) on the development of liver pathologies by respectively describing the induction of hepatic inflammatory reactions [184], and the oxidative stress, DNA damage, and lipid peroxidation induced in hepatic cells [185]. As the crosstalk is bilateral, data has also revealed a range of pulmonary abnormalities (e.g. dyspnea, hydrothorax) associated with liver diseases [186].

As previously described, toxicity can also arise from secondary metabolites. Guo's study on pregnant rats showed how the hepatic metabolization of pyrrolizidine alkaloids favors the development of fetal abnormalities in the liver and lungs. Indeed, the biotransformation of the alkaloids by the maternal liver generated by-products capable of crossing the placental barrier and inducing hepatic and pulmonary tissue abnormalities in the fetus [187].
Although this interaction has been discovered through pathologies and disorders, the lung-liver crosstalk has recently been considered a therapeutic tool to convey insulin delivery for type 1 and 2 diabetes patients [188].

1.4 The liver

1.4.1 Anatomy and physiology

The human liver is a 1.5 kg gland, located in the abdominal area, divided into a left and right lobe, both separated by the falciform ligament and enveloped by an external thin and fibrous layer called Glisson's capsule. Each lobe consists of numerous hexagonal lobules, which represent the functional units of the liver [189]. These lobules hold parenchymal cells (hepatocytes) and non-parenchymal cells (e.g. endothelial cells, biliary epithelial cells, Kupffer cells and hepatic stellate cells (HSC)). Each functional unit is irrigated by means of a central vein and portal triads, present at each of the lobule's corners, which comprise a bile duct and a branch of the hepatic artery, and the portal vein (Fig 1.9).

The liver is a highly vascularized organ through which flows two liters of blood per minute. This bloodstream circulates through the hepatic artery and the portal vein which respectively supply the liver with oxygen and nutrient-rich blood. Both bloods mix and flow from the portal triads towards the central vein through sinusoidal capillary networks. A multitude of exchanges occur and impact blood composition during this circulation, dividing lobules into 3 zones according to the Rappaport acinus model [191]:

- The periportal zone located near the portal triads where blood is enriched with oxygen, nutrients and carries xenobiotics.
- The transitional zone.
- The pericentral zone where the blood composition contrasts with that found in the periportal area, i.e. it is low in oxygen and nutrients, and carries little xenobiotic compounds.

The oxygen and nutrient gradients from the periportal to the pericentral zone leads to a metabolic zonation of cell activity, therefore creating a diversity of hepatocyte functional status (Fig. 1.10).
Meanwhile, bile flows through bile canaliculi towards the bile duct of the portal triad to aid its evacuation from the liver into the gallbladder [193].

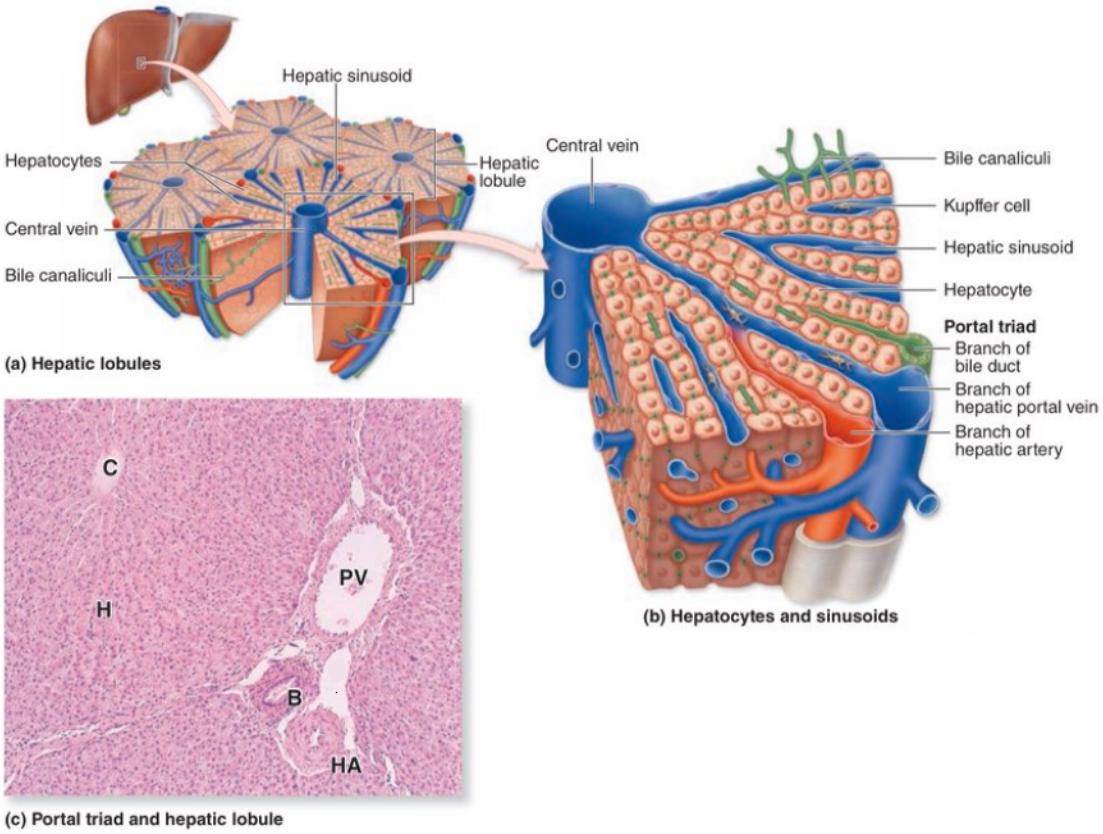

FIGURE 1.9: Diagram showing the liver and its structural hepatic lobule units (a) comprising a central vein and surrounded by portal triads at the corners. (b) Blood vessels of the portal triad travel to the central vein through sinusoids, which run between plates of hepatocytes. (c) Micrograph of a lobule showing the central vein (C), hepatocyte plates (H), and components of the portal triad: a portal vein (PV), a hepatic arteriole (HA) and a bile ductile (B) (x220, hematoxylin and eosin staining). Adapted from [190].

The human liver possesses more than 500 physiological functions revolving around three pillars: biotransformation, storage and synthesis [194]. Given that it receives about 80% of its blood supply from the gastrointestinal tract via the hepatic portal vein, the liver is prone to ensure metabolic and immune functions [195].

To fulfil them, the liver is composed of numerous different cell types. Hepatocytes represent the majority of the liver's cellular composition, comprising 60% of hepatic cells, and deal with hepatic metabolism (e.g. plasmatic protein synthesis, bile secretion or xenobiotic metabolism) [197]. Hepatocytes are hepatic parenchymal cells, central for basic liver function. As the first organ exposed to venous blood from the gut, the liver has developed advanced filtration capacities to process dietary nutrients (e.g. glucose, lipids, iron), and eliminate toxins. Overall, hepatocytes are involved in the secretion of proteins and lipids, the formation of bile, endocytosis-based filtering of blood, and detoxification of xenobiotics. As a result, this translates on a cellular level to the presence of numerous mitochondria (responsible for energy production), and large amounts of endoplasmic

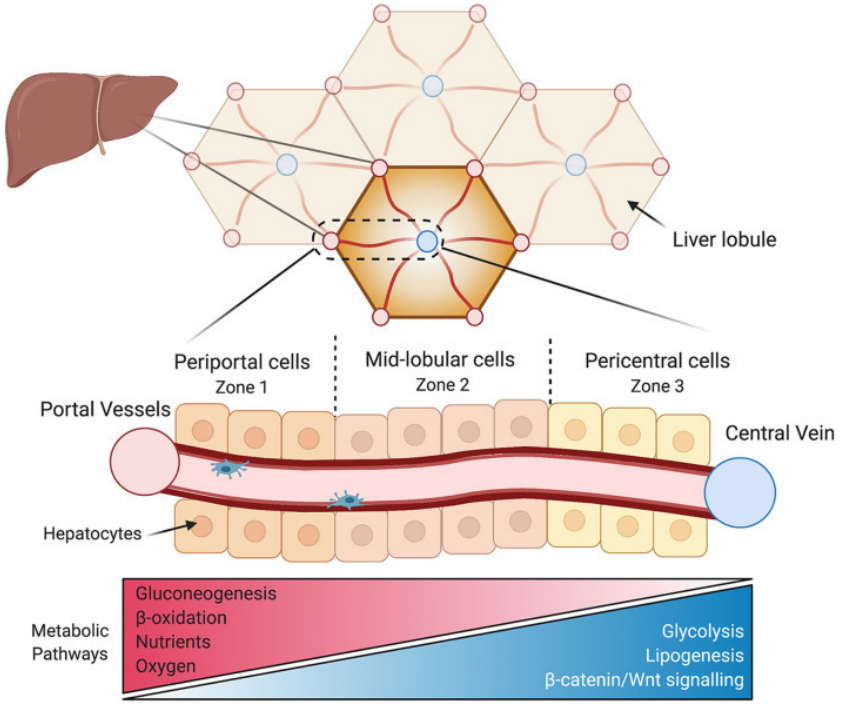

FIGURE 1.10: Hepatic zonation along the periportal-pericentral axis resulting in graded gene expression and the spatial separation of certain metabolic processes to periportal (red) and pericentral (blue) regions. Adapted from [192].

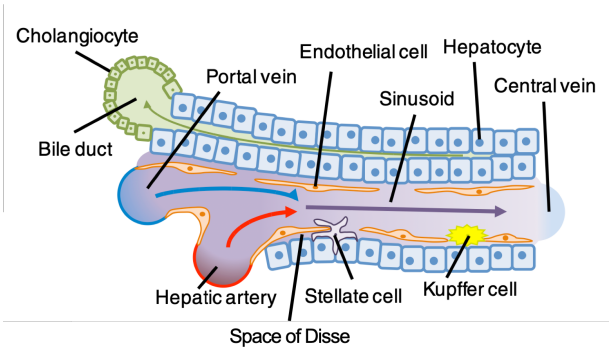

FIGURE 1.11: Diagram of the organization of the different cell types surrounding a hepatic sinusoid. Adapted from [196].

reticulum, where ribosome containing rough endoplasmic reticulum supports protein synthesis activities, whereas the smooth endoplasmic reticulum incorporates biotransformation enzymes.

Hepatocytes synthesize and secrete a variety of key proteins into the bloodstream, including transferrin (iron transporting glycoprotein), plasminogen (anticoagulant), and fibrinogen (coagulant). Among all, serum albumin is the most highly secreted liver-specific protein. Albumin is involved in the maintenance of osmotic pressure [198], features antioxidant properties, as it possesses abundant reduced sulfhydryl groups that scavenge oxygen-free radicals such as nitric oxide [199], and displays interesting binding functions (e.g. bilirubin, calcium) [200] that can influence the bioavailability of circulating

compounds.
Hepatocytes are also implicated in the systemic regulation of glucose and lipids as they carry out the metabolism of carbohydrates (namely glycogenesis, glucogenesis, and glycolysis) and lipids to maintain proper homeostasis. Several forms of regulation exist for these metabolic processes, including substrate concentration, and hormonal levels (e.g. insulin) [201].
From a structural point of view, *in vivo* hepatocytes are organized into plates, called liver plate, which accommodate a polarized cell layer that separates sinusoidal blood from canalicular bile [202]. Hepatocytes possess a unique polarity (canalicular apical, and sinusoidal basolateral membranes) important for bile purposes which aid the removal of xenobiotics and endogenous waste [193]. Following synthesis, bile is carried out across the apical membrane into the bile canaliculi, which empties into the gall bladder before being released into the intestine. Cholangiocytes form the intra- and extrahepatic bile ducts [203].
On the basolateral side, the liver sinusoidal endothelial cells (LSEC) form the wall of hepatic sinusoids through which blood circulates in the liver, and display several functions:

- They form a permeable exchange barrier, thanks to their fenestration (open pores of 100 nm), of solutes between blood and the space of Disse. The space of Disse is a perisinusoidal space, located between hepatocytes and a sinusoid, that contains blood plasma. Hepatocytes microvillis extend into this space, allowing proteins and other plasma components from the sinusoids to be absorbed by the hepatocytes [204].

- They maintain immune homeostasis by mediating immune responses ranging from filtration, endocytosis, antigen presentation to leukocyte recruitment [205].

- They maintain immune homeostasis by mediating immune responses ranging from filtration, endocytosis, antigen presentation to leukocyte recruitment [205].

Kupffer cells are also involved in the hepatic inflammatory response. They are hepatic macrophages residing in the lumen of the hepatic sinusoids. They are found throughout the liver but especially in the periportal zone. They are involved in the maintenance of hepatic homeostasis and the acute and chronic hepatic response to stress, through phagocytosis and immune signaling [206]. Pit cells are another kind of hepatic sinusoidal cell that contribute to the immune response in the liver. They act as natural killer (NK) cells, and are located inside the sinusoidal lumen, where they adhere to endothelial and Kupffer cells [207]. The Disse space also contains HSC, also known as Ito cells. They are versatile mesenchymal cells capable of storing vitamin A droplets, and are key players of liver regeneration upon injury as they have the ability to transdifferentiate into myofibroblasts-like cells and produce collagen extracellular matrix [208].
The liver is involved in the maintenance of essential processes [209] but hepatic zonation imposes a regionalization of functionality according to the lobular region. Oxygen and nutrient supply regulate the metabolic capacity of hepatocytes and thus the diversity of

their activities (Fig. 1.10). The periportal zone concentrates gluconeogenesis, albumin synthesis and ureagenesis, while the pericentral zone favors glycogenesis, glycolysis, lipogenesis, bile production and xenobiotic metabolism [210].

1.4.2 Hepatic detoxification metabolism

Organs communicate through a systemic cardiovascular closed circulatory loop, which allows endogenous and exogenous compounds (e.g. hormones, drugs) to travel through the body and into other organs via the endothelium. Regarding the liver, the hepatic artery supplies 25% of the blood flow, while 75% originates from the portal vein which is perfused by splanchnic blood (25% from the spleen and the pancreas, and 75% from the stomach and the intestines). The liver is the main site of clearance of xenobiotics in the body. The associated metabolism follows the phase I to III ADME phases previously described in 1.2.3.2.1.Briefly, the associated metabolism converts compounds into further hydrophilic derivatives to facilitate their excretion. However, in some cases, metabolic enzymes convert substances into their active or reactive form. Metabolite conjugates are then excreted into the biliary system by efflux pumps (e.g. MRP2) (Fig.1.12).

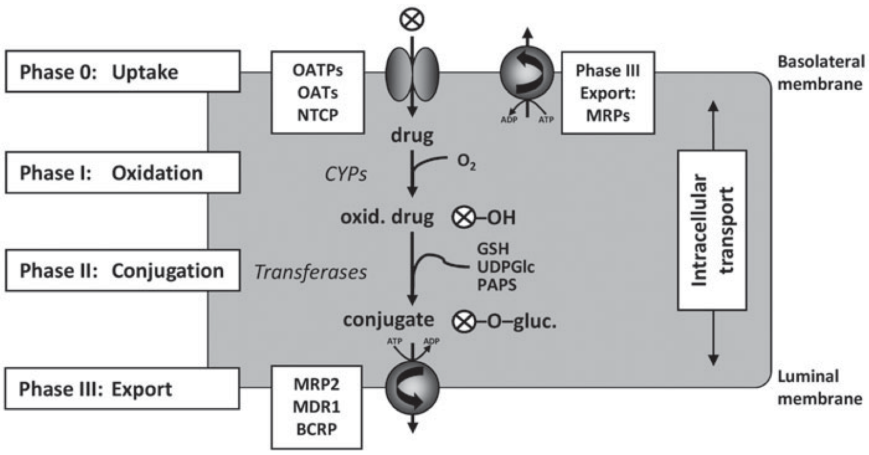

FIGURE 1.12: Sequential steps of drug elimination by metabolism and membrane transport. The diagram depicts the situation in the liver. Phase 0 delivers drugs by carrier-mediated uptake (i.e. organic anion transporters (OATs), organic anion transporting polypeptide (OATP), and Na+-dependent taurocholate cotransporting polypeptide (NTCP)) from the blood into a metabolizing cell. The excretion phase III of metabolite conjugates is achieved by transporter pumps such as MRP2, multidrug-resistance protein 1 (MDR1)/P-gp and breast cancer–resistant protein (BCRP) at the canalicular hepatocyte membrane. If this route is disturbed, efflux pumps at the basolateral blood-facing membrane are inserted by demand – such as MRP3, 4 and 6 – for metabolite elimination. Reproduced with permission from [155].

Hepatic biotransformation can be impacted by lobular microarchitecture [211], blood flow [212], [213], or even enterohepatic circulation [214].

1.4.2.1 Acetaminophen case study

Acetaminophen (APAP), also known as paracetamol, is the most commonly used over-the-counter analgesic worldwide [215]. When taken at the recommended doses, APAP is safe and causes only minimal side effects. However, overdosage results in hepatotoxicity [14]. Acetaminophen-induced liver damage is the most prevalent drug-induced liver injury [216], [217].

The liver is the primary site of the metabolism of APAP. Phase II conjugating enzymes mainly metabolize APAP into non-toxic acetaminophen-sulfate (APAP-SULF) or acetaminophen-glucuronide (APAP-GLU) metabolites, which are effectively eliminated in urine. However, toxic doses of APAP lead to saturation of the sulfate, and glucuronide pathways [218] and therefore the metabolization of APAP is overridden by oxidizing CYP450 enzymes, and more specifically by CYP2E1, CYP1A2, and CYP3A4. The switch towards phase I metabolizing pathways favors the production of a toxic reactive metabolite called N-acetyl-p-benzoquinone imine (NAPQI) [219] which leads to the depletion of the detoxifying glutathione pathway, and the formation of hepatotoxic NAPQI-protein adducts which, in excess, cause mitochondrial oxidative stress [220]. High levels of stress result in the loss of mitochondrial membrane potential, the stop of ATP production, and the initiation of cell death [22].

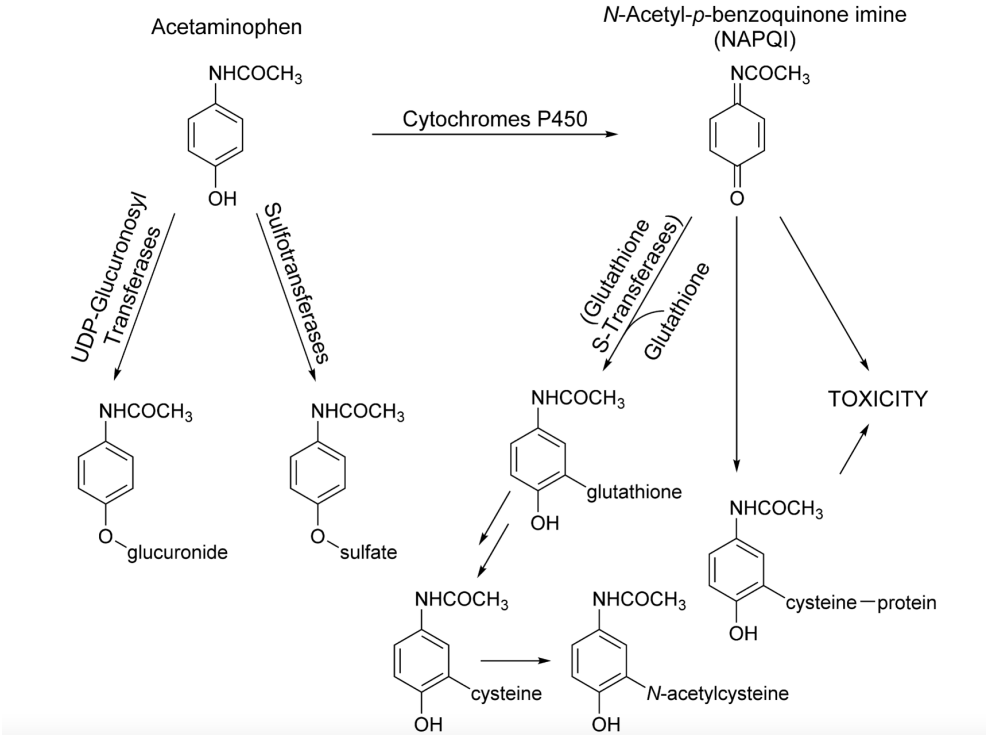

FIGURE 1.13: Major APAP metabolic pathways. Reproduced with permission from [221].

Consequently, as the metabolic pathways associated to the biotransformation of APAP are well understood, it is frequently utilized as a model hepatotoxicant [4], [5], [222].

1.5 Predictive studies for inhalation toxicology

Early inhalation toxicology investigations, up until the 1950s, were primarily concerned with military and industrial hazards relating to foundries, mining activities, and high exposure concentrations [223], [224]. To assess the toxicity of inhalants, the standard endpoint was to study acute and chronic-like exposures [225], associated induced pathologies, and test animal lethality by measuring the lethal concentration 50 (LC50), which corresponds to the exposure concentration that induces lethality of half of the tested animals. Data acquired by these tests were not sufficient to obtain proper extrapolation of toxicological data from animals to humans [226]. Since the 1990s, epidemiological data highlighted the link between low-level PM exposures, associated with urbanism, and mortality and morbidity rates [227]–[231]. Respiratory toxicology research has continuously adapted to the evolution of lifestyle and emerging technologies to improve the predictivity of data to the diversification of airborne hazard sources. Air pollution has become the leading environmental cause of death in the world. Interindividual variability, immune response, and physicochemical properties of inhalants are among the key aspects investigated to empower the accuracy of predictive studies.

1.5.1 *In vivo* models

Epidemiologic studies are often the starting point of public health research. Data obtained from regional outbreaks and real clinical cases are particularly relevant to mapping and understanding the determinants of a disease or a disorder. Associated toxicity mechanisms are complex and involve local and systemic biological responses. Because of this physiological complexity, animals are considered prime study models. Animal models have allowed considerable progress in this field since they maintain the intricacy of living systems and therefore make an assessment of organ–organ crosstalk and nontarget organ toxicity possible [232]. However, the inherent complexity of interconnected tissues makes mechanistic pathway analysis unsure and hardly identifiable, which confuses data [233].

Furthermore, animals have shown to display very different responses to stress compared to their human counterparts. Indeed, animals present basic anatomical, physiological, and biochemical differences that introduce translational gaps [234]. For instance, structural differences exist between human and rodent lungs: the basal cells that allow epithelial regeneration in humans are present only in the trachea of mice [98], and mucus cells are less prevalent in mouse models [235]. Oesch and coworkers also addressed this issue by extensively reviewing the DME found within human lungs and contrasted data from various animal and human studies, emphasizing the need of considering interspecies variations when researching pulmonary drug metabolism [236]. These significant physiological differences perturb the predictivity related to clinical outcomes and explain the frequent failure of clinical trials [237], [238]. In addition to the scientific bias induced by the use of animal models, this kind of experimentation suffers from numerous other limitations such as high costs, labor intensive and time-consuming experiments, and most

importantly ethical concerns as animals are sensitive beings capable of consciously perceiving pain and experiencing suffering.

1.5.2 European research framework: reduction, replacement and refinement (Three Rs) of animal use for scientific purposes

English researchers, William Russel and Rex Burch wrote and published in 1959 the foundation of what is well known to regulate Europe's animal experimentation policies nowadays, the 3Rs. « The Principles of Humane Experimental Techniques » placed animal welfare at the heart of applied sciences and good laboratory practices [239]. Their goals were to establish and outline the best practices for experimental scientists when designing *in vivo* studies while considering any potential replacement, reduction, or refining of animal use [240]. According to the authors, the regulation of the use of animals through the 3R rule would involve a series of considerations:

- « Replacement » intends to evaluate the contribution that animal experimentation would bring to the advancement of a scientific project and therefore if the importance of use of animals is strictly necessary or can be compensated by other means.
- If animal experimentation has been identified as essential to scientific research, « Reduction » is concerned with reducing the amount of animal resources used to the strict minimum.
- « Refinement » focused on avoiding or minimizing at best the suffering caused by animal experimentation.

The 3Rs reinforce the ethical considerations around pain, harm, and suffering caused to animals during experimentation in basic research context but also for higher education or training purposes. In the European Union, transparency and report obligations for this matter are reinforced by the Directive 2010/63/EU amended by Regulation (EU) 2019/1010. Animal accommodation and care guidelines are delivered by the Recommendation 2007/526/EU, and a status report on the evaluation of animal experimentation practices is also to be sent to the European Commission for examination. To facilitate and standardize the delivered reports, the Decision 2020/569/EU has established a common submitting format. Therefore, advanced *in vitro* approaches continue to be developed and establish themselves as promising alternative methods able to coherently emulate human physiology.

1.5.3 *In silico* modeling

In silico methods refer to computer-aided simulations, based on the mathematical modeling of qualitative and quantitative *vivo* and *vitro* data, to predict *in vivo* biological outcomes. They draw their resources from databases and use machine learning techniques, such as active learning, to empower predictions [241]. *In silico* models are controllable,

cost- and time-effective, as they minimize expenses related to conventional trial and error approaches in the laboratory. Although they can store and analyze large amounts of data, the reliability of their predictions depends primarily on the accuracy of the data on which the algorithms are based.
In silico modeling is particularly used in the pharmaceutical industry for drug screening purposes. PBPK (Physiologically Based Pharmacokinetics) and QSAR (Quantitative Structure-Activity Relationship) models are particularly relevant to predicting the ADME phases of a drug. The PBPK model converts the ADME features of organs into mathematical functions and compartmentalizes related biotransformation kinetics to determine a drug's pharmacokinetics profile in plasma and tissues to predict its bioavailability *in vivo* [242]. Whereas the QSAR models are used to predict the physicochemical, and biological behaviors of compounds in a given *vivo* setting based on their chemical structure as the model assumes that compounds with comparable molecular structures have similar biological activities [243]. Both methods can be tuned to exposure conditions (e.g. administration routes, exposure duration, doses) and models (e.g. human, mouse), and are therefore versatile and adaptable [244].

1.5.4 *In vitro* modeling

In vitro cell culture systems enable the growth of cells, derived from living organisms, out of their biological setting and in a miniaturized controlled environment supplemented with a synthetic medium. Depending on the culture mode, native and tissue-specific cellular behaviors such as proliferation and metabolic capacities can be emulated. *In vitro* models are good alternatives to animal models as they are simpler and less expensive to implement, and more importantly, they offer the possibility of working with tissue and cells of human origin, which empowers the accuracy of *in vitro* to *in vivo* extrapolation.

1.5.4.1 Cell sources

A variety of cell types are available for *in vitro* tissue engineering, and the following is a brief description of their characteristics.
Cell lines are characterized by an unlimited life span, which makes them highly proliferative and stable cells. This proliferative feature allows cell lines to be maintained in culture for long periods through consecutive subculturing. They can be pooled from active tumors or based on normal cells and immortalized (e.g. by viral transfection of an oncogene). The cellular degeneration resulting from these genetic changes gives them the main disadvantage of generally losing some or all functionality of the tissue they originate from. Nevertheless, cell lines are abundantly available and are therefore suitable for large-scale studies such as high-throughput toxicity screening.
Primary cells are directly harvested from biopsies of living organs; thus, they maintain better physiological functions than any other cell type used for *vitro* modeling. *Vitro* culture settings are far from physiological *vivo* environments cells originate from, which is

why their lifespan is limited to few subculturing cycles. Their use *in vitro* is frequently associated with dedifferentiation because cells tend to favor proliferation over functionality. Nevertheless, *in vitro* culture techniques are working towards model complexification by offering 3D culture modes that better mimic the physiological context and reduce phenotypical damages. Availability of primary cells is however limited, access to biopsies is restricted, and inter-individual variability in between donors is a bias to factor into robustness aspects of primary cell-based models.
Stem cells are characterized by their self-renewal capacity and their ability to differentiate into any cell type, which is why they appear as a promising alternative to primary cell cultures as they offer unlimited and stable sources of multiple cell types [245].
The choice of cell type will be based on the scientific and technical aspects related to the underlying research topic. Cell lines have proven particularly relevant for high-throughput studies, especially for pharmacological screening. Whereas a more mechanistic approach to study biological responses involved in cell toxicity phenomena would require the use of primary cultures for which native viability and functionality parameters are better preserved [246].

1.5.4.2 Pulmonary models

Tissue engineering has enabled the creation of *in vitro* respiratory tissue models for clinical and fundamental research applications, with a primary focus on the rebuilding of the tracheal and proximal (bronchial tissue) and distal (alveoli) airways.

Two-dimensional (2D) models

2D monocultures can be achieved in culture flasks and plates under submerged conditions. Most commonly used culture surfaces are polystyrene-based. As polystyrene is naturally unfit for cell anchorage, plasma treatments or surface coatings (e.g. collagen or polylysine) can be carried out to enable cell adhesion [247]. To better approximate *vivo* environments, as lungs are constantly and directly exposed to atmospheric air, culture inserts (e.g. permeable polyester membrane) have been developed to lift 2D cultures at the air-liquid interface (ALI) to better approximate a physiological environment. In this setting, the basolateral section is submerged in a culture medium while the apical side of the epithelium is exposed to air. This culture mode has proven to empower the differentiation of respiratory epithelia on a morphological and functional level [248]–[250]. The ALI culture mode also benefits inhalation studies as it allows to expose the epithelia to physiological modes of exposure that include gaseous and aerosolized exposures, representative of inhalation routes (e.g. vacuum chamber, VitroCell® nebulizer) [27]. *In vitro* pulmonary epithelia are widely reconstructed using cancerous cell lines such as A549 and Calu-3. Although they only partially retain phenotypical and functional capacities, they allow for stable, reproducible, easily scalable, and cost-effective modeling. *In vitro* tissue reconstruction can also be achieved using artificially immortalized cell lines, such as BEAS-2B, and $16HBE14^{\circ-}$ that are normal cells immortalized by viral transduction. Recently developed hAELVI cell line displays promising potential to improve the accuracy

of *in vitro* models, as they were immortalized from primary alveolar cells and display *vivo*-like phenotypes and alveolar permeability functions. Details referring to their cellular characteristics are recapitulated in 1.1. This table is meant to outline the key properties of the most commonly used cell types for *in vitro* lung tissue reconstruction.

TABLE 1.1: Brief recapitulate of the distinct characteristics of commonly used human pulmonary cells for *in vitro* modeling [28], [251]–[258]

Cell identity	Cell type	Description
Calu-3	Bronchial epithelial-like	- Derived from a pulmonary adenocarcinoma from submucosal gland serous cells - Fully differentiated ciliated and mucus-producing epithelial layer displaying strong barrier functions (tight junctions, adherent junctions, desmosomes)
BEAS-2B	Bronchial epithelial-like	- Normal cells immortalized using adenovirus 12-SV40 viral transduction - Weak barrier function (lack mucus secretion, tight junctions and cilia) - Secrete cytokines and anti-oxidants
$16HBE14^{\circ-}$	Bronchial epithelial-like	- Normal cells immortalized using adenovirus $SV40^{\circ-}$ viral transduction - Limited barrier function (cilia and tight junctions network only) - Differentiated and multi-layered epithelium - Secrete cytokines
A549	Alveolar type II pneumocytes-like	- Derived from a pulmonary adenocarcinoma - Produce surfactant - Lack tight junction network
NCI-H441	Possess alveolar type II pneumocytes-like and bronchiolar epithelial cell characteristics (i.e. Clara cells)	- Isolated from a pulmonary papillary adenocarcinoma - Form polarized tight monolayers and express organic cation transporters with P-glycoprotein (relevant to pharmaceutical research) - Secrete surfactant - Higher transepithelial electrical resistance values than A549
hAELVI	Alveolar type I pneumocytes-like	- Primary human alveolar epithelial cells immortalized by lentiviral transduction - Strong barrier functions (tight junctions network, high TEER) - Reflects *vivo*-like alveolar permeability

However, cell lines are very homogeneous populations that don't recapitulate the complexity of airway epithelia. For this reason, the use of primary cells in already commercially available tissue models (e.g. MatTek's EpiAirway, Epithelix's MucilAir), or isolated

from partial lung resections, or bronchial brushes, allow for greater *vivo*-like morphological and functional pulmonary representation although they introduce limitations such as donor variability, sourcing limitations and high experimental costs. Primary human bronchial and alveolar cells, along with primary rat alveolar cells are the most commonly used for *in vitro* modeling. The exposure of primary cells to the ALI empowers cellular differentiation into basal, ciliated, and goblet cells resulting in an overall better functionalization of the tissue through the production of mucins, the empowerment of barrier functions through, for example, tight junction networks, and cilia beating motions [259]. Even though 2D models are relevant to studying barrier transport and permeability kinetics [260], cell behavior is altered because environmental cues are different from native tissues [261]. This has led to an increase in the development of more complex three-dimensional (3D) models. 3D human airway models have been proven to improve the toxicity prediction accuracy of inhaled substances [262], [263].
Inhalation toxicology also tends to move towards models that include two or more cell types (co- or multicultural systems), and that can also comprise an extracellular matrix. Whilst the alveolar/bronchial cells are primarily responsible for barrier formation, cocultures [264], [265], tricultures [266], [267], and even tetracultures [268] have been developed to recreate the physiological complexity that occurs during local cellular crosstalk in the lungs, such as inflammatory responses involving pneumocyte and alveolar macrophage interactions. Cocultures are typically seeded and cultured on culture inserts (Fig. 1.14).

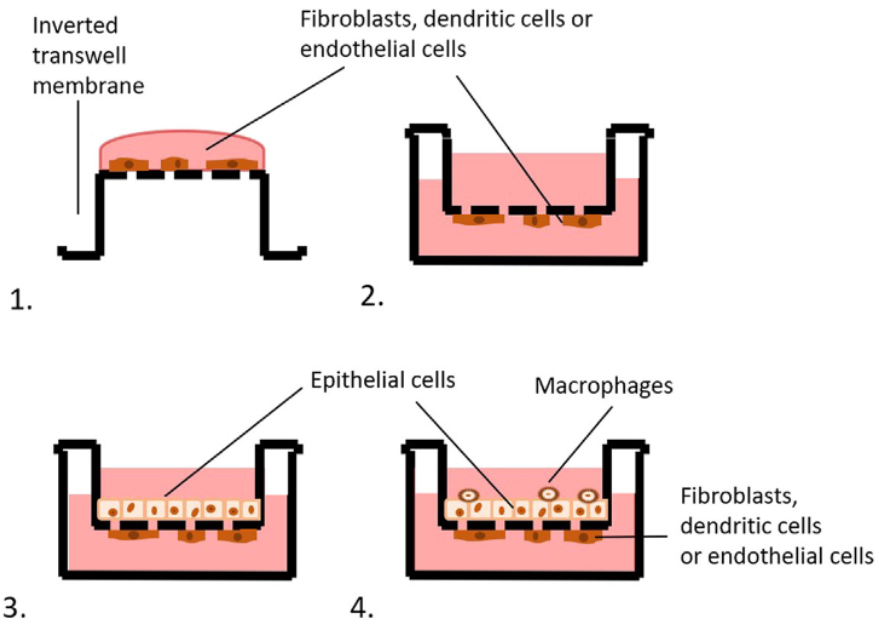

FIGURE 1.14: Diagram showing a method for triple co-culture of cells as a complex *in vitro* permeability model. Fibroblasts, dendritic or endothelial cells adhere to the inverted basolateral side of a culture insert (1, 2), the culture insert is replaced into the receiver well so that epithelial cells may be cultured on the apical side (3), and macrophages may also be added to apical side of the culture insert. Reproduced with permission from [158].

Spheroids and organoids

3D multicellular models, such as spheroids and organoids, serve as biomimetic platforms for investigating intracellular communications, cell-extra cellular matrix (ECM) interactions, and overall organ development as they further approach *in vivo*-like environments (Fig. 1.15). Spheroids self-assembled cell clusters, established from cell lines or patient-derived cells [269]. They are constituted of an internal necrotic core that develops from a lack of nutrients and oxygen along with a waste buildup, and outer layers made of active and proliferating cells [270]. Even though spheroids are not architecturally relevant as barrier models, their culture offers interesting prospects to expand *in vitro* pulmonary functionalities, Takahashi et al. [271] demonstrated how AEC2 spheroids revealed the expression of alveolar specific protein (SP-C) which until then had not been expressed in other *in vitro* alveolar models, and offer new prospects to *in vitro* tumor modeling [272]. Organoids are also capable of self-assembly and can be produced from both stem cells and patient-derived cells. They comprise multiple cell types, can self-renew, and display sufficient differentiation to mimic some level of functionality of the native target organ [273]. They present themselves as powerful disease modeling tools for personalized medicine as patient-derived diseased cells have been revealed to self-assemble into organoids that replicated the associated genetic disorders and phenotypes [274]. Basal, secretory, and type II alveolar cells are the key pulmonary cell types that have been used to engineer lung organoids. They can replicate some aspects of the intricate pulmonary architecture, especially that of the alveolar sac in the distal area, and the associated functional heterogeneity.

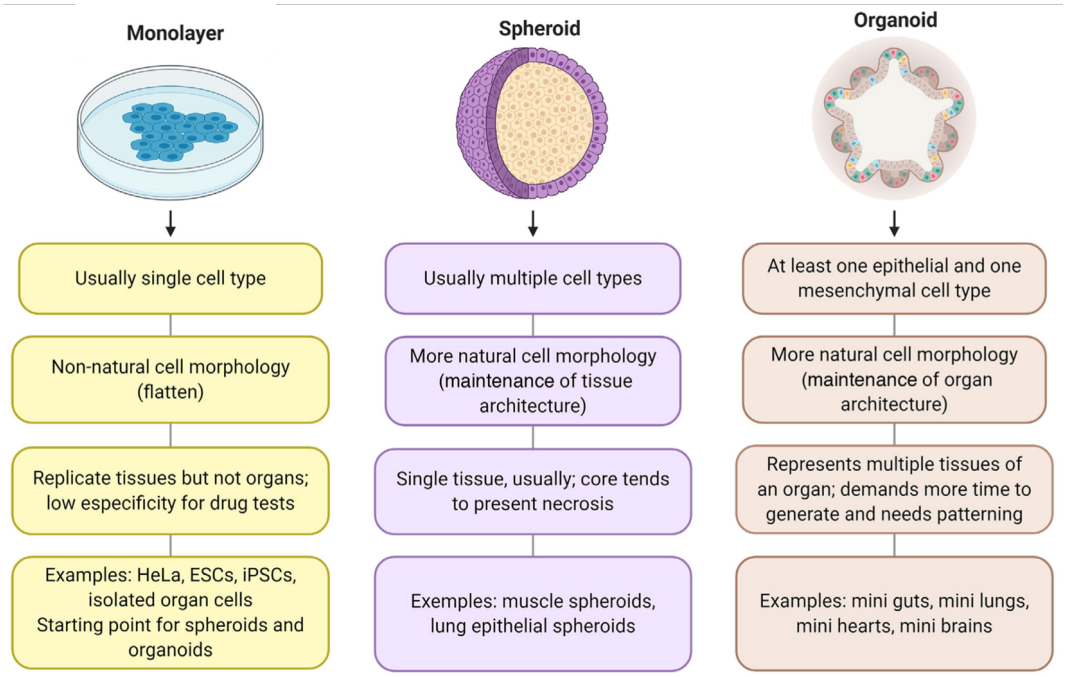

FIGURE 1.15: Main characteristics of 2D monolayered cell culture, and 3D spheroid and organoid cultures. Adapted from [275].

Decellularized ECM and biomaterial-based scaffolds

Scaffolds are great structural tools to guide *in vitro* tissue reconstruction. Decellularized lungs offer a unique native-like scaffold that, combined with specialized bioreactors, recapitulates vascularization, and ventilation processes [276]. Whole or resected lungs are treated with detergent-based protocols to strip the cellular components out of the tissues while maintaining the extracellular matrix and 3D microarchitectures of the airways and vascular channels as intact as possible (Fig. 1.16) [277], [278]. Decellularized scaffolds have proven particularly relevant to guiding the physiological differentiation of embryonic stem cell derived-embryoid bodies into AEC2, AEC1 and Club cell like-cells [279].

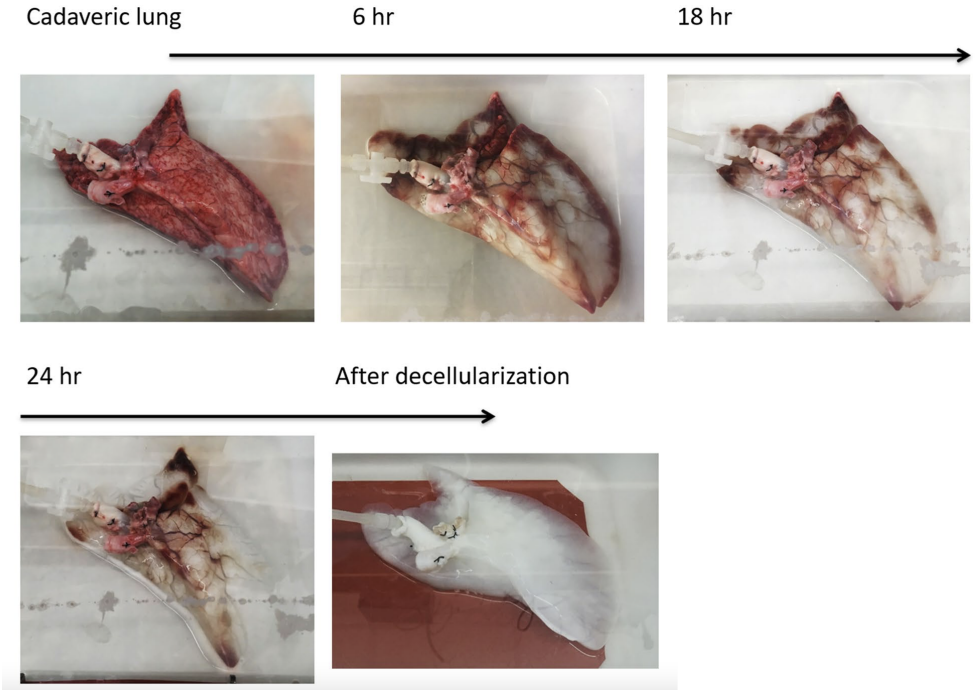

FIGURE 1.16: Pictures recapitulating the decellularization process of a porcine lung resulting in the loss of opacity caused by the evacuation of cellular material [276].

Because human decellularized ECM is difficult to come by, natural collagen and gelatin, as well as synthetic poly(ϵ-caprolactone) (PCL), are employed to create scaffolds [280], [281]. Hybrid scaffolds can also be useful for tissue reconstruction, they are created by combining natural and synthetic biomaterials.

Scaffolds can then be electrospun or 3D bioprinted into patterns of interest [282].

Electrospinning consists of a jet-like extrusion, conducted by an electrostatic force, collected onto a charged collector forming a network of continuous polymer fibers [283]. This technique allows for a high degree of control over fiber diameter, alignment, and porosity of the generated scaffold. Several reports have demonstrated the potential of electrospun meshes for the development of lung biomimetic platforms, showing suitability for mono- or coculture settings [284], [285].

3D bioprinting is an additive manufacturing technique that involves a printing system able to precisely deposit biological material such as cells and biocompatible matrices into

complex and functional 3D architectures to reconstruct living tissues and organs. Bioprinting offers controlled deposition of biomaterial and the ability to build precise 3D reconstructs layer-by-layer. Depending on the physicochemical properties of the bioink, the extrusion can be adapted to three extrusion techniques: laser, inkjet, or microextrusion-based bioprinting, respectively from the finest to the largest deposition [286]. This technique has been successfully used for healthy [287], and pathological lung modeling [288].

Lung-on-a-chip

Organ-on-chip technology is being increasingly harnessed to model pulmonary tissue engineered constructs. Interest is growing as these sophisticated microstructured devices enable dynamically-stimulated cell culture environments thanks to continuous perfusion of microfluidic flow. Huh et al. described the first lung-on-chip in 2010 [289]. They created their chip using a lithography-based manufacturing process, with central upper and lower channels separated by a flexible and microporous membrane, and surrounded by two vacuum chambers. The upper channel was used to cultivate alveolar cells at the ALI, while the bottom channel was used to culture endothelial cells under continuous microfluidic perfusion (Fig. 1.17). The vacuum chambers created cyclic deformations of the tissues that resembled *in vivo* breathing patterns, allowing to reproduce *in vitro* alveolar dilation.

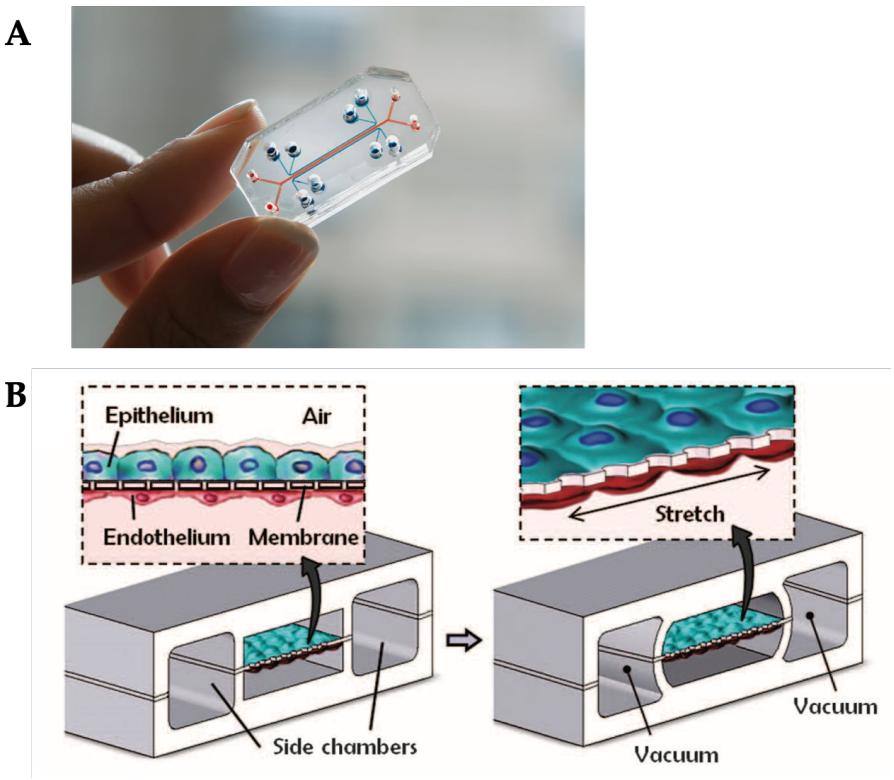

FIGURE 1.17: (A) Human breathing lung-on-a-chip polydimethylsiloxane (PDMS) microdevice. (Wyss Institute) (B) Scheme of the compartmentalized cell culture inside the chip, stimulated the mechanical stretching of physiological-like breathing movements [289].

Since, lung-on-chips have been adapted to different architectures and designs (e.g. hexagonal mesh culture membrane, additional channels, fluidic coupling to culture chamber bioreactors), and variations of pulmonary cocultures (e.g. pulmonary fibroblasts to consider tissue remodeling properties) [290], [291]. They even have been integrated into broader systemic platforms that integrate other tissue constructs, to recreate multiorgan microengineered platforms that consider inter-organ crosstalks [292].

1.5.4.3 Hepatic models

Before any kind of sophisticated *in vitro* modeling techniques, liver tissue slices were used for toxicity testing as they could, to some extent, retain native functionality features [293], [294], for up to 3 days [295]. Nevertheless, tissue functions decrease overall rapidly and necrosis is unavoidable, making the use of tissue slices a non-viable option, in addition to the fact that their also subject to inter-individual variation.
Many of the *vitro* models currently developed still use cell lines as they are well-characterized, robust, and highly proliferating cells that require lower handling costs than primary human hepatocyte (PHH) or stem cell cultures. HepaRG and HepG2 are the most commonly used.
HepaRG is a bipotent human progenitor cell line, isolated from a hepatocholangiocarcinoma, able to differentiate into hepatocyte-like and cholangiocyte-like cells. Many hepatic activities, such as CYP450 and phase II enzymes, are retained in hepatocyte-like cells, making them especially useful to toxicity and drug screening studies [296]. Because of their high proliferative capacity, partially preserved xenobiotic activities, and ability to provide repeatable data, they constitute valuable alternatives to PHH [297].
HepG2 cell line, is derived from a human hepatocellular carcinoma, and is most commonly used in hepatotoxicity pathway analysis studies [298]. Cells display an epithelial-like morphology and fulfill a variety of differentiated hepatic functions (e.g. glycogenesis, plasma proteins secretion) [296]. However, expression levels of phase I and II enzymes and uptake transporters are shown to be lower than in human hepatocytes, and rates also seem to differ between passages [299]. Even though they are not representative of PHH, they are a well characterized cell line, with abundant available data, and the low basal activity of CYP450 (especially CYP1A2, CYP2B6, and CYP3A4) make them good candidates in studies of CYP inducers [300]. Therefore, primary cells are still considered to be the most relevant for *in vitro* modeling as they retain native metabolic functions [301]. They are particularly relevant for fundamental research purposes, such as better understanding hepatic mechanistic regulation processes. However, the maintenance of viability and functionality is delicate, and tends to fade rapidly as they are extremely sensitive to the cell culture conditions. Added to the fact that they are difficult to source and costly to handle, primary hepatic cells present significant limitations to their use for *in vitro* modeling [302].
However, in recent years the use of stem cells has helped to overcome these limitations. The most highly explored stem cells for hepatic cells differentiation are induced pluripotent stem cells (iPSCs) [303]. Differentiation protocols vary depending on the targeted cell

type. Hepatocyte-like cells derived from iPSCs exhibit little batch variability and native-like metabolic functions, most interestingly xenobiotic-related functions. The limitations related to the use of these kind of cells lay in the terminal differentiation of the differentiated cells, and the high cost, time-consuming, and delicate handling of experimentations.

2D models

Standard static 2D monolayer culture systems are traditionally directly plated on a culture treated Petri dish to form a tissue. Although these models are easy, reproducible and cost-effective to manipulate, they lack the architectural complexity of *in vivo* tissues, and culture conditions only allow the maintenance of proper phenotypes for short periods of time before morphological alterations leading to loss of hepatic-like functions occur [304].

Sandwich culture

This culture method recreates the natural linear alignment of hepatocytes *in vivo*, i.e. the sandwich culture configuration involves growing cells between two layers of ECM (e.g. collagen or Matrigel^{TM}). The composition of the ECM is primordial as it influences cellular behavior [305], as Moghe et al. documented how collagen sandwich promoted further polarized differentiation of hepatocytes compared to Matrigel^{TM} sandwich configuration [306]. Sandwich hepatic cultures are particularly interesting for hepatotoxicity and hepatobiliary transport studies. Cell-cell contacts and cell-matrix interactions are facilitated by this configuration, as cells can attach three-dimensionally. These biological behaviors promote the responsiveness of cultured hepatic tissues to stress [307], along with hepatic-specific metabolic functions [308]. However, sandwich cultures can usually only be sustained for short periods as liver-specific functions are unstable and decrease over time [309]. Therefore, long-term hepatotoxicity assessments are not suited to these kinds of models.

Still, the sandwich culture has been of particular interest to recreate naturally-occurring *in vivo* spacing, such as the space of Disse [310].

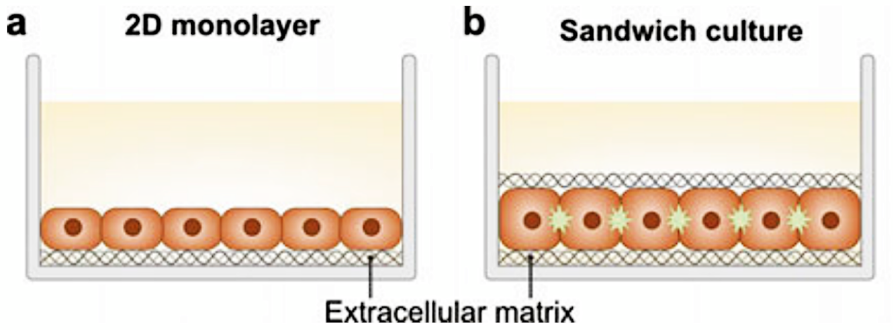

FIGURE 1.18: Diagram of hepatic culture configurations. (a) Conventional 2D monolayer. (b) Sandwich culture method. [311].

Spheroids

Spheroid offer a scaffold-free approach to 3D culture. They can be obtained by different

means (Fig. 1.19):

- The hanging drop method: a drop of hepatic cell suspension is placed on the bottom of a Petri dish lid, where gravity causes the cells to aggregate and self-assemble into spheroids [312].
- Non-adhesive agglomeration: when cells are seeded onto low-attachment culture plates, they spontaneously self-assemble [313].

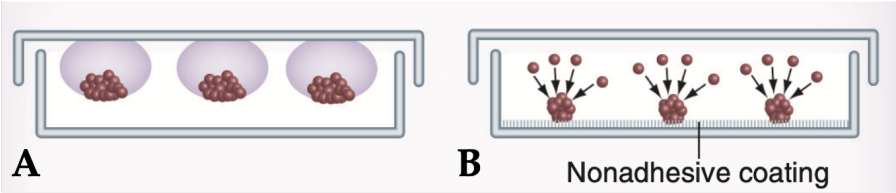

FIGURE 1.19: Diagram of 3D spheroids generated by hanging drop method (A) or by cell culture on non-adhesive surfaces (B). Adapted from [314].

Because their organization is based on random self-assembly, they do not relevantly recreate *vivo*-like structures, however, spheroid culture promotes increases viability, as long as the diameter does not exceed 200 μm (particularly for PHH), and retains proper xenobiotic phase I and II enzymes for several weeks [313]. Their functions can be increased if they are paired to dynamic culture conditions (bioreactors) as nutrient and oxygen are constantly being resupplied [315].

Liver-on-a-chip

Because hemodynamics and other fluid shear stress are biomechanical constraints inherent to the liver [316], [317], perfusion systems known as bioreactors have been developed to better approach physiological hepatic microenvironments, such as zonation [318]. The dynamic culture conditions emulated by native-like mechanical cues have proven to elongate the survival, and empower the functionality of hepatic cells. Specificities relating to biochips have been previously described in 1.5.4.2.

The choice of material and design of a biochip are key parameters that allow to modulate culture conditions to support different types of modeling (e.g. sandwich culture, spheroids). PDMS-based chips have proven to be of particular interest for hepatocyte *vitro* culture as they offer transparency, oxygen-permeability, and biocompatibility features [6]. However, other materials have been used, and thermoplastics offer interesting scalable and low-cost alternatives [319]. According to the material, biochip microfabrication can be achieved through different methods such as photolithography, hot embossing or 3D printing [320], [321].

Liver-on-chips can accommodate different type kinds of *vitro* modeling:

- Monolayered cultures can be used for monoculture or coculture purposes. Hepatic cocultures often involve hepatocytes in conjunction with non-parenchymal cells

(e.g. circulating Kupffer cells). Sandwich cell cultures can assist in tissue reconstruction inside biochips. For instance, primary hepatocyte culture was aided by a sandwich method, and paired with a compartmentalization of the biochip, via the addition of a porous membrane, to recapitulate the indirect sheer stress that hepatocytes undergo *in vivo* (Fig. 1.20) [322].

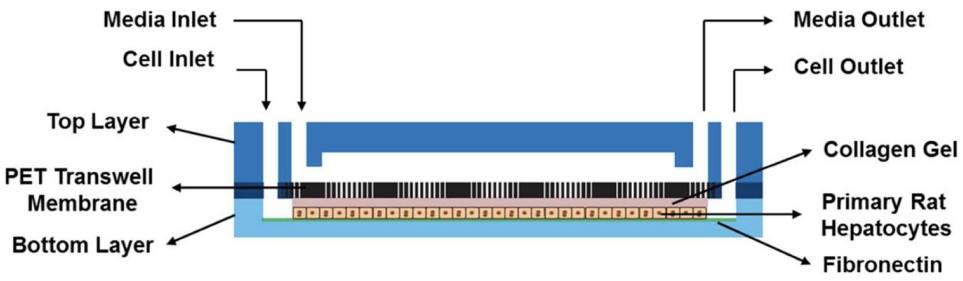

FIGURE 1.20: Cross-sectional diagram of a sandwich cultured hepatocyte monoculture [322].

- Spheroids-on-a-chip can be achieved by playing with the microarchitecture of the inner cell cultivating surface to control organotypic cell assembly [323]. For instance, a succession of concave microchambers were designed to favor cell aggregations into spheroids in the a dynamically perfused hepatic biochip [324]. Or by patterning cell deposition and adjusting a directional medium flow, that mimics portal to central vein blood flow, to create spheroids that served as building blocks to shape lobule-like constructs [325].

- Scaffolds can be embedded into biochips to provide *vivo*-like mechanical, biochemical, and structural environments of healthy or diseased *vivo* liver. For instance, an alginate-based cryogel allowed to reproduce the elastic properties of a cirrhotic tissue [326]. Decellularized liver matrix or gelatin metharcyloyl (GelMA) are other commonly used scaffolds.

Overall, the versatility of tissue reconstruction that can be carried out in biochips empowers the differentiation and functionality of liver-on-chip models which makes them promising *vitro* alternatives to investigate *vivo*-like biological behaviors.

1.6 Objectives and approach of the thesis: The Lung/Liver coculture platform

The respiratory system is exposed daily to a wide range of airborne xenobiotics. Toxicity mechanisms are complex and involve local and systemic responses that can aggravate, stabilize, or protect our bodies from adverse effects. Because of this complexity, animals are considered prime study models. However, in the European context of animal experimentation reduction (3Rs), we developed and investigated a new alternative method to emulate *in vitro* dynamic interactions between the lungs and the liver. In the context of respiratory toxicity, *in vitro* cocultures have contributed value to studies by increasing biological complexity and therefore better mimicking *in vivo* environments [327]–[330]. Since our multi-organ platform is intended for toxicological research, we included a liver construct because of how closely toxicity in the body is tied to hepatic xenobiotic metabolism. In addition, and according to literature, both organs reportedly also interact under stress (1.3). This approach allows to consider pulmonary and hepatic inter-organ crosstalks as possible modulators of toxicity and therefore acknowledge toxicity at a more systemic level when it comes to evaluating associated risks and hazards of inhaled xenobiotics.
As the coculture platform is currently in the development phase, experimental robustness is at the heart of the project. The main goal of this thesis was to use a model substance to highlight the passage and circulation of a xenobiotic through the device and to show the relevance of both compartments to respond simultaneously to xenobiotic stress. The project was therefore articulated into three experimental phases:

1. Characterization of tissue-specific toxicological behaviors of lung and liver constructs through monoculture settings. Viability, functionality and metabolic activities of both compartments were separately assessed following exposure to the model substance.

2. An adaptation and preparation both monocultures to coculture settings was conducted prior to coculture (e.g. common media, characterization of dynamic culture conditions) in order to best preserve optimal viability and functionality.

3. Pulmonary and hepatic culture compartments were united and jointly cultured into a single closed circuited coculture platform. The coculture was exposed, through the pulmonary to mimic in an inhalation-like exposure mode, to the model substance. Assessment of tissue viability and functionality parameters were used to highlight any associated crosstalk behaviors compared to monoculture settings.

Chapter 2

Material and methods

2.1 Cell sources

2.1.1 Bronchial cells

Calu-3 are human bronchial epithelial cells isolated from a lung adenocarcinoma: This cell line was obtained from the American Type Culture Collection (ATCC) (reference ATCC-HTB-55).

2.1.2 Hepatic cells

HepG2/C3A is a clonal derivative of HepG2 human hepatocypte cell line isolated from a hepatocellular carcinoma. This cell line was obtained from the ATCC (reference CRL-10741).

2.2 Pulmonary monoculture

2.2.1 Culture media

Cryopreserved Calu-3 cells were grown and expanded using Roswell Park Memorial Institute 1640 supplemented with stable L-Glutamine (RPMI 1640 GlutaMAX Supplement, ThermoFischer Scientific), and completed with 10% of Fetal Bovine Serum (FBS, Gibco) and 1% of 100 units/mL Penicillin-Streptomycin (PAN Biotech).

2.2.2 Cell culture

Calu-3 cells were expanded in two-dimensional (2D) monolayers in 75 cm^2 flasks (Corning, Falcon) seeded at an initial density of 20 000 cells per cm^2, in a 5% CO_2 supplied incubator at 37°C, reaching 70 to 80% confluence in 7 days. Cells were cultured from passage 32 through 40.

2.2.3 Tissue reconstruction

Calu-3 2D monolayers were amplified up to 80% of confluence. Calu-3 cells were then detached using 0.25% Trypsin-EDTA (1X) (Gibco) and seeded, at 200.10^3 cells per insert,

onto Transwell polystyrene membrane culture inserts (Transwell Permeable Supports, Costar). To complete proper barrier reconstruction, tissues were grown under submerged conditions for 11 days. Late differentiation stages were complexified in "semi" air-liquid interfaced (semi-ALI) conditions where tissues were subject to 24-hour air-lifted culture at day 10. Medium changes occurred every 2 days (Fig. 2.1).

2.2.4 Experimental setup

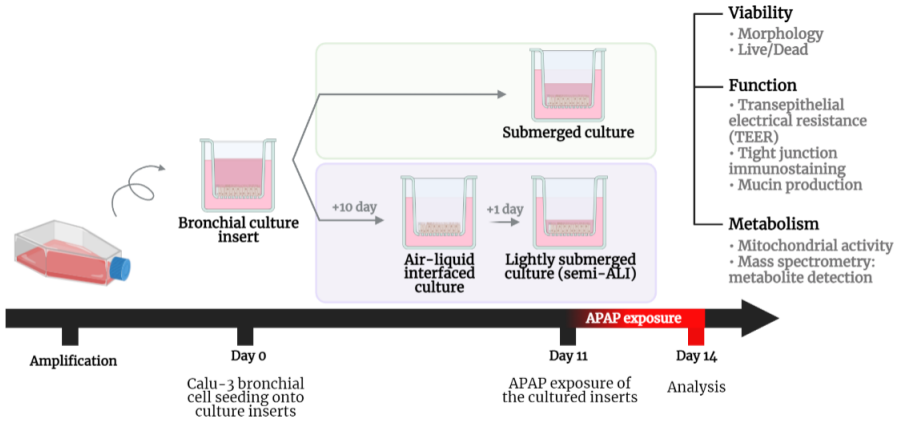

FIGURE 2.1: Experimental design of bronchial tissue reconstruction according to culture conditions.

As soon as the bronchial barrier completes reconstruction (when trans-epithelial resistance (TEER) measurements exceed 1000 $\Omega.cm^2$), 72-hour exposure to solubilized APAP was carried out. Submerged tissues received 1 mL of solution apically and semi-ALI tissues received 200 µL (Fig. 2.1). Following exposure, a variety of biochemical assays (protocols will be later described) were performed to assess associated biological behavior.

2.3 Hepatic monoculture: liver-on-a-chip

2.3.1 Biochip design and microfabrication

The inner microarchitecture of biochips is digitally conceived and printed by photolithography onto wafer containing SU-8 photoresist. The final design comprises two sides, a hollow media reservoir for the upper compartment and a series of microstructured chambers and channels for the bottom cell cultivating side (Fig. 2.2). 10:1 (w/w) polydimethylsiloxane (PDMS) and cross-linking agent (Sylgard 184, Dow Corning) mixture was used to manufacture biochips. The mix was poured onto the microdesigned molds and cured for 2 hours at 70°C. Both sides were sealed together through reactive air plasma treatment of their surfaces to achieve the completed biochip. The final assembled biochip holds a total volume of 40 µL and covers a cell growth area of $2cm^2$. This design has been documented in a previous study [7].

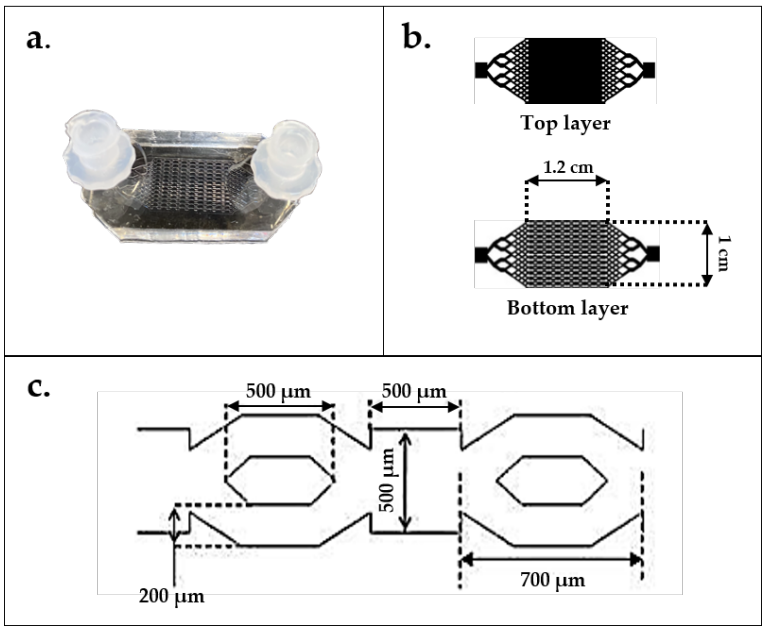

FIGURE 2.2: Sketch and photos of the PDMS microsystem (**a**) comprising an upper smooth side and a bottom microstructured compartment (**b**) made of a succession of channels and chambers (**c**).

2.3.2 Culture media

Cryopreserved HepG2/C3A cells were grown and expanded using Minimum Essential Medium (MEM, Corning) supplemented with 10% of Fetal Bovine Serum (FBS, Gibco), 1% of Penicillin-Streptomycin (10 000 U/mL Penicillin and 10 mg/mL Streptomycin) (PAN Biotech), 1% of L-Glutamine (100X) (PAN Biotech), 1% of N-2-hydroxyethylpiperazine-N-2-ethane sulfonic acid (HEPES) buffer (1M) (Gibco), 1% of Sodium Pyruvate (100X) (Gibco) and 1% of MEM non-essential amino acids (BioWest).

2.3.3 2D culture

HepG2/C3A cells were amplified in two-dimensional (2D) monolayers in 75 cm^2 flasks (Corning, Falcon), seeded at an initial density of 20 000 cells per cm^2, in a 5% CO_2 supplied incubator at 37°C, reaching up to 90% of confluence in 7 days. Cells were cultured from passage 6 through 15.

2.3.4 3D culture

Hepatic tissue reconstruction takes place in previously described biochips which provide a dynamically stimulated environment. All cell culture material was sterilized prior to experimentation thanks to an autoclave cycle peeking at 120°C for 20 minutes. Prior to cell culture, biochips had to firstly be coated with a 0.36 mg/ml Collagen I (Corning Life Science) solution to allow cell adhesion. This solution was prepared in Phosphate Buffer Saline (PBS, Gibco) (1X, pH 7.4). Coated biochips are then kept at rest for 1 hour in a 5% CO_2 incubator at 37°C before being rinsed with culture media. Amplified

HepG2/C3A cells were detached using 0.25% Trypsin-EDTA (1X) (Gibco) and seeded into culture ready-biochips at an initial density of 500.10^3 cells per biochip. Seeded microsystems are then kept at rest 24 hours, in a 5% CO_2 incubator at 37°C, to complete cell adhesion. Hepatic biochips were then boxed into an Integrated Dynamic Cell Culture in Microsystems (IDCCM) device to proceed to tissue reconstruction (Fig. 2.3). IDCCM box was a polycarbonate-based culture platform accommodating up to 12 parallelized microchips. It is composed of a bottom part, comprising attachments for biochips and associated media reservoirs, and a top part for tubing. Both parts are joined and sealed together by a silicon seal and a metal clamping system. Once mounted, the device is set at a continuous microfluidic flow rate of 25 µL per min, through and out of the microchannels, thanks to a peristaltic pump. This specific culture device was developed in UTC's Biomechanics and Bioengineering (BMBI) Laboratory and patented in 2011 [331].

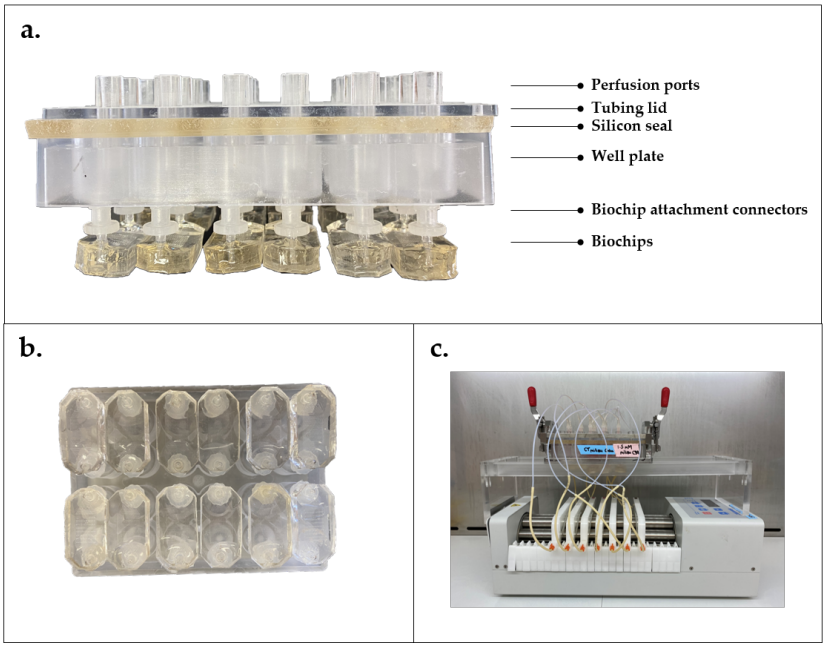

FIGURE 2.3: IDCCM box. Side (a) and bottom (b) photo of the device enabling parallelized dynamic monoculture of hepatic biochips. (c) Mounted culture-ready device. Based on [332].

2.3.5 Experimental setup

Biochips are coated and seeded at day 0. Boxed and dynamically cultured from day 1 to 4, during which 72-hour exposures to solubilized APAP were carried out (Fig. 2.4). APAP solution was prepared in hepatic culture media. Chosen exposure concentrations rely on documented hepatotoxicity thresholds: 1.5 mM and 3 mM [4]. A variety of biochemical assays (protocols will be later described) were performed post-exposure to assess associated biological behavior.

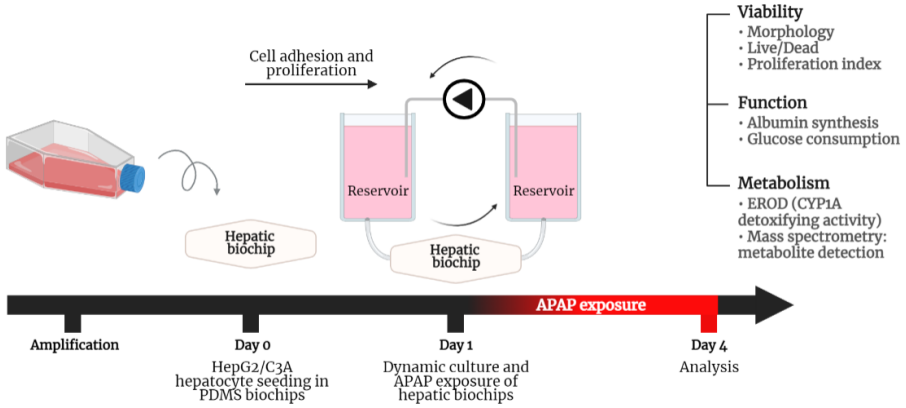

FIGURE 2.4: Experimental design of hepatic tissue reconstruction.

2.4 Lung/Liver coculture: the Lung/Liver (LuLi) platform

2.4.1 Coculture platform: Integrated Insert in a Dynamic Microfluidic Platform (IIDMP)

Both compartments were serially connected (Fig. 2.5) using the Integrated Insert in Dynamic Microfluidic Platform (IIDMP) device. This coculture platform is a polycarbonate-based box able to accommodate 3 parallelized cocultures. It is composed of a bottom part, comprising wells for 6-plate sized Transwell culture inserts, attachments for biochips and associated media reservoirs, and a top part for tubing (Fig. 2.6). Both parts are joined and sealed together by a silicon seal and screws. Once mounted (Fig. 2.7), the device is set at a continuous microfluidic flow rate of 25 µL per min, thanks to a peristaltic pump. Flow was directed from the insert to the biochip in a closed loop. In this study, dynamic cocultures were maintained for 72 hours, in a 5% CO_2 incubator at 37°C. Two IIDMPs were used per experiment, accommodating a total of 6 parallelized coculture circuits. This specific culture device was developed in UTC's Biomechanics and Bioengineering (BMBI) Laboratory in 2014 [333].

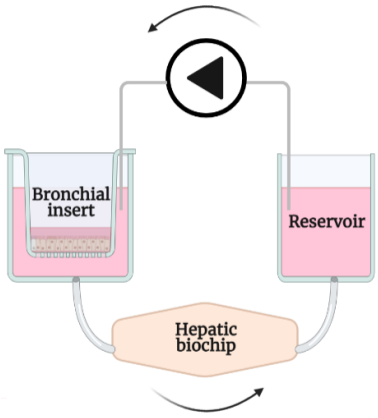

FIGURE 2.5: Schematic close-up of a functional unit of the IIDMP box.

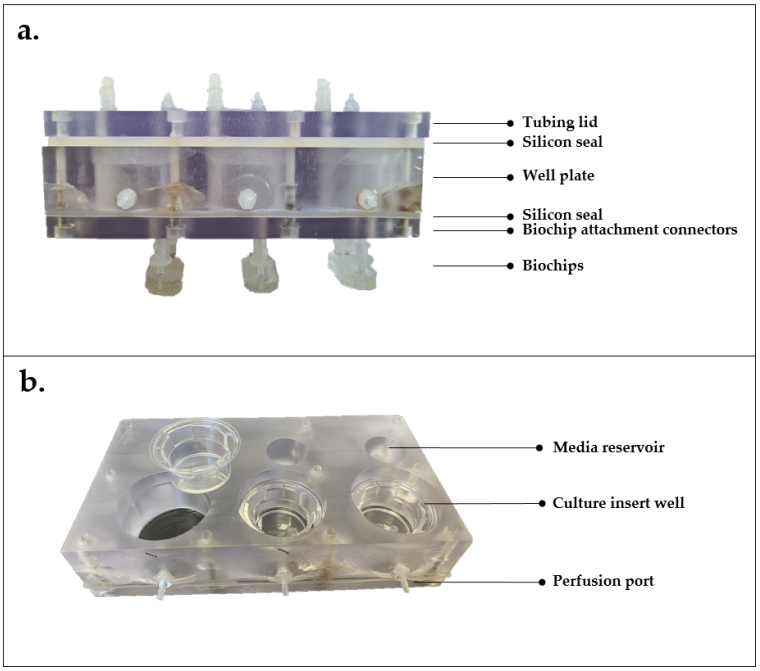

FIGURE 2.6: Photos of the global structure of the IIDMP box.

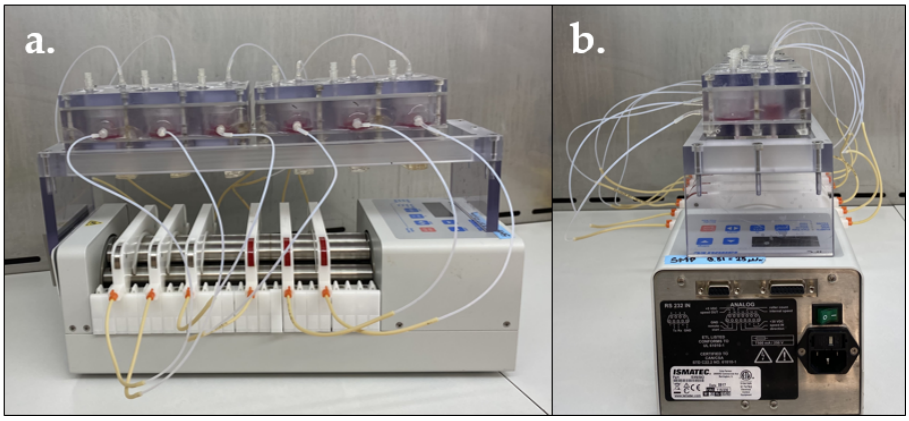

FIGURE 2.7: Side photos of two mounted culture-ready IIDMP boxes on a peristaltic pump.

2.4.2 Bronchial and hepatic coculture

2.4.2.1 Coculture media

Subject of a later study detailed in Chapter 4.

2.4.2.2 Experimental setup

Pulmonary inserts and hepatic biochips were matured separately, respectively up to day 11 and 1, according to previously described protocols. In the same way as monocultures, lung/liver cocultures were carried out in 2 modes: submerged and semi-ALI. These culture conditions concern the pulmonary compartments which received respectively 2 mL

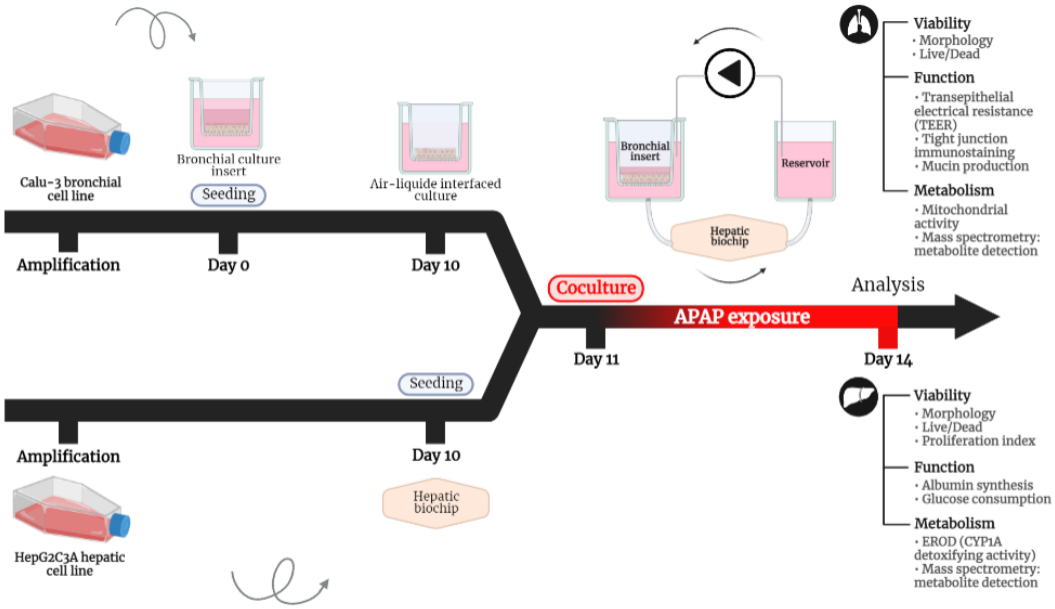

FIGURE 2.8: Experimental design of pulmonary and hepatic coculture.

and 200 µL of media or solubilized APAP solution apically. A variety of biochemical assays (protocols will be later described) were performed post-culture to assess associated biological behavior.

2.4.2.3 The developmental model

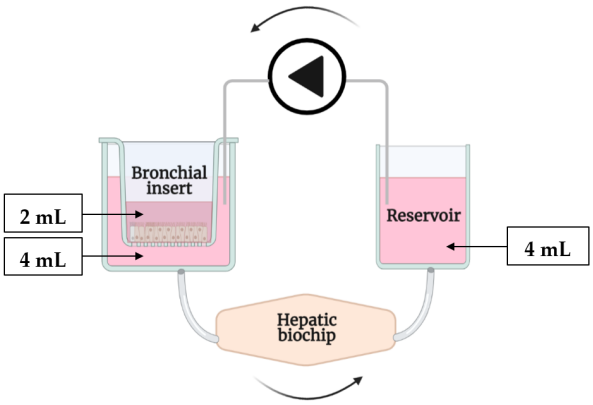

FIGURE 2.9: Schematic representation of the associated volumes of the developmental model functional coculture unit.

The submerged coculture condition was our developmental model. The full circuit encloses a total volume of 10 mL (Fig. 2.9). APAP exposure solutions were deposited on the pulmonary barrier at concentrations recalled as local exposure concentrations, which were imposed at 7.5 mM and 15 mM. When APAP passes the barrier to join dynamic circulation within the device, it is further diluted into the circulating media hence decreasing the recalled systemic exposure concentrations to respectively 1.5 mM and 3 mM (Fig. 2.10).

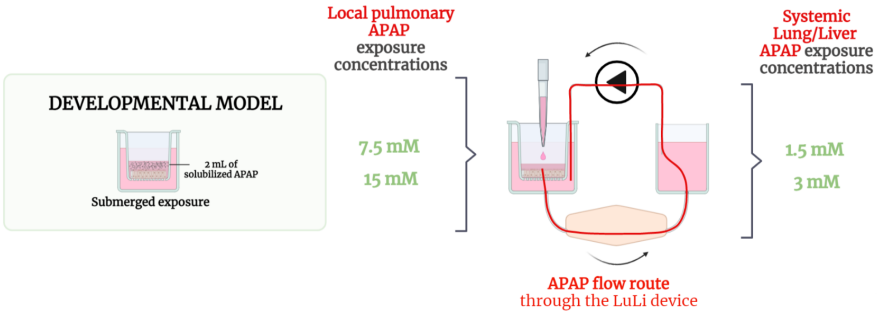

FIGURE 2.10: Schematic illustration of the associated local and systemic APAP exposure concentrations of the developmental model.

2.4.2.4 The physiological-like model

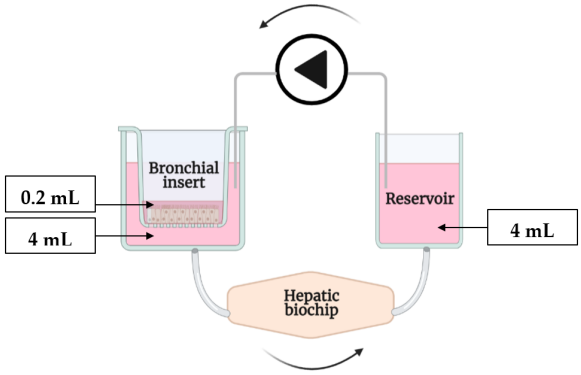

FIGURE 2.11: Schematic representation of the associated volumes of the physiological-like model functional coculture unit.

The semi-ALI coculture condition was considered to be a physiological-like model because of differentiation and exposure modes. The full circuit encloses a total volume of 8.5 mL, setting systemic APAP exposure concentrations at 12 µM and 24 µM. Associated local concentrations imposed through the pulmonary compartment were respectively 0.5 mM and 1 mM.

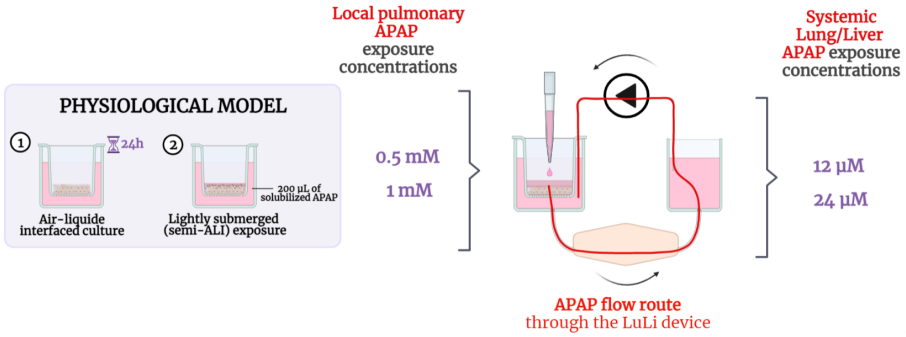

FIGURE 2.12: Schematic illustration of the associated local and systemic APAP exposure concentrations of the physiological-like model.

2.5 Biological assays

2.5.1 Pulmonary viability assay

2.5.1.1 Mitochondrial activity assessment

Mitochondrial activity was assessed by Prestoblue assay (Prestoblue^{TM} Cell viability Reagent, Fischer Scientific). Non-cytotoxic fluorogenic probe passively entered living cells in its non-fluorescent form (reazurin) and reduced into resorufin by mitochondria, a soluble red fluorescent product, that diffused out of the cells and was directly measured by spectrophotometry (excitation wavelength of 535 nm and emission wavelength of 595 nm, Spectafluor Plus, TECAN).

2.5.1.2 Live and Dead assay

Pulmonary inserts were washed with Hanks' Balanced Salt solution (with $CaCl_2$ and $MgCl_2$, pH 7.4) (HBSS) (Invitrogen) and incubated, 20 minutes at 37°C away from light, in a solution of calcein-AM and ethidium bromide according to manufacturer instructions (Live/deadTM Viability/Cytotoxicity Kit, for mammalian cells, ThermoFisher). Nuclei were stained by 3 μM of Hoechst 33342 dye (Fischer Scientific). Samples were visualized by epifluorescence microscopy (Leica DMI6000 B).

2.5.2 Pulmonary functionality: barrier properties

2.5.2.1 Trans-epithelial electrical resistance measurement

The quantitative measurement of barrier integrity was achieved using double electrodes (STX2 set and EndOhm-24SNAP 147581 from World Precision Instruments) connected to Millicell-ERS (Electrical Resistance System) (Millipore) to measure passing current. Every series of measurements, included measuring the blank resistance (R_{BLANK}) of an acellularized membrane and the resistance across a cellularized membrane (R_{TOTAL}). TEER values are reported ($TEER_{REPORTED}$) in units of $\Omega.cm^2$ and calculated as:

$$TEER_{REPORTED} = (R_{TOTAL} - R_{BLANK})(\Omega) \times M_{AREA}(cm^2) \tag{2.1}$$

2.5.2.2 Lucifer Yellow permeability assay

Barrier function was quantified by Lucifer Yellow permeability assay (LY) (Lucifer Yellow CH dipotassium salt, Sigma-Aldrich) on post-culture Calu-3 tissues. Briefly, tissues were washed with pre-warmed (37°C) HBSS (with $CaCl_2$ and $MgCl_2$, pH 7.4) (Invitrogen) on both apical and baso-lateral compartments. Lucifer Yellow CH dipotassium salt was then diluted in HBSS and added to the donor compartment (either apical or basal side to measure respectively apical to basal or basal to apical permeability) at a final concentration of 100 μg/mL. After 1 hour of incubation at 37°C and 5% CO_2, aliquots from the donor and receiver compartments were collected in a black 96-well micro-plate for determination of fluorescence leakage of the LY with a fluorescence microplate reader (TECAN,

Spectrafluor plus) ($\lambda_{excitation}$ = 485 nm, $\lambda_{emission}$ = 530 nm). The apparent permeability coefficient (P_{app}, unit: cm.s^{-1}) was calculated as follows:

$$P_{app} = \frac{dQ}{dt} \times \frac{1}{AC_0} \tag{2.2}$$

Where dQ/dt was the amount of compound transported per second (mg.s^{-1}), A was the surface area of the culture membrane (cm^2) and C_0 the initial donor concentration (mg/mL). The mass balance (R, unit: %) was calculated as:

$$R = 100 \times \frac{A + D}{D_0} \tag{2.3}$$

Where A and D were the amounts of compounds in the apical and basal compartments respectively, and D0 the initial amount of Lucifer Yellow introduced at t0 in the donor compartment. Mass balances of all compounds were between 46 and 86%.

2.5.2.3 Tight junction immunostaining

Post-culture exposed and non-exposed samples were collected, rinsed 3 times with PBS (1X, pH 7.4) (Gibco) and fixed with 4% paraformaldehyde (PFA) solution. Cells were permeabilized with 100X Triton (BDH) à 0,1% at room temperature. Non-specific sites were blocked by immersing the sections into 2% bovine serum albumin (BSA, Gibco). E-cadherin immunostaining procedure: primary antibodies (purified mouse anti-E-cadherin, BD Laboratories) were added at 5 µg/mL to the sections for 1 hour at room temperature. Then, the sections were rinsed 3 times with Phosphate Buffer Saline (PBS) at room temperature. Secondary antibodies (Goat Anti-Mouse Cyanine 3, Jackson ImmunoResearch), diluted in the range recommended by the manufacturer, were added to the sections for 1 hour at room temperature in a dark chamber. Then, the sections were rinsed 3 last times with PBS at room temperature. Claudin-1 immunostaining procedure: primary antibodies (Rabbit anti-Claudin-1 polyclonal antibody MH25, Invitrogen) were added at 20 µg/mL to the sections for 1 hour at room temperature. Then, the sections were rinsed 3 times with PBS at room temperature. Secondary antibodies (Alexa 488 goat anti-rabbit IgG (H+L), Thermo Scientific), diluted in the range recommended by the manufacturer, were added to the sections for 1 hour at room temperature in a dark chamber. Then, the sections were rinsed 3 last times with PBS at room temperature. Due to antibody depletion of the initially utilized stocks, initial protocol was adapted to a new set of antibodies: rabbit anti-Claudin-1 primary antibody (Claudin 1 antibodies (MH25), Invitrogen) at 20 µg/mL, paired with 4 µg/mL AlexaFluor 680 goat anti-rabbit IgG secondary antibody (Thermo Scientific) and rat anti-CD324 antibody (Invitrogen) at 5 µg/mL (Invitrogen) paired with 1:100 diluted Cyanine 2 AffiniPure goat anti-rat IgG secondary antibody (Jackson ImmunoResearch). Despite antibody changes, all images in this thesis were standardized in order to represent green and red staining respectively as Claudin-1 and E-Cadherin tight junctions. All samples also received a 1 mg/mL 4,6-diamidino-2-phenylindole (DAPI) immunostaining (MBD0015, Merck) and final mounting between a

slide and a glass. Immunofluorescence microscopy scans where achieved with confocal microscopy (Zeiss LSM 710).

2.5.2.4 Periodic acid Schiff (PAS) staining

Periodic acid–Schiff is a staining method that offers the opportunity to quantitatively visualize carbohydrates, such as glycoproteins, in tissues. We used this technique to observe mucin secretion of post-cultured bronchial tissues. Calu-3 reconstructs were harvested on day 14 and rinsed with HBSS (with $CaCl_2$ and $MgCl_2$, pH 7.4) (Invitrogen) before being fixed with 4% paraformaldehyde solution. Fixed tissues were then rinsed 3 times with deionized water and oxidized in contact with 0.5% periodic acid solution (Sigma) for 5 minutes. After that, they were rinsed 3 additional times with deionized water before they were stained by Schiff reagent (Merck) for 15 minutes. Stained tissues were then rinsed 3 times with tap water before a final 1-minute hematoxylin counterstaining. PAS stained tissues were then rinsed 3 final times with tap water. Tissues were observed using Leica's TL3000 Ergo transmitted light base.

2.5.2.5 Mucin secretion

Quantitative detection of MUC5AC in post-culture supernatants samples was achieved using the Human MUC5AC ELISA kit (CliniSciences) according to manufacturer instructions.

2.5.3 Hepatic viability assay

2.5.3.1 Cell count

HepG2/C3A cells within post-culture biochips were detached using 0.25% Trypsin-EDTA (1X) (Gibco) and counted using a Malassez' hemocytometer. Cell viability was assessed by Trypan blue dye exclusion.

2.5.3.2 Live and Dead assay

Cellularized biochips were carefully washed with PBS (Gibco) (1X, pH 7.4), using a micropipette, and incubated, 20 minutes at 37°C away from light, in a solution of calcein-AM and ethidium bromide according to manufacturer instructions (Live/deadTM Viability/Cytotoxicity Kit, for mammalian cells, ThermoFisher). Nuclei were stained by 3 μM of Hoechst 33342 dye (Fischer Scientific). Samples were visualized by epifluorescence microscopy (Leica DMI6000 B).

2.5.4 Hepatic functionality assay

2.5.4.1 Glucose consumption

Glucose consumption was quantified in post-culture media samples using the glucose oxidase method comprising two enzymatic phases: oxidation of glucose into gluconodelta- lactone and H_2O_2, by the glucose oxidase enzyme (GOD), followed by the reaction of H_2O_2 with 4-aminoantipyrine and phenol forming a red quinone imine, catalyzed by the peroxidase enzyme (POD). Enzymatic reactions were performed and measured by a chemistry analyzer (INDIKO, ThermoFisher) with the GOD-POD system glucose reagents kit (ThermoFisher).

2.5.4.2 Albumin synthesis

Hepatic albumin secretion was quantified in post-culture media samples by ELISA assay according to manufacturer instructions (Human albumin ELISA Quantitation Set, Bethyl Laboratories).

2.5.5 Hepatic metabolism

2.5.5.1 EROD assay (CYPA1/2 and CYP2B detoxifying activity)

CYP1A1/2 and CYP2B activity levels of post-culture hepatic biochips were measured using 5-ethoxyresorufin (10 mM) as substrate. Resorufin formation by 7-ethoxyresorufin O-deethylation (EROD) was quantified by fluorescence intensity measurement ($\lambda_{excitation}$ = 535 nm, $\lambda_{emission}$ = 595 nm) (TECAN, Spectrafluor plus) after 1 h incubation in presence of salicylamide (3 mM), which inhibits phase II enzymes.

2.5.6 Metabolic assay: mass spectrometry: metabolite detection

Samples were treated externally by the mass spectrometry platform of the Enzyme and Cell Engineering (GEC) department (UMR CNRS 7025) in UTC.
An Agilent QQQ 6460 mass spectrometer with a jet stream electrospray ion source and an Agilent 1200 series fast resolution LC system (Wilmington, DE) was employed to detect acetaminophen and associated metabolites in culture medium samples. MassHunter software was used for system control, data acquisition, and data processing. LC separation was performed on an Agilent poroshel C18 reverse phase column (100 mm x 4.6 mm i.d., 2.6 μm particle size) with a gradient program at a flow rate of 1 mL/min. The mobile phase A consisted of 100% HPLC grade water with 0.1% formic acid and mobile phase B consisted of 100% HPLC grade acetonitrile. The gradient started with 2% solvent B, held at 2% B for 1 minute before being increased to 20% B then increased to 95% in 1 minute and was then held at 95% B for 2 additional minutes. The column was re-equilibrated with 2% B for 3 minutes. Total run time was 12 minutes with a 10 μL injection volume. The mass spectrometer was operated in positive and negative jet stream ESI modes. Nitrogen was used as a nebulizer, turbo (heater) gas, curtain, and

collision-activated dissociation gas. The capillary voltage was +3800 V and 3500 B. The ion source gas temperatures were 350°C with flows of 12 L/min. Jetstream gas temperatures were 350°C with flows of 12 L/min. APAP and metabolites were measured by selective reaction monitoring (SRM). Fig. 2.13 lists the optimal mass spectrometric settings (fragmentor and collision energy) for each quantifying and qualifying transition. The calibration curve was performed with internal calibration using 0.5 μm APAP-D4 in acetonitrile. The samples are prepared by taking 20 μL of medium and adding 80 μL of the internal standard solution to the actenotrile in a 1 mL glass vial, then centrifuged for 5 minutes at 13500 rpm before being transferred from a vial with a 200 μL glass insert.

Stream

Time Segment 1

Scan Segments

Cpd Name	ISTD?	Prec Ion	MS1 Res	Prod Ion	MS2 Res	Dwell	Frag (V)	CE (V)	Cell Acc (V)	Polarity
APAP D4	Yes	156	Unit/Enh (6490)	114	Unit/Enh (6490)	20	80	8	7	Positive
APAP	No	152.07	Unit/Enh (6490)	110.1	Unit/Enh (6490)	20	80	12	7	Positive
APAP	No	152.07	Unit/Enh (6490)	65.1	Unit/Enh (6490)	20	80	32	7	Positive
APAP GSH	No	326.1	Unit/Enh (6490)	150.1	Unit/Enh (6490)	20	120	10	7	Negative
APAP GSH	No	326.1	Unit/Enh (6490)	107	Unit/Enh (6490)	20	120	10	7	Negative
APAP SULF	No	230.1	Unit/Enh (6490)	150	Unit/Enh (6490)	10	120	12	7	Negative
APAP SULF	No	230.1	Unit/Enh (6490)	107	Unit/Enh (6490)	10	120	20	7	Negative

FIGURE 2.13: Optimal mass spectrometric settings for each quantifying and qualifying transition.

2.5.7 Statistical analysis

Data are presented as the mean ± standard deviations. Histogram charts are complemented by scatter plots, which gather the samples that constitute the groups. n represents the number of independent experiments performed. Group comparison statistical tests were chosen based on analysis of dataset variance and normality (Fig. 2.14).

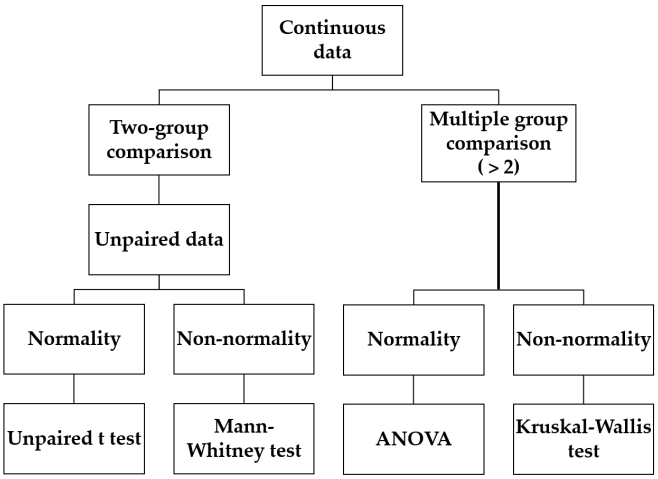

FIGURE 2.14: Statistical decision tree employed in this thesis.

Statistical analysis was performed using GraphPad Instat v.3.10. P values less than 0.05 were considered statistically significant and are presented as follow: * $p < 0.05$, ** $p < 0.01$, *** $p < 0.001$.

Chapter 3

Evaluating cytotoxic profile of a model molecule in hepatic and pulmonary monocultures: an acetaminophen case study

The present coculture platform was at the early stages of development, which is why experimental robustness was at the heart of our project. The focus was to demonstrate the value and utility of our model to study toxicology at a further systemic level, by considering organ crosstalk as possible modulators of toxicity. As the developed model is intended to be used to investigate toxicity related to airborne pollution exposure, inhaled through the respiratory tract, the lung compartment is the key study target. To prove our concept, we had to ensure that the associated hepatic compartment could access and respond to xenobiotic exposure when carried out through the pulmonary barrier. Our study began by choosing an appropriate model substance which's passage and circulation could quantitatively be followed through the device. APAP was our xenobiotic of choice, as it is known and well-documented to induce significant hepatic toxicity. Thus, causing notable biological responses during its transit through the device, and especially in contact with hepatic cells, would attest to the capacity of a given xenobiotic to navigate through both compartments of the coculture. Before using it in a joined culture configuration, we characterized tissue-specific biological behaviors in response to APAP by exposing lung and liver monocultures in individual settings. This chapter unfolds the associated results.

3.1 Assessing hepatic response to hepatotoxic stress

3.1.1 Morphological observations do not reveal noticeable differences at 1.5 mM and 3 mM APAP exposure concentrations

HepG2/C3A cells were inoculated into pre-sterilized and collagen I-coated biochips. The biochips were incubated for 24 hours at 37°C to facilitate cell adhesion before being dynamically cultured under a continuous microfluidic flow for 24 hours.

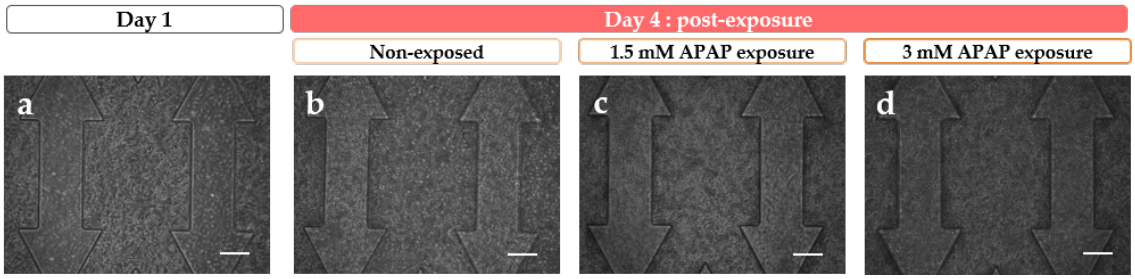

FIGURE 3.1: Phase contrast microscopy of monocultured HepG2/C3A biochips (a) on day 1 and (b, c, d) day 4 of untreated (b) and 72-hour exposed samples (c, d) (1.5 mM APAP or 3 mM APAP). (Scale bar = 100 μm)

Phase contrast microscopy showed that inoculation and adhesion of hepatocytes to the biochips were successful, as cells are elongated and homogeneously dispersed throughout the microchambers and channels of the system (3.1 a). Cell proliferation was obvious from day 1 to 4 as cell shapes are further blurred into each other because of high density proximity. Following 72-hour dynamic monocultures, non-exposed and exposed samples displayed similar morphological features (3.1 a, c and d). As confluence was high, cellular phenotype was hard to assess, however microscopic observations showed no significant differences despite APAP exposure and regardless of increasing exposure concentrations: cellular density organization and morphology seemed to remain intact at 1.5 mM and 3 mM exposure concentrations.

3.1.2 Viability assays highlight a significant decrease of live cells

HepG2/C3A cells were stained using a Live/Dead^{TM} viability/cytotoxicity kit, and counted by Trypan blue dye exclusion, on day 4, to determine the effect of APAP on cell viability following 72h of exposure. As biochips were cultured in a perfused environment, dead cells were carried away by the flow, we, therefore, focused our interest on the evaluation of green fluorescence intensity, associated with live-cell labeling. Epifluorescent microscopic observations (Fig. 3.2) showed that treated samples displayed a gradual decrease of green fluorescent signal correlated to increasing concentrations of APAP exposure. Qualitative data was paired with quantitative cell counts (Fig. 3.3) which revealed a significant drop of live cells correlated with APAP treatment and exposure concentration. Collected viability data suggested that APAP induced dose-dependent hepatic toxicity at 3 mM in a dynamic exposure configuration.

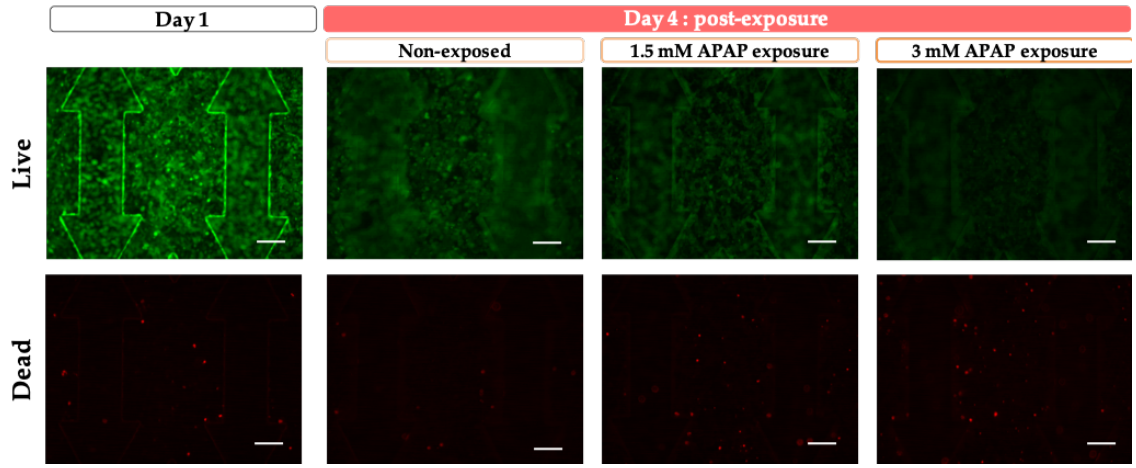

FIGURE 3.2: Cytotoxicity assay (Live and Dead) on day 1 and 4 of untreated and APAP-exposed HepG2/C3A biochips. Red fluorescence: calcein AM staining of dead cells, green fluorescence: ethidium bromide staining of live cells. Scale bar: 100 μm

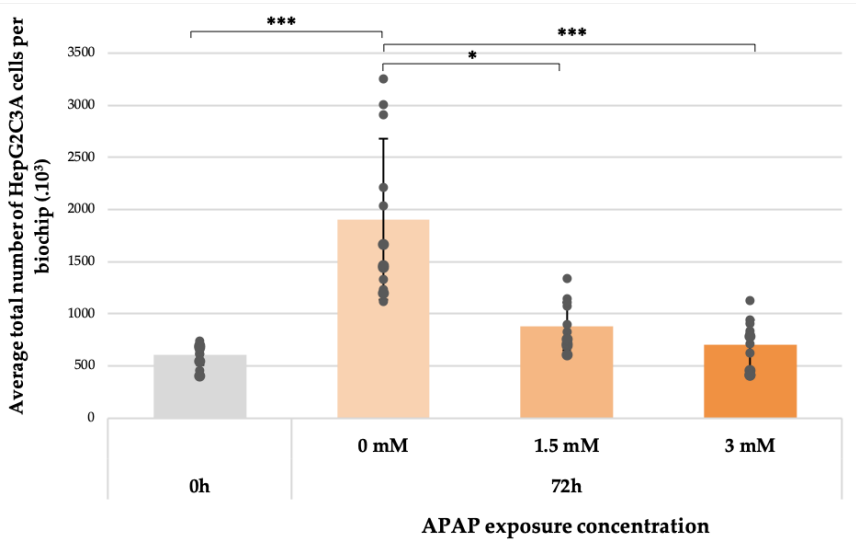

FIGURE 3.3: Evolution of monocultured HepG2/C3A cell proliferation rates according to APAP exposure concentration (significance analyzed by Kruskal-Wallis test. $n \geq 4$)

3.1.3 APAP exposure does not impair hepatic differentiation

Measurement of albumin secretion rate was investigated (Fig. 3.4) to provide more dynamic insight into the impact of APAP on modulation of albumin metabolism and therefore hepatic functionality of monocultured HepG2/C3A cells. In non-exposed and exposed culture conditions, albumin synthesis was detected. Rates were variable as standard deviations were spread, production varied on average from 88.94 ± 50.91 to 188.53 ± 129 ng/10^6 cells/h. Results showed comparable metabolic activities despite APAP exposure. The statistical ANOVA test did not reveal any significant differences between the three tested conditions. APAP did not impact hepatic functionality at 1.5 mM and 3 mM exposure concentrations.

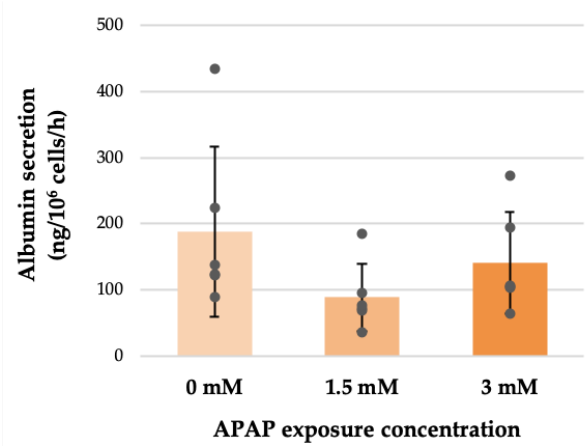

FIGURE 3.4: Albumin secretion rates of HepG2/C3A on day 4 according to APAP treatment. Statistically analyzed by one-way analysis of variance (ANOVA) test. n = 3.

3.1.4 Functional characterization reveals increased metabolic activities following exposures

Glucose is a vital fuel for proper cell machinery function, and CYP1A1/2 are prominent detoxifying enzymes, analyzing basal and xenobiotic metabolisms allowed for a better understanding of hepatic response to a stress-induced environment. Both parameters gave an overview of the metabolic profiles of monocultured HepG2/C3A cells in response to APAP. Glucose rates were analyzed, in post-cultured supernatants, collected data is displayed in Fig. 3.5.

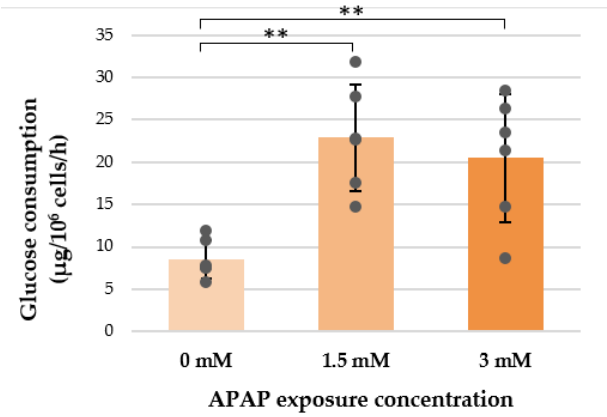

FIGURE 3.5: Glucose consumption of HepG2/C3A cells cultured in perfused biochips for 72 hours, with or without APAP. Statistically analyzed by ANOVA test, Tukey-Kramer post-hoc multiple comparisons test. n = 3.

Results showed that cell consumption increased when tissues were treated with APAP. HepG2/C3A cells consumed up to 2.5 times more glucose in an APAP-exposed environment. However, no dose-dependent effect of exposure was found.

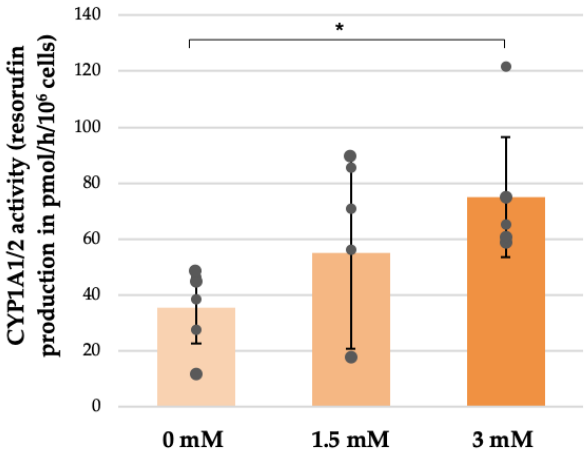

FIGURE 3.6: Comparison of CYP1A1/2 detoxifying activities on day 4 according to APAP exposure concentrations. Statistically analyzed by Kruskal Wallis test. $n \geq 3$.

In parallel, CYP1A1/2 activity was significantly stronger when APAP was present. Figure 3.6 shows how the collected data highlighted a significant difference between the CYP activity of 3 mM-exposed and non-exposed samples. These results suggest that APAP stimulates the induction of CYP1A1/2 activities as of 3 mM exposures.

3.2 Investigating APAP toxicity on the bronchial barrier: the submerged bronchial monoculture standard

3.2.1 Viability assays show tissue response to hepatotoxic exposure concentrations

At the end of the culture on day 14, the cell viability of untreated and treated Calu-3 bronchial tissues was measured. Untreated samples were considered as fully viable standards to which APAP-exposed tissues were compared with.

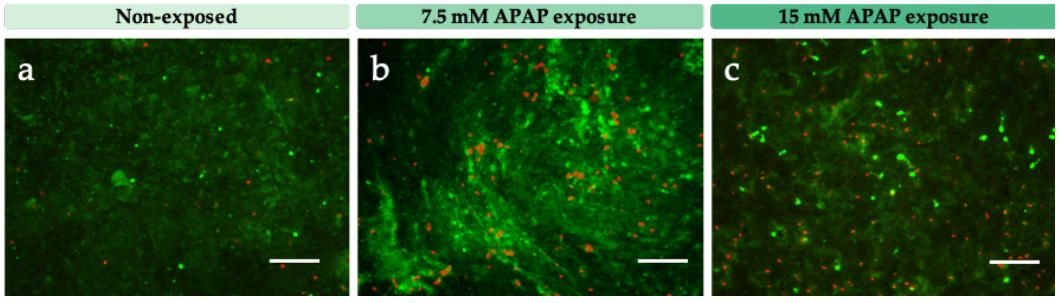

FIGURE 3.7: Viability of submerged monocultures of Calu-3 bronchial tissues (Live and Dead assay) tissues on day 14 exposed and non-exposed to APAP. Green – Calcein AM-stained: viable cells; Red – Ethidium homodimer-stained: dead cells. Scale bar: 100 μ m

Live and Dead stainings showed an increased amount of red signaling, associated with cell mortality (Fig. 3.7). These results tied with basal cell activity measurements, associated with mitochondrial resorufin production assay (Fig. 3.8), which significantly dropped in the presence of APAP. Overall, it seemed that viability of treated tissues was significantly impacted by exposure.

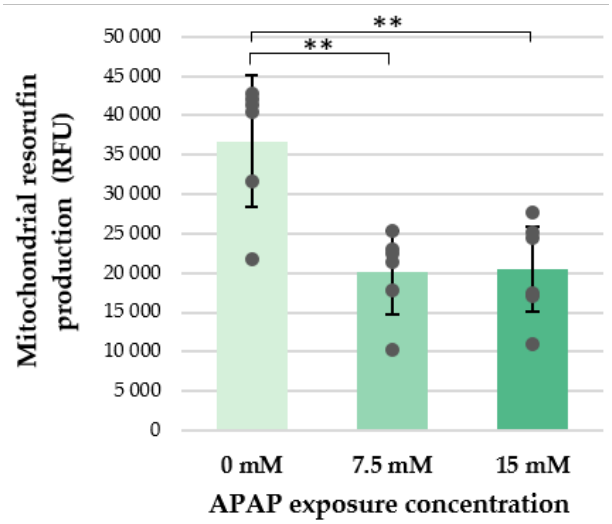

FIGURE 3.8: Relative mitochondrial activity of APAP-exposed monocultured Calu-3 bronchial tissues compared to non-exposed samples, measured by PrestoBlue^{TM} through fluorescent resorufin production, on day 14 after 72h exposures to various APAP concentrations. Statistically analyzed by ANOVA, post-hoc Tukey-Kramer multiple comparisons test. $n \geq 6$.

3.2.2 Immunostaining reveals barrier architecture disruption following APAP exposures

Immunofluorescence staining of Calu-3 bronchial epithelia exposed or unexposed to APAP were analyzed using confocal microscopy. Established culture protocols allowed for effectively reconstructed tissues, as immunofluorescence showed that the epithelial cells were linked by continuous staining of adherens junction protein E-Cadherin, and tight junction protein Claudin-1 (Fig. 3.9 a, b). Both highly colocalized along cell peripheries while Claudin-1 also diffused within the cytoplasm. APAP exposure did not perturb E-Cadherin expression and localization (Fig. 3.9 b, c), however labeling revealed a morphological change in cellular phenotype, as cell size increased. Meanwhile, APAP-treated tissues demonstrated discontinuous staining of Claudin-1 proteins (Fig. 3.9 e, f), indicating disruption of tight junctions. No dose-dependent effect was found between treated conditions.

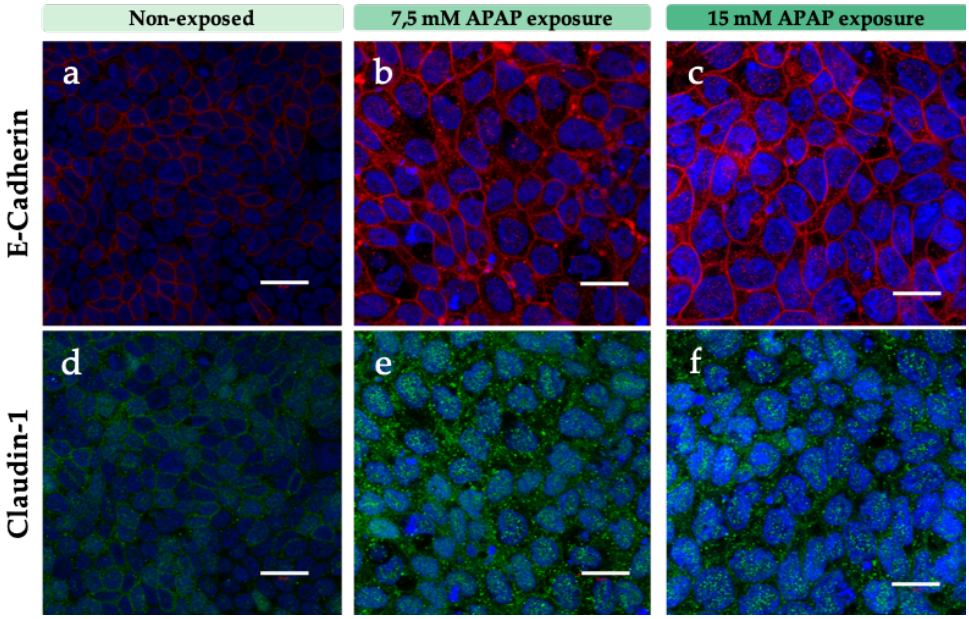

FIGURE 3.9: Confocal microscopy imaging of nuclei (blue), E-Cadherin (red), and Claudin-1 (green) immunostained adherens and tight junction complexes on day 14 in APAP-exposed (b, c, e, f) and non-exposed (a, d) submerged Calu-3 monocultures. Scale bar: 20 μ m

3.2.3 Functional assays confirm impaired barrier functions

Integrity, permeability, and mucin secretion of Calu-3 reconstructs were monitored to evaluate barrier properties. Non-invasive TEER measurements revealed that bronchial tissues continued to grow up to day 11, as Kruskal Wallis comparisons test revealed a significant increase in resistance values from day 10 to 11 (Fig. 3.10), the resistance then plateaued, and measurements culminated on average up to $3228 \pm 1507\,\Omega.cm^2$ highlighting the development of a strongly cohesive barrier at day 14. When tissues were grown in the presence of APAP, the measured electrical resistance significantly dropped by 3000 $\Omega.cm^2$ ($168 \pm 54\,\Omega.cm^2$) compared to non-exposed tissues.

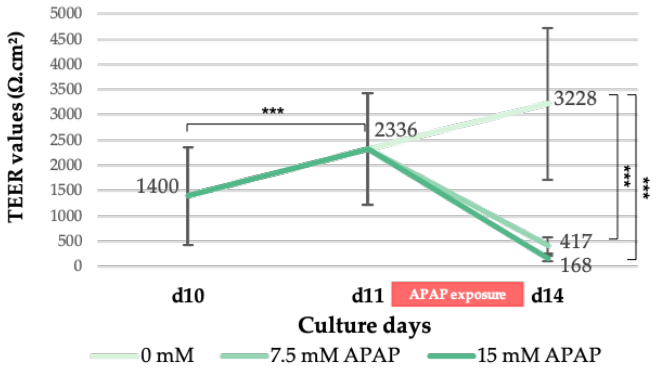

FIGURE 3.10: Transepithelial electrical resistance (TEER) measurement of submerged Calu-3 bronchial tissues over time following 72h APAP exposures. Statistically analyzed by Kruskal-Wallis Comparisons Test. n = 6.

To better understand this phenomenon, we used Lucifer Yellow dye to evaluate permeability of exposed tissues (Fig. 3.11). Results confirmed TEER data. Associated P_{app} values significantly increased in a non-dose-dependent manner from untreated barriers approaching average P_{app} values of 0.029 x 10^{-6} ± 0.02 cm.s^{-1} to 15 mM APAP-exposed tissues leveling up to 3.736 x 10^{-6} ± 1.09 cm.s^{-1}.

		Papp (x10^{-6} cm.s^{-1})		Permeability rate (%)
Cell free culture insert *Apical* permeability		60,581		100
Submerged	**0 mM**	0,029 ± 0,02	***	0,05
	7.5 mM	1,031 ± 0,14		1,70
	15 mM	3,736 ± 1,09		6,17

FIGURE 3.11: Permeability of non-exposed and APAP exposed Calu-3 bronchial tissues (P_{app} values) measured through the transport of 100 μg/mL Lucifer Yellow (from the apical to the basal compartment). Statistically analyzed by Kruskal Wallis test. n = 3.

To further functionally characterize the effect of exposure on Calu-3, Periodic acid-Schiff stainings were carried out on fixed post-culture tissue to visually assess mucin secretion, as the mucus layer is a core protective function of bronchial tissue [334]. Associated observations are displayed in Fig. 3.12, and showed a gradual dose-dependent decrease in stain intensity.

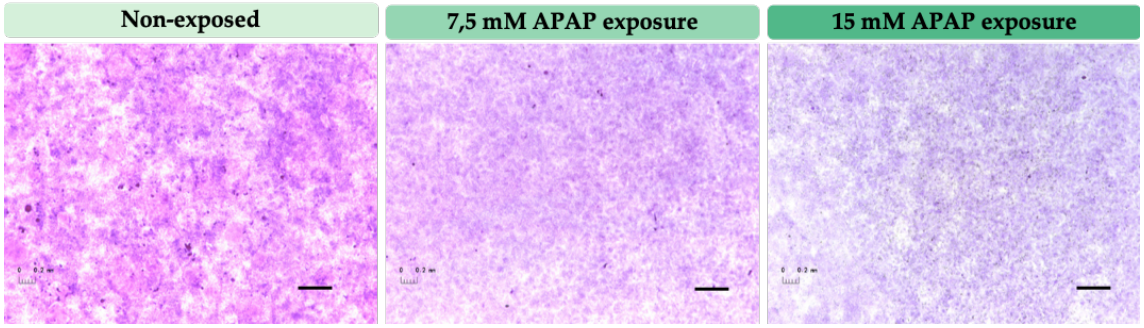

FIGURE 3.12: Correlation between PAS stained-mucin secretion and APAP exposure concentrations. Scale bar = 400 μm.

Regarding the MUC5AC dosage, the results presented in Fig.3.13 show a drastic drop in the concentrations of mucins detected in the supernatants of samples exposed to APAP. There is no dose-dependent effect at the tested exposure concentrations tested as the mucins concentration averages found for the samples exposed to 7.5 and 15 mM are similar.

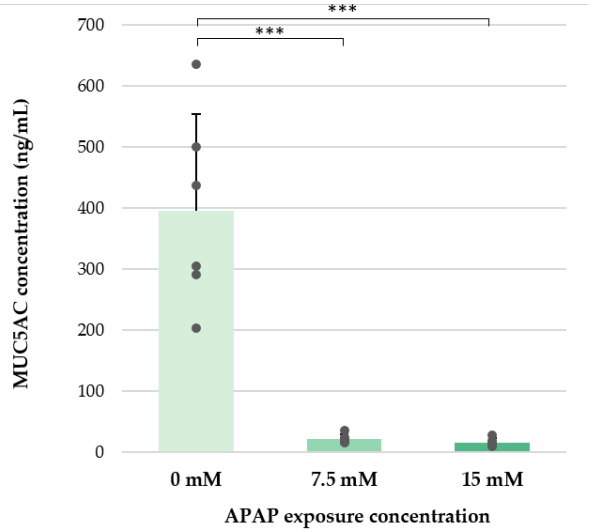

FIGURE 3.13: Measurements of MUC5AC concentrations of submerged Calu-3 bronchial tissues according to APAP exposure. Statistically analyzed by ANOVA, Tukey-Kramer post-hoc multiple comparisons test. n = 6.

3.3 Empowering pulmonary model relevance: introducing a physiological-like bronchial model

Because submerged tissue reconstruction overlooked *vivo* pulmonary physiology, we complexified the bronchial model to obtain further relevantly differentiated tissues. *In vitro* air-liquid interfaced (ALI) lung cell culture models have proven to enhance physiological differentiation [27] [335], because of how closely apically air-exposed cells mimic healthy human *in vivo* anatomical features of cells in the respiratory tract [336]. We considered that relevantly complexifying the cell function of the pulmonary barrier would empower the predictability of our coculture model. Calu-3 tissues were grown under submerged cultures conditions for 10 days, until confluence was reached. An additional ALI period was imposed for 24 hours for the semi-ALI monocultured condition from day 10 to 11 (see 2.2.4 in Chapter 2). Thus, tissue morphology was followed from day 11 until the end of culture period on day 14 (Fig. 3.14). Contrast phase microscopy showed that as soon as tissue reached the ALI (d11), an opaque veil appeared, covering the surface of the epithelial tissues. This specific veil sparsened when a thin layer of culture medium (200 μL) was added to the apical side from day 11 to 14, however it appeared to remain present compared to the submerged tissues.

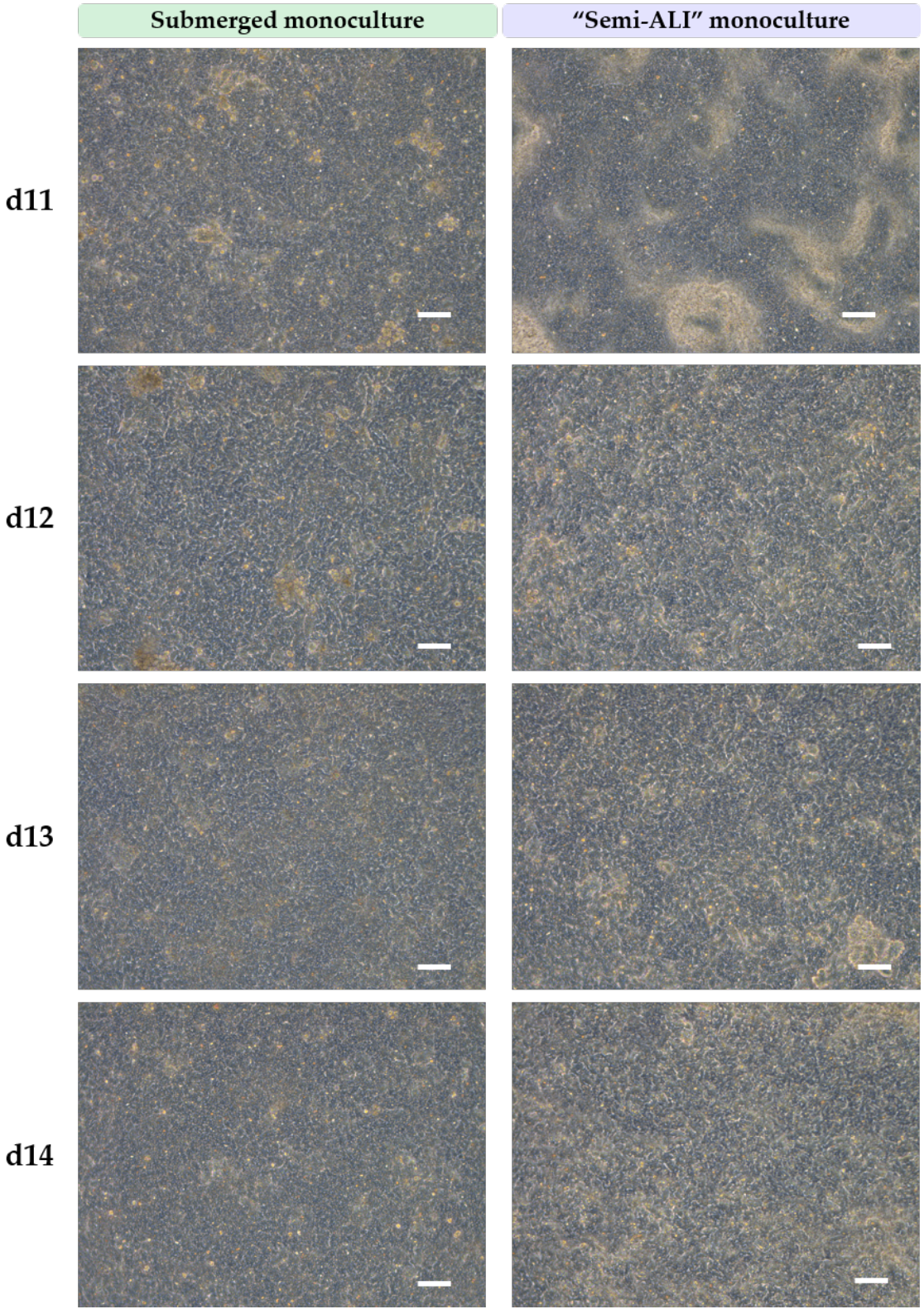

FIGURE 3.14: Phase contrast microscopy observations of Calu-3 bronchial tissue reconstruction evolution through time according to culture conditions (scale bar = 100 μm).

Regarding tissue functionality, it appeared that culture mode did not impact barrier permeability as Lucifer Yellow assay did not reveal any significant difference between submerged and semi-ALI P_{app} values (Fig. 3.15).

	Papp ($x10^{-6}$ $cm.s^{-1}$)	Permeability rate (%)
Cell free culture insert *Apical* permeability	60,581	100
Liquid-Liquid Interfaced Culture	0,029 ± 0,02	0,048
Semi Air-Liquid Interfaced Culture	0,033 ± 0,03	0,054

FIGURE 3.15: Permeability of submerged and "semi-ALI" Calu-3 bronchial tissues (P_{app} values) measured through the transport of 100 μg/mL Lucifer Yellow (from the apical to the basal compartment). Statistically analyzed by unpaired t test. n = 3.

PAS staining did not reveal any obvious staining differences between submerged and semi-ALI samples with regards to color intensity. However, the subtle variation concerned the organization patterns of mucins visible at the tissue surface of semi-ALI samples. Indeed, a few small agglomerates of intense staining were sparsely observable (Fig. 3.16A). This difference was quantitatively reflected when MUC5AC dosage was assayed (Fig. 3.16B). The results in Fig. 3.16B showed that the concentration of mucins found at the surface of semi-ALI tissues was 4 times higher than those of submerged tissues. ALI culture would therefore favor the development of better mucin-loaded tissues.

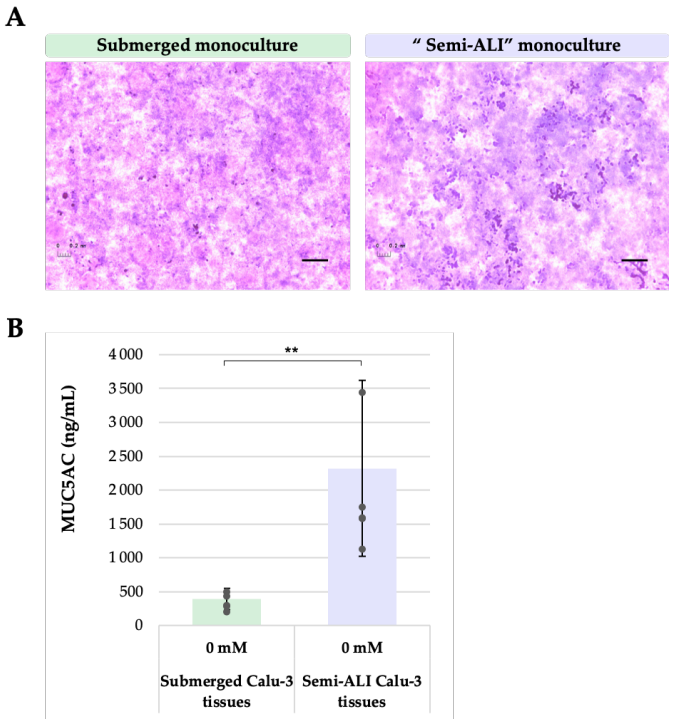

FIGURE 3.16: (A) PAS staining of submerged and semi-ALI non-exposed Calu-3 tissues at day 14. Scale bar = 400 μm. (B) Quantification of MUC5AC concentrations measured in post-culture apical supernatant of submerged and semi-ALI Calu-3 tissues at day 14. Statistically analyzed by Mann-Whitney test. n = 6.

3.4 Exploring bronchial sensibility to low dose exposures: partial air-liquid interfaced monoculture

In the semi-ALI culture setting, Calu-3 tissues are covered with a small volume of medium (200 μL) to better approximate physiological exposure conditions. APAP exposure concentrations were lowered to 0.5 mM and 1 mM because of solubilization thresholds (14 mg/mL at 25°C) [337].

3.4.1 Morphology, viability and function remain unchanged

Phase contrast microscopy showed cohesive Calu-3 bronchial reconstructs up till the end of the culture on day 14, despite APAP exposure (Fig. 3.17A). No obvious differences were noted between untreated and treated samples. APAP did not seem to impact morphology at the tissue level. This observation was confirmed by adherens and tight junction immunostaining (Fig. 3.17B). Indeed, tissue cohesiveness remained unchanged as E-Cadherin and Claudin-1 stainings stayed localized, at the cell-cell contact sites, regardless of exposure (Fig. 3.17Ba, Bb).

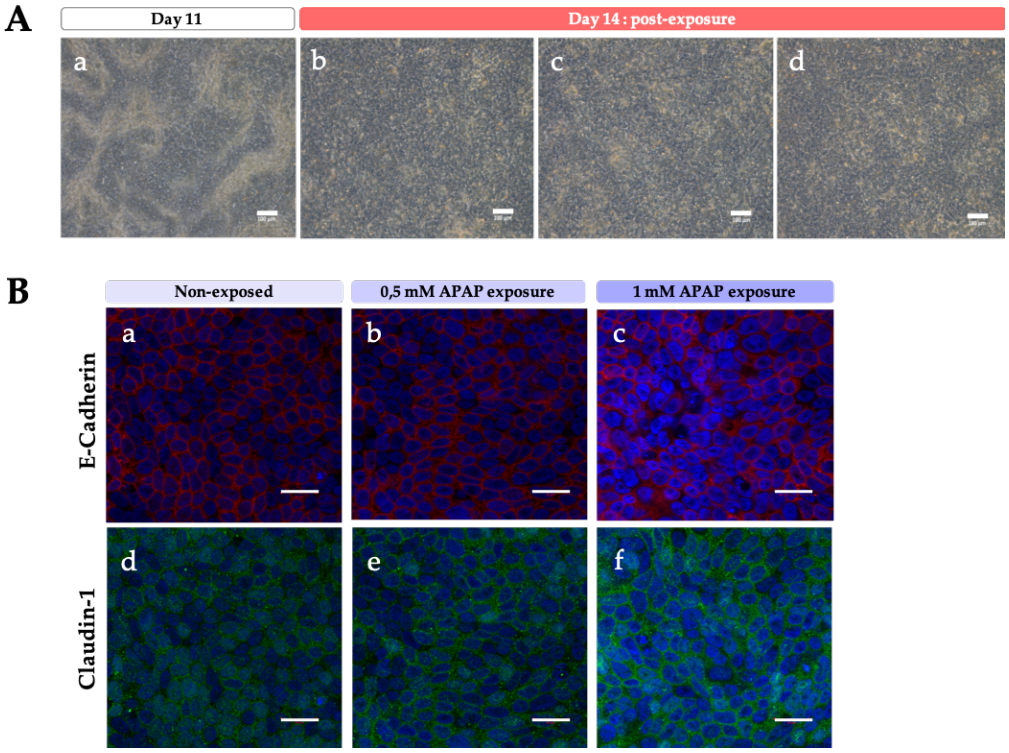

FIGURE 3.17: (A) Phase contrast microscopic imaging of semi air-liquid interfaced monocultures of Calu-3 bronchial tissues cultured up to maturation on day 11 (a) and on 14 days (b, c, d) post-acetaminophen exposures at 0,5 mM (c) and 1 mM (d). Non-exposed samples (a) were kept within every experiment as controls (scale bar = 100 μm). (B) Confocal microscopy imaging of nuclein (blue), Claudin-1 (green), E-Cadherin (red) immunostained adherens and tight junction complexes in semi air-liquid interfaced monocultures of Calu-3 bronchial tissues at day 14 exposed (b, c, e, f) and non-exposed (a, d) to APAP. Scale bar = 20 μm).

Concerning tissue viability, Live/Dead assay did not reveal any increase in dead cells between conditions (Fig.3.18A) as red signaling remained minimal throughout all conditions. Similarly, one-way analysis of variance (ANOVA) did not reveal any significant changes in basal metabolic cell function, as APAP-treated tissues reported steady mitochondrial resorufin activity close to the values of the unexposed control (Fig.3.18B). Overall, according to our results, APAP did not have any impact on the viability of Calu-3 tissue reconstructs.

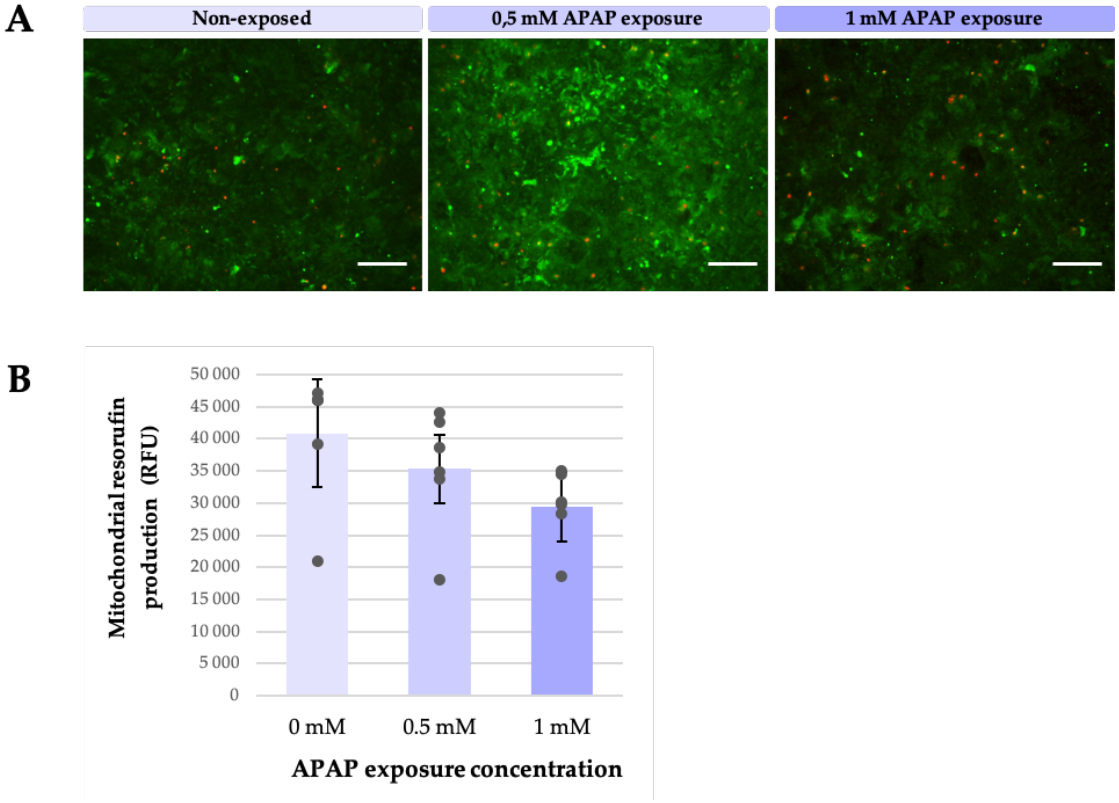

FIGURE 3.18: Viability assays of semi-ALI monocultured Calu-3 bronchial tissues post-culture on day 14. (A) Live and Dead assay of exposed and non-exposed samples to APAP. Green – Calcein AM-stained viable cells; Red – Ethidium homodimer-stained dead cells. Scale bar = 100 μm). (B) Mitochondrial activity measured by PrestoBlue^{TM} through fluorescent resorufin production, according to various APAP exposure concentrations. Statistically analyzed by ANOVA test. n = 6.

Along the same lines as previously presented data, the Calu-3 barrier function remained strong in the presence of APAP, TEER measurements revealed stable electrical resistance values (Fig.3.19) peaking at $2696 \pm 1153\,\Omega.cm^2$. However, even though exposure doses were low, Calu-3 semi-ALI tissues seemed to perceive a stress-induced environment as Kruskal Wallis statistical analysis revealed a significant increase of resistance from day 11 to day 14 only for non-exposed samples, meaning that APAP interrupted tissue growth.

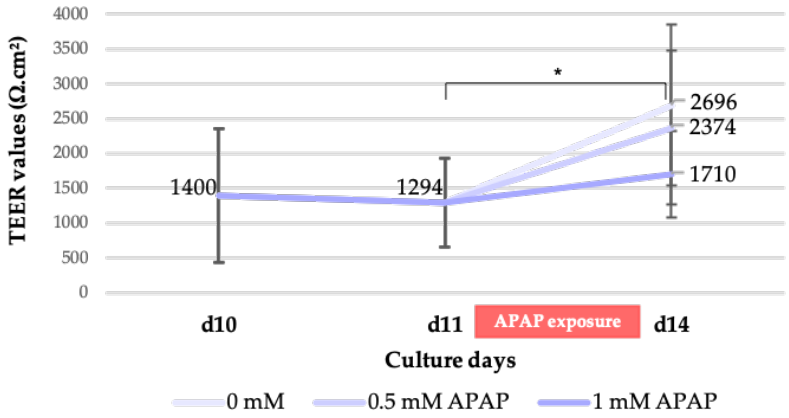

FIGURE 3.19: Transepithelial electrical resistance (TEER) measurement of semi-ALI Calu-3 bronchial tissues over time according to 72h APAP exposures. Statistically analyzed by Kruskal Wallis test. $n \geq 6$.

In order to get more of an insight into tissue functionality of semi-ALI samples, PAS staining, MUC5AC concentrations and Lucifer Yellow permeability assays were measured. PAS stainings revealed the same kinds of dispersion patterns as previously mentioned in section 3.3. Agglomerates of intense staining on the surface of the tissues are present as seen previously on unexposed tissues and also on those exposed to APAP (Fig. 3.20). There was no discernible difference between the three studied culture conditions in terms of coloring intensity or organization.

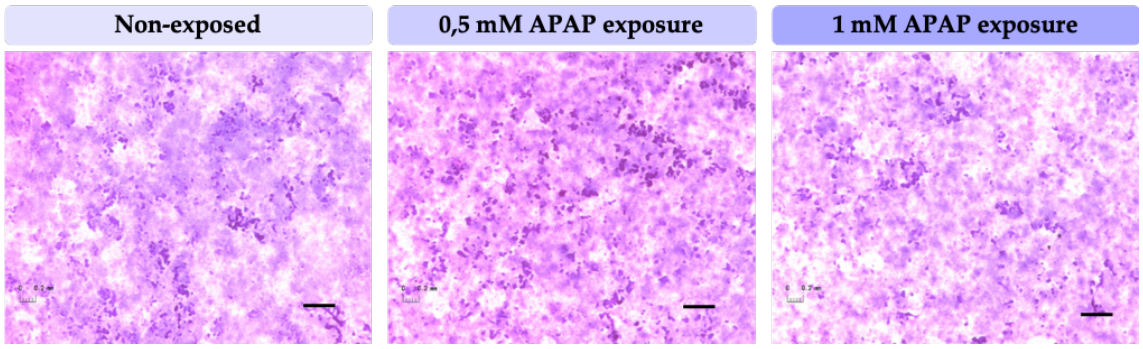

FIGURE 3.20: PAS staining of semi-ALI cultured bronchial tissues on day 14 according to APAP exposure. Scale bar = 400 μm.

These qualitative observations were confirmed by the quantitative results obtained from the dosage of MUC5AC concentrations measured in post-culture supernatants (Fig 3.21). No significant concentrations differences were noted between non-exposed and exposed tissues. All means average around 2000 ng/mL. APAP did not impact the MUC5AC homeostasis of semi-ALI monocultured Calu-3 tissues.

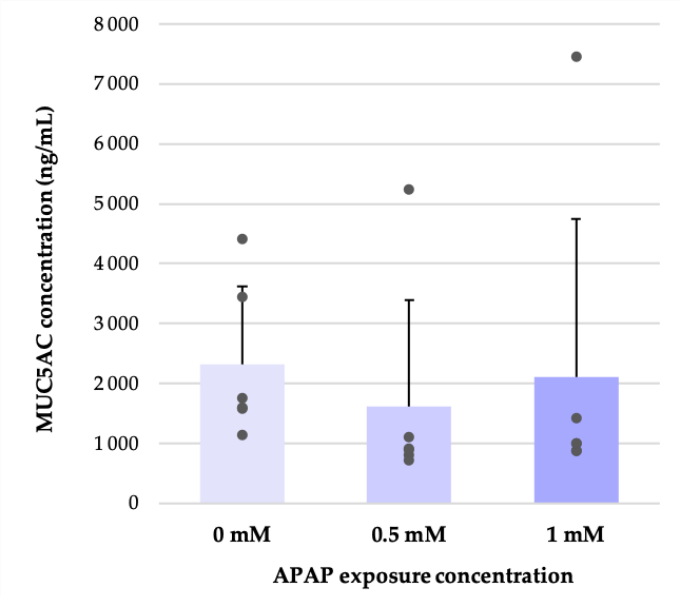

FIGURE 3.21: Measurement of MUC5AC concentrations in the supernatants of post-cultured semi-ALI bronchial tissues according to APAP exposure. Statistically analyzed by ANOVA test. n = 6.

Kruskal Wallis statistical analysis did not reveal any significative difference between Papp values of semi-ALI tissues. APAP exposure did not perturn barrier functions of Calu-3 tissues (Fig. 3.22).

		Papp ($x10^{-6}$ $cm.s^{-1}$)	Permeability rate (%)
Cell free culture insert *Apical* permeability		60,581	100
Semi-ALI	0 mM	0,033 ± 0,03	0,054
	0.5 mM	0,042 ± 0,06	0,070
	1 mM	0,013 ± 0,01	0,022

FIGURE 3.22: Permeability of non-exposed and APAP exposed semi-ALI Calu-3 bronchial tissues (P_{app} values) measured through the transport of 100 μg/mL Lucifer Yellow (from the apical to the basal compartment). Statistically analyzed by Kruskal Wallis test. n = 3.

3.5 Discussion

The pulmonary and hepatic *in vitro* models represent the building blocks of the coculture model. To demonstrate the relevancy of the model for systemic-like toxicological investigations, we chose to work with robust and already characterized *in vitro* reconstructs that displayed active metabolic features.

3.5.1 Recreating a metabolically competent hepatic construct

The hepatic compartment was established using a previously developed and characterized PDMS microstructured biochip [4]–[10]. Among other applications, this culture

mode has been utilized for the culture of HepG2/C3A cells and has proven to improve *in vitro* hepatic functionality and more interestingly enhance cellular cytoprotective mechanisms notably through the upregulating of gene-related expressions and activities of phase I and II drug-metabolizing enzymes [8]. Improved hepatic metabolism in microfluidic biochips has been linked to culture media renewal, which ensures continuous transport of nutrients and oxygen, and the mechanical stimulation imposed by the perfusion [11]. The improvement of these metabolic capacities is of particular significance in drug metabolism investigations, and therefore relevant for the proof of concept of the lung/liver coculture model. The present results appeared consistent with previous studies based on morphological observations, albumin secretion, CYP1A activity, and glucose consumption rates. Overall, data indicate that the dynamic culture allowed for the establishment of differentiated, and metabolically active HepG2/C3A cells at the basal and xenobiotic metabolic levels.

The mechanisms related to APAP hepatoxicity have already been extensively investigated. The goal was to expand on this pool of data by utilizing APAP as a tool to define the tissue-specific toxicological profile of the hepatic compartment under our study's culture settings. The biological responses of HepG2/C3A biochips to APAP exposure have already been investigated, however at lower doses of no more than 1 mM [5], [8]. The tested 1.5 and 3 mM APAP-induced cell culture environments, induced perceivable adverse effects on HepG2/C3A biochips. As previously described, the hepatoxicity of APAP is related to the production of the reactive metabolite NAPQI. NAPQI is normally conjugated to glutathione (GSH) via GSTs to produce a non-toxic APAP-glutathione (APAP-GSH) metabolite. However, excessive NAPQI production depletes GSH stocks, causing NAPQI to accumulate. CYP activities are involved in the biotransformation of APAP to NAPQI [12]. Consistent with Prot et al. monitoring CYP1A activity in HepG2/C3A cells, through EROD assay, allows following the production of NAPQI [13]. The results indicate that APAP induces CYP1A metabolism as of 3 mM exposures, and perhaps as early as 1.5 mM since the values tend to be already higher than the baseline activity of controls at these doses, implying that NAPQI metabolites are being increasingly produced. To follow the detoxification process of NAPQI, APAP-GSH conjugates should be quantified through mass spectrometry in post-culture supernatants [14]. However, detoxification of NAPQI to APAP-GSH is unlikely as exposures cause a substantial increase in cell mortality (Live and Dead assays, and cell counts). Therefore, the measured glucose consumption corresponds to the activity of a reduced cell number, which implies that the significant increase in glucose consumption is related to a significant increase in cell activity. Despite the hepatotoxicity, the measured albumin levels indicate that the differentiation of HepG2/C3A cells was not impacted.

According to the present results, HepG2/C3A biochips sense and react to APAP exposures, which cause substantial hepatotoxicity in HepG2/C3A biochips at 1.5 mM exposures, which rises at 3 mM exposures via an increase in cell activity and cell death. However, toxicity does not seem to induce their dedifferentiation. The characterization of these biological responses provides a base to better identify possible lung/liver crosstalk

behaviors within coculture conditions.

3.5.2 Investigating the effects of APAP on the bronchial Calu-3 barrier

As the pulmonary barrier is intended for drug permeation investigations the primary requirement is that it should provide correct barrier functions, which is why we chose to work with the Calu-3 cell line as associated confluent monolayers display strong barrier functions. Even though Calu-3 are immortalized cells, they still possess many relevant characteristics of primary airway cells (e.g. TEER, permeability) including an active xenobiotic metabolism through the presence of active phase I CYPs (1A1, 2B6, and 2E1), phase II UGTs, and phase III efflux transporters (e.g. MRP1, P-gp), making them appropriate study models for toxicological investigations [15]–[19].
The submerged bronchial monoculture allowed to benefit of a consequent apical exposure volume at the tissue surface to reach high exposure concentrations, as APAP solubility is a constraining technical factor. The results indicate no dose-dependent differences in the effects of 7.5 and 15 mM APAP exposure doses. APAP induced apparent cytotoxicity that was notably reflected by an increase in cell death (Live/Dead), and an increase in cell size. Abnormally large morphology has been correlated *in vitro* to senescent cells. According to the literature, increasing cell size causes an increase in the cytoplasm to DNA ratio, which contributes to cell cycle arrest in senescent cells [20]. Furthermore, APAP also affected the mitochondrial metabolism of Calu-3 cells as the activity decreased by almost half of what it was in the basal state. This could be attributed to NAPQI accumulation due to phase II metabolizing enzyme saturation caused by APAP overdose, as studies report that mitochondrial proteins are the main targets of NAPQI in the injury process of APAP hepatotoxicity proteins [21]. As this phenomenon translates into mitochondrial oxidative stress in the liver [22], additional Reactive Oxygen Species (ROS) measurements could be carried out to investigate if the reduction of mitochondrial activity could be linked to mitochondrial oxidative stress, as it is in the liver, and therefore could be associated to NAPQI accumulation. This loss of viability could impact the tissue cohesion and thus explain the loss of barrier function that became apparent, particularly through a drop in TEER, which according to the classification established in the literature makes the Calu-3 epithelium pass from "tight", with values exceeding 2000 $\Omega.cm^2$, to "intermediate" tending more towards "leaky" as the values are around or less than 300 $\Omega.cm^2$ [23]. Barrier function is strongly linked to the state of intercellular junctions. The barrier's integrity is determined by the cellular continuity of tissue and the effectiveness of adhesions formed with neighboring cells [24]. Immunostaining of E-Cadherin adherens junctions and Claudin-1 tight junctions revealed that APAP disrupted Claudin-1 architecture. Tight junctions are particularly involved in the regulation of macromolecular and ionic permeability, by regulating access to the paracellular spaces [25], which explains the increase in tissue permeability measured by Lucifer Yellow. The loss of the barrier function was also reflected by the decrease in the level of MUC5AC mucins detected on the surface of Calu-3 tissues, as it has been established that the diffusion of small hydrophobic molecules is slowed down by mucus [338] due to transient interactions with

mucins - glycoproteins rich in cysteine [339], a hydrophobic amino acid, which makes up 2% of mucus [340]. While the literature reports that *in vivo*, external aggressions (e.g. infectious pathogens) drive airway remodeling, notably through goblet cell hyperplasia, which activates airway mucin production [26], it appears that APAP treatment limits the mucin production of Calu-3 cells. This may be due to the fact that the cells are already too damaged by exposure to maintain an active metabolism. Therefore, the measured MUC5AC may come from the secretions before APAP altered the metabolism.

3.5.3 Complexification of the bronchial model portfolio towards more physiological culture and exposure conditions

The reconstruction protocol, incorporating 24 hours of ALI differentiation, and lower volume (200 μL) and exposure doses (0.5 and 1 mM), provide semi-ALI tissues with culture conditions that better approximate a *vivo* environment. The physiologically enhanced differentiation of tissues in ALI has been widely documented and valued for the functional benefits it confers to lung tissues [27], concerning Calu-3 tissues, Forbes and Kristan's teams documented how ALI produced tissues more similar to *vivo* airway epithelia as they displayed higher quantity of mucus covering the cell surface, and a pseudostratification of the tissue with more columnar cells [28], [29], which also translated in our present semi-ALI Calu-3 bronchial constructs. TEER values and permeability of ALI tissues often exceed those of submerged tissues; however, this was not the case in our experiments. This is most likely due to the tissues not having enough time to fully readapt to the culture after the passage to the ALI, i.e. when the apical medium is removed, an abrupt loss of apical nutrient supply occurs along with changes in oxygen levels, this adaptation phase could cause a momentary lag phase in the culture.
Overall, because of tissue differentiation enhancement, semi-ALI samples should be associated with higher cytoprotective tissue properties, therefore adverse effects linked to APAP exposures are expected to be lessened. Because there has been no documented assessment of the effect of direct APAP exposure on lung models *in vitro*, the only data we can use are the traditionally documented effects of APAP on liver cells. While Prot et al. reports that acetaminophen led to an EC50 at a 1 mM concentration for 72 hours of contact in HepG2/C3A biochips [8], the viability and functionality of Calu-3 tissues remain stable at 0.5 and 1 mM exposure. The absence of significant adverse effects could be due to the improved mucus production which could modulate the toxicity of APAP [29]. Since APAP is hydrophobic, the mucus may briefly and partially retain it. Therefore, reducing or at least delaying the exposure of Calu-3 cells to APAP might reduce its toxicity. However, there appears to be a progressive trend of dose-dependent toxicity causing increasingly subtle changes in mitochondrial activities and TEER.
Although our primary interest was not to study the effect of APAP on the pulmonary barrier per se because APAP medication is orally ingested, direct exposure to the pulmonary barrier has no physiological significance. It seems that the effect of APAP on the lungs is gaining interest as studies increasingly link chronic exposure to APAP to asthma

and COPD [341]. Therefore, the present findings could contribute to the growing body of knowledge on the mechanisms that APAP triggers to produce pulmonary toxicity.

3.6 Conclusion

To conclude, the utilization of cell lines benefited in generating robust and reproducible data making the interpretation of data clearer. The fact that bronchial and hepatic tissues were reconstructed respectively on culture inserts and biochips, facilitates their handling, and observation (transparent silicone for the biochip, semi-opaque membrane for the insert). Overall, the present data shows that the liver and lung constructs were successfully reconstructed as they resulted in differentiated and viable tissues. Both compartments metabolically respond to hepatotoxicant exposures while remaining viable throughout.

Chapter 4

Ensuring stable transition of monocultured pulmonary and hepatic compartments into a coculture setting

We have demonstrated the relevancy of the culture and reconstruction protocols, described in the Chapter 2, for the proper differentiation of bronchial, and hepatic tissues as constructs displayed distinct key organ functions, even though they were established from cell lines. Before joining both constructs in culture, some tests and adjustments were conducted to ensure that the culture conditions allowed to maintain the viability and the cellular and tissue functionalities of both compartments established in the Chapter 3. The coculture setting involves a common culture space where a common media flows continuously thanks to microfluidic perfusion. Within the framework of the project, and in the time allotted to us, we have chosen to study the following main parameters to monitor the evolution and adaptation of the tissues to the new culture mode:

- Choice and impact of a common coculture medium on tissue viability and functionality
- The effect of microfluidic perfusion on the development of the bronchial barrier
- Passive absorption potential of the cell culture equipment (e.g. coculture box, tubing)
- Recirculation of the common medium within the closed-circuit during the culture period

If any of the previously described parameters cannot be adapted to the coculture setting, they will be accounted for during result interpretation. The results presented in this chapter represent important technical input to better comprehend the biological phenomena at stake during coculture, and therefore allow for relevant interpretation as technical biases will be discriminated from cocultured-related biological responses. This will allow us to better define the functionality range of the device.

4.1 Choosing a relevant common media to support functional hepato-pulmonary coculture: characterization of hepatic biochip culture in RPMI 1640 supplemented media

Many culture media have been developed, and are available on the market, making the *vitro* culture of many different cell types possible. The composition of the media is based on key components, such as buffering agents (regulates pH), carbohydrates (source of energy), amino acids (source of energy), salts (maintains osmotic balance), proteins (e.g. albumin, transferrin), lipids, and vitamins (essential to cell growth and proliferation). The ratio of these constituents vary according to cell culture needs. Media are considered "defined" if their composition is known and determined.
RPMI 1640 is a general-purpose media used to culture a broad range of cells (in Chapter 2) for the culture of Calu-3 has also been reportedly used for the culture of hepatic cell lines [342]. As the Calu-3 RPMI-based culture media is richer in supplements and additives than the HepG2/C3A MEM-based media, we chose to test its potential as a coculture media, by testing its compatibility for the culture of HepG2/C3A.

4.1.1 Non-exposed dynamic culture condition

All biochips are seeded in the same MEM-based culture medium, which explains why phase contrast microscopy shows that cell adhesion is the same in all biochips at d1. After 72 hours of monoculture, under the same dynamic culture conditions as described in Chapter 3, no visible change occurred in terms of cell density in the microchannels and microchambres of the MEM-based and RPMI-based hepatic biochips cultures. The proliferation of HepG2/C3A cells seemed to follow the same trend as in their native MEM-based medium (Fig 4.1).

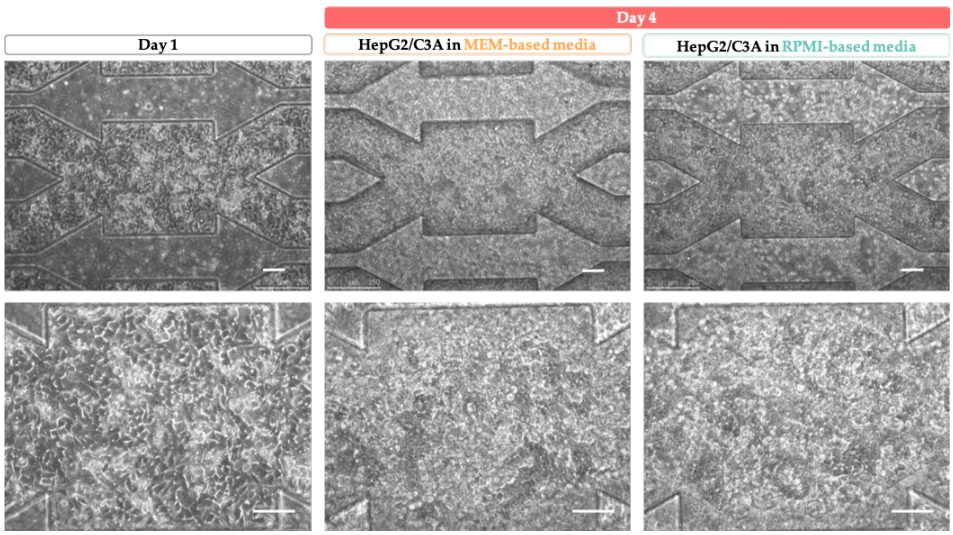

FIGURE 4.1: Phase contrast microscopy of monocultured HepG2/C3A biochips on day 1 and day 4 after 72-hour dynamic culture in MEM-based or RPMI-based culture medium. (Scale bar = 100 μm).

These qualitative observations were paired to quantitative cell counts. Results show a slight decrease of cells when HepG2/C3A are cultured in a RPMI-based medium compared to the cell count of MEM-based biochip cultures, however this was not significant (Fig 4.2).

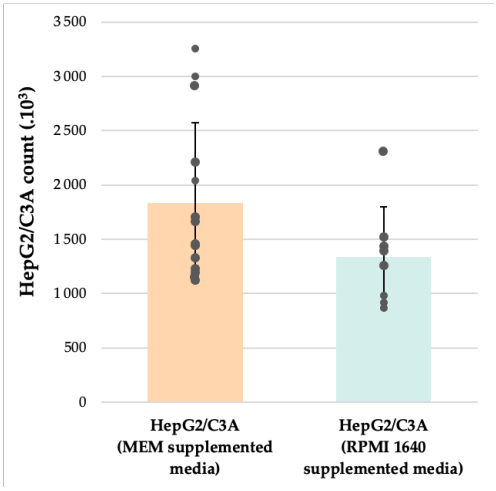

FIGURE 4.2: Monocultured HepG2/C3A cell count according to culture media. Statistically analyzed by unpaired t test. $n \geq 6$.

Albumin synthesis rates were investigated (Fig. 4.3A) to explore hepatic differentiation. Even though cells cultured in RPMI-based medium continued to secrete albumin, measurements revealed that the medium impacted the production rates. The Mann-Whitney statistical test revealed a significant decrease between both culture media. Hepatic tissues cultured in RPMI-based medium secrete on average 3 times less, the values dropped from 186 ± 129 to 60 ± 43 ng/10^6 cells/h. Mann-Whitney's statistical test revealed that the drop was significant.

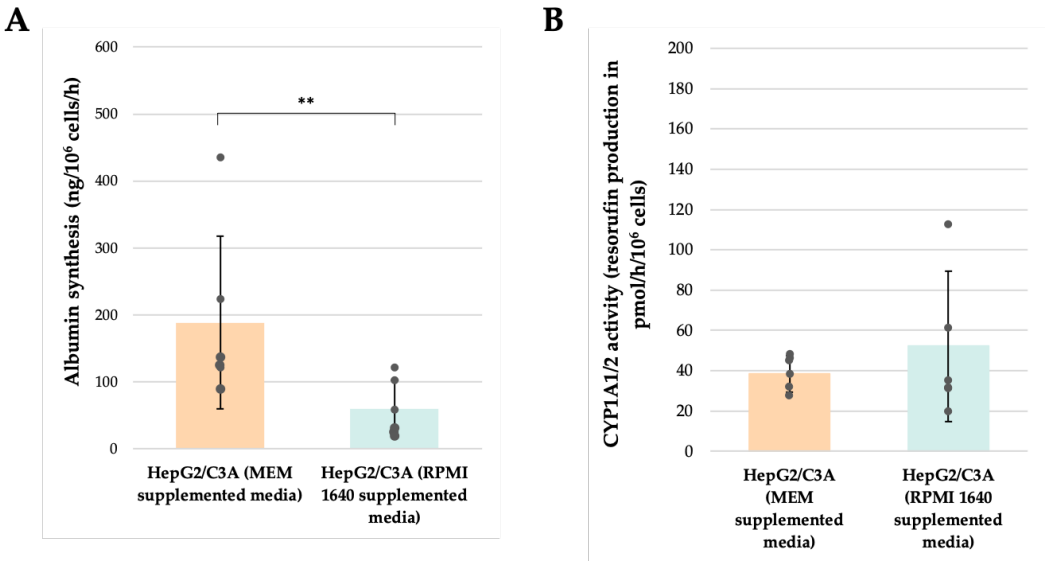

FIGURE 4.3: Metabolic insight of HepG2/C3A biochips according to culture medium. (A) Albumin secretion rates. (B) CYP1A1/2 activity. Statistically analyzed by Mann-Whitney test. $n \geq 3$.

To test whether the change in medium stimulates the metabolic activity of HepG2/C3A cells, CYP1A/2 activity was measured (Fig 4.3B). Although the standard deviation was large, the metabolic activity levels of cells grown in MEM-based and RPMI-based media were similar, respectively at 39 ± 9 and 52 ± 37 pmol/10^6 cell/h. Thus, the medium change did not induce an induction of the detoxification metabolism of HepG2/C3A.

4.1.2 Dynamic hepatotoxic exposure culture condition

After documenting the effect of culture medium on the basal state of hepatic cells, the impact of medium change was investigated under stress conditions, i.e. exposure to APAP. The results presented in the Chapter 3 showed that the effects imposed by APAP exposure are roughly the same at 1.5 mM or 3 mM, which is why we chose to work with a 3 mM APAP exposure in the context of the tests carried out to select the culture medium. APAP exposure induced the same type of cell confluence in both MEM and RPMI-based cultures. Even though cell morphology is hardly distinguishable because of high cell density, phase contrast microscopy does not reveal any more major notable differences in between culture settings (Fig. 4.4).

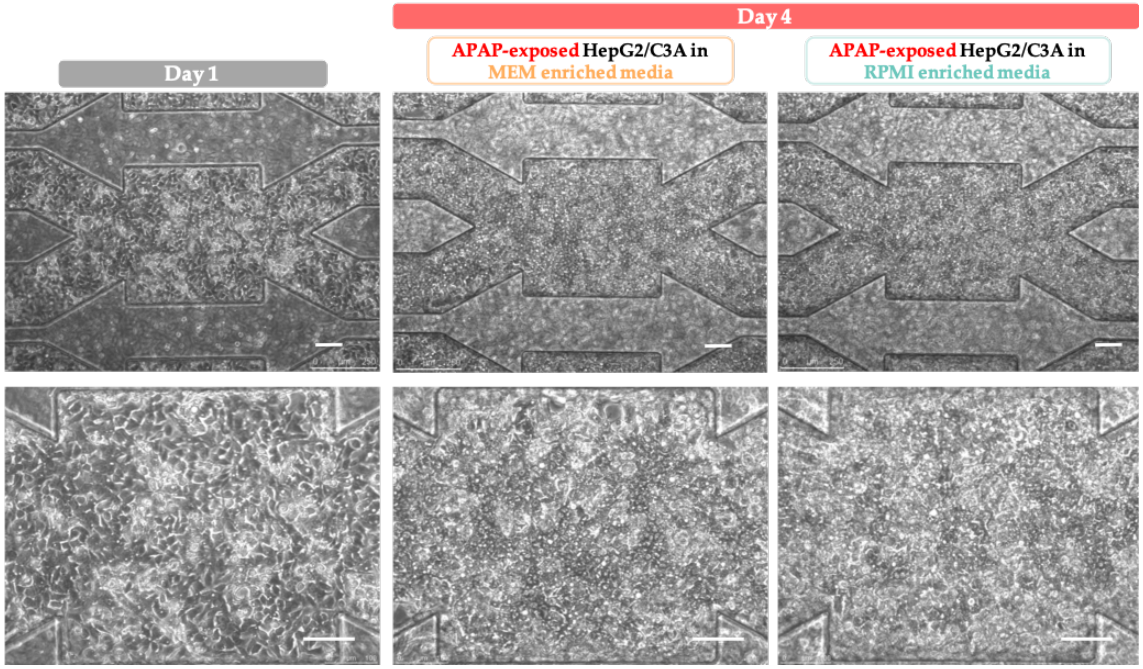

FIGURE 4.4: Phase contrast microscopy of monocultured APAP-exposed HepG2/C3A biochips on day 1 and day 4 after 72-hour dynamic culture in MEM-based or RPMI-based culture medium. (Scale bar = 100 μm).

Similarly, to the observations in Fig. 4.4 the results of cell counts showed that the culture medium did not further disrupt the perceived hepatotoxic stress of HepG2/C3A. Mean values approached 600,000 cells per biochip at d4 after 72 hours of continuous exposure (Fig 4.5A). Regarding the metabolic response, the induction of CYP1A1/2 activity (Fig 4.5B) was impacted by the change of medium. Indeed, the cells show on average an activity nearly 2 times higher than in MEM-based medium.

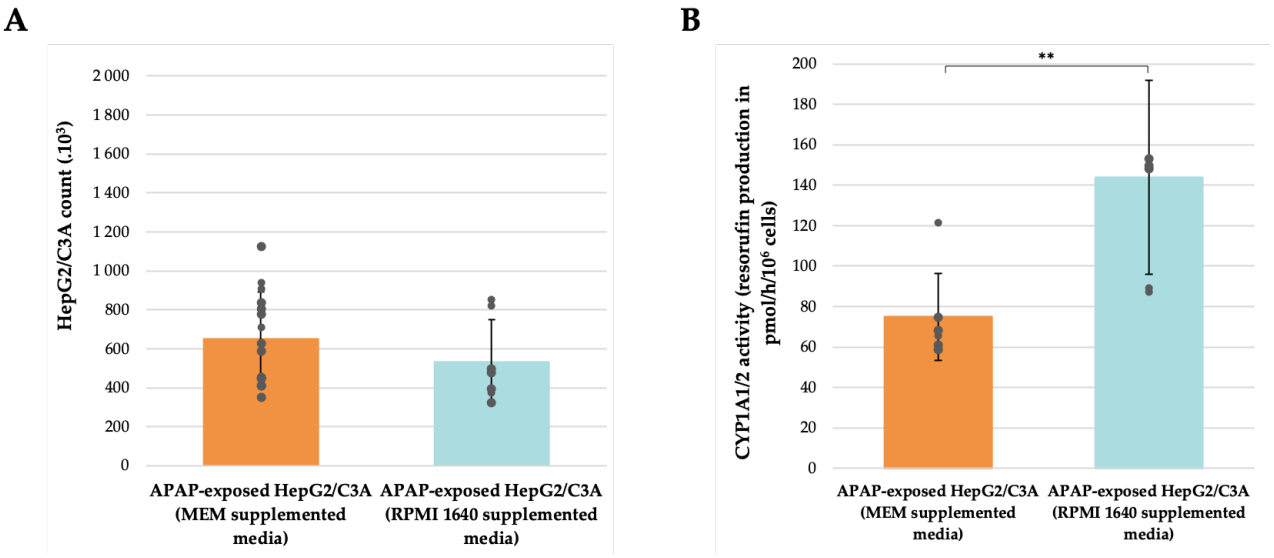

FIGURE 4.5: Monocultured APAP-exposed HepG2/C3A biochip (A) cell count and (B) CYP1A1/2 activities according to culture media. Statistically analyzed respectively by (A) unpaired t test and (B) Mann-Whitney test. $n \geq 3$.

Thus, it appeared that culturing HepG2/C3A exposed to APAP in RPMI-based medium does not elevate mortality but changes the way cells respond to stress.

4.2 Assessing the effect of dynamic flow on the epithelial barrier

Calu-3 bronchial tissues have so far been classically grown in static culture conditions. In contrast to monoculture settings, the culture medium dynamically circulates through the coculture box to facilitate communication between the various tissue compartments. Only the basolateral side of the bronchial barrier perceives medium perfusion, which is continuously maintained during the entire culture period. To comprehend the impact of flow on the bronchial barrier, coculture-specific dynamic culture conditions were replicated and adapted to a Calu-3 monoculture setting. Viability and barrier function properties were investigated. To gain perspective on the matter, the experiments were carried out on Calu-3 submerged tissues, both unexposed and 15 mM-exposed to APAP (for the same reasons as previously stated in section 4.1.2), and semi-ALI-grown tissues. Because the exposure doses (0.5 and 1 mM) did not elicit any particular biological responses in semi-ALI-cultured tissues, none of the APAP-exposed semi-ALI tissues were evaluated for this study (cf. Chapter 3). As a result, unexposed semi-ALI tissues were considered to be sufficiently representative of this group of cultures.

4.2.1 Culture conditions affect the morphology of Calu-3 tissues

After 72 hours of basolateral perfusion, Calu-3 tissues remained cohesive and confluent (Fig. 4.6). In contrast to what was previously observed in static culture, APAP no longer

incited morphological change when exposure was coupled to dynamic tissue culture. Indeed, although cells were hardly distinguishable because of the confluence of the tissue, the difference in cell refringence that was observed following exposure in static conditions for submerged tissues did not persist in dynamic conditions. The impact of the culture mode was also noticeable in samples grown in semi-ALI conditions. The cell relief that appeared as aggregates under static conditions appeared much more intense and homogeneous under dynamic culture conditions.

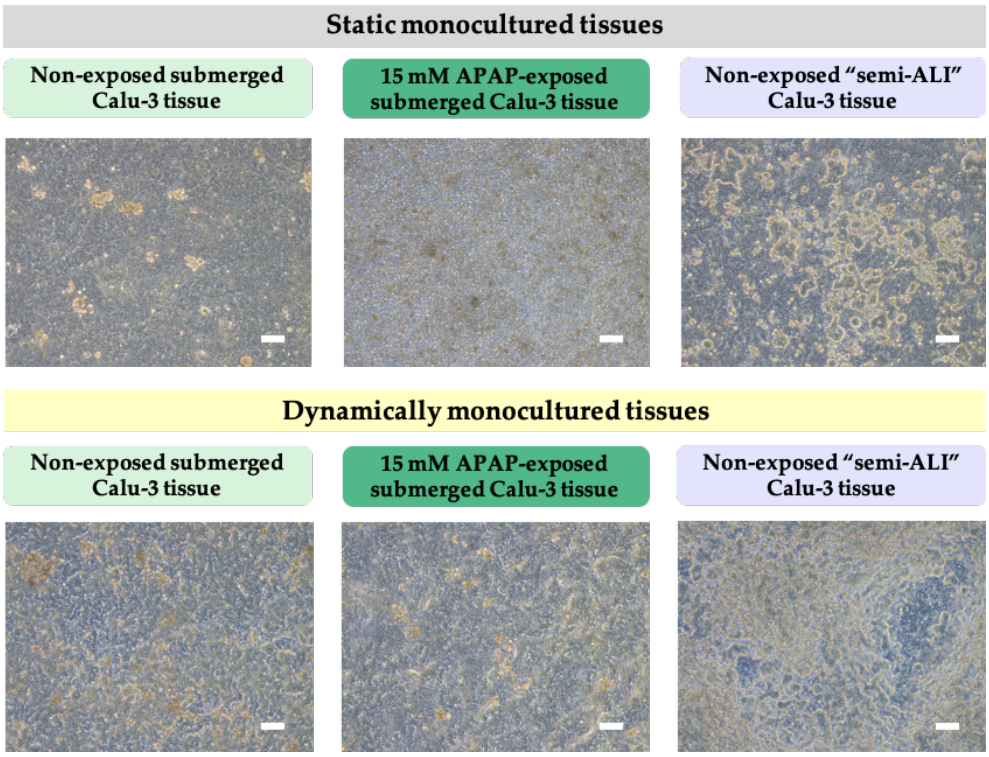

FIGURE 4.6: Phase contrast microscopy observations of submerged and semi-ALI Calu-3 bronchial tissue constructs according to culture conditions and APAP exposure. (Scale bar = 100 μm).

These morphological differences were confirmed when Claudin-1 and E-Cadherin cell junctions were immunolabeled. The samples displayed in (Fig. 4.7) were nor stained or imaged at the same time, for this reason, only localization of stainings can be compared. While it was observed that APAP exposure and ALI culture conditions caused a change in labeling in static culture conditions, this was no longer the case for dynamically cultured tissues. Not only were the labelings much less diffuse and more localized to the intercellular zone, but they were also far better preserved across exposures than what was observed under static conditions. Moreover, it appeared that exposure to APAP had much less impact on dynamically grown tissues. Indeed, while APAP caused an increase in cell size under static conditions, dynamically grown tissues maintained similar cell sizes to unexposed tissues even though cellular phenotypes displayed an elongated shapes. Thus, it seemed that flow contributed to the retention of the morphological features of the bronchial tissues under stress conditions. Regarding semi-ALI tissues, the localization of

E-Cadherin labeling remained similar between culture modes, except that Claudin-1 labeling appeared much less diffuse in dynamically cultured samples. It seemed that the effects of the flow are less perceptible on tissues grown in semi-ALI than in submerged conditions.

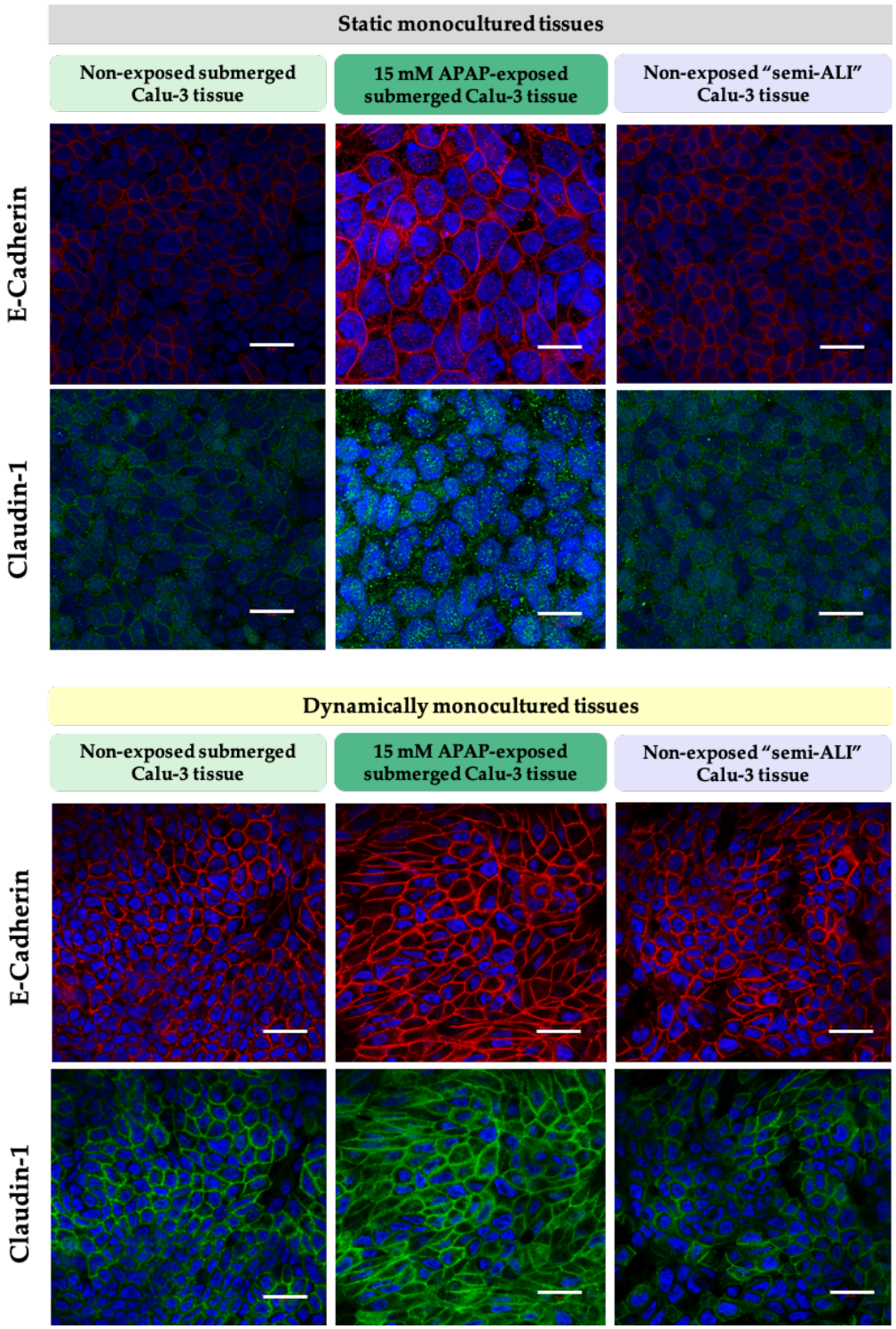

FIGURE 4.7: Confocal microscopy imaging of nuclei (blue), E-Cadherin (red) and Claudin-1 (green) immunostained adherens and tight junction complexes in Calu-3 tissues on day 14 according to culture conditions and APAP exposure. Scale bar = 20 μm).

4.2.2 The flow does not interfere with basal Calu-3 metabolism

In the same way that perfusion improved the morphology of Calu-3 tissues, it also contributed to the maintenance of cell viability, as shown in Figure 4.8. The collected data showed that measurements of mitochondrial activity were similar to those in static cultures, as unpaired t-test analysis revealed no significant differences between culture settings. The exposure of APAP leading to decrease in resorufin production observed in static culture conditions persisted in dynamic culture conditions.

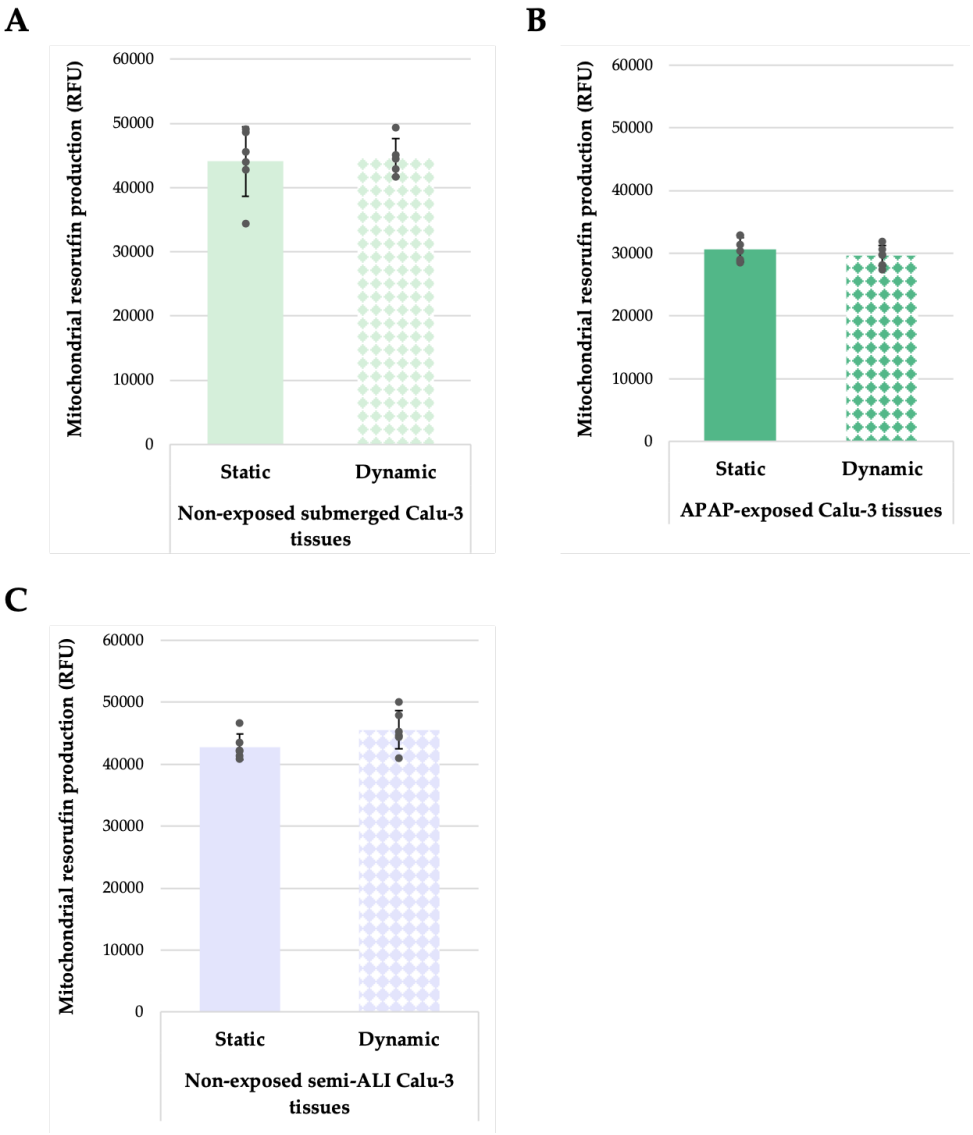

FIGURE 4.8: Relative mitochondrial activity of monocultured non-exposed submerged (A) and semi-ALI (C), and APAP-exposed submerged (B) Calu-3 bronchial tissues, measured by *PrestoBlue*^{TM} through fluorescent resorufin production, on day 14 according to culture conditions and APAP exposure. Statistically analyzed by unpaired t test. $n \geq 5$.

4.2.3 Dynamic flow tends to empower bronchial resilience to stress

To investigate the effect of basolateral perfusion on the barrier function of Calu-3 tissues, TEER measurements, Lucifer Yellow permeability assays, PAS labeling, and MUC5AC mucin assay were performed.

TEER measurements confirmed that the cohesive reconstruction of the bronchial barrier carried on despite the change in culture conditions, as the culture mode did not cause any significant fluctuations in TEER of submerged and semi-ALI-cultured control samples (Fig. 4.9).

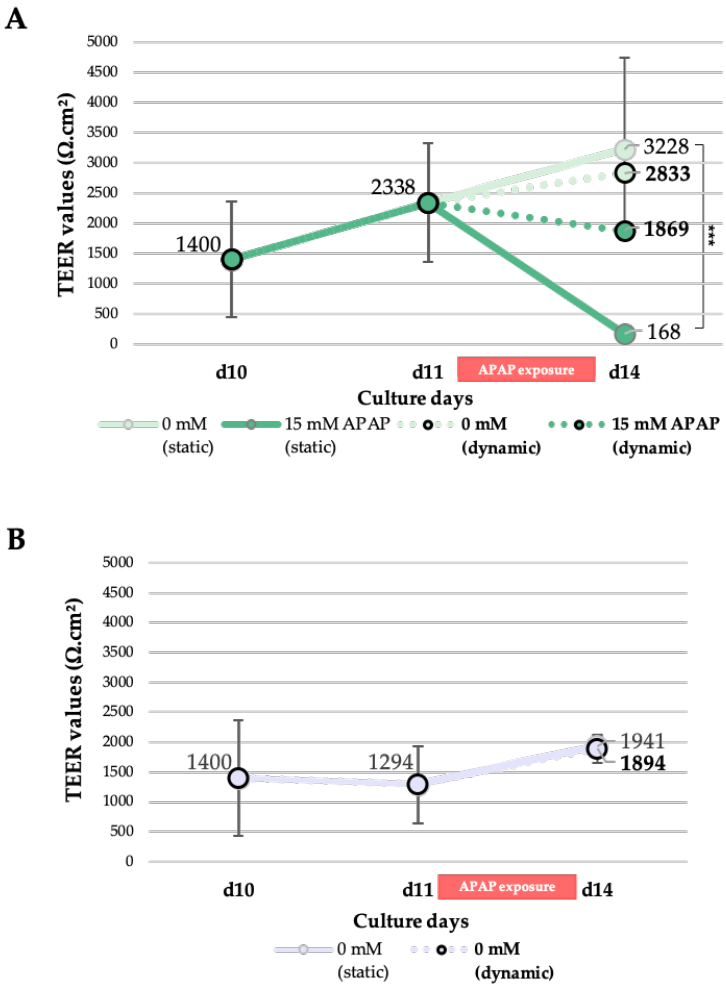

FIGURE 4.9: TEER measurements of (A) submerged and (B) semi-ALI cultured Calu-3 bronchial tissues according to culture mode and APAP exposure. Statistically analyzed respectively by (A) Kruskal Wallis and (B) Mann-Whitney tests. $n \geq 5$.

The TEERs of static submerged Calu-3 cultures were significantly higher than those of semi-ALI tissues. This gap persisted under dynamic culture circumstances, but decreased. The dynamic culture setting also benefited the maintenance of barrier integrity in the face of a stress-induced environment as no TEER disruption was reported following APAP exposure of submerged tissues, as opposed to what had been reported in static cultures.

Indeed, the substantial statistical significance between TEER values of non-exposed and APAP-exposed submerged samples was lost under a dynamic culture setting (Fig. 4.9A). The apparent permeability data obtained from Lucifer Yellow assays supported the previously described TEER results (Fig. 4.10).

		Papp ($x10^{-6}$ cm.s^{-1})		Permeability rate (%)	
		Static monoculture	*Dynamic* monoculture	*Static* monoculture	*Dynamic* monoculture
Cell free culture insert *Apical* permeability		60,581		100	
Submerged	**0 mM**	0,029 ± 0,02	0,023 ± 0,02	0,05	0,04
	15 mM	3,736 ± 1,09 ***	0,049 ± 0,01	6,17	0,08
Semi-ALI	**0 mM**	0,033 ± 0,03	0,050 ± 0,07	0,05	0,08

FIGURE 4.10: Papp values of static and dynamic Calu-3 bronchial tissue cultures measured through the transport of 100 µg/mL Lucifer Yellow (from the apical to the basal compartment). Statistically analyzed by Kruskal Wallis test. $n \geq 5$.

While APAP initially caused a 120 fold increase of permeability in submerged tissues, their dynamic counterparts maintained similar permeability to unexposed tissues. Regarding semi-ALI tissues, Kruskal-Wallis statistical analysis did not reveal any fluctuation in Papp values between static and dynamically cultured tissues. Not only did the culture mode change not perturb barrier function but it seemed that perfusion had the potential to empower tissue resistance to stress.

PAS labeling allowed for visually assessing the presence and organization of mucins found on the surface of Calu-3 tissues. The macroscopic images in Fig 4.11 showed that although static submerged and semi-ALI tissues displayed similar labelings, it seemed that a subtle difference in color dispersion began to appear on semi-ALI constructs.

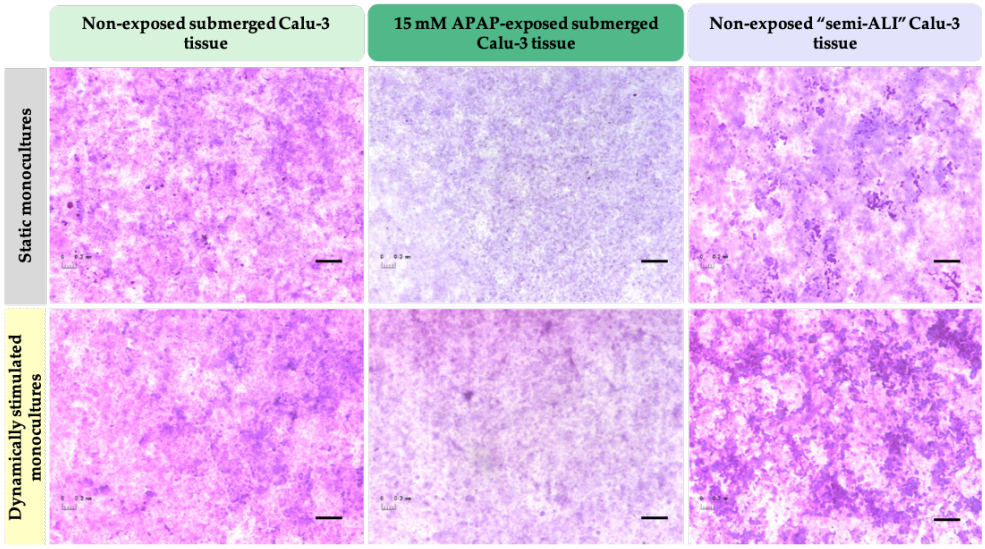

FIGURE 4.11: Brighfield macroscopic imaging of PAS staining of Calu-3 bronchial tissue surfaces according to culture settings and APAP exposure. Scale bar = 400 μm.

Dynamic culture conditions further revealed these staining differences as staining patterns of submerged samples remained diffuse and homogeneous throughout the tissue while semi-ALI barriers displayed more intense and cluster-structured stainings. The decrease in staining intensity associated with APAP exposure remained the same as in the static culture conditions. PAS staining revealed that dynamic culture settings induce similar mucin-related behaviors but overall intensified the concentration and dispersion patterns.

ELISAs were used to detect MUC5AC in cell supernatants (Fig. 4.12). The results showed that the concentration of dosed mucins decreased drastically for all cultures tested, especially for the unexposed submerged and semi-ALI controls.

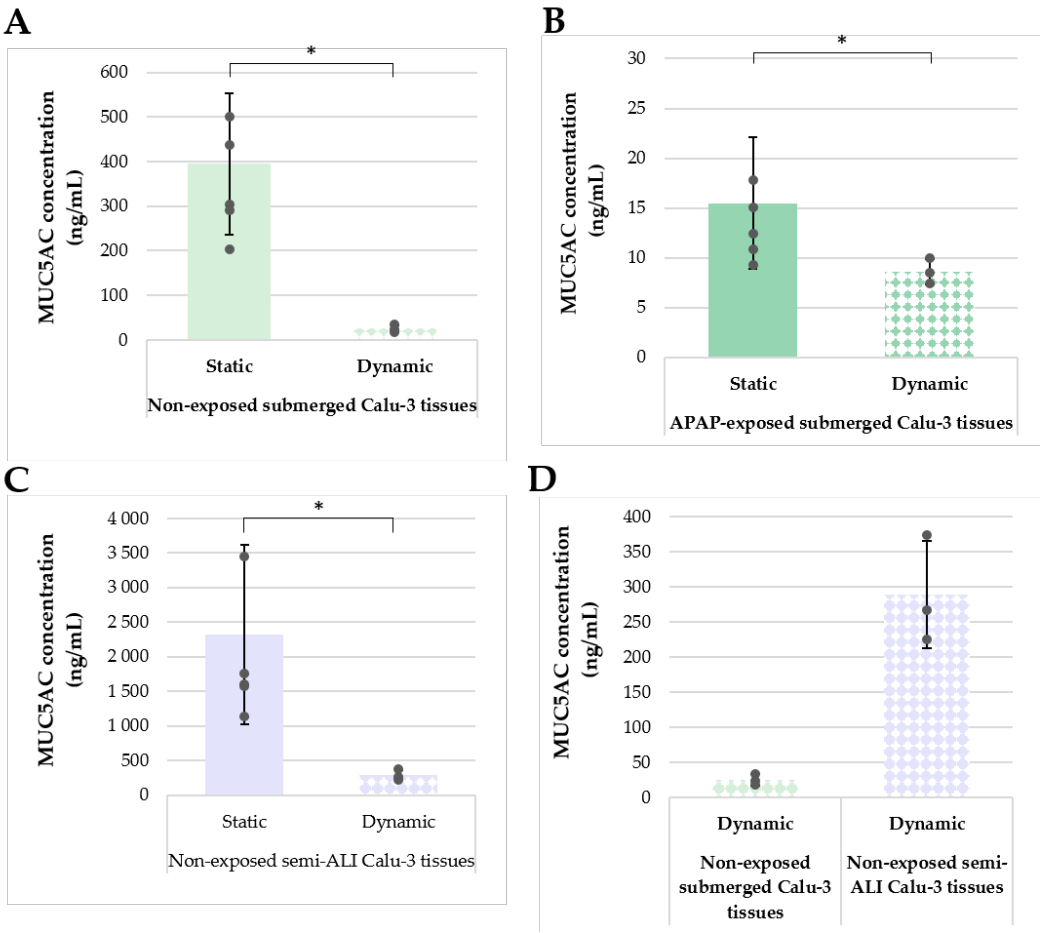

FIGURE 4.12: Measurements of MUC5AC concentrations of non-exposed submerged (A), non-exposed semi-ALI (C), and APAP-exposed submerged (B) Calu-3 bronchial tissues according to culture conditions. (D) compares MUC5AC concentrations of dynamically cultured non-exposed submerged and semi-ALI samples. Statistically analyzed by Mann-Whitney test. $n \geq 2$.

Indeed, measurements revealed that concentrations dropped respectively on average from 395 to 25 and 2318 to 289 ng of MUC5AC per mL. Even though the assays were performed on a small number of samples, the results indicated that the flow impacted the mucins of Calu-3 tissues. Even yet, MUC5AC concentrations in semi-ALI tissues

were on average 11 times higher than in submerged tissues (Fig. 4.12D).

4.3 Considering potential cell culture equipment bias

4.3.1 Investigating passive uptake of APAP by the coculture equipment

The goal was to investigate whether the culture equipment (IIDMP coculture box, culture insert, biochip, tubing) could induce possible biases by passively absorbing a part of the exposed APAP during the culture period. This kind of phenomenon would impact the exposure conditions as it would consequently reduce the fraction available to the cells. For this, the coculture conditions were recreated but in an acellular environment, and the culture supernatants were recovered at the end of the experiment to analyze their APAP content by mass spectrometry. The 1.5 and 3 mM APAP exposure conditions were tested for this purpose.
The results are presented in Fig. 4.13 They show that the concentrations initially introduced in the system at t0 are found at the same concentrations after 72 hours of dynamic culture.

		APAP (mM)
Apical	**1.5 mM**	1.3128
Basal		1.3518
Apical	**3 mM**	2.7189
Basal		2.6675

FIGURE 4.13: Mass spectrometry measurements of APAP levels after 72 hours of acellular culture in the IIDMP box. n = 1.

These findings imply that even at the greatest exposure levels, APAP is not absorbed by the culture equipment.

4.3.2 Estimating recirculation of APAP through the coculture system

As the coculture medium circulates in a closed circuit continuously for 72 hours, it was necessary to determine the basolateral permeability of the cellularized culture insert to assess whether recirculation and therefore re-exposure of the tissue to APAP and its associated metabolites was possible. To do so, Calu-3 monocultures were grown under coculture conditions, in the same way as for the tests previously presented in the section 4.2. They were collected at the end of the culture period and used for Lucifer Yellow tests. Instead of measuring the transport of the reagent from the apical to the basal compartment, Lucifer Yellow was introduced into the basal side of the insert to assess the transport from the basal to the apical compartment to assess basal-to-apical permeability. Measured Papp values are indicated in Figure 4.14. Even though the rates were low, the results show that the tissues also supported basal to apical transport. The basal permeability was even higher than those measured apically (cf. 4.2.3). The permeability did

		Papp ($x10^{-6}$ $cm.s^{-1}$) *Basal-to-apical permeability coefficient*	Permeability rate (%)
Cell free culture insert *Basal* permeability		24,267	100
Submerged	**0 mM**	0,058 ± 0,08	0,241
	15 mM	0,071 ± 0,03	0,291
Semi-ALI	**0 mM**	0,108 ± 0,10	0,446

FIGURE 4.14: Papp values of dynamically monocultured Calu-3 bronchial tissues measured through the transport of 100 µg/mL Lucifer Yellow (from the basal to the apical compartment). n = 2.

not seem to be affected by high exposure concentrations, but it appeared to be sensitive to the culture mode since the semi-ALI tissues had a permeability almost twice as high as the submerged tissues.

4.4 Discussion

4.4.1 APAP bioavailability features in the coculture setting

The quantification of APAP concentrations within the acellular coculture platform confirms the previously documented data by T. Bricks [343] which reveals that the materials of the present culture equipment don't absorb APAP passively and therefore that the bioavailability of paracetamol in coculture conditions remains the same as the initial exposure. The observed experimental biological effects can therefore be related to the theoretical exposure concentrations.

4.4.2 Adapting HepG2/C3A biochip culture to RPMI-based culture

The lung and liver compartments are reconstructed based on distinct protocols involving different culture media. As the coculture model is in the early stages of development and the choice of culture medium is a full-fledged study, the optimization of the culture medium composition was not yet a primary focus. This kind of investigation belongs to later stages of model optimization. Nevertheless, as the coculture model is intended to study the interaction between both tissues, the common media should only minimally interfere with tissue viability and differentiation features.
We started by characterizing the effect of RPMI-based medium (Calu-3 culture medium) on HepG2/C3A monoculture. Although there was a large dispersion of data, it does not appear that the medium induces cell death or increased CYP1A activities, which means that the cells did not seem to perceive any cytotoxicity or cellular stress. Indeed, as CYP1A play a prominent role in the oxidative metabolism of xenobiotics, their activation would mean that the cells could be detoxifying the culture media. However, hepatic albumin secretion is reduced in RPMI-based medium, which could mean that HepG2/C3A differentiation was impacted by the medium change. To test whether this

presumed dedifferentiation could affect the cellular stress response, HepG2/C3A cells were treated with 3 mM APAP for 72 hours in RPMI-based medium. The results show that the medium change did not cause increased mortality rates however did seem to induce higher activation of CYP1A detoxification activities. Even if the induction values seem higher in RPMI-based monocultures, they remain in the same range as those of similarly cultured and exposed HepG2/C3A biochip monocultures [7], i.e. even though the measured activity is more intense, it does not appear abnormally high. The key aspect is that the behavior of HepG2/C3A cells in RPMI-based medium remains the same as in MEM-based medium, i.e. HepG2/C3A biochips remain sensitive to APAP exposure and the induction intensity between untreated and APAP-treated samples is similar. Moreover, due to the size of the standard deviations and the lack of experimental replicates, we cannot definitively conclude that the RPMI-based medium induces lower albumin secretion rates and higher CYP1A activities in HepG2/C3A biochips.
Even if the coculture medium could be further optimized to ensure complete preservation of the original MEM-based hepatic functions, the cellular behaviors of HepG2/C3A in both tested media remain comparable, indicating that the cells are capable of adapting to the change in media, thus RPMI-based medium can be used for coculture purposes.

4.4.3 Identifying coculture setting bias

In vivo, the bronchial region predominantly undergoes compressive cyclic motions caused by bronchoconstriction, as they participate in the breathing motions that bring the air in and out of the respiratory system [344]. In the context of our project, the mechanical stimulation of the lung compartment is minor, under coculture conditions Calu-3 culture inserts are embedded within a microfluidized circuit, therefore the generated sheer stress only concerns the basal region of the membrane, imposing indirect frictional forces to the epithelial barrier. However, because the physical microenvironment locally sensed by cells has been documented to contribute to their differentiation (e.g. substrate stiffness, cyclic stretch, air-liquid interface) it was important to verify how the basal flow affected the development of the Calu-3 compartment.
Even though submerged and semi-ALI tissues react differently to flow, dynamic culture appears to promote improved epithelial development. Immunostainings show significantly enhanced labeling localization of adherens (E-cadherin) and tight (Claudin-1) junctions, creating a network of continuous intercellular junctions at their native cell-cell contact sites, which could lead to a better tissue differentiation and functionality through an enhanced tissue polarization as tight and adherens junctions reportedly interact to establish apical–basal epithelial cell polarity [345]. The fluorescent labelings also appear more contrasted, the shaded areas do not reflect discontinuities but rather the relief of pseudostratified tissue, which further resembles *vivo* physiology. These observations are also visible on the phase contrast microscopy images. Immunostaining also reveals a morphological change in the cells shape, which appear to be slightly more elongated and flattened overall, which could be attributed to the fact that tight junction transmembrane proteins are linked to the actin cytoskeleton via protein complexes containing zonula

occludens (ZO) proteins. Thus, to determine if the flow causes a directional reorganization of the cytoskeleton, actin labeling may be employed. This epithelial architectural rearrangement might explain why submerged tissues are more resistant to APAP exposure. The considerable decrease in TEER and increase in permeability generated by the treatment do not translate to the dynamic culture state. However, despite the benefits of microfluidization of Calu-3 tissue culture, it appears that APAP continues to disrupt mucin metabolism in the same way as in static culture.

While APAP exposures have usually only been considered on the apical side of the bronchial barrier, it is presumed that within the coculture platform APAP and its associated metabolites recirculate continuously throughout the culture period, which would mean that the bronchial compartment could suffer a continuous re-exposure through its basal cell pole. The quantification of the basal permeability of the tissues indicates that such an APAP re-exposure is plausible as basal tissue permeability is superior to apical permeability, especially given the pores of the culture membrane are 0.4 um wide and APAP and NAPQI (cytotoxic metabolites) are respectively 49.3 and 46.5 $Å^2$ [337], [346] i.e. 4.93 et 4.65 nm^2 and could therefore readily breach the membrane and fall back into contact with the cells.

Overall, the adaptation of Calu-3 cells towards further physiological behaviors in dynamic culture settings is not surprising, despite their immortalized nature, as airway epithelial cells are known to respond *in vivo* to mechanical forces and control the airway response to applied loads by modulating key aspects of inflammation and produce factors that influence the activity of fibroblasts and smooth muscle cells [347]. Besides, it has been documented that dynamic culture has been used as a tool to emulate native microenvironments that enhance 2D pulmonary cultures [348].

Chapter 5

Analysis of hepatic and bronchial coculture dynamics in response to acetaminophen exposure for organ-to-organ interaction studies

Environmental, occupational, or other external airborne sources of pollution have been increasingly jeopardizing human health worldwide [1]–[3] propelling respiratory toxicology to the forefront [349].

Understanding biological mechanisms involved in the deterioration of human health due to air pollution could allow for further global risk assessment and management. Animal models are a reference tool for predictive studies of the toxicological effects of inhaled substances. However, in the European context of reduced animal testing (REACH, and the 3R rules), the development of reliable alternative methods has become a necessity. Conventionally used animal models have also demonstrated inter-species variability which challenges transferability of data from animal to human studies. *In vitro* models present as alternative candidates to fill these translational gaps [350]. They are simpler and less expensive to implement than *in vivo* models and allow working with human cells or tissues which allows for better approximation of *vivo* physiological conditions and therefore empowers their relevance for accurate predictability. However, limited extrapolation from *vitro* to *vivo* is often linked to a lack of complexity in cell culture models, particularly due to the absence of multi-organ crosstalks emulation. Restricted physiological pertinence of current *in vitro* assays prevents the implementation of alternative and more predictive methods in inhalation toxicology. Multi-organ-on-chip technologies seek to overcome these limitations by connecting several metabolically active and complex tissue entities within the same culture circuit to reproduce systemic *vivo* interactions. It is in this context that our project stemmed, here, we describe a model that enables *in vitro* coculture of a pulmonary barrier (route of entry of inhaled xenobiotics) with a detoxifying organ such as the liver. This approach allows to consider biotransformation of inhaled compounds and inter-organ crosstalks as possible modulators of toxicity and therefore acknowledges toxicity at a further systemic level when it comes to

evaluating associated risks and hazards of inhaled xenobiotics. Currently still in the development phase of the coculture model, experimental robustness was at the heart of the project. The present model was characterized using the previously described hepatotoxicant APAP. Exposure to the pulmonary barrier is not accurate but allowed us to visibly observe the passage and circulation of a xenobiotic through the device as APAP interfered with hepatic viability and metabolic performances. Moreover, previously obtained monoculture data gave us an insight into the individual specificity of each compartment's biological responses, therefore, new behavioral patterns could be directly associated with the synergic culture of hepatic and pulmonary compartments.
2 types of LuLi models were developed:

- The developmental model allowed for the technical setup of the coculture platform.

  This configuration comprised a classically cultured submerged Calu-3 bronchial tissue connected to a HepG2/C3A hepatic biochip. The chosen exposure concentrations for this model relied on documented hepatotoxicity thresholds, 1.5 mM and 3 mM, to allow better quantification of biological responses. These concentrations correspond to so-called "systemic" concentrations, to which the hepatic compartment will have access through the flow, following dilution into the circulating media. The concentrations of APAP locally deposited upstream on the barrier take into account the dilution of the total medium that follows. To reach systemic values of 1.5 mM and 3 mM the local exposures were set at 7.5 mM and 15 mM on the pulmonary side respectively (previously described in Chapter 2 Fig. 2.9).

- The physiological model allowed for further complexification of the model to better approximate a human *vivo* situation. The culture setup is the same as the previously described developmental model, however, includes an additional differentiation stage which comprises a bronchial air-liquid interfaced culture period. The exposure mode also was adapted, and liquid inoculation of APAP solutions was lowered to a smaller volume of 200 µL (previously described in Chapter 2 Fig. 2.11) to mimic further physiological exposure conditions. Locally deposited APAP concentrations for this model were set at 0.5 mM and 1 mM, because of solubilization threshold restrictions at this volume. Associated systemic concentrations, reaching the flowing circulation and the hepatic compartment, were respectively 12 μM and 24 μM.

Although the interactions between the lungs and the liver in toxicology are recognized [184], [187], [351], dedicated study models still rely on the use of *in vivo* tests. This chapter recapitulates the results and potential of our newly developed microphysiological system to study the absorption, distribution, metabolism, elimination and potential toxicity (ADMET) of airborne xenobiotics [352], [353].

5.1 The developmental model: a tool for the coculture platform validation

5.1.1 APAP passes the bronchial barrier, joins the systemic circulation and is metabolized by the lung/liver coculture

To verify that APAP is able to cross the bronchial barrier into the systemic circulation of the coculture platform, we quantified APAP levels in post-culture supernatants from lung/liver cocultures. Following the 72 hour coculture period, samples were taken from the apical compartment of the bronchial insert, and from the basal side which corresponds to the circulating culture medium. As a reminder, in order to reach systemic exposure concentrations of 1.5 mM and 3 mM, initial and local exposure concentrations were 7.5 mM and 15 mM respectively on the apical side of the Calu-3 barrier. The results are shown in Fig. 5.1 and revealed that APAP passed the bronchial barrier and reached the circulating medium as it was detected on the apical and basal side. The coculture systems reached equilibrium as the measured levels approached the theoretical concentrations of 1.5 mM and 3 mM.
In addition to APAP levels, the secondary metabolites APAP-SULF and APAP-GLU were determined. Both were found mainly in the basal compartments. They were found at the same final concentrations for the 1.5 mM and 3 mM exposures. This suggests that the lung/liver coculture was capable of metabolizing APAP at hepatotoxic exposure concentrations.

	Coculture			
	APAP exposure concentration (mM)	**APAP (mM)**	**APAP-GLU (mM)**	**APAP-SULF (mM)**
Apical	0	0,013 ± 0,008	0 ± 0	0 ± 0
Basal	0	0,005 ± 0,002	0 ± 0	0 ± 0
Apical	7.5	1,844 ± 0,587	0,039 ± 0,092	0 ± 0
Basal	1.5	1,872 ± 0,378	0,135 ± 0,140	0,0120 ± 0,0133
Apical	15	2,267 ± 1,259	0 ± 0	0 ± 0
Basal	3	3,178 ± 0,756	0,089 ± 0,122	0,0072 ± 0,0095

FIGURE 5.1: Mass spectrometry measurements of APAP, APAP-GLU and APAP-SULF levels in post-culture supernatants of bronchial and hepatic submerged cocultures according to APAP exposure.

5.1.2 Both compartments display higher viability compared to monoculture conditions

Because the results in Chapter 4, revealed that perfusion impacts the morphology of Calu-3 submerged tissues, cocultured tissue morphology presented in Fig.5.2 will be compared to dynamically monocultured tissues.
At the end of the coculture period, in an APAP-exposed or unexposed environment,

both compartments were collected and tissue morphology was observed through phase-contrast microscopy to assess the effects of exposure and culture conditions on tissue growth (Fig.5.2).
Calu-3 bronchial tissues remained confluent and cohesive under coculture settings, regardless of the stress-induced environment (co-cultured non-exposed samples in Fig. 5.2).

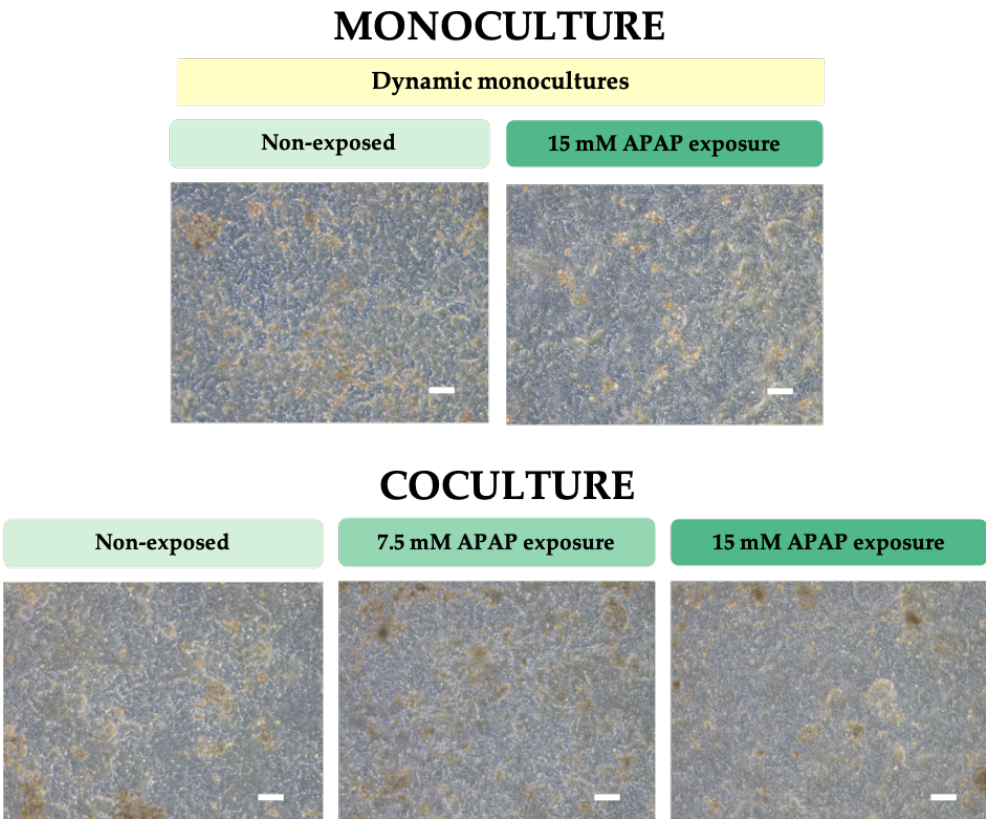

FIGURE 5.2: Phase contrast microscopy of monocultured and cocultured submerged untreated and 72-hour APAP-exposed Calu-3 bronchial tissues (7.5 mM APAP or 15 mM APAP) on day 14. Scale bar = 100 μm.

Overall their morphology remained unchanged, throughout both 7.5 mM and 15 mM APAP exposures, compared to monocultures. Indeed, where monoculture exposures led to a clear dose-dependent change in cell refringency (monocultured exposed samples in Fig. 5.2), this morphological pattern did not translate to cocultured tissues.
Cocultured bronchial tissues were also subject to PrestoBlue assays, to pair previously presented qualitative morphological observations (Fig. 5.2) with quantitative viability measurements. Monoculture and coculture results were compared back to back in Fig. 5.3.

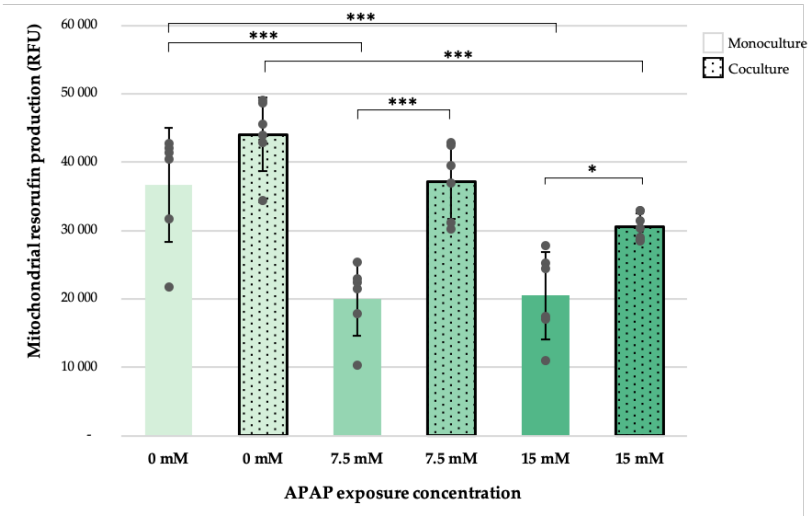

FIGURE 5.3: Bronchial mitochondrial activity of monocultured vs cocultured APAP-exposed submerged Calu-3 tissues measured by PrestoBlue^{TM} at d14 after 72h exposures. Statistical analysis assessed by Kruskal Wallis multiple comparisons. $n \geq 4$

Statistical analysis revealed that the exposure-dependent decrease of mitochondrial activity observed during monoculture exposures carried on to the coculture setting, although adverse effects were decreased. Metabolisms associated with 7.5 mM and 15 mM APAP exposures were significantly increased in the coculture setting. No dose-dependent effects were detected in monocultures, as both exposure concentrations significantly induced an activity drop. While coculture settings led to a significant drop only at 15 mM. In the same way, as for the pulmonary compartment, the hepatic biochip underwent a series of viability assessments to investigate the effect of coculture on tissue growth. In Fig. 5.4, we recapitulate microscopic observations of post-cocultured hepatic compartments.

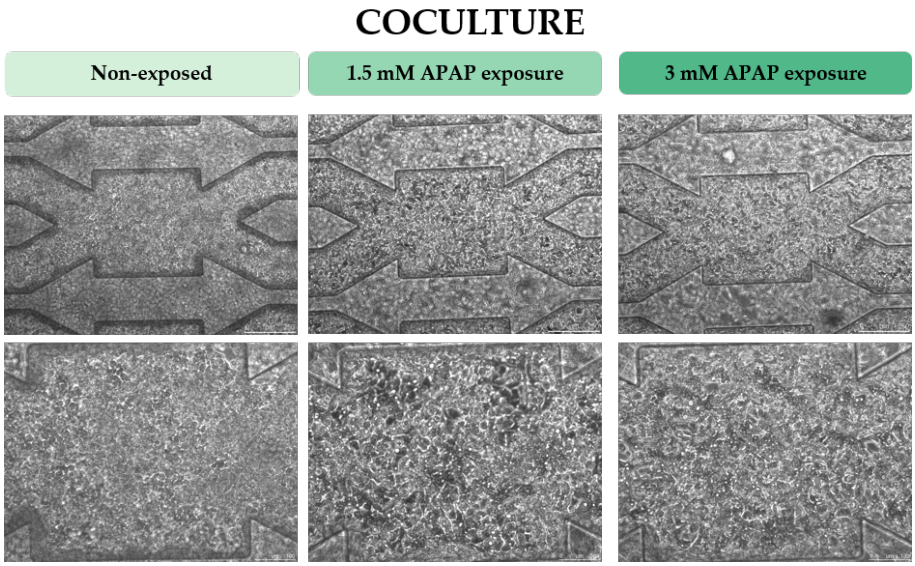

FIGURE 5.4: Phase contrast microscopy of cocultured untreated and 72-hour APAP-exposed HepG2/C3A biochips (1.5 mM APAP or 3 mM APAP) on day 4.

These results showed that the biochips remained confluent up until the end of the culture period, even when APAP was perfused through the platform. Typical cuboidal-shaped phenotypes, characteristic of hepatocyte-like HepG2/C3A cells, were recognizable. The tissue within biochips was dense but appeared to sparsen, in an exposure-dependent manner, as cell shapes seemed to be better distinguishable.

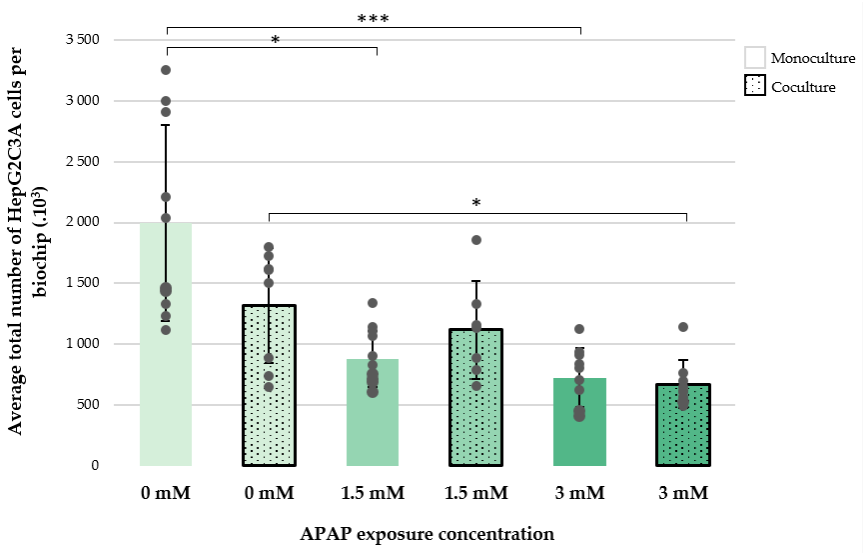

FIGURE 5.5: Evolution of monocultured vs cocultured HepG2/C3A cell proliferation according to APAP exposure concentration and culture mode (significance analyzed by Kruskal-Wallis Comparisons Test with post-hoc Dunn's test for multiple comparisons). $n \geq 3$

Similarly to the previously presented bronchial data trends, cell count (Fig. 5.5) showed that the dose-dependent drops induced by APAP in monoculture settings diminished in coculture configurations. Statistical analysis revealed alleviated differences between APAP-exposed cell counts as cocultured exposed biochips featured smaller cell count variations.

5.1.3 Coculture benefits the maintenance of bronchial barrier functions up to 15 mM APAP exposures

Based on the results previously described in Chapter 4, continuous perfusion during dynamic monoculture conditions has shown to influence the development of Calu-3 barrier. Therefore, the coculture TEER, Lucifer Yellow, MUC5AC and immunostaining results presented in this section were compared to dynamic rather than static monoculture data. Kruskal Wallis analysis showed that the coculture did not disturb the growth of the bronchial barrier, as no statistical significance was found between the means of the different culture modes. Resistance values remained high and were in the range of $2833 \pm 558\,\Omega.cm^2$ and $1443 \pm 583\,\Omega.cm^2$. The TEER gap between unexposed and APAP-exposed tissues decreased under coculture conditions. It seemed that the addition of a liver compartment to the bronchial culture might strengthen the integrity of the barrier under hepatotoxic stress conditions.

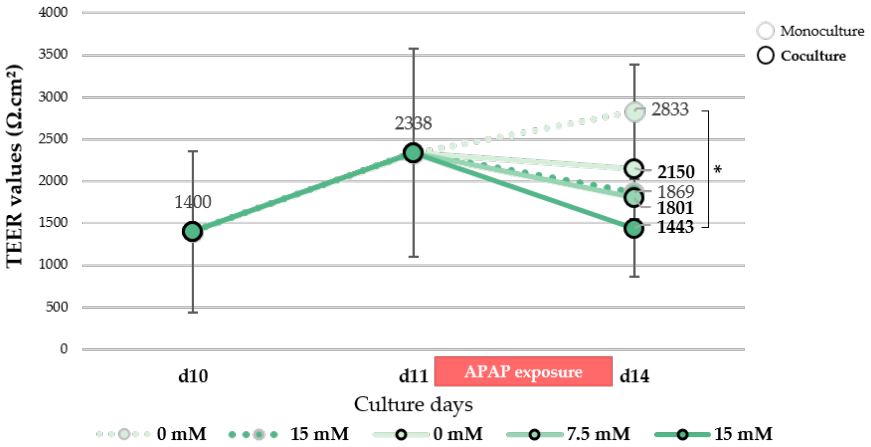

FIGURE 5.6: Transepithelial electrical resistance (TEER) measurement of monocultured and cocultured submerged Calu-3 bronchial tissues over time following 72h APAP exposures. Statistically analyzed by Kruskal-Wallis Comparisons Test. $n \geq 5$

Intercellular junction immunostainings allowed us to further depict the barrier integrity status of cocultured tissues. The samples shown in Fig. 5.7 were not stained or confocally imaged at the same time or following the same staining protocols. It is for this reason that the staining intensity between samples can not be compared, only the localization of stainings can be criticized.

Coculture seemed to impact the junctional architecture of Calu-3 tissues, regardless of APAP exposure, as Claudin-1 stainings appeared disrupted from their native peripheral localization compared to monocultured samples. However, with respect to the adherens E-Cadherin junctions, the associated stainings remained localized at the cell-cell interface without any diffusion. Moreover, APAP exposures no longer destabilized cellular phenotypical features of Calu-3 tissues (previously enlarged and elongated in monocultures), as exposed-cocultured tissues displayed similar cell size and shape to unexposed tissues. Therefore, coculture seemed to benefit the maintenance of bronchial phenotypical features and adherens junctional architecture in the face of hepatotoxic stress.

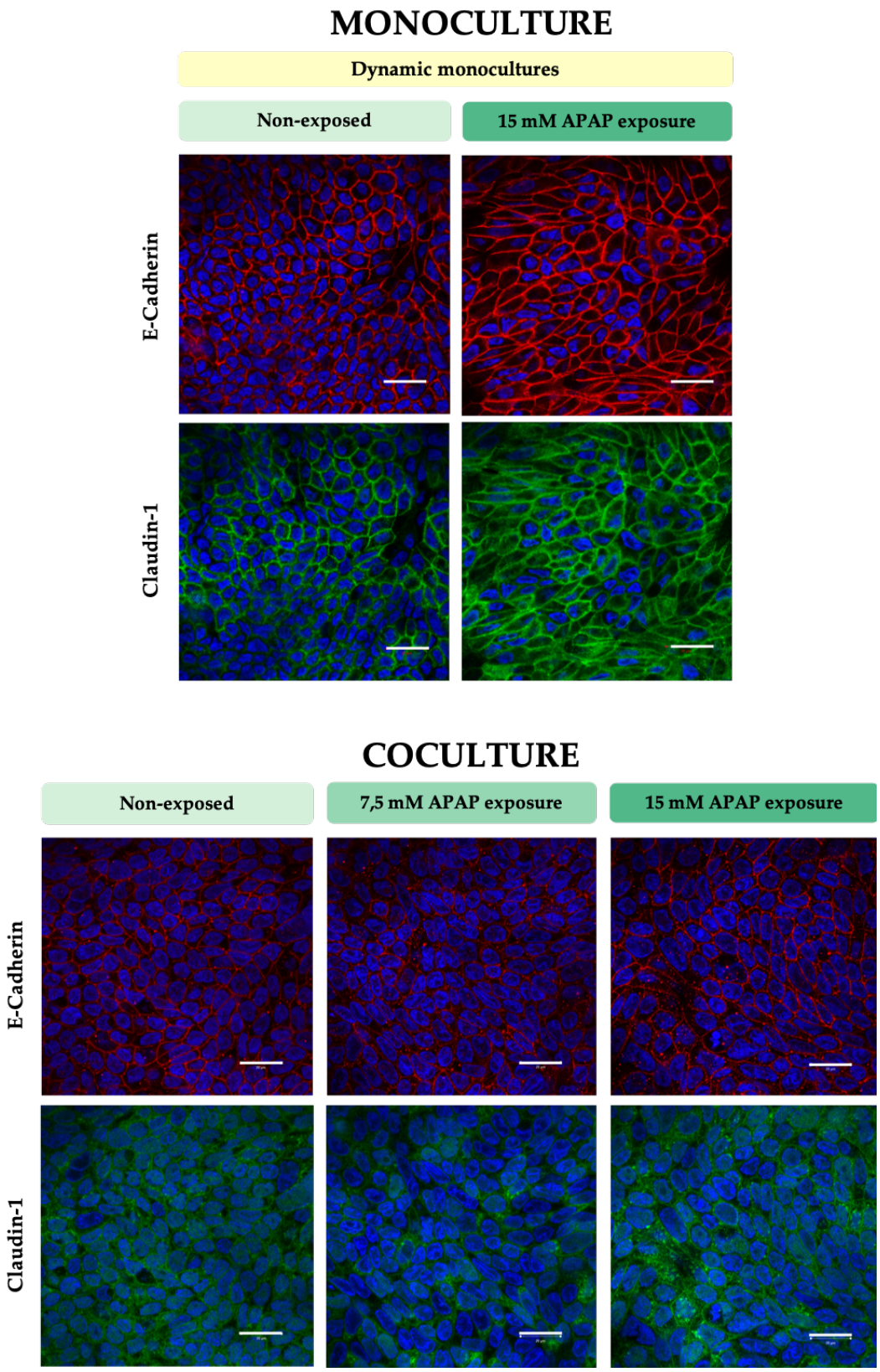

FIGURE 5.7: Confocal microscopy imaging of nuclei (blue), Claudin-1 (green) and E-Cadherin (red) immunostained adherens and tight junction complexes in submerged monocultures and cocultures of Calu-3 bronchial tissues at day 14 exposed and non-exposed to APAP. Scale bar = 20 μm).

To further investigate barrier functionality, Lucifer Yellow assays were carried out (Fig. 5.8). Even if there is no statistical significance in the Papp results because data was obtained on a limited number of samples, a tendency toward a slight increase in permeability from an exposure of 15 mM of APAP emerged in coculture settings. Overall, cocultured-bronchial permeability remained minimal, under 1%. Coculture did not disrupt the permeability of the barrier.

		Papp ($x10^{-6}$ $cm.s^{-1}$)	Permeability rate (%)
Cell free culture insert *Apical* permeability		60,581	100
		Monoculture	
	0 mM	0,028 ± 0,02	0,045
	15 mM	0,049 ± 0,01	0,081
		Coculture	
	0 mM	0,041 ± 0,04	0,067
Submerged	**7.5 mM**	0,052 ± 0,03	0,085
	15 mM	0,143 ± 0,08	0,235

FIGURE 5.8: Papp measurements of cocultured Calu-3 tissues compared to monocultures according to APAP exposure. Statistically analyzed by Kruskal Wallis test. $n \geq 3$

The apparent biological pattern observed in the Lucifer Yellow permeability results was reinforced by the results of the MUC5AC assays shown in Fig. 5.9. Indeed, the MUC5AC were not impacted by the culture mode as the concentrations of the unexposed cocultured tissues are similar to those of the monocultures. In the same way, as described in monoculture, APAP affects the MUC5AC of Calu-3 tissues, especially as of 15 mM exposures. These effects were exacerbated in coculture, as concentrations dropped from 8.603 ± 1.3 ng/mL to 0.075 ± 0.2 ng/mL, which represented a 115-fold decrease.

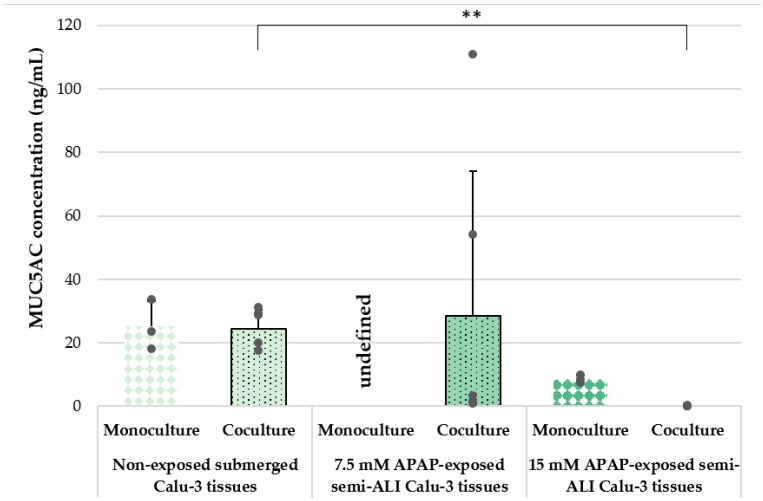

FIGURE 5.9: MUC5AC concentrations measured by ELISA in post-culture supernatants of submerged monocultured and cocultured Calu-3 tissues. Statistically analyzed by Kruskal-Wallis test. $n \geq 2$

5.1.4 Coculture improves and protects hepatic differentiation

The results presented in Fig. 5.10 compare the quantification of albumin, determined from post-culture supernatants, measured in monocultured and cocultured HepG2/C3A biochips. Although the amount of data collected was limited, particular biological behaviors emerged. The results suggested that coculture induced an increase in albumin synthesis of about 40 ng/10^6 cells/h compared to monocultures. While albumin concentrations decreased in monocultures following APAP exposure, these ratios did not change in coculture. Not only did coculture benefit albumin synthesis for HepG2/C3A biochips, but it also enhanced the resistance of the hepatic compartment to hepatotoxic APAP exposures.

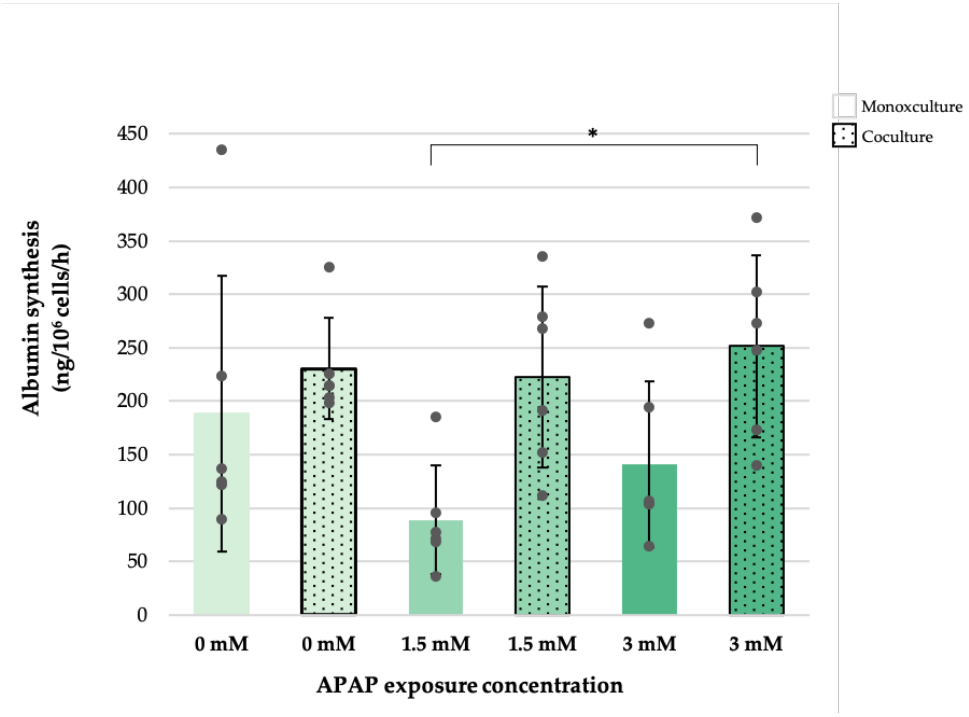

FIGURE 5.10: Albumin secretion rates of monocultured and submerged cocultured HepG2/C3A biochips according to APAP treatment. Statistically analyzed by ANOVA, Tukey-Kramer post-hoc multiple comparisons test. $n \geq 3$.

5.1.5 Coculture induces early hepatic xenobiotic metabolic responses to stress-induced environments

Here, we were interested in the metabolic activity of CYP1A1/2, from HepG2/C3A cocultured cells, involved in the metabolization of APAP in NAPQI [354][14].
The statistical analysis of data was performed in three steps, first independently, blue significance indicates monoculture data comparison, and yellow significance points to coculture data comparison. Monoculture to coculture data comparison is shown as the black significance.

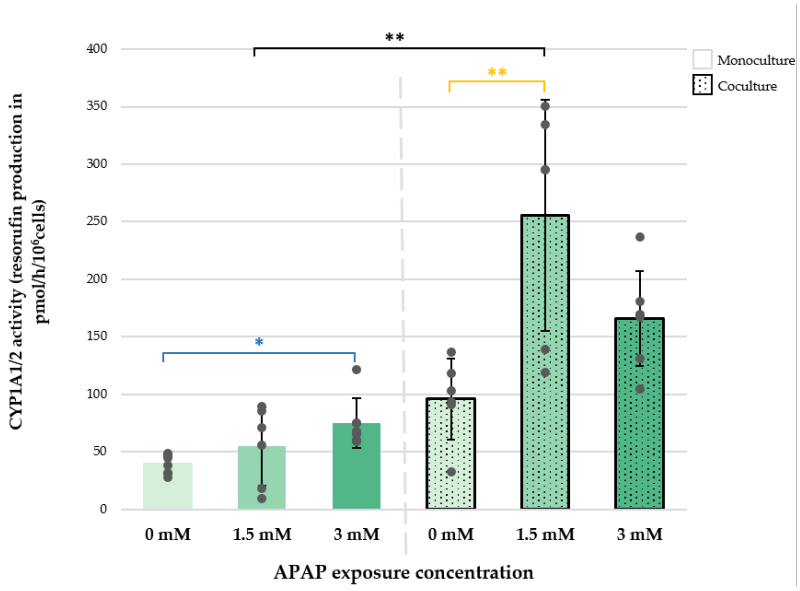

FIGURE 5.11: Comparison of CYP1A1/2 activities in monocultured and cocultured HepG2/C3A cells on day 4 according to APAP exposure concentrations. Statistically analyzed by Kruskal-Wallis test. $n \geq 3$.

Even though the results presented in Fig. 5.11 did not show any statistical significant increase, it seems that the culture mode influenced the metabolic state of the tissues as EROD values for both non-exposed cocultured controls were higher than monocultures. Upon contact with APAP, the biological responses differed according to culture conditions: cocultured HepG2/C3A cells were subject to an earlier induction of CYP1A1/2 activity at 1.5 mM APAP exposure concentration whereas the stimulation of the activity in monocultured cells only occurs at 3 mM. Moreover, at the same exposure dose (1.5 mM), the cocultured cells respond significantly stronger. The maximum intensity of CYP activity perceived under coculture conditions was about 5 times greater than that under monoculture. Maximum CYP activity peaked at 256 ± 101 pmol of resorufin per hour per 10^6 cells, whilst in monoculture the maximum only reached 75 ± 21 pmol of resorufin per hour per 10^6 cells. Thus, the presence of a bronchial barrier influenced the metabolic response of the hepatic cells to APAP.

5.2 The physiological-like model: a step towards complexifying the coculture design

For the same reason as previously described in the section 5.1, the cocultured tissue morphology, immunostainings and MUC5AC concentrations will be compared to dynamically monocultured tissues.

5.2.1 Mass spectrometry highlights the coculture's capacity to perceive and metabolize low concentrations of APAP

Similar to the developmental model, APAP levels were determined in the apical compartment of the bronchial and basal barrier common to the systemic and common segment of the coculture platform. The results showed that APAP was detected in the device at concentrations approaching equilibrium for exposures of 12 μM. Traces of the secondary metabolites APAP-GLU and APAP-SULF were also revealed by mass spectrometry. The measured doses were higher in the apical compartment of the barrier than on the basal side. These results suggest that APAP was able to cross the pulmonary barrier into the systemic circulation and was metabolized by the coculture.

	Coculture			
	APAP exposure concentration (mM)	**APAP (mM)**	**APAP-GLU (mM)**	**APAP-SULF (mM)**
Apical	0	0,0006 ± 0,0012	0 ± 0	0 ± 0
Basal	0	0,0011 ± 0,0019	5E-05 ± 0,0001	8E-06 ± 2E-05
Apical	0.012	0,0106 ± 0,0034	0,0986 ± 0,1060	0,0016 ± 0,0023
Basal	0.012	0,0108 ± 0,0010	0,0126 ± 0,0036	0,0003 ± 0,0001
Apical	0.024	0,0176 ± 0,0131	0,1666 ± 0,1841	0,0004 ± 0,0006
Basal	0.024	0,0127 ± 0,0004	0,0101 ± 0,0039	0,0002 ± 6E-05

FIGURE 5.12: Mass spectrometry measurements of APAP, APAP-GLU and APAP-SULF levels in post-culture supernatants of bronchial and hepatic semi-ALI cocultures according to APAP exposure.

5.2.2 Both compartments show viable and differentiated tissue properties

At the end of each experiment, culture inserts were collected and morphology was routinely monitored, by phase-contrast microscopy, to get a brief overview of tissue differentiation. A representative sample of these observations is showcased in Fig.5.13.
Phase-contrast observations (Fig. 5.13) showed us that the pluristratification phenomenon observed in monoculture conditions persisted in coculture while becoming more homogenized. The refractive clusters corresponded more to a stratification of the tissue than to the secretion of mucus because it rather leaved a semi-opaque veil on the surface of the tissue that it covered, letting the tissue beneath show through (monocultured non-exposed controls in Fig. 5.13), but this was not the case here.

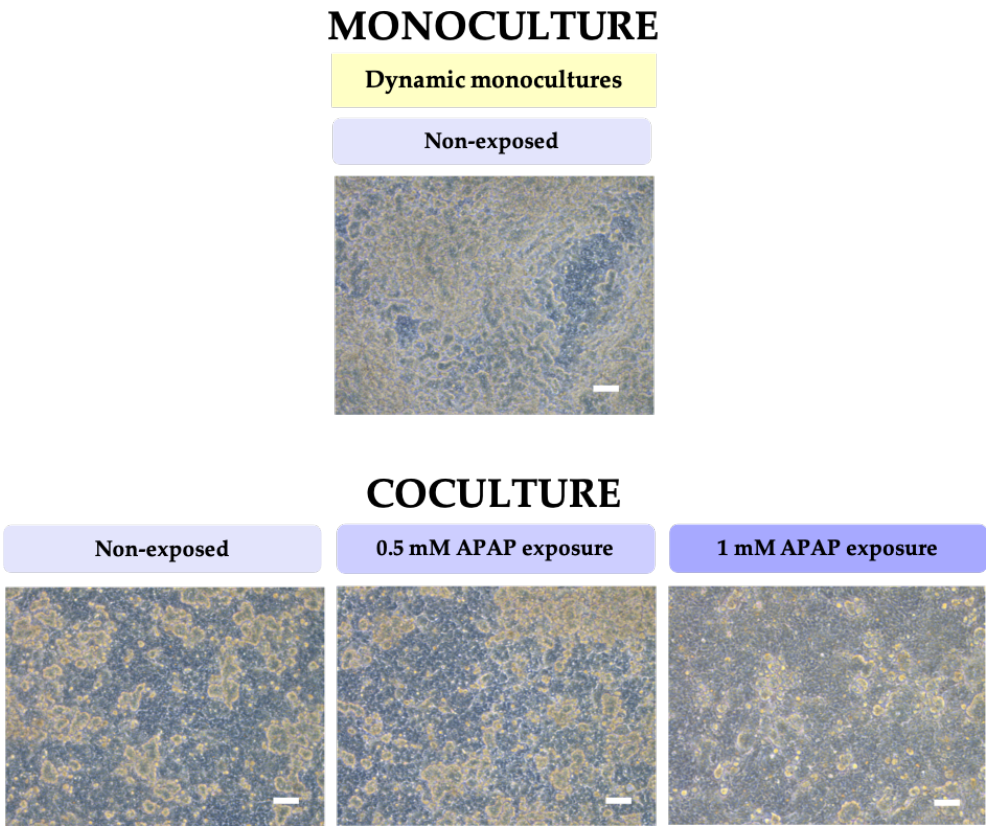

FIGURE 5.13: Phase contrast microscopy of monocultured and cocultured semi-ALI untreated and 72-hour APAP-exposed Calu-3 bronchial tissues on day 14. (Scale bar = 100 μm.

Pluristratification seemed to be more homogeneous on cocultured tissues because the refringency is better diffused than that of the agglomerates observed in monoculture conditions. No obvious morphological difference between exposed and unexposed tissues were noticed. It seemed that APAP did not modify the morphology of the lung compartment cultured in semi-ALI conditions.

The immunolabeling results presented in Fig.5.14 showed that the contiguous adherens junctions formed under monoculture conditions did not persist for E-Cadherin in coculture settings. While the labeling remained highly localized for Claudin-1, E-Cadherin underwent configuration changes that mostly delocalized its initial cell periphery labeling. It should also be noted that although the majority of junctions have been disrupted, some of them remained in their original conformation in the cell periphery.

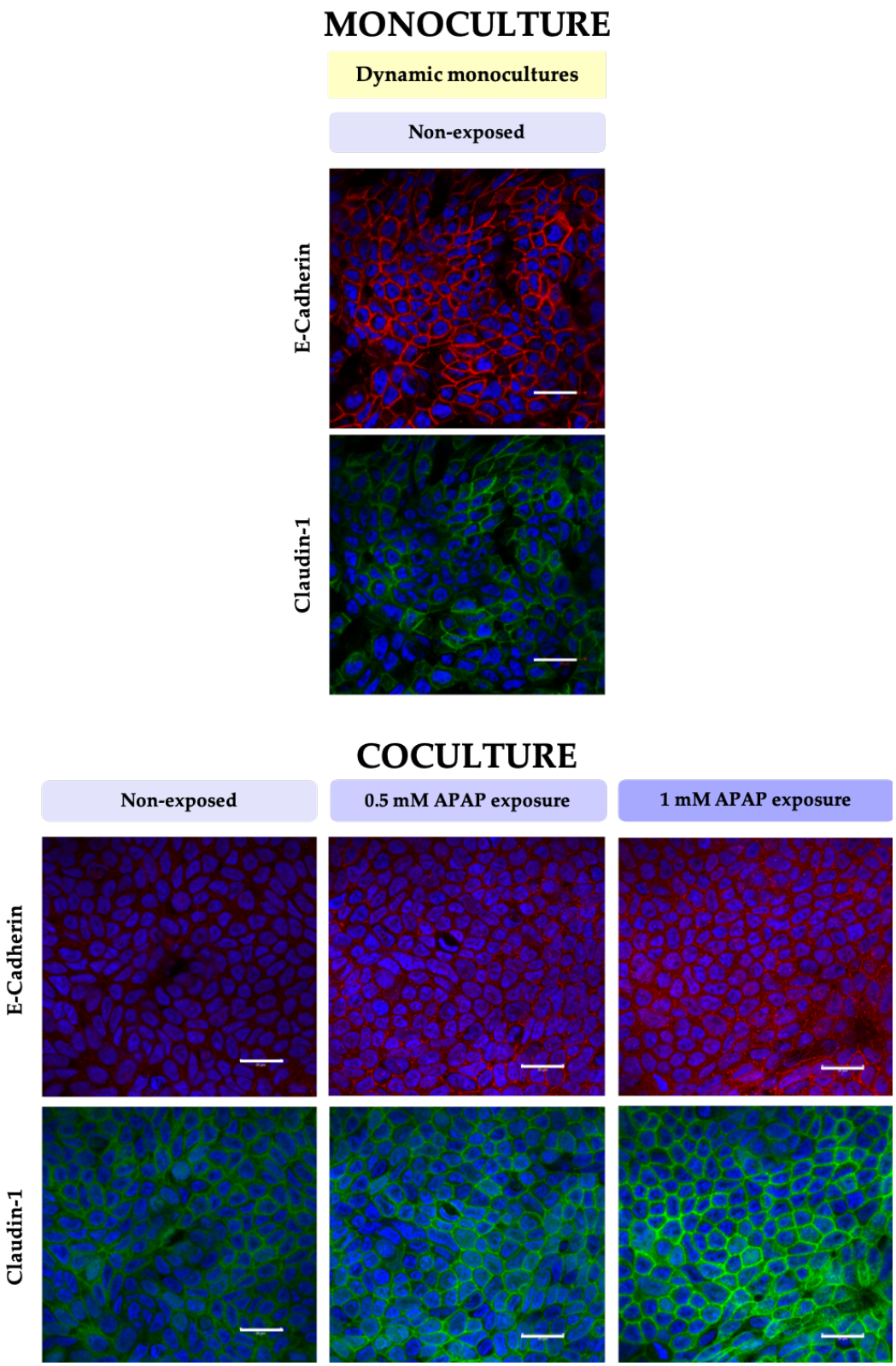

FIGURE 5.14: Confocal microscopy imaging of nuclei (blue), Claudin-1 (green) and E-Cadherin (red) immunostained tight and adherens junction complexes in semi-ALI monocultures and cocultures of Calu-3 bronchial tissues at day 14 exposed and non-exposed to APAP. (Scale bar = 20 μm).

Given that immunostainings revealed a configuration change in bronchial tight junctions, affected by the culture mode, TEER measurements were conducted to further characterize barrier functionality. Quantitative results are presented in Fig.5.15. In monoculture conditions, TEER results had shown us (previously described in Chapter 3) that APAP exposure (0.5 mM and 1 mM) disturbed the proper development of Calu-3 tissue cohesion. Indeed, statistical analysis of the results had pointed out a significant difference between resistance values at d11 and d14 only regarding unexposed conditions ($2696 \pm 1153\,\Omega.cm^2$), which attested to the progression of tissue integrity through time. This effect faded in coculture, where APAP no longer had an impact on tissue integrity as Kruskal Wallis Comparisons Test did not reveal any tissue resistance differences during the culture period.

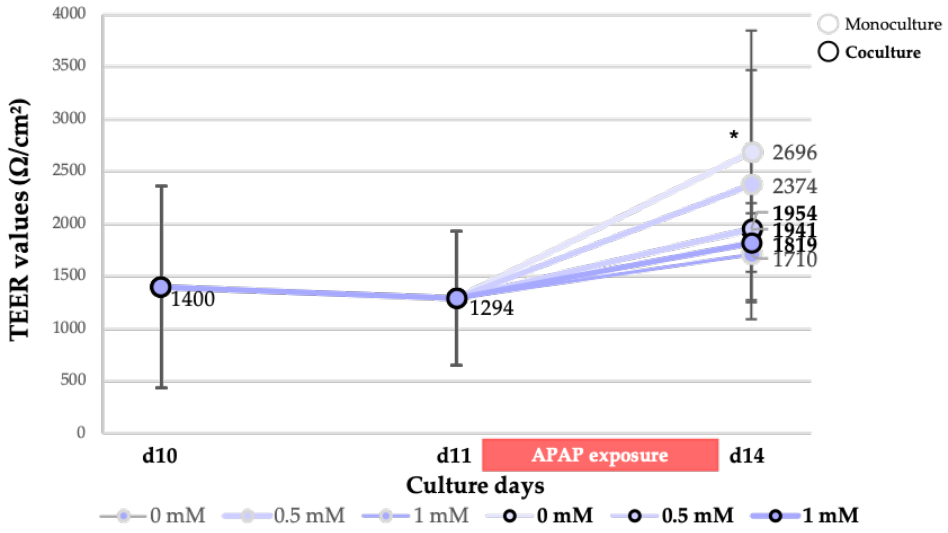

FIGURE 5.15: Transepithelial electrical resistance (TEER) measurement of monocultured and cocultured semi-ALI Calu-3 bronchial tissues over time following 72h APAP exposures. Statistically analyzed by Kruskal-Wallis test. $n \geq 4$

To further investigate cocultured Calu-3 barrier functions, MUC5AC were measured by ELISA and the results are presented in Fig. 3.21. As for previous measurements described in this thesis, the assays were carried out on post-culture supernatants. Event though data samples were small it does not seem that MUC5AC concentrations of cocultured bronchial tissues were different from monocultures. In addition, average MUC concentrations did not vary between APAP-exposed and non-exposed samples. These measurements suggested that neither the culture mode nor the exposure of APAP at 0.5 mM and 1 mM impaired the development of semi-ALI bronchial tissues. However, because the available data was so limited, further quantification is required to support this hypothesis.

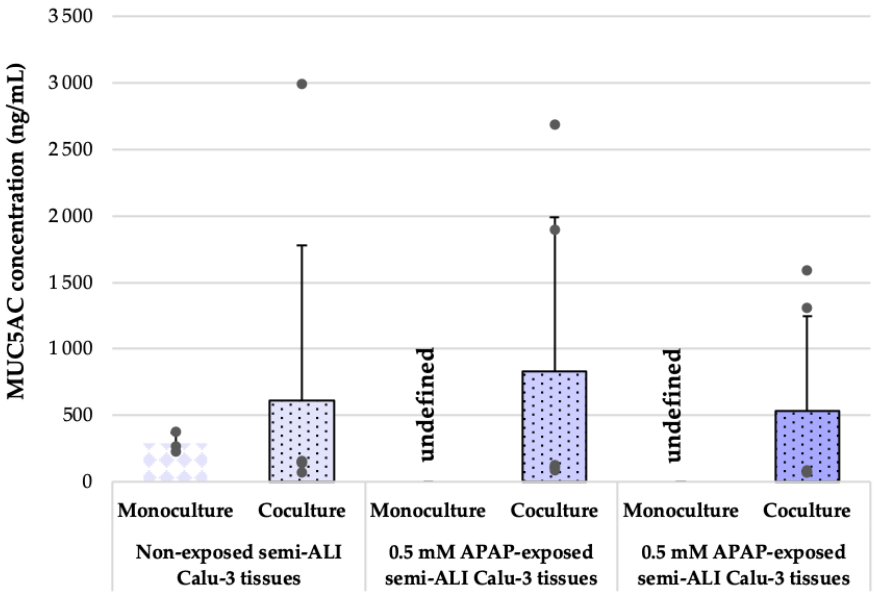

FIGURE 5.16: MUC5AC concentrations measured by ELISA in post-culture supernatants of semi-ALI monocultured and cocultured Calu-3 bronchial tissues. Statistically analyzed by Kruskal-Wallis test. $n \geq 2$

PrestoBlue measurements were performed to gain insight into the barrier's viability (Fig. 5.17). The added presence of a hepatic biochip to the circuit did not seem to disturb the bronchial mitochondrial activity.

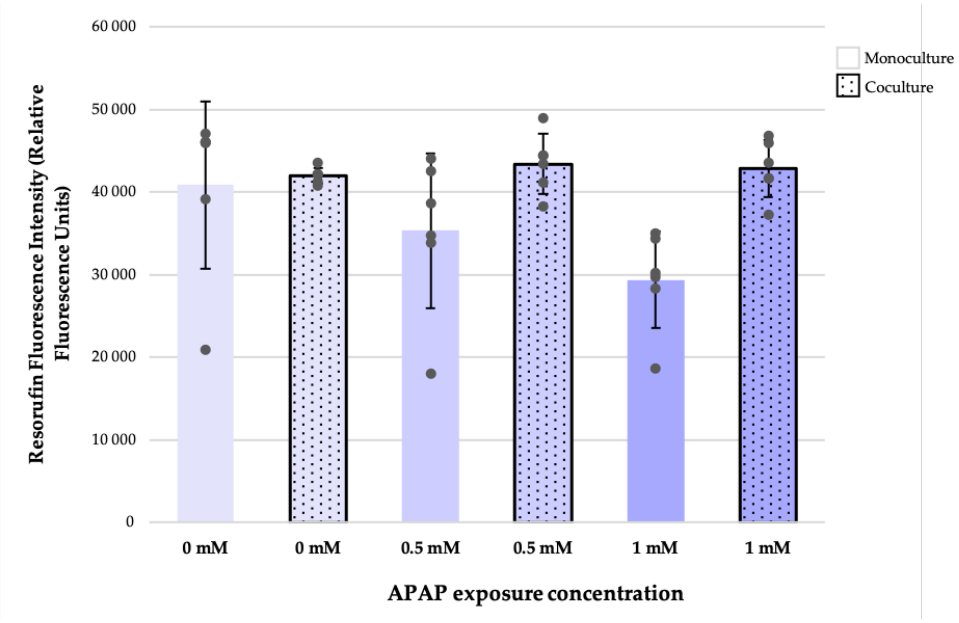

FIGURE 5.17: Bronchial mitochondrial activity of monocultured vs cocultured APAP-exposed semi-ALI Calu-3 tissues measured by PrestoBlue^{TM} at d14 after 72h exposures. Statistically analyzed by Kruskal-Wallis test. $n \geq 3$

Indeed, the measured activities remained comparable to the previously collected monoculture data. Mitochondrial biotransformation of reazurin in fluorescent resorufin remained regular, despite 0.5 mM and 1 mM APAP exposures, no significant differences were found between the different stress-induced conditions and culture modes.
Along with the controls performed on the lung compartment, we also monitored the liver compartment by assessing the same kinds of parameters, i.e. viability and cell metabolism, to attest to the impact of the presence of the bronchial barrier to the circuit, and if this affected the biological response of the hepatic tissue to APAP exposure.
Trypan Blue cell counts were performed on biochips recovered at the end of the culture. Quantitative data are shown in Fig. 5.18. Statistical analysis using the Kruskal-Wallis test followed by the Dunn's Multiple Comparisons Test, described that the cell counts collected on the unexposed and 0.5 mM and 1 mM exposed biochips did not show any significant cell count differences. APAP did not induce any cell death under co-culture conditions and at the tested concentrations.

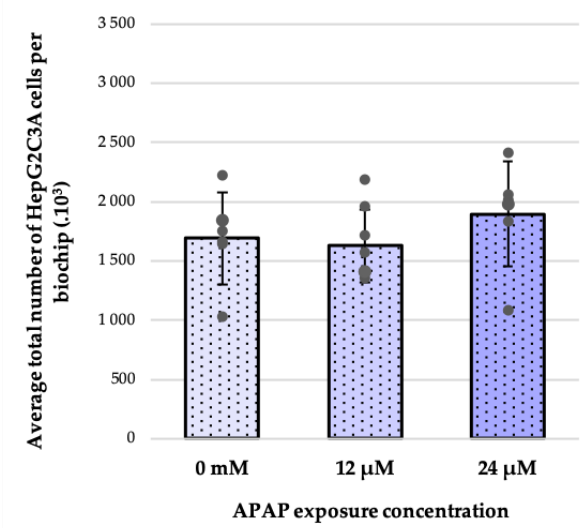

FIGURE 5.18: Evolution of cell proliferation of cocultured HepG2/C3A in semi-ALI coculture mode according to APAP exposure concentration. Statistically analyzed by Kruskal-Wallis test. $n \geq 3$

To monitor hepatic differentiation status of HepG2/C3A biochips, albumin production was measured in post-culture supernatants and results are shown in Fig. 5.19.
The collected data suggested that coculture albumin rates remain stable regardless of APAP exposure. ANOVA statistical test revealed a significant decrease of albumin at 24 μM APAP exposure, which means that HepG2/C3A cocultured biochips perceive the exposure as of 24 μM. Hepatic differentiation of hepatocyte-like cells was affected by low exposure concentrations of APAP, starting from 24 μM.
To investigate if low exposure concentrations also induce the xenobiotic metabolism of HepG2/C3A biochips, EROD assay were implemented.In addition, and as previously mentioned, it was also relevant to investigate CYP1A1/2 activites since they are involved in the metabolism of APAP to NAPQI, one of its secondary metabolites responsible for its cytotoxicity.

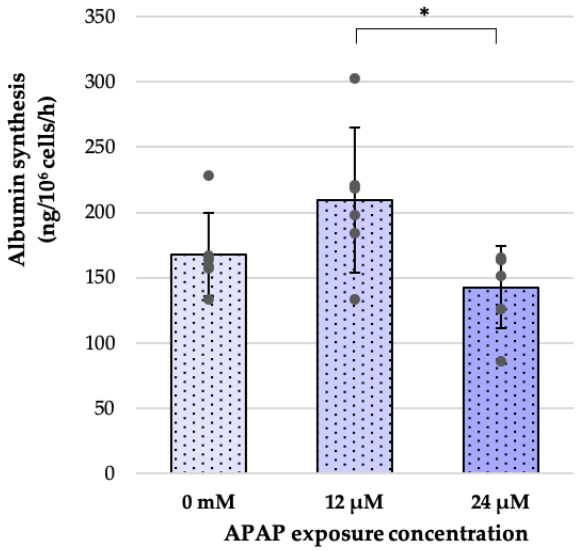

FIGURE 5.19: Albumin secretion rates of semi-ALI cocultured HepG2/C3A biochips according to APAP treatment. Statistically analyzed by ANOVA test, Tukey-Kramer post-hoc multiple comparisons test. $n \geq 3$.

The results obtained are shown in Fig.5.20 and showed that hepatic cells comprised active CYP1A1/2, displaying a basal activity level of approximately 61 $\pm$ 34 pmol of resorufin per hour per 10^6 cells (unexposed tissue). Statistical testing revealed no significant difference between the unexposed control and the exposed samples. CYP activity stabilized at around 49 $\pm$ 24 pmol of resorufin per hour per 10^6 cells. Thus, APAP did not induce an increase in CYP1A1/2 activity at the 0.5 mM and 1 mM exposure concentrations over a 72-hour exposure period.

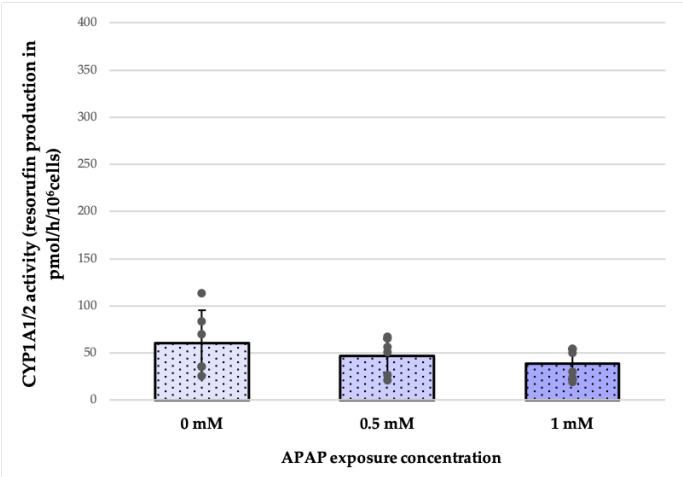

FIGURE 5.20: Comparison of CYP1A1/2 activities in semi-ALI cocultured HepG2/C3A biochips according to APAP exposure concentrations. Statistically analyzed by ANOVA test. $n \geq 3$.

5.3 Discussion

5.3.1 Highlighting the impact of coculture on the modulation of Calu-3 and HepG2/C3A cellular stress response

Overall, present results show that the lung and liver compartments can be successfully cocultured during 72 hours of joint culture as they display stable and functional cellular behaviors, similar to monoculture. The presence of a foreign tissue did not induce a stressful culture environment for either of the tissues, a ROS assay would help confirm this hypothesis, however, it did cause a reorganization of the Calu-3 tissue architecture. The loss of Claudin-1 labeling at cell-cell contact sites should have resulted in increased permeability of the barrier, as they are responsible for regulating access to paracellular spaces [25], yet this was not the case. Mucociliary clearance, intercellular apical junctional complexes, and protective mucus production all contribute to the barrier function of the airway epithelial tract *in vivo*. As mucin metabolism was not altered in coculture, and mucociliary clearance mechanisms do not apply to insert culture mode because the system is closed, neither could have compensated for the preservation of Calu-3 permeability. Understanding the involvement of the HepG2/C3A cells in maintaining Calu-3 permeability despite the loss of paracellular diffusion integrity would require further study. As the lungs and liver do not interact directly *in vivo*, these effects have not been observed or studied in the literature.
Nevertheless, the coculture setting allowed the passage of APAP through the Calu-3 barrier and into the circulatory system. Indeed, APAP was detected in the circulating medium and likely reached the liver compartment as the hepatic homeostasis of the biochip was impaired.
Overall APAP exposures elicited similar cellular behavior patterns, meaning that APAP presence was associated with apparent cytotoxicity, however, the intensity of associated adverse effects was reduced, and tissue responses followed a different kinetic in the coculture setting. While the presence of APAP-SULF and APAP-GLU in the medium is indicative of active phase II metabolism, CYP1A activities allow following the production of reactive NAPQI [13]. Indeed, while CYP1A were barely induced in monocultured 3 mM APAP-exposed biochips, activity measurements of cocultured HepG2/C3A biochips reveal an earlier and 5-fold intenser induction, probably associated with increased production of toxic NAPQI, however, associated cytotoxic effects are not proportional which would mean that the detoxification of NAPQI is actively occurring. Moreover, given that the literature documents that NAPQI targets mitochondrial proteins [21], its possible detoxification would also explain why the mitochondrial metabolism of Calu-3 is higher than in the monoculture setting. Quantification of the APAP-GSH metabolite, resulting from the detoxification of NAPQI, could clarify this hypothesis. However, it is important to emphasize that the current data is not sufficient to identify the implication levels of bronchial and hepatic metabolism in the biotransformation of APAP. For this purpose, further metabolic screening of the hepatic biochip should be performed and the Calu-3 compartment should be subjected to an array of metabolic tests to estimate the

activity levels of phase I and II DMEs.
As the exposure concentration raises (3 mM), cocultures seem to display disrupted hepatic and bronchial xenobiotic metabolism respectively as CYP1A activity reduce and APAP-GLU and APAP-SULF metabolites are absence of the apical side of the bronchial barrier. As a result, produced NAPQI could freely circulate through the coculture, no longer undergoing enhanced detoxification processes previously described, which would explain why the adverse effects are more pronounced than for 1.5 mM-APAP exposed cocultures. However, even so, the effects remain diminished compared to their monocultured counterpart where NAPQI was probably not detoxified either. Delayed cytotoxicity suggests that at least a part of the NAPQI was metabolized into a non-toxic metabolite (APAP-GSH), implying that the detoxification metabolism would have been at least momentarily active during the 72-hour culture period, before the exhaustion of cellular defense mechanisms. To verify this hypothesis, the state of Calu-3 and HepG2/C3A metabolisms could be punctually assessed throughout the coculture period to verify if a gradual decrease occurs.
The present developmental model shows that a Calu-3 bronchial barrier and a HepG2/C3A biochip can successfully be maintained viable and functional in a dynamic coculture setting within the IIDMP box for 3 days. The hepatic and bronchial cellular responses to APAP exposure were modified in a coculture setting, notably by the enhancement of cytoprotective detoxification processes resulting in delayed cytotoxicity, highlighting active and functional organ crosstalk between both compartments of the coculture model. Similar observations were assessed in other recently developed lung/liver models where a delayed and protective decrease of toxicity was also observed following aflatoxin B1 exposures [30], [31].

5.3.2 Revealing the sensitivity of the coculture model to low exposure doses

Present data show that ALI differentiation did not perturb the coculture model, i.e. both bronchial barrier and HepG2/C3A can maintain viability and functionality in a joint culture setting. Much like the developmental model, it appears that the presence of the HepG2/C3A biochip disrupted the architecture of the semi-ALI Calu-3 tissue through the loss of E-Cadherin labeling. E-Cadherin adherens junctions are calcium-dependent junctions responsible for cell-cell adhesion and are also involved in the regulation of epithelial differentiation and the immune response in stress-induced environments. While it seems that tissue cohesiveness has not been compromised, the lack of differentiation can be seen in the tissue's loss of pseudostratification. Further investigation is required to comprehend the influence of the HepG2/C3A biochip on the development of Calu-3 tissue. However, before considering any model complexification, commonly through the inclusion of immune cells (e.g. macrophages) in toxicological models, E-Cadherin loss should be addressed and corrected as they also are involved in the immune response in stress-induced environments, as their absence correlates with an increase in proinflammatory activity in bronchial epithelium (e.g. increased T helper type 2-mediated factors)

which could constitute an epithelial molecular switch from a tolerogenic to an immunogenic phenotype [355]. Thus, disruption of the E-Cadherin network in Calu-3 tissues would therefore compromise the relevance of predictive studies.
Nevertheless, APAP was able to cross the barrier of the physiological-like model and join the circulating media, and even at low exposure concentrations, APAP still appears to be able to reach the hepatic compartment, as evidenced by the slight changes in hepatic albumin synthesis. The cellular behaviors of the coculture in response to APAP treatments are similar to those observed in monocultures, i.e., no reported interferences with the viability or functionality of the hepatic and bronchial compartments.
The present coculture model is metabolically competent enough to handle low exposure doses as APAP-GLU and APAP-SULF metabolites were strongly detected in post-culture media, and it seems that both hepatic and bronchial metabolism are involved in the biotransformation of APAP as metabolites were found in apical and basal compartments of the culture platform. Even though the present physiological-like model requires further adjusting to enable the proper differentiation of the Calu-3 barrier, ALI systems seem promising to refine pulmonary responsiveness of epithelial cells to xenobiotic exposure as the literature reported that this was the case for other pulmonary cells such as ALI cocultured A549 and THP-1, in response to ceria and titania nanoparticle exposure [356]. Panas et al. revealed also how ALI increased the release of IL-8 in A549 in stress-induced environments, a major mediator of the inflammatory response, compared to submerged conditions [357].

Conclusion and perspectives

In an effort to contribute to the emergence of new alternative approaches for improved inhalation risk assessments, we introduce a new lung/liver coculture model allowing to acknowledge toxicity at a further systemic level.
During this thesis, we successfully recreated HepG2/C3A biochip and Calu-3 bronchial barrier models to use as the building blocks of the present lung/liver coculture model. Characterizing tissue-specific behaviors of monocultures prior to coculture allowed to better understand and identify lung/liver-specific interactions. The present model was characterized using a well-documented hepatotoxicant: APAP. APAP exposure to the pulmonary barrier is not physiological but allowed for quantitative passage and circulation through the device, as it interfered with hepatic homeostasis, proving that a given substance was capable of transiting and interacting with both compartments of the platform. 2 kinds of lung/liver models were developed:

- The developmental model allowed the technical set up of the model.
- The physiological-like model began to better approximate human *vivo* differentiation and exposure conditions, as ALI opens the way to physiological aerosolized exposures (e.g. nebulized exposure via the VitroCell® Cloud device).

Although preliminary, present results report that the developed model emulates active and functional *in vitro* crosstalk between a bronchial barrier and a liver biochip, and that this interaction is seemingly responsive to high and low xenobiotic exposure doses. In the context of APAP-induced toxicity, the crosstalk induced a modulation of stress response dynamics, delaying cytotoxicity, proving that xenobiotic fate, biological behaviors and cellular stress responses can be modulated in a broader systemic-like environment.
Although the existing interactions between the lungs and the liver are recognized, dedicated study models continue to rely on the use of *in vivo* tests. The literature reports a rise of lung/liver coculture platforms that offer the possibility to connect pulmonary tissue models (bronchial or alveolar) with hepatocytes for the evaluation of inhaled xenobiotics [30], [31], [358]. The present coculture model offers a novel way of cost-effectively coculturing pulmonary and hepatic reconstructs and its apparent functionality allows to obtain preliminary investigate predictions in 72 hours. The present model offers a huge culture versatility, as the IIDMP box that houses the coculture displays a plug-and-go design. Indeed, culture platform integrates culture insert and biochip culture modes, both of which have been utilized for many kinds of cultures. Studies of complexification of the pulmonary compartment are underway, in particular by using hAELVI cells (healthy

human alveolar cell line) in order to recreate an alveolar-capillary barrier. This versatility could allow to modulate the model according to the molecule of interest, bearing in mind that the physico-chemical properties influence the *in vivo* deposition in the respiratory tract, the current configuration allows to modify the nature of the pulmonary compartment according to the study. Considering that epithelial barrier functions are driven by mucus secretion, junctional network but also immune signaling, the addition of immune cells could also improve the relevancy of observed biological outcomes. Thus, immunocompetent pulmonary *in vitro* models are emerging in toxicology intended models [359], [360]. Regarding the hepatic compartment, the biochip used during this study has been previously declined through architecture and cellular composition accessing a portfolio of different hepatic models, notably leveraging the culture of different cell types such as primary human and animal cells, and iPSCs [361]–[363].
The culture versatility offered by the culture supports used in this model suggest that the lung/liver device could easily be tailored to offer better functionality and *vitro* to *vivo* extrapolation, to empower the predictivity of the coculture model.
Overall, the model will likely benefit from improvements to optimize ALI exposure mode and to complexify pulmonary and hepatic reconstructs to obtain a better representation of the *vivo*. The present lung/liver co-culture displays promising potential to empower the prediction of inhalation-like exposures.

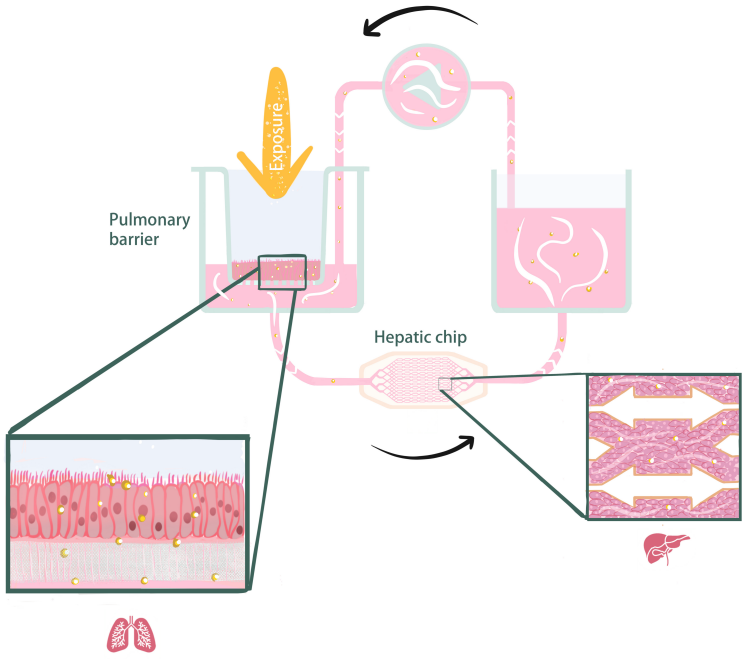

FIGURE 5.21: Schematic representation of the present coculture model comprising a pulmonary barrier and a hepatic biochip joined in a closed microfluidic culture circuit. Made by Dr. Augustin Lerebours.

Communications

International Congress

S. Madiedo-Podvršan, S. Bacari, F. Zhu, M. Cattelin, T. Martinez, L Sebillet, R. Jellali, G. Lacroix, M. Vayssade, "Characterization of a new in vitro lung and liver coculture model for the study of inhaled xenobiotics" - Poster
EUROTOX 2021, September 2021

S. Madiedo-Podvršan, S. Bacari, F. Zhu, M. Cattelin, T. Martinez, L Sebillet, R. Jellali, G. Lacroix, M. Vayssade, "Development of a hepato-pulmonary in vitro model for the toxicological study of inhaled pollutants " - Poster presentation
6th TERMIS World Congress, November 2021

Other international communication

S. Madiedo-Podvršan, F. Zhu, M. Cattelin, T. Martinez, L Sebillet, R. Jellali, G. Lacroix, M. Vayssade, "Development of a new in vitro device for risk assessment of inhaled xenobiotics : Lung/Liver " - Poster presentation
JRC Summer School 2021, May 2021
ESTIV Best Poster Award

S. Madiedo-Podvršan, S. Bacari, F. Zhu, M. Cattelin, T. Martinez, L Sebillet, R. Jellali, G. Lacroix, M. Vayssade, "Developing and investigating a new in vitro hepato-pulmonary coculture model for the toxicological study of inhaled xenobiotic" - Presentation
Early Career Scientists Workshop on Non-Animal New Approach Methodologies (NAMs) in Biomedical Research, November 2021

S. Madiedo-Podvršan, S. Bacari, F. Zhu, M. Cattelin, T. Martinez, L Sebillet, R. Jellali, G. Lacroix, M. Vayssade, "Developing and investigating a new in vitro hepato-pulmonary coculture model for the toxicological study of inhaled xenobiotic" - Presentation
ESTIV and ASCCT webinar, March 2022

Publications

In preparation:
S. Madiedo-Podvršan, S. Bacari, L Sebillet, T. Martinez, F. Zhu, M. Cattelin, F. Merlier, R. Jellali, G. Lacroix, M. Vayssade, "Development of a lung-liver *in vitro* coculture model for the risk assessment of inhaled xenobiotics "

Bibliography

[1] P. A. Solomon, M. Costantini, T. J. Grahame, *et al.*, "Air pollution and health: Bridging the gap from sources to health outcomes: Conference summary," *Air Quality, Atmosphere &Amp; Health*, vol. 5, no. 1, pp. 9–62, Mar. 2011, ISSN: 18739318. DOI: 10.1007/S11869-011-0161-4.

[2] M. S. O'Neill, C. V. Breton, R. B. Devlin, and M. J. Utell, "Air pollution and health: Emerging information on susceptible populations," *Air Quality, Atmosphere &Amp; Health*, vol. 5, no. 2, pp. 189–201, Jun. 2011, ISSN: 18739318. DOI: 10.1007/S11869-011-0150-7.

[3] A. J. Cohen, M. Brauer, R. Burnett, *et al.*, "Estimates and 25-year trends of the global burden of disease attributable to ambient air pollution: An analysis of data from the Global Burden of Diseases Study 2015," *The Lancet*, vol. 389, no. 10082, pp. 1907–1918, May 2017, Publisher: Lancet Publishing Group, ISSN: 1474547X. DOI: 10.1016/S0140-6736(17)30505-6.

[4] J. M. Prot, A. Bunescu, B. Elena-Herrmann, *et al.*, "Predictive toxicology using systemic biology and liver microfluidic "on chip" approaches: Application to acetaminophen injury," *Toxicology and applied pharmacology*, vol. 259, no. 3, pp. 270–280, Mar. 2012, Publisher: Toxicol Appl Pharmacol, ISSN: 1096-0333. DOI: 10.1016/J.TAAP.2011.12.017.

[5] E. Leclerc, J. Hamon, I. Claude, R. Jellali, M. Naudot, and F. Bois, "Investigation of acetaminophen toxicity in HepG2/C3a microscale cultures using a system biology model of glutathione depletion," en, *Cell Biology and Toxicology*, vol. 31, no. 3, pp. 173–185, Jun. 2015, ISSN: 1573-6822. DOI: 10.1007/s10565-015-9302-0.

[6] E. Leclerc, Y. Sakai, and T. Fujii, "Microfluidic PDMS (polydimethylsiloxane) bioreactor for large-scale culture of hepatocytes," eng, *Biotechnology Progress*, vol. 20, no. 3, pp. 750–755, Jun. 2004, ISSN: 8756-7938. DOI: 10.1021/bp0300568.

[7] R. Baudoin, L. Griscom, J. M. Prot, C. Legallais, and E. Leclerc, "Behavior of HepG2/C3A cell cultures in a microfluidic bioreactor," *Biochemical Engineering Journal*, vol. 53, no. 2, pp. 172–181, Jan. 2011, ISSN: 1369703X. DOI: 10.1016/j.bej.2010.10.007.

[8] J. M. Prot, C. Aninat, L. Griscom, *et al.*, "Improvement of HepG2/C3a cell functions in a microfluidic biochip," *Biotechnology and Bioengineering*, vol. 108, no. 7, pp. 1704–1715, 2011, ISSN: 00063592. DOI: 10.1002/bit.23104.

[9] J.-M. Prot, O. Videau, C. Brochot, C. Legallais, H. Bénech, and E. Leclerc, "A cocktail of metabolic probes demonstrates the relevance of primary human hepatocyte cultures in a microfluidic biochip for pharmaceutical drug screening," *International Journal of Pharmaceutics*, vol. 408, no. 1-2, Apr. 2011, ISSN: 03785173. DOI: 10.1016/j.ijpharm.2011.01.054.

[10] R. Baudoin, J. M. Prot, G. Nicolas, *et al.*, "Evaluation of seven drug metabolisms and clearances by cryopreserved human primary hepatocytes cultivated in microfluidic biochips," *Xenobiotica; the fate of foreign compounds in biological systems*, vol. 43, no. 2, pp. 140–52, 2012, ISSN: 1366-5928. DOI: 10.3109/00498254.2012.706725.

[11] A. W. Tilles, H. Baskaran, P. Roy, M. L. Yarmush, and M. Toner, "Effects of oxygenation and flow on the viability and function of rat hepatocytes cocultured in a microchannel flat-plate bioreactor," eng, *Biotechnology and Bioengineering*, vol. 73, no. 5, pp. 379–389, Jun. 2001, ISSN: 0006-3592. DOI: 10.1002/bit.1071.

[12] J. E. Laine, S. Auriola, M. Pasanen, and R. O. Juvonen, "Acetaminophen bioactivation by human cytochrome P450 enzymes and animal microsomes," eng, *Xenobiotica; the Fate of Foreign Compounds in Biological Systems*, vol. 39, no. 1, pp. 11–21, Jan. 2009, ISSN: 1366-5928. DOI: 10.1080/00498250802512830.

[13] J. M. Prot, A.-S. Briffaut, F. Letourneur, *et al.*, "Integrated proteomic and transcriptomic investigation of the acetaminophen toxicity in liver microfluidic biochip," eng, *PloS One*, vol. 6, no. 8, e21268, 2011, ISSN: 1932-6203. DOI: 10.1371/journal.pone.0021268.

[14] L. L. Mazaleuskaya, K. Sangkuhl, C. F. Thorn, G. A. Fitzgerald, R. B. Altman, and T. E. Klein, "PharmGKB summary: Pathways of acetaminophen metabolism at the therapeutic versus toxic doses," *Pharmacogenetics and Genomics*, vol. 25, no. 8, pp. 416–426, Jul. 2015, Publisher: Lippincott Williams and Wilkins, ISSN: 17446880. DOI: 10.1097/FPC.0000000000000150.

[15] Y. Zhu, A. Chidekel, and T. H. Shaffer, "Cultured human airway epithelial cells (calu-3): A model of human respiratory function, structure, and inflammatory responses," eng, *Critical Care Research and Practice*, vol. 2010, p. 394 578, 2010, ISSN: 2090-1313. DOI: 10.1155/2010/394578.

[16] K. O. Hamilton, E. Topp, I. Makagiansar, T. Siahaan, M. Yazdanian, and K. L. Audus, "Multidrug resistance-associated protein-1 functional activity in Calu-3 cells," eng, *The Journal of Pharmacology and Experimental Therapeutics*, vol. 298, no. 3, pp. 1199–1205, Sep. 2001, ISSN: 0022-3565.

[17] K. O. Hamilton, G. Backstrom, M. A. Yazdanian, and K. L. Audus, "P-glycoprotein efflux pump expression and activity in Calu-3 cells," eng, *Journal of Pharmaceutical Sciences*, vol. 90, no. 5, pp. 647–658, May 2001, ISSN: 0022-3549. DOI: 10.1002/1520-6017(200105)90:5<647::aid-jps1021>3.0.co;2-g.

[18] Y. Kuzuya, T. Adachi, H. Hara, A. Anan, K. Izuhara, and H. Nagai, "Induction of Drug-metabolizing Enzymes and Transporters in Human Bronchial Epithelial Cells by Beclomethasone Dipropionate," en, *IUBMB Life*, vol. 56, no. 6, pp. 355–359, 2004, ISSN: 1521-6551. DOI: 10.1080/10258140412331286946.

[19] K. A. Foster, M. L. Avery, M. Yazdanian, and K. L. Audus, "Characterization of the Calu-3 cell line as a tool to screen pulmonary drug delivery," en, *International Journal of Pharmaceutics*, vol. 208, no. 1, pp. 1–11, Nov. 2000, ISSN: 0378-5173. DOI: 10.1016/S0378-5173(00)00452-X.

[20] G. E. Neurohr, R. L. Terry, J. Lengefeld, *et al.*, "Excessive Cell Growth Causes Cytoplasm Dilution And Contributes to Senescence," en, *Cell*, vol. 176, no. 5, 1083–1097.e18, Feb. 2019, ISSN: 0092-8674. DOI: 10.1016/j.cell.2019.01.018.

[21] Y. Qiu, L. Z. Benet, and A. L. Burlingame, "Identification of the hepatic protein targets of reactive metabolites of acetaminophen in vivo in mice using two-dimensional gel electrophoresis and mass spectrometry," eng, *The Journal of Biological Chemistry*, vol. 273, no. 28, pp. 17 940–17 953, Jul. 1998, ISSN: 0021-9258. DOI: 10.1074/jbc.273.28.17940.

[22] H. Jaeschke, M. R. McGill, and A. Ramachandran, "Oxidant stress, mitochondria, and cell death mechanisms in drug-induced liver injury: Lessons learned from acetaminophen hepatotoxicity," *Drug metabolism reviews*, vol. 44, no. 1, pp. 88–106, Feb. 2012, Publisher: Drug Metab Rev, ISSN: 1097-9883. DOI: 10.3109/03602532.2011.602688.

[23] B. Srinivasan, A. R. Kolli, M. B. Esch, H. E. Abaci, M. L. Shuler, and J. J. Hickman, "TEER measurement techniques for in vitro barrier model systems," eng, *Journal of Laboratory Automation*, vol. 20, no. 2, pp. 107–126, Apr. 2015, ISSN: 2211-0690. DOI: 10.1177/2211068214561025.

[24] C. Robinson, "10 - The Airway Epithelium: The Origin and Target of Inflammatory Airways Disease and Injury," en, in *Immunopharmacology of Respiratory System*, ser. Handbook of Immunopharmacology, S. T. Holgate, Ed., London: Academic Press, Jan. 1995, pp. 187–III, ISBN: 978-0-12-352325-9. DOI: 10.1016/B978-012352325-9/50012-5.

[25] J. M. Anderson and C. M. Van Itallie, "Tight junctions and the molecular basis for regulation of paracellular permeability," eng, *The American Journal of Physiology*, vol. 269, no. 4 Pt 1, G467–475, Oct. 1995, ISSN: 0002-9513. DOI: 10.1152/ajpgi.1995.269.4.G467.

[26] E. P. Lillehoj, K. Kato, W. Lu, and K. C. Kim, "Cellular and Molecular Biology of Airway Mucins," *International review of cell and molecular biology*, vol. 303, pp. 139–202, 2013, ISSN: 1937-6448. DOI: 10.1016/B978-0-12-407697-6.00004-0.

[27] G. Lacroix, W. Koch, D. Ritter, *et al.*, "Air-Liquid Interface in Vitro Models for Respiratory Toxicology Research: Consensus Workshop and Recommendations," *Applied In Vitro Toxicology*, vol. 4, no. 2, pp. 91–106, 2018, Publisher: Mary Ann Liebert Inc., ISSN: 23321539. DOI: 10.1089/aivt.2017.0034.

[28] M. E. Kreft, U. D. Jerman, E. Lasič, *et al.*, "The characterization of the human cell line Calu-3 under different culture conditions and its use as an optimized in vitro model to investigate bronchial epithelial function.," *European journal of pharmaceutical sciences : official journal of the European Federation for Pharmaceutical Sciences*, vol. 69, pp. 1–9, 2015, ISSN: 1879-0720. DOI: 10.1016/j.ejps.2014.12.017.

[29] C. I. Grainger, L. L. Greenwell, D. J. Lockley, G. P. Martin, and B. Forbes, "Culture of Calu-3 cells at the air interface provides a representative model of the airway epithelial barrier," *Pharmaceutical Research*, vol. 23, no. 7, pp. 1482–1490, 2006, ISSN: 07248741. DOI: 10.1007/s11095-006-0255-0.

[30] D. Bovard, A. Sandoz, K. Luettich, *et al.*, "A lung/liver-on-a-chip platform for acute and chronic toxicity studies," en, *Lab on a Chip*, vol. 18, no. 24, pp. 3814–3829, 2018, ISSN: 1473-0197, 1473-0189. DOI: 10.1039/C8LC01029C.

[31] K. Schimek, S. Frentzel, K. Luettich, *et al.*, "Human multi-organ chip co-culture of bronchial lung culture and liver spheroids for substance exposure studies," en, *Scientific Reports*, vol. 10, no. 1, p. 7865, Dec. 2020, ISSN: 2045-2322. DOI: 10.1038/s41598-020-64219-6.

[32] World Health Organization (WHO), *Air pollution*, 2022.

[33] J. Currie and M. Neidell, "Air Pollution and Infant Health: What Can We Learn from California's Recent Experience?" *The Quarterly Journal of Economics*, vol. 120, no. 3, pp. 1003–1030, Aug. 2005, ISSN: 0033-5533. DOI: 10.1093/qje/120.3.1003.

[34] Y. Chen, A. Ebenstein, M. Greenstone, and H. Li, "Evidence on the impact of sustained exposure to air pollution on life expectancy from China's Huai River policy," *Proceedings of the National Academy of Sciences of the United States of America*, vol. 110, no. 32, pp. 12 936–12 941, Aug. 2013, Publisher: National Academy of Sciences, ISSN: 00278424. DOI: 10.1073/PNAS.1300018110/SUPPL_FILE/SAPP.PDF.

[35] T. Deryugina, G. Heutel, N. H. Miller, D. Molitor, and J. Reif, "The Mortality and Medical Costs of Air Pollution: Evidence from Changes in Wind Direction," *American Economic Review*, vol. 109, no. 12, pp. 4178–4219, 2019, Publisher: American Economic Association, ISSN: 0002-8282. DOI: 10.1257/AER.20180279.

[36] R. S. Sokhi and International Union of Air Pollution Prevention and Environmental Protection Associations., "World atlas of atmospheric pollution," p. 120, 2008, Publisher: Anthem Press ISBN: 9780857288592.

[37] I. Colbeck, "Air Pollution: History of Actions and Effectiveness of Change," *The SAGE Handbook of Environment and Society*, pp. 374–384, May 2012, Publisher: SAGE Publications Ltd. DOI: 10.4135/9781848607873.N26.

[38] A. J. A. J. McMichael, "Human frontiers, environments, and disease : Past patterns, uncertain futures," p. 413, 2001, Publisher: Cambridge University Press ISBN: 9780521004947.

[39] R. P. Sieferle, *The Subterranean Forest Energy Systems and the Industrial Revolution*. Cambridge: The White Horse Press, 2001, ISBN: 978-1-874267-59-1.

[40] S. Mosley, "Environmental History of Air Pollution and Protection," in *Environmental History (Netherlands)*, vol. 4, ISSN: 22119027, Springer Science and Business Media B.V., 2014, pp. 143–169. DOI: 10.1007/978-3-319-09180-8_5.

[41] B. J. Polivka, "The Great London Smog of 1952," *AJN, American Journal of Nursing*, vol. 118, no. 4, pp. 57–61, Apr. 2018, ISSN: 0002-936X. DOI: 10.1097/01.NAJ.0000532078.72372.c3.

[42] E. K. Shuman, "Global climate change and infectious diseases," eng, *The International Journal of Occupational and Environmental Medicine*, vol. 2, no. 1, pp. 11–19, Jan. 2011, ISSN: 2008-6520.

[43] C Ayres, R Costanza, R Goldemberg, *et al.*, *Encyclopedia of Energy. Six-Volume Set, 1-6*. Elsevier Science, 2004.

[44] M. S. Bućko, T. Magiera, B. Johanson, E. Petrovský, and L. J. Pesonen, "Identification of magnetic particulates in road dust accumulated on roadside snow using magnetic, geochemical and micro-morphological analyses," *Environmental Pollution*, vol. 159, no. 5, pp. 1266–1276, May 2011, ISSN: 02697491. DOI: 10.1016/j.envpol.2011.01.030.

[45] B. Freedman, "AIR POLLUTION," in *Environmental Ecology*, Elsevier, 1995, pp. 11–61. DOI: 10.1016/B978-0-08-050577-0.50007-8.

[46] N Englert, "Fine particles and human health—a review of epidemiological studies," *Toxicology Letters*, vol. 149, no. 1-3, pp. 235–242, Apr. 2004, ISSN: 03784274. DOI: 10.1016/j.toxlet.2003.12.035.

[47] *Conséquences des incendies de Gironde : Épisode de pollution athmosphérique en Gironde*, Aug. 2022.

[48] U. Kulshrestha and M. Mishra, "Chapter 3 - Atmospheric chemistry in Asia: Need of integrated approach," en, in *Asian Atmospheric Pollution*, R. P. Singh, Ed., Elsevier, Jan. 2022, pp. 55–74, ISBN: 978-0-12-816693-2. DOI: 10.1016/B978-0-12-816693-2.00002-0.

[49] M. Masilamani, S. Commins, and W. Shreffler, "Determinants of Food Allergy," *Immunology and Allergy Clinics of North America*, vol. 32, no. 1, pp. 11–33, Feb. 2012, ISSN: 08898561. DOI: 10.1016/j.iac.2011.12.003.

[50] C. F. Schuler Iv and J. M. Montejo, "Allergic Rhinitis in Children and Adolescents.," *Pediatric clinics of North America*, vol. 66, no. 5, pp. 981–993, 2019, ISSN: 1557-8240. DOI: 10.1016/j.pcl.2019.06.004.

[51] C. Traidl-Hoffmann, A. Kasche, A. Menzel, *et al.*, "Impact of Pollen on Human Health: More Than Allergen Carriers?" *International Archives of Allergy and Immunology*, vol. 131, no. 1, pp. 1–13, 2003, ISSN: 1018-2438. DOI: 10.1159/000070428.

[52] G. D'Amato, S. T. Holgate, R. Pawankar, *et al.*, "Meteorological conditions, climate change, new emerging factors, and asthma and related allergic disorders. A statement of the World Allergy Organization," *World Allergy Organization Journal*, vol. 8, p. 25, 2015, ISSN: 19394551. DOI: 10.1186/s40413-015-0073-0.

[53] K. M. Shea, R. T. Truckner, R. W. Weber, and D. B. Peden, "Climate change and allergic disease," *Journal of Allergy and Clinical Immunology*, vol. 122, no. 3, pp. 443–453, Sep. 2008, ISSN: 00916749. DOI: 10.1016/j.jaci.2008.06.032.

[54] F. Thien, P. J. Beggs, D. Csutoros, *et al.*, "The Melbourne epidemic thunderstorm asthma event 2016: An investigation of environmental triggers, effect on health services, and patient risk factors," eng, *The Lancet. Planetary Health*, vol. 2, no. 6, e255–e263, Jun. 2018, ISSN: 2542-5196. DOI: 10.1016/S2542-5196(18)30120-7.

[55] A. Monteiro, V. Carvalho, T. Oliveira, and C. Sousa, "Excess mortality and morbidity during the July 2006 heat wave in Porto, Portugal," *International Journal of Biometeorology*, vol. 57, no. 1, pp. 155–167, Jan. 2013, ISSN: 0020-7128. DOI: 10.1007/s00484-012-0543-9.

[56] National Research Council, *Climate Stabilization Targets*. Washington, D.C.: National Academies Press, Feb. 2011, ISBN: 978-0-309-15176-4. DOI: 10.17226/12877.

[57] C. Ziegler, V. Morelli, and O. Fawibe, "Climate Change and Underserved Communities," eng, *Primary Care*, vol. 44, no. 1, pp. 171–184, Mar. 2017, ISSN: 1558-299X. DOI: 10.1016/j.pop.2016.09.017.

[58] W. G. Lindsley, J. D. Noti, F. M. Blachere, *et al.*, "Viable influenza A virus in airborne particles from human coughs," *Journal of occupational and environmental hygiene*, vol. 12, no. 2, pp. 107–113, Feb. 2015, Publisher: J Occup Environ Hyg, ISSN: 1545-9632. DOI: 10.1080/15459624.2014.973113.

[59] K. P. Fennelly, J. W. Martyny, K. E. Fulton, I. M. Orme, D. M. Cave, and L. B. Heifets, "Cough-generated aerosols of Mycobacterium tuberculosis: A new method to study infectiousness," *American journal of respiratory and critical care medicine*, vol. 169, no. 5, pp. 604–609, Mar. 2004, Publisher: Am J Respir Crit Care Med, ISSN: 1073-449X. DOI: 10.1164/RCCM.200308-1101OC.

[60] E. A. Nardell, "Indoor environmental control of tuberculosis and other airborne infections," *Indoor air*, vol. 26, no. 1, pp. 79–87, Feb. 2016, Publisher: Indoor Air, ISSN: 1600-0668. DOI: 10.1111/INA.12232.

[61] Canadian Tuberculosis Committee, "Housing conditions that serve as risk factors for tuberculosis infection and disease. An Advisory Committee Statement (ACS).," *Canada communicable disease report = Releve des maladies transmissibles au Canada*, vol. 33, no. ACS-9, pp. 1–13, Oct. 2007, ISSN: 1481-8531.

[62] E. G. Holmes and A. Rambaut, "Viral evolution and the emergence of SARS coronavirus," *Philosophical transactions of the Royal Society of London. Series B, Biological sciences*, vol. 359, no. 1447, pp. 1059–1065, Jul. 2004, Publisher: Philos Trans R Soc Lond B Biol Sci, ISSN: 0962-8436. DOI: 10.1098/RSTB.2004.1478.

[63] G. Neumann, T. Noda, and Y. Kawaoka, "Emergence and pandemic potential of swine-origin H1N1 influenza virus," *Nature 2009 459:7249*, vol. 459, no. 7249, pp. 931–939, Jun. 2009, Publisher: Nature Publishing Group, ISSN: 1476-4687. DOI: 10.1038/nature08157.

[64] E. A. Wrigley, *Energy and the English Industrial Revolution*. Cambridge University Press, Aug. 2010, ISBN: 978-0-521-76693-7. DOI: 10.1017/CBO9780511779619.

[65] J.-F. Lamarque, T. C. Bond, V. Eyring, *et al.*, "Historical (1850–2000) gridded anthropogenic and biomass burning emissions of reactive gases and aerosols: Methodology and application," *Atmospheric Chemistry and Physics*, vol. 10, no. 15, pp. 7017–7039, Aug. 2010, ISSN: 1680-7324. DOI: 10.5194/acp-10-7017-2010.

[66] D. S. Reay, E. A. Davidson, K. A. Smith, *et al.*, "Global agriculture and nitrous oxide emissions," *Nature Climate Change*, vol. 2, no. 6, pp. 410–416, Jun. 2012, ISSN: 1758-678X. DOI: 10.1038/nclimate1458.

[67] V. P. Aneja, W. H. Schlesinger, and J. W. Erisman, "Farming pollution," *Nature Geoscience*, vol. 1, no. 7, pp. 409–411, Jul. 2008, ISSN: 1752-0894. DOI: 10.1038/ngeo236.

[68] M. Wu, G. Li, P. Li, *et al.*, "Assessing the ecological risk of pesticides should not ignore the impact of their transformation byproducts – The case of chlorantraniliprole," en, *Journal of Hazardous Materials*, vol. 418, p. 126 270, Sep. 2021, ISSN: 0304-3894. DOI: 10.1016/j.jhazmat.2021.126270.

[69] T. F. Stocker, D. Qin, G.-K. Plattner, *et al.*, *Climate Change 2013. The Physical Science Basis. Working Group I Contribution to the Fifth Assessment Report of the Intergovernmental Panel on Climate Change - Abstract for decision-makers; Changements climatiques 2013. Les elements scientifiques. Contribution du groupe de travail I au cinquieme rapport d'evaluation du groupe d'experts intergouvernemental sur l'evolution du CLIMAT - Resume a l'intention des decideurs*, 2013.

[70] W. M. Hodan and W. R. Barnard, "Evaluating the Contribution of PM2.5 Precursor Gases and Re-entrained Road Emissions to Mobile Source PM2.5 Particulate Matter Emissions Prepared by MACTEC Under Contract to the Federal Highway Administration," MACTEC Federal Programs, Tech. Rep., 2004, Publication Title: Environmental Science.

[71] T. F. Mar and J. Q. Koenig, "Relationship between visits to emergency departments for asthma and ozone exposure in greater Seattle, Washington," *Annals of Allergy, Asthma & Immunology*, vol. 103, no. 6, pp. 474–479, Dec. 2009, ISSN: 10811206. DOI: 10.1016/S1081-1206(10)60263-3.

[72] M. Jerrett, R. T. Burnett, C. A. Pope, *et al.*, "Long-Term Ozone Exposure and Mortality," *New England Journal of Medicine*, vol. 360, no. 11, pp. 1085–1095, Mar. 2009, ISSN: 0028-4793. DOI: 10.1056/NEJMoa0803894.

[73] Q. Di, L. Dai, Y. Wang, *et al.*, "Association of Short-term Exposure to Air Pollution With Mortality in Older Adults," *JAMA*, vol. 318, no. 24, p. 2446, Dec. 2017, ISSN: 0098-7484. DOI: 10.1001/jama.2017.17923.

[74] World Health Organization (WHO), *Household air pollution and health*, 2022.

[75] S. Gupta, A. Kankaria, and B. Nongkynrih, "Indoor air pollution in India: Implications on health and its control," *Indian Journal of Community Medicine*, vol. 39, no. 4, p. 203, 2014, ISSN: 0970-0218. DOI: 10.4103/0970-0218.143019.

[76] I. Parajuli, H. Lee, and K. R. Shrestha, "Indoor Air Quality and ventilation assessment of rural mountainous households of Nepal," *International Journal of Sustainable Built Environment*, vol. 5, no. 2, pp. 301–311, Dec. 2016, ISSN: 22126090. DOI: 10.1016/j.ijsbe.2016.08.003.

[77] W. W. Nazaroff, "Indoor bioaerosol dynamics," eng, *Indoor Air*, vol. 26, no. 1, pp. 61–78, Feb. 2016, ISSN: 1600-0668. DOI: 10.1111/ina.12174.

[78] G. Buonanno, L. Stabile, and L. Morawska, "Personal exposure to ultrafine particles: The influence of time-activity patterns," *The Science of the total environment*, vol. 468-469, pp. 903–907, Jan. 2014, Publisher: Sci Total Environ, ISSN: 1879-1026. DOI: 10.1016/J.SCITOTENV.2013.09.016.

[79] J. R. Marlon, B. Bloodhart, M. T. Ballew, *et al.*, "How Hope and Doubt Affect Climate Change Mobilization," *Frontiers in Communication*, vol. 4, May 2019, ISSN: 2297-900X. DOI: 10.3389/fcomm.2019.00020.

[80] M. Dherani, D. Pope, M. Mascarenhas, K. R. Smith, M. Weber, and N. Bruce, "Indoor air pollution from unprocessed solid fuel use and pneumonia risk in children aged under five years: A systematic review and meta-analysis," *Bulletin of the World Health Organization*, vol. 86, no. 5, pp. 390–394, May 2008, Publisher: Bull World Health Organ, ISSN: 1564-0604. DOI: 10.2471/BLT.07.044529.

[81] J. B. Newbury, R. Stewart, H. L. Fisher, *et al.*, "Association between air pollution exposure and mental health service use among individuals with first presentations of psychotic and mood disorders: Retrospective cohort study," *The British Journal of Psychiatry*, vol. 219, no. 6, pp. 678–685, Dec. 2021, ISSN: 0007-1250. DOI: 10.1192/bjp.2021.119.

[82] M. Newlands, "Environmental Activism, Environmental Politics, and Representation: The Framing of the British Environmental Activist Movement," Ph.D. dissertation, University of East London, London, 2013.

[83] Environmental Protection Agency, *Air Pollution: Current and Future Challenges*.

[84] European Environment Agency, "Comparison of the EU and US Air Quality Standards and Planning Requirements," Tech. Rep., 2004.

[85] P. Schlosser, B. Asgharian, and M. Medinsky, "Inhalation Exposure and Absorption of Toxicants," in *Comprehensive Toxicology*, Elsevier, 2010, pp. 75–109. DOI: 10.1016/B978-0-08-046884-6.00104-4.

[86] B. Schlingmann, S. A. Molina, and M. Koval, "Claudins: Gatekeepers of lung epithelial function," *Seminars in cell & developmental biology*, vol. 42, pp. 47–57, Jun. 2015, ISSN: 1084-9521. DOI: 10.1016/j.semcdb.2015.04.009.

[87] A. L. Harris, "Emerging issues of connexin channels: Biophysics fills the gap," eng, *Quarterly Reviews of Biophysics*, vol. 34, no. 3, pp. 325–472, Aug. 2001, ISSN: 0033-5835. DOI: 10.1017/s0033583501003705.

[88] A. I. Ivanov and N. G. Naydenov, "Dynamics and regulation of epithelial adherens junctions: Recent discoveries and controversies," eng, *International Review of Cell and Molecular Biology*, vol. 303, pp. 27–99, 2013, ISSN: 1937-6448. DOI: 10.1016/B978-0-12-407697-6.00002-7.

[89] M. Paulsson, "Basement membrane proteins: Structure, assembly, and cellular interactions," eng, *Critical Reviews in Biochemistry and Molecular Biology*, vol. 27, no. 1-2, pp. 93–127, 1992, ISSN: 1040-9238. DOI: 10.3109/10409239209082560.

[90] A. M. Marchiando, W. V. Graham, and J. R. Turner, "Epithelial barriers in homeostasis and disease," eng, *Annual Review of Pathology*, vol. 5, pp. 119–144, 2010, ISSN: 1553-4014. DOI: 10.1146/annurev.pathol.4.110807.092135.

[91] K. Bérubé, Z. Prytherch, C. Job, and T. Hughes, "Human primary bronchial lung cell constructs: The new respiratory models," eng, *Toxicology*, vol. 278, no. 3, pp. 311–318, Dec. 2010, ISSN: 1879-3185. DOI: 10.1016/j.tox.2010.04.004.

[92] N. Kia'i and T. Bajaj, *Histology, Respiratory Epithelium*. 2022.

[93] E. R. Weibel, B. Sapoval, and M. Filoche, "Design of peripheral airways for efficient gas exchange," *Respiratory Physiology and Neurobiology*, vol. 148, no. 1-2 SPEC. ISS. Pp. 3–21, Aug. 2005, ISSN: 15699048. DOI: 10.1016/J.RESP.2005.03.005.

[94] D. Spina, "Epithelium smooth muscle regulation and interactions," *American journal of respiratory and critical care medicine*, vol. 158, no. 5 Pt 3, 1998, Publisher: Am J Respir Crit Care Med, ISSN: 1073-449X. DOI: 10.1164/AJRCCM.158.SUPPLEMENT_2.13TAC100A.

[95] M. J. Evans and C. G. Plopper, "The role of basal cells in adhesion of columnar epithelium to airway basement membrane," *The American review of respiratory disease*, vol. 138, no. 2, pp. 481–483, 1988, Publisher: Am Rev Respir Dis, ISSN: 0003-0805. DOI: 10.1164/AJRCCM/138.2.481.

[96] J. Kajstura, M. Rota, S. R. Hall, *et al.*, "Evidence for Human Lung Stem Cells," *New England Journal of Medicine*, vol. 364, no. 19, pp. 1795–1806, May 2011, Publisher: Massachusetts Medical Society, ISSN: 0028-4793. DOI: 10.1056/NEJMOA1101324/SUPPL_FILE/NEJMOA1101324_DISCLOSURES.PDF.

[97] R. Hajj, T. Baranek, R. Le Naour, P. Lesimple, E. Puchelle, and C. Coraux, "Basal cells of the human adult airway surface epithelium retain transit-amplifying cell properties," *Stem cells (Dayton, Ohio)*, vol. 25, no. 1, pp. 139–148, Jan. 2007, Publisher: Stem Cells, ISSN: 1066-5099. DOI: 10.1634/STEMCELLS.2006-0288.

[98] J. E. Boers, A. W. Ambergen, and F. B. Thunnissen, "Number and proliferation of clara cells in normal human airway epithelium," *American journal of respiratory and critical care medicine*, vol. 159, no. 5 Pt 1, pp. 1585–1591, 1999, Publisher: Am J Respir Crit Care Med, ISSN: 1073-449X. DOI: 10.1164/AJRCCM.159.5.9806044.

[99] F. Broeckaert, A. Clippe, B. Knoops, C. Hermans, and A. Bernard, "Clara cell secretory protein (CC16): Features as a peripheral lung biomarker," *Annals of the New York Academy of Sciences*, vol. 923, pp. 68–77, 2000, Publisher: Ann N Y Acad Sci, ISSN: 0077-8923. DOI: 10.1111/J.1749-6632.2000.TB05520.X.

[100] P. T. Nhamburo, S. Kimura, H. V. Gelboin, F. J. Gonzalez, O. Wesley McBride, and C. A. Kozak, "The Human CYP2F Gene Subfamily: Identification of a cDNA Encoding a New Cytochrome P450, cDNA-Directed Expression, and Chromosome Mapping," *Biochemistry*, vol. 29, no. 23, pp. 5491–5499, Jun. 1990, Publisher: American Chemical Society, ISSN: 15204995. DOI: 10.1021/BI00475A012/ASSET/BI00475A012.FP.PNG_V03.

[101] D. Gras, P. Chanez, I. Vachier, A. Petit, and A. Bourdin, "Bronchial epithelium as a target for innovative treatments in asthma," *Pharmacology & therapeutics*, vol. 140, no. 3, pp. 290–305, 2013, Publisher: Pharmacol Ther, ISSN: 1879-016X. DOI: 10.1016/J.PHARMTHERA.2013.07.008.

[102] A. K. T. Perl, D. Riethmacher, and J. A. Whitsett, "Conditional depletion of airway progenitor cells induces peribronchiolar fibrosis," *American journal of respiratory and critical care medicine*, vol. 183, no. 4, pp. 511–521, Feb. 2011, Publisher: Am J Respir Crit Care Med, ISSN: 1535-4970. DOI: 10.1164/RCCM.201005-0744OC.

[103] A. Yaghi and M. B. Dolovich, "Airway Epithelial Cell Cilia and Obstructive Lung Disease," eng, *Cells*, vol. 5, no. 4, E40, Nov. 2016, ISSN: 2073-4409. DOI: 10.3390/cells5040040.

[104] J. H. WATSON and G. L. BRINKMAN, "ELECTRON MICROSCOPY OF THE EPITHELIAL CELLS OF NORMAL AND BRONCHITIC HUMAN BRONCHUS," *The American review of respiratory disease*, vol. 90, pp. 851–866, Dec. 1964, Publisher: Am Rev Respir Dis, ISSN: 0003-0805. DOI: 10.1164/ARRD.1964.90.6.851.

[105] X. M. Bustamante-Marin and L. E. Ostrowski, "Cilia and Mucociliary Clearance," *Cold Spring Harbor Perspectives in Biology*, vol. 9, no. 4, a028241, Apr. 2017, ISSN: 1943-0264. DOI: 10.1101/cshperspect.a028241.

[106] R. G. Breeze and E. B. Wheeldon, "The cells of the pulmonary airways," *The American review of respiratory disease*, vol. 116, no. 4, pp. 705–777, 1977, Publisher: Am Rev Respir Dis, ISSN: 0003-0805. DOI: 10.1164/ARRD.1977.116.4.705.

[107] J. Harkema, A. Mariassy, J. A. George, D. Hyde, and C. Plopper, "Epithelial cells of the conducting airways : A species comparison," *Lung biology in health and disease*, vol. 55, pp. 3–39, 1991.

[108] J. Ma, B. K. Rubin, and J. A. Voynow, "Mucins, Mucus, and Goblet Cells," *Chest*, vol. 154, no. 1, pp. 169–176, Jul. 2018, ISSN: 00123692. DOI: 10.1016/j.chest.2017.11.008.

[109] W. E. Finkbeiner, "Physiology and pathology of tracheobronchial glands," *Respiration physiology*, vol. 118, no. 2-3, pp. 77–83, Dec. 1999, Publisher: Respir Physiol, ISSN: 0034-5687. DOI: 10.1016/S0034-5687(99)00080-8.

[110] C. B. Basbaum, B. Jany, and W. E. Finkbeiner, "The serous cell," *Annual review of physiology*, vol. 52, no. 1, pp. 97–113, 1990, Publisher: Annu Rev Physiol, ISSN: 0066-4278. DOI: 10.1146/ANNUREV.PH.52.030190.000525.

[111] D. A. Knight and S. T. Holgate, "The airway epithelium: Structural and functional properties in health and disease," *Respirology*, vol. 8, no. 4, pp. 432–446, Dec. 2003, Publisher: John Wiley & Sons, Ltd, ISSN: 1440-1843. DOI: 10.1046/J.1440-1843.2003.00493.X.

[112] J. Xu, H. Yu, and X. Sun, "Less Is More: Rare Pulmonary Neuroendocrine Cells Function as Critical Sensors in Lung," *Developmental Cell*, vol. 55, no. 2, pp. 123–132, Oct. 2020, ISSN: 15345807. DOI: 10.1016/j.devcel.2020.09.024.

[113] J. F. Collawn, A. Lazrak, Z. Bebok, and S. Matalon, "The CFTR and ENaC debate: How important is ENaC in CF lung disease?" *American Journal of Physiology-Lung Cellular and Molecular Physiology*, vol. 302, no. 11, pp. L1141–L1146, Jun. 2012, ISSN: 1040-0605. DOI: 10.1152/ajplung.00036.2012.

[114] G. E. Angus and W. M. Thurlbeck, "Number of alveoli in the human lung," *Journal of applied physiology*, vol. 32, no. 4, pp. 483–485, 1972, Publisher: J Appl Physiol, ISSN: 0021-8987. DOI: 10.1152/JAPPL.1972.32.4.483.

[115] P. Gehr, M. Bachofen, and E. R. Weibel, "The normal human lung: Ultrastructure and morphometric estimation of diffusion capacity," *Respiration physiology*, vol. 32, no. 2, pp. 121–140, 1978, Publisher: Respir Physiol, ISSN: 0034-5687. DOI: 10.1016/0034-5687(78)90104-4.

[116] M. Ochs, J. R. Nyengaard, A. Jung, *et al.*, "The number of alveoli in the human lung," *American journal of respiratory and critical care medicine*, vol. 169, no. 1, pp. 120–124, Jan. 2004, Publisher: Am J Respir Crit Care Med, ISSN: 1073-449X. DOI: 10.1164/RCCM.200308-1107OC.

[117] M. C. Williams, "Alveolar type I cells: Molecular phenotype and development," *Annual review of physiology*, vol. 65, pp. 669–695, 2003, Publisher: Annu Rev Physiol, ISSN: 0066-4278. DOI: 10.1146/ANNUREV.PHYSIOL.65.092101.142446.

[118] H Fehrenbach, "Alveolar epithelial type II cell: Defender of the alveolus revisited.," *Respiratory research*, vol. 2, no. 1, pp. 33–46, 2001, ISSN: 1465-9921. DOI: 10.1186/rr36.

[119] J. D. Crapo, B. E. Barry, P Gehr, M Bachofen, and E. R. Weibel, "Cell number and cell characteristics of the normal human lung.," *The American review of respiratory disease*, vol. 126, no. 2, pp. 332–7, Aug. 1982, ISSN: 0003-0805. DOI: 10.1164/arrd.1982.126.2.332.

[120] A. B. Thompson, R. A. Robbins, D. J. Romberger, *et al.*, "Immunological functions of the pulmonary epithelium," *The European respiratory journal*, vol. 8, no. 1, pp. 127–149, 1995, Publisher: Eur Respir J, ISSN: 0903-1936. DOI: 10.1183/09031936.95.08010127.

[121] S. T. Holgate, "Epithelial damage and response," eng, *Clinical and Experimental Allergy: Journal of the British Society for Allergy and Clinical Immunology*, vol. 30 Suppl 1, pp. 37–41, Jun. 2000, ISSN: 0954-7894. DOI: 10.1046/j.1365-2222.2000.00095.x.

[122] H. Tandel, K. Florence, and A. Misra, "Protein and Peptide Delivery through Respiratory Pathway," in *Challenges in Delivery of Therapeutic Genomics and Proteomics*, Elsevier, 2011, pp. 429–479. DOI: 10.1016/B978-0-12-384964-9.00009-8.

[123] W. C. Hinds, "Aerosol Technology Properties, Behavior, and Measurement of Airborne Particles," *John Wiley & Sons, Inc.*, 1999.

[124] K. Nazridoust and B. Asgharian, "Unsteady-state airflow and particle deposition in a three-generation human lung geometry," *Inhalation toxicology*, vol. 20, no. 6, pp. 595–610, Apr. 2008, Publisher: Inhal Toxicol, ISSN: 1091-7691. DOI: 10.1080/08958370801939374.

[125] O. Raabe, H.-C. Yeah, M. Schum, and R. Phalen, "Tracheobronchial Geometry: Human, Dog, Rat, Hamster - A Compilation of Selected Data from the Project Respiratory Tract Deposition Models," Tech. Rep., 1976, Publication Title: Biology.

[126] E. R. Weibel, "Morphometry of the Human Lung," *Morphometry of the Human Lung*, 1963, Publisher: Springer Berlin Heidelberg. DOI: 10.1007/978-3-642-87553-3.

[127] Price OT, Asgharian B, Miller FJ, Cassee FR, and de Winter-Sorkina R, "Multiple Path Particle Dosimetry model (MPPD v1.0): A model for human and rat airway particle dosimetry 650010030," National Institute for Public Health and the Environment (RIVM), Tech. Rep., 2002.

[128] G. Pilcer and K. Amighi, "Formulation strategy and use of excipients in pulmonary drug delivery," *International journal of pharmaceutics*, vol. 392, no. 1-2, pp. 1–19, Jun. 2010, Publisher: Int J Pharm, ISSN: 1873-3476. DOI: 10.1016/J.IJPHARM.2010.03.017.

[129] M. Geiser and W. G. Kreyling, "Deposition and biokinetics of inhaled nanoparticles," *Particle and Fibre Toxicology*, vol. 7, no. 1, p. 2, Jan. 2010, ISSN: 1743-8977. DOI: 10.1186/1743-8977-7-2.

[130] G. J. Laurent and S. D. Shapiro, *Encyclopedia of respiratory medicine*. Academic Press Elsevier, 2006, ISBN: 978-0-12-438360-9.

[131] C. Darquenne, "Deposition Mechanisms," *Journal of aerosol medicine and pulmonary drug delivery*, vol. 33, no. 4, pp. 181–185, Aug. 2020, Publisher: J Aerosol Med Pulm Drug Deliv, ISSN: 1941-2703. DOI: 10.1089/JAMP.2020.29029.CD.

[132] J. A. Whitsett, "Airway Epithelial Differentiation and Mucociliary Clearance," *Annals of the American Thoracic Society*, vol. 15, no. Suppl 3, S143–S148, Nov. 2018, Publisher: Ann Am Thorac Soc, ISSN: 2325-6621. DOI: 10.1513/ANNALSATS.201802-128AW.

[133] H. Takizawa, M. Tanaka, K. Takami, *et al.*, "Increased expression of transforming growth factor-beta1 in small airway epithelium from tobacco smokers and patients with chronic obstructive pulmonary disease (COPD)," *American journal of respiratory and critical care medicine*, vol. 163, no. 6, pp. 1476–1483, 2001, Publisher: Am J Respir Crit Care Med, ISSN: 1073-449X. DOI: 10.1164/AJRCCM.163.6.9908135.

[134] P. Puneet, S. Moochhala, and M. Bhatia, "Chemokines in acute respiratory distress syndrome," *American journal of physiology. Lung cellular and molecular physiology*, vol. 288, no. 1, Jan. 2005, Publisher: Am J Physiol Lung Cell Mol Physiol, ISSN: 1040-0605. DOI: 10.1152/AJPLUNG.00405.2003.

[135] F. Puttur, L. G. Gregory, and C. M. Lloyd, "Airway macrophages as the guardians of tissue repair in the lung," *Immunology and cell biology*, vol. 97, no. 3, pp. 246–257, Mar. 2019, Publisher: Immunol Cell Biol, ISSN: 1440-1711. DOI: 10.1111/IMCB.12235.

[136] J. Wong, B. E. Magun, and L. J. Wood, "Lung inflammation caused by inhaled toxicants: A review," *International journal of chronic obstructive pulmonary disease*, vol. 11, no. 1, pp. 1391–1401, Jun. 2016, Publisher: Int J Chron Obstruct Pulmon Dis, ISSN: 1178-2005. DOI: 10.2147/COPD.S106009.

[137] B. Asgharian, "A Model of Deposition of Hygroscopic Particles in the Human Lung," *Aerosol Science and Technology*, vol. 38, no. 9, pp. 938–947, Sep. 2004, ISSN: 0278-6826. DOI: 10.1080/027868290511236.

[138] T. S. Wiedmann, R. Bhatia, and L. W. Wattenberg, "Drug solubilization in lung surfactant," *Journal of controlled release : official journal of the Controlled Release Society*, vol. 65, no. 1-2, pp. 43–47, Mar. 2000, Publisher: J Control Release, ISSN: 0168-3659. DOI: 10.1016/S0168-3659(99)00230-8.

[139] J. D. Schroeter, J. S. Kimbell, E. A. Gross, *et al.*, "Application of physiological computational fluid dynamics models to predict interspecies nasal dosimetry of inhaled acrolein," *Inhalation toxicology*, vol. 20, no. 3, pp. 227–243, Feb. 2008, Publisher: Inhal Toxicol, ISSN: 1091-7691. DOI: 10.1080/08958370701864235.

[140] J. G. Garcia, "Pulmonary Circulation and Regulation of Fluid Balance," in *Murray and Nadel's Textbook of Respiratory Medicine*, Elsevier, 2016, 92–110.e8. DOI: 10.1016/B978-1-4557-3383-5.00006-3.

[141] B. Testa, A. Pedretti, and G. Vistoli, "Reactions and enzymes in the metabolism of drugs and other xenobiotics," *Drug discovery today*, vol. 17, no. 11-12, pp. 549–560, Jun. 2012, Publisher: Drug Discov Today, ISSN: 1878-5832. DOI: 10.1016/J.DRUDIS.2012.01.017.

[142] R. J. Bertz and G. R. Granneman, "Use of in vitro and in vivo data to estimate the likelihood of metabolic pharmacokinetic interactions," *Clinical pharmacokinetics*, vol. 32, no. 3, pp. 210–258, 1997, Publisher: Clin Pharmacokinet, ISSN: 0312-5963. DOI: 10.2165/00003088-199732030-00004.

[143] E. Petzinger and J. Geyer, "Drug transporters in pharmacokinetics," *Naunyn-Schmiedeberg's archives of pharmacology*, vol. 372, no. 6, pp. 465–475, Mar. 2006, Publisher: Naunyn Schmiedebergs Arch Pharmacol, ISSN: 0028-1298. DOI: 10.1007/S00210-006-0042-9.

[144] B. Hagenbuch and B. Stieger, "The SLCO (former SLC21) superfamily of transporters," *Molecular aspects of medicine*, vol. 34, no. 2-3, pp. 396–412, Apr. 2013, Publisher: Mol Aspects Med, ISSN: 1872-9452. DOI: 10.1016/J.MAM.2012.10.009.

[145] A. Obaidat, M. Roth, and B. Hagenbuch, "The expression and function of organic anion transporting polypeptides in normal tissues and in cancer," *Annual review of pharmacology and toxicology*, vol. 52, pp. 135–151, 2012, Publisher: Annu Rev Pharmacol Toxicol, ISSN: 1545-4304. DOI: 10.1146/ANNUREV-PHARMTOX-010510-100556.

[146] M. S. Benedetti, R. Whomsley, I. Poggesi, *et al.*, "Drug metabolism and pharmacokinetics," *Drug metabolism reviews*, vol. 41, no. 3, pp. 344–390, Aug. 2009, Publisher: Drug Metab Rev, ISSN: 1097-9883. DOI: 10.1080/10837450902891295.

[147] Parkinson A, Ogilvie BW, Buckley DB, Kazmi F, Czerwinski M, and Parkinson O, "Biotransformation of Xenobiotics," in *Casarett and Doull's Toxicology: The Basic Science of Poisons, Eighth Edition.* 2013.

[148] B. S. P. P.B. Danielson, "The cytochrome P450 superfamily: Biochemistry, evolution and drug metabolism in humans," *Current drug metabolism*, vol. 3, no. 6, pp. 561–597, Mar. 2002, Publisher: Curr Drug Metab, ISSN: 1389-2002. DOI: 10.2174/1389200023337054.

[149] B. Achour, J. Barber, and A. Rostami-Hodjegan, "Expression of hepatic drug-metabolizing cytochrome p450 enzymes and their intercorrelations: A meta-analysis," *Drug metabolism and disposition: the biological fate of chemicals*, vol. 42, no. 8, pp. 1349–1356, 2014, Publisher: Drug Metab Dispos, ISSN: 1521-009X. DOI: 10.1124/DMD.114.058834.

[150] M. R. Caira and C. Ionescu, *Drug Metabolism: Current Concepts*. Springer, 2005, ISBN: 978-1-4020-4141-9.

[151] S. C. Khojasteh, H. Wong, and C. E. Hop, *Drug Metabolism and Pharmacokinetics Quick Guide*. New York, NY: Springer New York, 2011, ISBN: 978-1-4419-5628-6. DOI: 10.1007/978-1-4419-5629-3.

[152] Y. Yilmaz, G. Williams, M. Walles, N. Manevski, S. Krähenbühl, and G. Camenisch, "Comparison of Rat and Human Pulmonary Metabolism Using Precision-cut Lung Slices (PCLS)," *Drug metabolism letters*, vol. 13, no. 1, pp. 53–63, Oct. 2019, Publisher: Drug Metab Lett, ISSN: 1874-0758. DOI: 10.2174/1872312812666181022114622.

[153] S. Kadlubar and F. F. Kadlubar, "Enzymatic Basis of Phase I and Phase II Drug Metabolism," in *Enzyme- and Transporter-Based Drug-Drug Interactions*, New York, NY: Springer New York, 2010, pp. 3–25. DOI: 10.1007/978-1-4419-0840-7_1.

[154] C. H. Johnson, A. D. Patterson, J. R. Idle, and F. J. Gonzalez, "Xenobiotic metabolomics: Major impact on the metabolome," *Annual review of pharmacology and toxicology*, vol. 52, pp. 37–56, 2012, Publisher: Annu Rev Pharmacol Toxicol, ISSN: 1545-4304. DOI: 10.1146/ANNUREV-PHARMTOX-010611-134748.

[155] B. Döring and E. Petzinger, "Phase 0 and phase III transport in various organs: Combined concept of phases in xenobiotic transport and metabolism," *Drug metabolism reviews*, vol. 46, no. 3, pp. 261–282, 2014, Publisher: Drug Metab Rev, ISSN: 1097-9883. DOI: 10.3109/03602532.2014.882353.

[156] T. Ishikawa, "The ATP-dependent glutathione S-conjugate export pump," *Trends in biochemical sciences*, vol. 17, no. 11, pp. 463–468, 1992, Publisher: Trends Biochem Sci, ISSN: 0968-0004. DOI: 10.1016/0968-0004(92)90489-V.

[157] E. Courcot, J. Leclerc, J. J. Lafitte, *et al.*, "Xenobiotic metabolism and disposition in human lung cell models: Comparison with in vivo expression profiles," *Drug metabolism and disposition: the biological fate of chemicals*, vol. 40, no. 10, pp. 1953–1965, Oct. 2012, Publisher: Drug Metab Dispos, ISSN: 1521-009X. DOI: 10.1124/DMD.112.046896.

[158] Z. Enlo-Scott, M. Swedrowska, and B. Forbes, "Epithelial permeability and drug absorption in the lungs," in *Inhaled Medicines*, Elsevier, 2021, pp. 267–299. DOI: 10.1016/B978-0-12-814974-4.00004-3.

[159] M. A. Sarkar, "Drug metabolism in the nasal mucosa," *Pharmaceutical research*, vol. 9, no. 1, pp. 1–9, 1992, Publisher: Pharm Res, ISSN: 0724-8741. DOI: 10.1023/A:1018911206646.

[160] J. Hukkanen, J. Hakkola, S. Anttila, *et al.*, "Detection of mRNA encoding xenobiotic-metabolizing cytochrome P450s in human bronchoalveolar macrophages and peripheral blood lymphocytes," *Molecular Carcinogenesis*, vol. 20, no. 2, pp. 224–230, Oct. 1997, ISSN: 08991987. DOI: 10.1002/(SICI)1098-2744(199710)20:2<224::AID-MC9>3.0.CO;2-M.

[161] Bogdanffy MS and Keller DA, "Metabolism of xenobiotics by the respiratory tract," in *Toxicology of the Lung*, Donald E. Gardner, James D Crapo, and Roger O. McClellan, Eds., vol. 3, Philadelphia: Taylor & Francis, 1999, pp. 85–123.

[162] I. M. Keith, E. B. Olson, N. M. Wilson, and C. R. Jefcoate, "Immunological identification and effects of 3-methylcholanthrene and phenobarbital on rat pulmonary cytochrome P-450.," *Cancer research*, vol. 47, no. 7, pp. 1878–82, Apr. 1987, ISSN: 0008-5472.

[163] A. Tronde, B. Nordén, H. Marchner, A. K. Wendel, H. Lennernäs, and U. H. Bengtsson, "Pulmonary absorption rate and bioavailability of drugs in vivo in rats: Structure-absorption relationships and physicochemical profiling of inhaled drugs," *Journal of pharmaceutical sciences*, vol. 92, no. 6, pp. 1216–1233, Jun. 2003, Publisher: J Pharm Sci, ISSN: 0022-3549. DOI: 10.1002/JPS.10386.

[164] J. S. Patton, C. S. Fishburn, and J. G. Weers, "The lungs as a portal of entry for systemic drug delivery," *Proceedings of the American Thoracic Society*, vol. 1, no. 4, pp. 338–344, 2004, Publisher: Proc Am Thorac Soc, ISSN: 1546-3222. DOI: 10.1513/PATS.200409-049TA.

[165] L. S. Schanker, "Drug absorption from the lung," eng, *Biochemical Pharmacology*, vol. 27, no. 4, pp. 381–385, Feb. 1978, ISSN: 0006-2952. DOI: 10.1016/0006-2952(78)90365-9.

[166] J. Yu and Y. W. Chien, "Significance of respiratory dynamics of the lung tissue in pulmonary drug permeation," *Pharmaceutical development and technology*, vol. 7, no. 2, pp. 215–225, 2002, Publisher: Pharm Dev Technol, ISSN: 1083-7450. DOI: 10.1081/PDT-120003489.

[167] D. W. Nebert, T. P. Dalton, A. B. Okey, and F. J. Gonzalez, "Role of aryl hydrocarbon receptor-mediated induction of the CYP1 enzymes in environmental toxicity and cancer," *The Journal of biological chemistry*, vol. 279, no. 23, pp. 23 847–23 850, Jun. 2004, Publisher: J Biol Chem, ISSN: 0021-9258. DOI: 10.1074/JBC.R400004200.

[168] M. McManus, A. Boobis, G. Pacifici, *et al.*, "Xenobiotic metabolism in the human lung," *Life Sciences*, vol. 26, no. 6, pp. 481–487, Feb. 1980, Publisher: Pergamon, ISSN: 0024-3205. DOI: 10.1016/0024-3205(80)90169-1.

[169] X. Ding and L. S. Kaminsky, "Human extrahepatic cytochromes P450: Function in xenobiotic metabolism and tissue-selective chemical toxicity in the respiratory and gastrointestinal tracts," *Annual review of pharmacology and toxicology*, vol. 43, pp. 149–173, 2003, Publisher: Annu Rev Pharmacol Toxicol, ISSN: 0362-1642. DOI: 10.1146/ANNUREV.PHARMTOX.43.100901.140251.

[170] J. Hukkanen, O. Pelkonen, J. Hakkola, and H. Raunio, "Expression and regulation of xenobiotic-metabolizing cytochrome P450 (CYP) enzymes in human lung," *Critical reviews in toxicology*, vol. 32, no. 5, pp. 391–411, 2002, Publisher: Crit Rev Toxicol, ISSN: 1040-8444. DOI: 10.1080/20024091064273.

[171] J. Zhang, Y. Fen Wang, and C. Prakash, "Xenobiotic-metabolizing enzymes in human lung," *Current drug metabolism*, vol. 7, no. 8, pp. 939–948, Nov. 2006, Publisher: Curr Drug Metab, ISSN: 1389-2002. DOI: 10.2174/138920006779010575.

[172] B. Olsson, E. Bondesson, L. Borgström, *et al.*, "Pulmonary Drug Metabolism, Clearance, and Absorption," in *Controlled Pulmonary Drug Delivery*, New York, NY: Springer New York, 2011, pp. 21–50. DOI: 10.1007/978-1-4419-9745-6_2.

[173] J. V. Castell, M. Teresa Donato, and M. J. Gómez-Lechón, "Metabolism and bioactivation of toxicants in the lung. The in vitro cellular approach," *Experimental and Toxicologic Pathology*, vol. 57, pp. 189–204, Jul. 2005, ISSN: 09402993. DOI: 10.1016/j.etp.2005.05.008.

[174] K. B. Okona-Mensah, J. Battershill, A. Boobis, and R. Fielder, "An approach to investigating the importance of high potency polycyclic aromatic hydrocarbons (PAHs) in the induction of lung cancer by air pollution," *Food and chemical toxicology : an international journal published for the British Industrial Biological Research Association*, vol. 43, no. 7, pp. 1103–1116, 2005, Publisher: Food Chem Toxicol, ISSN: 0278-6915. DOI: 10.1016/J.FCT.2005.03.001.

[175] V. I. Lushchak, T. M. Matviishyn, V. V. Husak, J. M. Storey, and K. B. Storey, "Pesticide toxicity: A mechanistic approach," *EXCLI Journal*, vol. 17, p. 1101, 2018, Publisher: Leibniz Research Centre for Working Environment and Human Factors, ISSN: 16112156. DOI: 10.17179/EXCLI2018-1710.

[176] J Jamaludin, N Marlin, H Wood, *et al.*, "Evaluating the impact of genotype on the relationship between impaired lung growth and chronic exposure to traffic derived pollutants," Sep. 2013, ISSN: 0903-1936.

[177] X. Tekpli, N. E. Landvik, K. H. Anmarkud, V. Skaug, A. Haugen, and S. Zienolddiny, "DNA methylation at promoter regions of interleukin 1B, interleukin 6, and interleukin 8 in non-small cell lung cancer," *Cancer immunology, immunotherapy : CII*, vol. 62, no. 2, pp. 337–345, Feb. 2013, Publisher: Cancer Immunol Immunother, ISSN: 1432-0851. DOI: 10.1007/S00262-012-1340-3.

[178] Z. Wang, Q. Pu, C. Huang, and M. Wu, "Crosstalk Between Lung and Extrapulmonary Organs in Infection and Inflammation," *Advances in experimental medicine and biology*, vol. 1303, pp. 333–350, 2021, Publisher: Adv Exp Med Biol, ISSN: 0065-2598. DOI: 10.1007/978-3-030-63046-1_18.

[179] S. Bollenbecker, B. Czaya, O. M. Gutierrez, and S. Krick, "Lung-kidney interactions and their role in chronic kidney disease-associated pulmonary diseases," *Lung Cellular and Molecular Physiology*, vol. 322, no. 5, pp. L625–L640, May 2022, Publisher: American Physiological Society Rockville, MD, ISSN: 15221504. DOI: 10.1152/AJPLUNG.00152.2021.

[180] H. Wang, J. S. Liu, S. H. Peng, *et al.*, "Gut-lung crosstalk in pulmonary involvement with inflammatory bowel diseases," *World journal of gastroenterology*, vol. 19, no. 40, pp. 6794–6804, Oct. 2013, Publisher: World J Gastroenterol, ISSN: 2219-2840. DOI: 10.3748/WJG.V19.I40.6794.

[181] S. Mrozek, J.-M. Constantin, and T. Geeraerts, "Brain-lung crosstalk: Implications for neurocritical care patients," *World journal of critical care medicine*, vol. 4, no. 3, p. 163, 2015, Publisher: World J Crit Care Med, ISSN: 2220-3141. DOI: 10.5492/WJCCM.V4.I3.163.

[182] W. Ye, H. Guo, J. Xu, *et al.*, "Heart-lung crosstalk in pulmonary arterial hypertension following myocardial infarction (Review)," *International Journal of Molecular Medicine*, vol. 46, no. 3, p. 913, Sep. 2020, Publisher: Spandidos Publications, ISSN: 1791244X. DOI: 10.3892/IJMM.2020.4650.

[183] A. M. Siore, R. E. Parker, A. A. Stecenko, *et al.*, "Endotoxin-induced acute lung injury requires interaction with the liver," *American journal of physiology. Lung cellular and molecular physiology*, vol. 289, no. 5, Nov. 2005, Publisher: Am J Physiol Lung Cell Mol Physiol, ISSN: 1040-0605. DOI: 10.1152/AJPLUNG.00137.2005.

[184] P. Ya, H. Xu, Y. Ma, *et al.*, "Liver injury induced in Balb/c mice by PM 2.5 exposure and its alleviation by compound essential oils," *Biomedicine & pharmacotherapy = Biomedecine & pharmacotherapie*, vol. 105, pp. 590–598, Sep. 2018, Publisher: Biomed Pharmacother, ISSN: 1950-6007. DOI: 10.1016/J.BIOPHA.2018.06.010.

[185] J. W. Kim, S. Park, C. W. Lim, K. Lee, and B. Kim, "The Role of Air Pollutants in Initiating Liver Disease," *Toxicological Research*, vol. 30, no. 2, Jun. 2014, ISSN: 1976-8257. DOI: 10.5487/TR.2014.30.2.065.

[186] C. Francoz, H. Mal, and F. Durand, "Anomalies pulmonaires au cours des maladies hépatiques," *EMC - Pneumologie*, vol. 2, no. 1, pp. 49–60, Feb. 2005, Publisher: Elsevier Masson, ISSN: 1762-4223. DOI: 10.1016/J.EMCPN.2004.10.003.

[187] Y. Guo, D. Xiao, X. Yang, *et al.*, "Prenatal exposure to pyrrolizidine alkaloids induced hepatotoxicity and pulmonary injury in fetal rats," *Reproductive toxicology (Elmsford, N.Y.)*, vol. 85, pp. 34–41, Apr. 2019, Publisher: Reprod Toxicol, ISSN: 1873-1708. DOI: 10.1016/J.REPROTOX.2019.02.006.

[188] H. Liu, X. Shan, J. Yu, X. Li, and L. Hu, "Recent Advances in Inhaled Formulations and Pulmonary Insulin Delivery Systems," *Current pharmaceutical biotechnology*, vol. 21, no. 3, pp. 180–193, Oct. 2020, Publisher: Curr Pharm Biotechnol, ISSN: 1873-4316. DOI: 10.2174/1389201020666191011152248.

[189] M. Krishna, "Microscopic anatomy of the liver," *Clinical Liver Disease*, vol. 2, no. S1, S4–S7, Mar. 2013, ISSN: 20462484. DOI: 10.1002/cld.147.

[190] A. Mescher, *Junqueira's Basic Histology: Text & Atlas (13th ed.), by Anthony L. Mescher*. Jan. 2013.

[191] A. M. Rappaport, Z. J. Borowy, W. M. Lougheed, and W. N. Lotto, "Subdivision of hexagonal liver lobules into a structural and functional unit. Role in hepatic physiology and pathology," *The Anatomical Record*, vol. 119, no. 1, pp. 11–33, May 1954, ISSN: 0003-276X. DOI: 10.1002/ar.1091190103.

[192] R. P. Cunningham and N. Porat-Shliom, "Liver Zonation - Revisiting Old Questions With New Technologies.," *Frontiers in physiology*, vol. 12, p. 732 929, 2021, ISSN: 1664-042X. DOI: 10.3389/fphys.2021.732929.

[193] J. L. Boyer, "Bile formation and secretion.," *Comprehensive Physiology*, vol. 3, no. 3, pp. 1035–78, Jul. 2013, ISSN: 2040-4603. DOI: 10.1002/cphy.c120027.

[194] C. Legallais, D. Kim, S. M. Mihaila, *et al.*, "Bioengineering Organs for Blood Detoxification," *Advanced healthcare materials*, vol. 7, no. 21, Nov. 2018, Publisher: Adv Healthc Mater, ISSN: 2192-2659. DOI: 10.1002/ADHM.201800430.

[195] R. P. Mathew and S. K. Venkatesh, "Liver vascular anatomy: A refresher," *Abdominal radiology (New York)*, vol. 43, no. 8, pp. 1886–1895, Aug. 2018, Publisher: Abdom Radiol (NY), ISSN: 2366-0058. DOI: 10.1007/S00261-018-1623-Z.

[196] E. Trefts, M. Gannon, and D. H. Wasserman, "The liver," *Current biology : CB*, vol. 27, no. 21, R1147–R1151, Nov. 2017, Publisher: Curr Biol, ISSN: 1879-0445. DOI: 10.1016/J.CUB.2017.09.019.

[197] D. E. Malarkey, K. Johnson, L. Ryan, G. Boorman, and R. R. Maronpot, "New Insights into Functional Aspects of Liver Morphology," *Toxicologic Pathology*, vol. 33, no. 1, pp. 27–34, Jan. 2005, ISSN: 0192-6233. DOI: 10.1080/01926230590881826.

[198] J. Dich, S. E. Hansen, and H. I. Thieden, "Effect of albumin concentration and colloid osmotic pressure on albumin synthesis in the perfused rat liver," eng, *Acta Physiologica Scandinavica*, vol. 89, no. 3, pp. 352–358, Nov. 1973, ISSN: 0001-6772. DOI: 10.1111/j.1748-1716.1973.tb05530.x.

[199] M. Taverna, A.-L. Marie, J.-P. Mira, and B. Guidet, "Specific antioxidant properties of human serum albumin," eng, *Annals of Intensive Care*, vol. 3, no. 1, p. 4, Feb. 2013, ISSN: 2110-5820. DOI: 10.1186/2110-5820-3-4.

[200] M. Fasano, S. Curry, E. Terreno, *et al.*, "The extraordinary ligand binding properties of human serum albumin," eng, *IUBMB life*, vol. 57, no. 12, pp. 787–796, Dec. 2005, ISSN: 1521-6543. DOI: 10.1080/15216540500404093.

[201] *Schiff's Diseases of the Liver - 10th Edition : Journal of the American College of Surgeons*.

[202] A. Müsch, "The unique Polarity Phenotype of Hepatocytes," *Experimental cell research*, vol. 328, no. 2, pp. 276–283, Nov. 2014, ISSN: 0014-4827. DOI: 10.1016/j.yexcr.2014.06.006.

[203] J. M. Banales, R. C. Huebert, T. Karlsen, M. Strazzabosco, N. F. LaRusso, and G. J. Gores, "Cholangiocyte pathobiology," eng, *Nature Reviews. Gastroenterology & Hepatology*, vol. 16, no. 5, pp. 269–281, May 2019, ISSN: 1759-5053. DOI: 10.1038/s41575-019-0125-y.

[204] J. Poisson, S. Lemoinne, C. Boulanger, *et al.*, "Liver sinusoidal endothelial cells: Physiology and role in liver diseases," *Journal of hepatology*, vol. 66, no. 1, pp. 212–227, Jan. 2017, Publisher: J Hepatol, ISSN: 1600-0641. DOI: 10.1016/J.JHEP.2016.07.009.

[205] S. Shetty, P. F. Lalor, and D. H. Adams, "Liver sinusoidal endothelial cells - gatekeepers of hepatic immunity.," *Nature reviews. Gastroenterology & hepatology*, vol. 15, no. 9, pp. 555–567, 2018, ISSN: 1759-5053. DOI: 10.1038/s41575-018-0020-y.

[206] L. J. Dixon, M. Barnes, H. Tang, M. T. Pritchard, and L. E. Nagy, "Kupffer cells in the liver," *Comprehensive Physiology*, vol. 3, no. 2, pp. 785–797, 2013, Publisher: Compr Physiol, ISSN: 2040-4603. DOI: 10.1002/CPHY.C120026.

[207] K. Nakatani, K. Kaneda, S. Seki, and Y. Nakajima, "Pit cells as liver-associated natural killer cells: Morphology and function.," *Medical electron microscopy : official journal of the Clinical Electron Microscopy Society of Japan*, vol. 37, no. 1, pp. 29–36, Mar. 2004, ISSN: 0918-4287. DOI: 10.1007/s00795-003-0229-9.

[208] S. L. Friedman, "Hepatic Stellate Cells: Protean, Multifunctional, and Enigmatic Cells of the Liver," *Physiological Reviews*, vol. 88, no. 1, pp. 125–172, Jan. 2008, ISSN: 0031-9333. DOI: 10.1152/physrev.00013.2007.

[209] I. M. Arias, H. J. Alter, J. L. Boyer, *et al.*, "The liver: Biology and pathobiology, fifth edition," *The Liver: Biology and Pathobiology*, pp. 1–1191, Jan. 2009, Publisher: wiley ISBN: 9780470747919. DOI: 10.1002/9780470747919.

[210] P. Godoy, N. J. Hewitt, U. Albrecht, *et al.*, "Recent advances in 2D and 3D in vitro systems using primary hepatocytes, alternative hepatocyte sources and non-parenchymal liver cells and their use in investigating mechanisms of hepatotoxicity, cell signaling and ADME," *Archives of Toxicology*, vol. 87, pp. 1315–1530, 2013. DOI: 10.1007/s00204-013-1078-5.

[211] S. A. Belinsky, F. C. Kauffman, S Ji, J. J. Lemasters, and R. G. Thurman, "Stimulation of mixed-function oxidation of 7-ethoxycoumarin in periportal and pericentral regions of the perfused rat liver by xylitol.," *European journal of biochemistry*, vol. 137, no. 1-2, pp. 1–6, Dec. 1983, ISSN: 0014-2956. DOI: 10.1111/j.1432-1033.1983.tb07787.x.

[212] A. S. Nies, D. G. Shand, and G. R. Wilkinson, "Altered hepatic blood flow and drug disposition.," *Clinical pharmacokinetics*, vol. 1, no. 2, pp. 135–55, 1976, ISSN: 0312-5963. DOI: 10.2165/00003088-197601020-00005.

[213] O Pelkonen and M Turpeinen, "In vitro-in vivo extrapolation of hepatic clearance: Biological tools, scaling factors, model assumptions and correct concentrations.," *Xenobiotica; the fate of foreign compounds in biological systems*, vol. 37, no. 10-11, pp. 1066–89, 2007, ISSN: 0049-8254. DOI: 10.1080/00498250701620726.

[214] M. S. Roberts, B. M. Magnusson, F. J. Burczynski, and M. Weiss, "Enterohepatic circulation: Physiological, pharmacokinetic and clinical implications.," *Clinical pharmacokinetics*, vol. 41, no. 10, pp. 751–90, 2002, ISSN: 0312-5963. DOI: 10.2165/00003088-200241100-00005.

[215] G. G. Graham, M. J. Davies, R. O. Day, A. Mohamudally, and K. F. Scott, "The modern pharmacology of paracetamol: Therapeutic actions, mechanism of action, metabolism, toxicity and recent pharmacological findings," *Inflammopharmacology*, vol. 21, no. 3, pp. 201–232, Jun. 2013, Publisher: Inflammopharmacology, ISSN: 1568-5608. DOI: 10.1007/S10787-013-0172-X.

[216] A. Reuben, D. G. Koch, and W. M. Lee, "Drug-induced acute liver failure: Results of a U.S. multicenter, prospective study," *Hepatology (Baltimore, Md.)*, vol. 52, no. 6, pp. 2065–2076, Dec. 2010, Publisher: Hepatology, ISSN: 1527-3350. DOI: 10.1002/HEP.23937.

[217] L. J. Chun, M. J. Tong, R. W. Busuttil, and J. R. Hiatt, "Acetaminophen hepatotoxicity and acute liver failure," *Journal of clinical gastroenterology*, vol. 43, no. 4, pp. 342–349, Apr. 2009, Publisher: J Clin Gastroenterol, ISSN: 1539-2031. DOI: 10.1097/MCG.0B013E31818A3854.

[218] A. Michaut, C. Moreau, M. A. Robin, and B. Fromenty, "Acetaminophen-induced liver injury in obesity and nonalcoholic fatty liver disease," *Liver international : official journal of the International Association for the Study of the Liver*, vol. 34, no. 7, e171–e179, 2014, Publisher: Liver Int, ISSN: 1478-3231. DOI: 10.1111/LIV.12514.

[219] S. S. Lee, J. T. Buters, T. Pineau, P. Fernandez-Salguero, and F. J. Gonzalez, "Role of CYP2E1 in the hepatotoxicity of acetaminophen," *The Journal of biological chemistry*, vol. 271, no. 20, pp. 12 063–12 067, 1996, Publisher: J Biol Chem, ISSN: 0021-9258. DOI: 10.1074/JBC.271.20.12063.

[220] M. R. McGill and H. Jaeschke, "Metabolism and disposition of acetaminophen: Recent advances in relation to hepatotoxicity and diagnosis," *Pharmaceutical research*, vol. 30, no. 9, pp. 2174–2187, Sep. 2013, Publisher: Pharm Res, ISSN: 1573-904X. DOI: 10.1007/S11095-013-1007-6.

[221] S. F. Cook, A. D. King, J. N. van den Anker, and D. G. Wilkins, "Simultaneous quantification of acetaminophen and five acetaminophen metabolites in human plasma and urine by high-performance liquid chromatography-electrospray ionization-tandem mass spectrometry: Method validation and application to a neonatal pharmacokinetic study," *Journal of chromatography. B, Analytical technologies in the biomedical and life sciences*, vol. 1007, pp. 30–42, Dec. 2015, Publisher: J Chromatogr B Analyt Technol Biomed Life Sci, ISSN: 1873-376X. DOI: 10.1016/J.JCHROMB.2015.10.013.

[222] B. Fromenty, "Bridging the gap between old and new concepts in drug-induced liver injury," *Clinics and research in hepatology and gastroenterology*, vol. 37, no. 1, pp. 6–9, Feb. 2013, Publisher: Clin Res Hepatol Gastroenterol, ISSN: 2210-741X. DOI: 10.1016/J.CLINRE.2012.12.003.

[223] E. Boyland, F. F. McDonald, and M. J. Rumens, "Variation in the toxicity of phosgene for small animals with the duration of exposure," *British Journal of Pharmacology and Chemotherapy*, vol. 1, no. 2, p. 81, Jun. 1946, Publisher: Wiley-Blackwell, ISSN: 0366-0826.

[224] S. C. RAY, E. J. KING, and C. V. HARRISON, "The Action of Anthracite and Bituminous Coal Dusts Mixed with Quartz on the Lungs of Rats," *British Journal of Industrial Medicine*, vol. 8, no. 2, p. 74, 1951, Publisher: BMJ Publishing Group, ISSN: 00071072. DOI: 10.1136/OEM.8.2.74.

[225] D. R. Coman, H. D. Bruner, R. C. Horn, *et al.*, "Studies on Experimental Phosgene Poisoning: I. The Pathologic Anatomy of Phosgene Poisoning, with Special Reference to the Early and Late Phases*," *The American Journal of Pathology*, vol. 23, no. 6, p. 1037, Nov. 1947, Publisher: American Society for Investigative Pathology, ISSN: 00029440.

[226] F. Sewell, I. Ragan, T. Marczylo, *et al.*, "A global initiative to refine acute inhalation studies through the use of 'evident toxicity' as an endpoint: Towards adoption of the fixed concentration procedure," *Regulatory toxicology and pharmacology : RTP*, vol. 73, no. 3, pp. 770–779, Dec. 2015, Publisher: Regul Toxicol Pharmacol, ISSN: 1096-0295. DOI: 10.1016/J.YRTPH.2015.10.018.

[227] C. A. Pope, D. W. Dockery, and J. Schwartz, "Review of Epidemiological Evidence of Health Effects of Particulate Air Pollution," *Inhalation Toxicology*, vol. 7, no. 1, pp. 1–18, Jan. 1995, ISSN: 0895-8378. DOI: 10.3109/08958379509014267.

[228] J. M. Samet, F. Dominici, F. C. Curriero, I. Coursac, and S. L. Zeger, "Fine particulate air pollution and mortality in 20 U.S. cities, 1987-1994," *The New England journal of medicine*, vol. 343, no. 24, pp. 1742–1749, Dec. 2000, Publisher: N Engl J Med, ISSN: 0028-4793. DOI: 10.1056/NEJM200012143432401.

[229] C. A. Pope, R. T. Burnett, G. D. Thurston, *et al.*, "Cardiovascular mortality and long-term exposure to particulate air pollution: Epidemiological evidence of general pathophysiological pathways of disease," *Circulation*, vol. 109, no. 1, pp. 71–77, Jan. 2004, Publisher: Circulation, ISSN: 1524-4539. DOI: 10.1161/01.CIR.0000108927.80044.7F.

[230] M. L. Bell, D. L. Davis, and T. Fletcher, "A retrospective assessment of mortality from the London smog episode of 1952: The role of influenza and pollution.," *Environmental Health Perspectives*, vol. 112, no. 1, pp. 6–8, Jan. 2004, ISSN: 0091-6765.

[231] I. C. Hanigan, M. I. Rolfe, L. D. Knibbs, *et al.*, "All-cause mortality and long-term exposure to low level air pollution in the '45 and up study' cohort, Sydney, Australia, 2006-2015," *Environment international*, vol. 126, pp. 762–770, May 2019, Publisher: Environ Int, ISSN: 1873-6750. DOI: 10.1016/J.ENVINT.2019.02.044.

[232] E. E. Morrisey and B. L. Hogan, "Preparing for the first breath: Genetic and cellular mechanisms in lung development," *Developmental cell*, vol. 18, no. 1, pp. 8–23, Jan. 2010, Publisher: Dev Cell, ISSN: 1878-1551. DOI: 10.1016/J.DEVCEL.2009.12.010.

[233] D. E. Ingber, "Is it Time for Reviewer 3 to Request Human Organ Chip Experiments Instead of Animal Validation Studies?" *Advanced Science*, vol. 7, no. 22, p. 2 002 030, Nov. 2020, Publisher: John Wiley & Sons, Ltd, ISSN: 2198-3844. DOI: 10.1002/ADVS.202002030.

[234] H. Hardin-Pouzet and S. Morosan, "Organismes-modèles et réglementation de la recherche animale," *médecine/sciences*, vol. 35, no. 2, pp. 153–156, Feb. 2019, ISSN: 0767-0974. DOI: 10.1051/medsci/2019006.

[235] J. R. Rock, S. H. Randell, and B. L. Hogan, "Airway basal stem cells: A perspective on their roles in epithelial homeostasis and remodeling," *Disease models & mechanisms*, vol. 3, no. 9-10, pp. 545–556, Sep. 2010, Publisher: Dis Model Mech, ISSN: 1754-8411. DOI: 10.1242/DMM.006031.

[236] F. Oesch, E. Fabian, and R. Landsiedel, "Xenobiotica-metabolizing enzymes in the lung of experimental animals, man and in human lung models," *Archives of toxicology*, vol. 93, no. 12, pp. 3419–3489, Dec. 2019, Publisher: Arch Toxicol, ISSN: 1432-0738. DOI: 10.1007/S00204-019-02602-7.

[237] R. Greek and A. Menache, "Systematic Reviews of Animal Models: Methodology versus Epistemology," *International Journal of Medical Sciences*, vol. 10, no. 3, pp. 206–221, 2013, ISSN: 1449-1907. DOI: 10.7150/ijms.5529.

[238] L. A. Low, C. Mummery, B. R. Berridge, C. P. Austin, and D. A. Tagle, "Organs-on-chips: Into the next decade," *Nature Reviews Drug Discovery*, Sep. 2020, ISSN: 1474-1776. DOI: 10.1038/s41573-020-0079-3.

[239] Russell WMS and Burch RL, "The Principles of Humane Experimental Technique," *Medical Journal of Australia*, vol. 1, no. 13, pp. 500–500, Mar. 1960, Publisher: John Wiley & Sons, Ltd, ISSN: 1326-5377. DOI: 10.5694/J.1326-5377.1960.TB73127.X.

[240] J. Tannenbaum and B. T. Bennett, "Russell and Burch's 3Rs Then and Now: The Need for Clarity in Definition and Purpose," *Journal of the American Association for Laboratory Animal Science : JAALAS*, vol. 54, no. 2, p. 120, Mar. 2015, Publisher: American Association for Laboratory Animal Science, ISSN: 15596109.

[241] T. Lookman, P. V. Balachandran, D. Xue, and R. Yuan, "Active learning in materials science with emphasis on adaptive sampling using uncertainties for targeted design," en, *npj Computational Materials*, vol. 5, no. 1, pp. 1–17, Feb. 2019, Number: 1 Publisher: Nature Publishing Group, ISSN: 2057-3960. DOI: 10.1038/s41524-019-0153-8.

[242] S. Alqahtani, "In silico ADME-Tox modeling: Progress and prospects," eng, *Expert Opinion on Drug Metabolism & Toxicology*, vol. 13, no. 11, pp. 1147–1158, Nov. 2017, ISSN: 1744-7607. DOI: 10.1080/17425255.2017.1389897.

[243] J. Verma, V. M. Khedkar, and E. C. Coutinho, "3D-QSAR in drug design–a review," eng, *Current Topics in Medicinal Chemistry*, vol. 10, no. 1, pp. 95–115, 2010, ISSN: 1873-4294. DOI: 10.2174/156802610790232260.

[244] P. Zhao, L. Zhang, J. A. Grillo, *et al.*, "Applications of physiologically based pharmacokinetic (PBPK) modeling and simulation during regulatory review," eng, *Clinical Pharmacology and Therapeutics*, vol. 89, no. 2, pp. 259–267, Feb. 2011, ISSN: 1532-6535. DOI: 10.1038/clpt.2010.298.

[245] L. Suter-Dick, P. M. Alves, B. J. Blaauboer, *et al.*, "Stem cell-derived systems in toxicology assessment," *Stem cells and development*, vol. 24, no. 11, pp. 1284–1296, Jun. 2015, Publisher: Stem Cells Dev, ISSN: 1557-8534. DOI: 10.1089/SCD.2014.0540.

[246] F. Marano, P. Hubert, L. Geoffroy, and H. Juin, *Quelles alternatives en expérimentation animale ? - Pratiques et éthique*, Quae éditions, Ed. 2020, ISSN: 1952-1251, ISBN: 978-2-7592-3187-4.

[247] A. S. Zeiger, B. Hinton, and K. J. Van Vliet, "Why the dish makes a difference: Quantitative comparison of polystyrene culture surfaces," eng, *Acta Biomaterialia*, vol. 9, no. 7, pp. 7354–7361, Jul. 2013, ISSN: 1878-7568. DOI: 10.1016/j.actbio.2013.02.035.

[248] C. Ehrhardt, J. Fiegel, S. Fuchs, *et al.*, "Drug Absorption by the Respiratory Mucosa: Cell Culture Models and Particulate Drug Carriers," *Journal of Aerosol Medicine*, vol. 15, no. 2, pp. 131–139, Jun. 2002, ISSN: 0894-2684. DOI: 10.1089/089426802320282257.

[249] N. R. Mathias, J. Timoszyk, P. I. Stetsko, J. R. Megill, R. L. Smith, and D. A. Wall, "Permeability Characteristics of Calu-3 Human Bronchial Epithelial Cells: In Vitro - In Vivo Correlation to Predict Lung Absorption in Rats," *Journal of Drug Targeting*, vol. 10, no. 1, pp. 31–40, Jan. 2002, ISSN: 1061-186X. DOI: 10.1080/10611860290007504.

[250] J. J. Boei, S. Vermeulen, B. Klein, *et al.*, "Xenobiotic metabolism in differentiated human bronchial epithelial cells," *Archives of toxicology*, vol. 91, no. 5, pp. 2093–2105, May 2017, Publisher: Arch Toxicol, ISSN: 1432-0738. DOI: 10.1007/S00204-016-1868-7.

[251] R. R. Reddel, Y Ke, B. I. Gerwin, *et al.*, "Transformation of human bronchial epithelial cells by infection with SV40 or adenovirus-12 SV40 hybrid virus, or transfection via strontium phosphate coprecipitation with a plasmid containing SV40 early region genes.," *Cancer research*, vol. 48, no. 7, pp. 1904–9, Apr. 1988, ISSN: 0008-5472.

[252] C. E. Stewart, E. E. Torr, N. H. Mohd Jamili, C. Bosquillon, and I. Sayers, "Evaluation of differentiated human bronchial epithelial cell culture systems for asthma research.," *Journal of allergy*, vol. 2012, p. 943 982, 2012, ISSN: 1687-9791. DOI: 10.1155/2012/943982.

[253] K. A. Foster, C. G. Oster, M. M. Mayer, M. L. Avery, and K. L. Audus, "Characterization of the A549 cell line as a type II pulmonary epithelial cell model for drug metabolism," *Experimental cell research*, vol. 243, no. 2, pp. 359–366, Sep. 1998, Publisher: Exp Cell Res, ISSN: 0014-4827. DOI: 10.1006/EXCR.1998.4172.

[254] B. Rothen-Rutishauser, F. Blank, C. Mühlfeld, and P. Gehr, "In vitro models of the human epithelial airway barrier to study the toxic potential of particulate matter," *Expert opinion on drug metabolism & toxicology*, vol. 4, no. 8, pp. 1075–1089, Aug. 2008, Publisher: Expert Opin Drug Metab Toxicol, ISSN: 1742-5255. DOI: 10.1517/17425255.4.8.1075.

[255] J. E. Duncan, J. A. Whitsett, and A. D. Horowitz, "Pulmonary surfactant inhibits cationic liposome-mediated gene delivery to respiratory epithelial cells in vitro," *Human gene therapy*, vol. 8, no. 4, pp. 431–438, Mar. 1997, Publisher: Hum Gene Ther, ISSN: 1043-0342. DOI: 10.1089/HUM.1997.8.4-431.

[256] K. Zscheppang, J. Berg, S. Hedtrich, *et al.*, "Human Pulmonary 3D Models For Translational Research," *Biotechnology journal*, vol. 13, no. 1, Jan. 2018, Publisher: Biotechnol J, ISSN: 1860-7314. DOI: 10.1002/BIOT.201700341.

[257] S. Kletting, S. Barthold, U. Repnik, *et al.*, "Co-culture of human alveolar epithelial (hAELVi) and macrophage (THP-1) cell lines," eng, *ALTEX*, vol. 35, no. 2, pp. 211–222, 2018, ISSN: 1868-8551. DOI: 10.14573/altex.1607191.

[258] A. Kuehn, S. Kletting, C. de Souza Carvalho-Wodarz, *et al.*, "Human alveolar epithelial cells expressing tight junctions to model the air-blood barrier.," *ALTEX*, vol. 33, no. 3, pp. 251–60, 2016, ISSN: 1868-8551. DOI: 10.14573/altex.1511131.

[259] A. Dvorak, A. E. Tilley, R. Shaykhiev, R. Wang, and R. G. Crystal, "Do airway epithelium air-liquid cultures represent the in vivo airway epithelium transcriptome?" *American journal of respiratory cell and molecular biology*, vol. 44, no. 4, pp. 465–473, Apr. 2011, Publisher: Am J Respir Cell Mol Biol, ISSN: 1535-4989. DOI: 10.1165/RCMB.2009-0453OC.

[260] M. F. Acosta, P. Muralidharan, S. A. Meenach, D. Hayes, S. M.-Black, and H. M. Mansour, "In Vitro Pulmonary Cell Culture in Pharmaceutical Inhalation Aerosol Delivery: 2-D, 3-D, and In Situ Bioimpactor Models," *Current pharmaceutical design*, vol. 22, no. 17, pp. 2522–2531, Feb. 2016, Publisher: Curr Pharm Des, ISSN: 1873-4286. DOI: 10.2174/1381612822666160202142104.

[261] C. Jensen and Y. Teng, "Is It Time to Start Transitioning From 2D to 3D Cell Culture?" *Frontiers in molecular biosciences*, vol. 7, Mar. 2020, Publisher: Front Mol Biosci, ISSN: 2296-889X. DOI: 10.3389/FMOLB.2020.00033.

[262] K. B. Sivars, U. Sivars, E. Hornberg, *et al.*, "A 3D Human Airway Model Enables Prediction of Respiratory Toxicity of Inhaled Drugs In Vitro," *Toxicological sciences : an official journal of the Society of Toxicology*, vol. 162, no. 1, pp. 301–308, Mar. 2018, Publisher: Toxicol Sci, ISSN: 1096-0929. DOI: 10.1093/TOXSCI/KFX255.

[263] A. J. Carterson, K. Höner Zu Bentrup, C. M. Ott, *et al.*, "A549 lung epithelial cells grown as three-dimensional aggregates: Alternative tissue culture model for Pseudomonas aeruginosa pathogenesis," *Infection and immunity*, vol. 73, no. 2, pp. 1129–1140, Feb. 2005, Publisher: Infect Immun, ISSN: 0019-9567. DOI: 10.1128/IAI.73.2.1129-1140.2005.

[264] M. I. Hermanns, S. Fuchs, M. Bock, *et al.*, "Primary human coculture model of alveolo-capillary unit to study mechanisms of injury to peripheral lung," *Cell and tissue research*, vol. 336, no. 1, pp. 91–105, 2009, Publisher: Cell Tissue Res, ISSN: 1432-0878. DOI: 10.1007/S00441-008-0750-1.

[265] J. Kasper, M. I. Hermanns, C. Bantz, *et al.*, "Inflammatory and cytotoxic responses of an alveolar-capillary coculture model to silica nanoparticles: Comparison with conventional monocultures," *Particle and fibre toxicology*, vol. 8, no. 1, Jan. 2011, Publisher: Part Fibre Toxicol, ISSN: 1743-8977. DOI: 10.1186/1743-8977-8-6.

[266] B. M. Rothen-Rutishauser, S. C. Kiama, and P. Gehr, "A three-dimensional cellular model of the human respiratory tract to study the interaction with particles," *American journal of respiratory cell and molecular biology*, vol. 32, no. 4, pp. 281–289, Apr. 2005, Publisher: Am J Respir Cell Mol Biol, ISSN: 1044-1549. DOI: 10.1165/RCMB.2004-0187OC.

[267] A. D. Lehmann, N. Daum, M. Bur, C. M. Lehr, P. Gehr, and B. M. Rothen-Rutishauser, "An in vitro triple cell co-culture model with primary cells mimicking the human alveolar epithelial barrier," *European journal of pharmaceutics and biopharmaceutics : official journal of Arbeitsgemeinschaft fur Pharmazeutische Verfahrenstechnik e.V*, vol. 77, no. 3, pp. 398–406, Apr. 2011, Publisher: Eur J Pharm Biopharm, ISSN: 1873-3441. DOI: 10.1016/J.EJPB.2010.10.014.

[268] E. Alfaro-Moreno, T. S. Nawrot, B. M. Vanaudenaerde, *et al.*, "Co-cultures of multiple cell types mimic pulmonary cell communication in response to urban PM10," *The European respiratory journal*, vol. 32, no. 5, pp. 1184–1194, Nov. 2008, Publisher: Eur Respir J, ISSN: 1399-3003. DOI: 10.1183/09031936.00044008.

[269] K. Sato, W. Zhang, S. Safarikia, *et al.*, "Organoids and Spheroids as Models for Studying Cholestatic Liver Injury and Cholangiocarcinoma," *Hepatology (Baltimore, Md.)*, vol. 74, no. 1, pp. 491–502, Jul. 2021, Publisher: Hepatology, ISSN: 1527-3350. DOI: 10.1002/HEP.31653.

[270] Z. Zhang, H. Wang, Q. Ding, *et al.*, "Establishment of patient-derived tumor spheroids for non-small cell lung cancer," *PloS one*, vol. 13, no. 3, Mar. 2018, Publisher: PLoS One, ISSN: 1932-6203. DOI: 10.1371/JOURNAL.PONE.0194016.

[271] K. Takahashi, M. Mitsui, K. Takeuchi, *et al.*, "Preservation of the characteristics of the cultured human type II alveolar epithelial cells," *Lung*, vol. 182, no. 4, pp. 213–226, 2004, Publisher: Lung, ISSN: 0341-2040. DOI: 10.1007/S00408-004-2504-5.

[272] D. A. Gendre, E. Ameti, W. Karenovics, N. Perriraz-Mayer, F. Triponez, and V. Serre-Beinier, "Optimization of tumor spheroid model in mesothelioma and lung cancers and anti-cancer drug testing in H2052/484 spheroids," *Oncotarget*, vol. 12, no. 24, pp. 2375–2387, Nov. 2021, ISSN: 1949-2553. DOI: 10.18632/oncotarget.28134.

[273] M. A. Lancaster and J. A. Knoblich, "Organogenesis in a dish: Modeling development and disease using organoid technologies," *Science (New York, N.Y.)*, vol. 345, no. 6194, 2014, Publisher: Science, ISSN: 1095-9203. DOI: 10.1126/SCIENCE.1247125.

[274] F. Schutgens and H. Clevers, "Human Organoids: Tools for Understanding Biology and Treating Diseases," *Annual review of pathology*, vol. 15, pp. 211–234, Jan. 2020, Publisher: Annu Rev Pathol, ISSN: 1553-4014. DOI: 10.1146/ANNUREV-PATHMECHDIS-012419-032611.

[275] M. E. Sakalem, M. T. De Sibio, F. A. d. S. da Costa, and M. de Oliveira, "Historical evolution of spheroids and organoids, and possibilities of use in life sciences and medicine," *Biotechnology Journal*, vol. 16, no. 5, p. 2 000 463, May 2021, ISSN: 1860-6768. DOI: 10.1002/biot.202000463.

[276] K. Ohata and H. C. Ott, "Human-scale lung regeneration based on decellularized matrix scaffolds as a biologic platform," *Surgery today*, vol. 50, no. 7, pp. 633–643, Jul. 2020, Publisher: Surg Today, ISSN: 1436-2813. DOI: 10.1007/S00595-020-02000-Y.

[277] H. Zhou, K. Kitano, X. Ren, *et al.*, "Bioengineering Human Lung Grafts on Porcine Matrix," *Annals of surgery*, vol. 267, no. 3, pp. 590–598, Mar. 2018, Publisher: Ann Surg, ISSN: 1528-1140. DOI: 10.1097/SLA.0000000000002129.

[278] O. Rosmark, E. Åhrman, C. Müller, *et al.*, "Quantifying extracellular matrix turnover in human lung scaffold cultures," *Scientific reports*, vol. 8, no. 1, Dec. 2018, Publisher: Sci Rep, ISSN: 2045-2322. DOI: 10.1038/S41598-018-23702-X.

[279] N. Kawai, Y. Ouji, M. Sakagami, *et al.*, "Induction of lung-like cells from mouse embryonic stem cells by decellularized lung matrix," *Biochemistry and Biophysics Reports*, vol. 15, p. 33, Sep. 2018, Publisher: Elsevier, ISSN: 24055808. DOI: 10.1016/J.BBREP.2018.06.005.

[280] L. Wang, Y. Zhao, F. Yang, *et al.*, "Biomimetic collagen biomaterial induces in situ lung regeneration by forming functional alveolar," *Biomaterials*, vol. 236, Apr. 2020, Publisher: Biomaterials, ISSN: 1878-5905. DOI: 10.1016/J.BIOMATERIALS.2020.119825.

[281] A. Kosmala, M. Fitzgerald, E. Moore, and F. Stam, "Evaluation of a Gelatin-Modified Poly(-Caprolactone) Film as a Scaffold for Lung Disease," *Analytical Letters*, vol. 50, no. 1, pp. 219–232, Jan. 2017, ISSN: 0003-2719. DOI: 10.1080/00032719.2016.1163363.

[282] P. D. Dalton, C. Vaquette, B. L. Farrugia, T. R. Dargaville, T. D. Brown, and D. W. Hutmacher, "Electrospinning and additive manufacturing: Converging technologies," *Biomaterials Science*, vol. 1, no. 2, pp. 171–185, Jan. 2013, Publisher: The Royal Society of Chemistry, ISSN: 2047-4849. DOI: 10.1039/C2BM00039C.

[283] H. Liu, X. Ding, G. Zhou, P. Li, X. Wei, and Y. Fan, "Electrospinning of Nanofibers for Tissue Engineering Applications," *Journal of Nanomaterials*, vol. 2013, pp. 1–11, 2013, ISSN: 1687-4110. DOI: 10.1155/2013/495708.

[284] B. Azimi, M. S. S. Bafqi, A. Fusco, *et al.*, "Electrospun ZnO/Poly(Vinylidene Fluoride-Trifluoroethylene) Scaffolds for Lung Tissue Engineering," *Tissue engineering. Part A*, vol. 26, no. 23-24, pp. 1312–1331, Dec. 2020, Publisher: Tissue Eng Part A, ISSN: 1937-335X. DOI: 10.1089/TEN.TEA.2020.0172.

[285] J. C. Bridge, J. W. Aylott, C. E. Brightling, *et al.*, "Adapting the Electrospinning Process to Provide Three Unique Environments for a Tri-layered In Vitro Model of the Airway Wall," *Journal of Visualized Experiments : JoVE*, vol. 2015, no. 101, pp. 1–11, Jul. 2015, Publisher: MyJoVE Corporation, ISSN: 1940087X. DOI: 10.3791/52986.

[286] J. Malda, J. Visser, F. P. Melchels, *et al.*, "25th anniversary article: Engineering hydrogels for biofabrication," *Advanced materials (Deerfield Beach, Fla.)*, vol. 25, no. 36, pp. 5011–5028, Sep. 2013, Publisher: Adv Mater, ISSN: 1521-4095. DOI: 10.1002/ADMA.201302042.

[287] L. Huang, W. Yuan, Y. Hong, *et al.*, "3D printed hydrogels with oxidized cellulose nanofibers and silk fibroin for the proliferation of lung epithelial stem cells," *Cellulose*, vol. 28, no. 1, pp. 241–257, Jan. 2021, Publisher: Springer Science and Business Media B.V., ISSN: 1572882X. DOI: 10.1007/S10570-020-03526-7/FIGURES/6.

[288] A. Mondal, A. Gebeyehu, M. Miranda, *et al.*, "Characterization and printability of Sodium alginate -Gelatin hydrogel for bioprinting NSCLC co-culture," *Scientific reports*, vol. 9, no. 1, Dec. 2019, Publisher: Sci Rep, ISSN: 2045-2322. DOI: 10.1038/S41598-019-55034-9.

[289] D. Huh, B. D. Matthews, A. Mammoto, M. Montoya-Zavala, H. Yuan Hsin, and D. E. Ingber, "Reconstituting organ-level lung functions on a chip," *Science*, vol. 328, no. 5986, pp. 1662–1668, 2010, ISSN: 00368075. DOI: 10.1126/science.1188302.

[290] P. Zamprogno, S. Wüthrich, S. Achenbach, *et al.*, "Second-generation lung-on-a-chip with an array of stretchable alveoli made with a biological membrane," *Communications biology*, vol. 4, no. 1, Dec. 2021, Publisher: Commun Biol, ISSN: 2399-3642. DOI: 10.1038/S42003-021-01695-0.

[291] K. L. Sellgren, E. J. Butala, B. P. Gilmour, S. H. Randell, and S. Grego, "A biomimetic multicellular model of the airways using primary human cells," *Lab on a Chip*, vol. 14, no. 17, pp. 3349–3358, Jul. 2014, Publisher: The Royal Society of Chemistry, ISSN: 1473-0189. DOI: 10.1039/C4LC00552J.

[292] A. Skardal, S. V. Murphy, M. Devarasetty, *et al.*, "Multi-tissue interactions in an integrated three-tissue organ-on-a-chip platform," *Scientific Reports*, vol. 7, no. 1, Dec. 2017, ISSN: 2045-2322. DOI: 10.1038/s41598-017-08879-x.

[293] E. Hashemi, C. Till, and C. Ioannides, "Stability of Phase II Conjugation Systems in Cultured Precision-cut Rat Hepatic Slices," *Toxicology in Vitro*, vol. 13, no. 3, pp. 459–466, Jun. 1999, Publisher: Pergamon, ISSN: 0887-2333. DOI: 10.1016/S0887-2333(99)00017-X.

[294] H. N. Ghantous, J. Fernando, A. J. Gandolfi, and K. Brendel, "Sevoflurane is biotransformed by guinea pig liver slices but causes minimal cytotoxicity," *Anesthesia and analgesia*, vol. 75, no. 3, pp. 436–440, 1992, Publisher: Anesth Analg, ISSN: 0003-2999. DOI: 10.1213/00000539-199209000-00021.

[295] R. J. Price, S. E. Ball, A. B. Renwick, P. T. Barton, J. A. Beamand, and B. G. Lake, "Use of precision-cut rat liver slices for studies of xenobiotic metabolism and toxicity: Comparison of the Krumdieck and Brendel tissue slicers," *Xenobiotica; the fate of foreign compounds in biological systems*, vol. 28, no. 4, pp. 361–371, 1998, Publisher: Xenobiotica, ISSN: 0049-8254. DOI: 10.1080/004982598239470.

[296] H. H. Gerets, K. Tilmant, B. Gerin, *et al.*, "Characterization of primary human hepatocytes, HepG2 cells, and HepaRG cells at the mRNA level and CYP activity in response to inducers and their predictivity for the detection of human hepatotoxins," *Cell biology and toxicology*, vol. 28, no. 2, pp. 69–87, Apr. 2012, Publisher: Cell Biol Toxicol, ISSN: 1573-6822. DOI: 10.1007/S10565-011-9208-4.

[297] M. Lübberstedt, U. Müller-Vieira, M. Mayer, *et al.*, "HepaRG human hepatic cell line utility as a surrogate for primary human hepatocytes in drug metabolism assessment in vitro.," *Journal of pharmacological and toxicological methods*, vol. 63, no. 1, pp. 59–68, 2010, ISSN: 1873-488X. DOI: 10.1016/j.vascn.2010.04.013.

[298] S. S. Palabiyik, E. Karakus, Z. Halici, *et al.*, "The protective effects of carvacrol and thymol against paracetamol-induced toxicity on human hepatocellular carcinoma cell lines (HepG2)," *Human & experimental toxicology*, vol. 35, no. 12, pp. 1252–1263, Dec. 2016, Publisher: Hum Exp Toxicol, ISSN: 1477-0903. DOI: 10.1177/0960327115627688.

[299] W. M. Westerink and W. G. Schoonen, "Cytochrome P450 enzyme levels in HepG2 cells and cryopreserved primary human hepatocytes and their induction in HepG2 cells," *Toxicology in vitro : an international journal published in association with BIBRA*, vol. 21, no. 8, pp. 1581–1591, Dec. 2007, Publisher: Toxicol In Vitro, ISSN: 0887-2333. DOI: 10.1016/J.TIV.2007.05.014.

[300] A. Takemura, S. Gong, T. Sato, *et al.*, "Evaluation of Parent- and Metabolite-Induced Mitochondrial Toxicities Using CYP-Introduced HepG2 cells," *Journal of pharmaceutical sciences*, vol. 110, no. 9, pp. 3306–3312, Sep. 2021, Publisher: J Pharm Sci, ISSN: 1520-6017. DOI: 10.1016/J.XPHS.2021.06.001.

[301] K. Zeilinger, N. Freyer, G. Damm, D. Seehofer, and F. Knö spel, *Cell sources for in vitro human liver cell culture models*, Pages: 1684-1698 Publication Title: Experimental Biology and Medicine Volume: 241, 2016. DOI: 10.1177/1535370216657448.

[302] E. L. LeCluyse, E. Alexandre, G. A. Hamilton, *et al.*, "Isolation and Culture of Primary Human Hepatocytes," in *Basic Cell Culture Protocols*, New Jersey: Humana Press, 2005, pp. 207–230. DOI: 10.1385/1-59259-838-2:207.

[303] L. Boeri, L. Izzo, L. Sardelli, M. Tunesi, D. Albani, and C. Giordano, "Advanced Organ-on-a-Chip Devices to Investigate Liver Multi-Organ Communication: Focus on Gut, Microbiota and Brain.," *Bioengineering (Basel, Switzerland)*, vol. 6, no. 4, Sep. 2019, ISSN: 2306-5354. DOI: 10.3390/bioengineering6040091.

[304] L. Schyschka, J. J. Sánchez, Z. Wang, *et al.*, "Hepatic 3D cultures but not 2D cultures preserve specific transporter activity for acetaminophen-induced hepatotoxicity," *Archives of toxicology*, vol. 87, no. 8, pp. 1581–1593, Aug. 2013, Publisher: Arch Toxicol, ISSN: 1432-0738. DOI: 10.1007/S00204-013-1080-Y.

[305] T. De Bruyn, S. Chatterjee, S. Fattah, *et al.*, "Sandwich-cultured hepatocytes: Utility for in vitro exploration of hepatobiliary drug disposition and drug-induced hepatotoxicity," *Expert opinion on drug metabolism & toxicology*, vol. 9, no. 5, pp. 589–616, May 2013, Publisher: Expert Opin Drug Metab Toxicol, ISSN: 1744-7607. DOI: 10.1517/17425255.2013.773973.

[306] P. V. Moghe, F. Berthiaume, R. M. Ezzell, M. Toner, R. G. Tompkins, and M. L. Yarmush, "Culture matrix configuration and composition in the maintenance of hepatocyte polarity and function," en, *Biomaterials*, Tissue Engineering II: Tissue Technologies and Soft Tissue Engineering, vol. 17, no. 3, pp. 373–385, Jan. 1996, ISSN: 0142-9612. DOI: 10.1016/0142-9612(96)85576-1.

[307] J. L. Page, M. C. Johnson, K. M. Olsavsky, S. C. Strom, H. Zarbl, and C. I. Omiecinski, "Gene expression profiling of extracellular matrix as an effector of human hepatocyte phenotype in primary cell culture," *Toxicological sciences : an official journal of the Society of Toxicology*, vol. 97, no. 2, pp. 384–397, Jun. 2007, Publisher: Toxicol Sci, ISSN: 1096-6080. DOI: 10.1093/TOXSCI/KFM034.

[308] Y. Kim, C. D. Lasher, L. M. Milford, T. M. Murali, and P. Rajagopalan, "A comparative study of genome-wide transcriptional profiles of primary hepatocytes in collagen sandwich and monolayer cultures," *Tissue engineering. Part C, Methods*, vol. 16, no. 6, pp. 1449–1460, Dec. 2010, Publisher: Tissue Eng Part C Methods, ISSN: 1937-3392. DOI: 10.1089/TEN.TEC.2010.0012.

[309] C. Rowe, C. E. P. Goldring, N. R. Kitteringham, *et al.*, "Network Analysis of Primary Hepatocyte Dedifferentiation Using a Shotgun Proteomics Approach," *Journal of Proteome Research*, vol. 9, no. 5, pp. 2658–2668, May 2010, ISSN: 1535-3893. DOI: 10.1021/pr1001687.

[310] S. S. Bale, I. Golberg, R. Jindal, *et al.*, "Long-Term Coculture Strategies for Primary Hepatocytes and Liver Sinusoidal Endothelial Cells," *Tissue Engineering Part C: Methods*, vol. 21, no. 4, pp. 413–422, Apr. 2015, ISSN: 1937-3384. DOI: 10.1089/ten.tec.2014.0152.

[311] Magnus Ölander, "Proteomic and Functional Analysis of In Vitro Systems for Studies of Drug Disposition in the Human Small Intestine and Liver," Ph.D. dissertation, Uppsala Universitet, 2019.

[312] E. Fennema, N. Rivron, J. Rouwkema, C. van Blitterswijk, and J. de Boer, "Spheroid culture as a tool for creating 3D complex tissues," *Trends in Biotechnology*, vol. 31, no. 2, pp. 108–115, Feb. 2013, ISSN: 01677799. DOI: 10.1016/j.tibtech.2012.12.003.

[313] C. C. Bell, D. F. Hendriks, S. M. Moro, *et al.*, "Characterization of primary human hepatocyte spheroids as a model system for drug-induced liver injury, liver function and disease," *Scientific reports*, vol. 6, May 2016, Publisher: Sci Rep, ISSN: 2045-2322. DOI: 10.1038/SREP25187.

[314] P. Benien and A. Swami, "3D tumor models: History, advances and future perspectives," *Future Oncology*, vol. 10, no. 7, pp. 1311–1327, May 2014, ISSN: 1479-6694. DOI: 10.2217/fon.13.274.

[315] R. M. Tostões, S. B. Leite, M. Serra, *et al.*, "Human liver cell spheroids in extended perfusion bioreactor culture for repeated-dose drug testing," *Hepatology*, vol. 55, no. 4, pp. 1227–1236, Apr. 2012, ISSN: 02709139. DOI: 10.1002/hep.24760.

[316] A. Dash, M. B. Simmers, T. G. Deering, *et al.*, "Hemodynamic flow improves rat hepatocyte morphology, function, and metabolic activity in vitro," *American Journal of Physiology-Cell Physiology*, vol. 304, no. 11, pp. C1053–C1063, Jun. 2013, ISSN: 0363-6143. DOI: 10.1152/ajpcell.00331.2012.

[317] H. Rashidi, S. Alhaque, D. Szkolnicka, O. Flint, and D. C. Hay, "Fluid shear stress modulation of hepatocyte-like cell function," *Archives of Toxicology*, vol. 90, no. 7, pp. 1757–1761, Jul. 2016, ISSN: 0340-5761. DOI: 10.1007/s00204-016-1689-8.

[318] S. Y. Lee, D. Kim, S. H. Lee, and J. H. Sung, "Microtechnology-based in vitro models: Mimicking liver function and pathophysiology," *APL Bioengineering*, vol. 5, no. 4, p. 041 505, Dec. 2021, ISSN: 2473-2877. DOI: 10.1063/5.0061896.

[319] K. Ren, J. Zhou, and H. Wu, "Materials for Microfluidic Chip Fabrication," *Accounts of Chemical Research*, vol. 46, no. 11, pp. 2396–2406, Nov. 2013, Publisher: American Chemical Society, ISSN: 0001-4842. DOI: 10.1021/ar300314s.

[320] F. Kurth, E. Györvary, S. Heub, *et al.*, "Chapter 3 - Organs-on-a-chip engineering," en, in *Organ-on-a-chip*, J. Hoeng, D. Bovard, and M. C. Peitsch, Eds., Academic Press, Jan. 2020, pp. 47–130, ISBN: 978-0-12-817202-5. DOI: 10.1016/B978-0-12-817202-5.00003-6.

[321] N. S. Bhise, V. Manoharan, S. Massa, *et al.*, "A liver-on-a-chip platform with bioprinted hepatic spheroids.," *Biofabrication*, vol. 8, no. 1, p. 014 101, Jan. 2016, ISSN: 1758-5090. DOI: 10.1088/1758-5090/8/1/014101.

[322] M. Hegde, R. Jindal, A. Bhushan, *et al.*, "Dynamic interplay of flow and collagen stabilizes primary hepatocytes culture in a microfluidic platform," *Lab Chip*, vol. 14, no. 12, pp. 2033–2039, 2014, ISSN: 1473-0197. DOI: 10.1039/C4LC00071D.

[323] L.-D. Ma, Y.-T. Wang, J.-R. Wang, *et al.*, "Design and fabrication of a liver-on-a-chip platform for convenient, highly efficient, and safe *in situ* perfusion culture of 3D hepatic spheroids," *Lab on a Chip*, vol. 18, no. 17, pp. 2547–2562, 2018, ISSN: 1473-0197. DOI: 10.1039/C8LC00333E.

[324] S.-A. Lee, D. Y. No, E. Kang, J. Ju, D.-S. Kim, and S.-H. Lee, "Spheroid-based three-dimensional liver-on-a-chip to investigate hepatocyte-hepatic stellate cell interactions and flow effects," eng, *Lab on a Chip*, vol. 13, no. 18, pp. 3529–3537, Sep. 2013, ISSN: 1473-0189. DOI: 10.1039/c3lc50197c.

[325] Y.-S. Weng, S.-F. Chang, M.-C. Shih, S.-H. Tseng, and C.-H. Lai, "Scaffold-Free Liver-On-A-Chip with Multiscale Organotypic Cultures," eng, *Advanced Materials (Deerfield Beach, Fla.)*, vol. 29, no. 36, Sep. 2017, ISSN: 1521-4095. DOI: 10.1002/adma.201701545.

[326] L. Boulais, R. Jellali, U. Pereira, E. Leclerc, S. A. Bencherif, and C. Legallais, "Cryogel-Integrated Biochip for Liver Tissue Engineering," *ACS Applied Bio Materials*, vol. 4, no. 7, pp. 5617–5626, Jul. 2021, ISSN: 2576-6422. DOI: 10.1021/acsabm.1c00425.

[327] S. G. Klein, T. Serchi, L. Hoffmann, B. Blömeke, and A. C. Gutleb, "An improved 3D tetraculture system mimicking the cellular organisation at the alveolar barrier to study the potential toxic effects of particles on the lung," *Particle and Fibre Toxicology*, vol. 10, no. 1, Jul. 2013, ISSN: 17438977. DOI: 10.1186/1743-8977-10-31.

[328] S. G. Klein, S. Cambier, J. Hennen, *et al.*, "Endothelial responses of the alveolar barrier in vitro in a dose-controlled exposure to diesel exhaust particulate matter," *Particle and Fibre Toxicology*, vol. 14, no. 1, Mar. 2017, Publisher: BioMed Central Ltd., ISSN: 17438977. DOI: 10.1186/S12989-017-0186-4.

[329] A. Chary, T. Serchi, E. Moschini, *et al.*, "An in vitro coculture system for the detection of sensitization following aerosol exposure," *Altex*, vol. 36, no. 3, pp. 403–418, Jul. 2019, Publisher: ALTEX Edition, ISSN: 18688551. DOI: 10.14573/ALTEX.1901241.

[330] I. Fizeșan, A. Chary, S. Cambier, *et al.*, "Responsiveness assessment of a 3D tetraculture alveolar model exposed to diesel exhaust particulate matter," *Toxicology in Vitro*, vol. 53, pp. 67–79, Dec. 2018, ISSN: 08872333. DOI: 10.1016/j.tiv.2018.07.019.

[331] Legallais C., Baudoin R., Leclerc E., Prot J.-M., and Paullier P., "US20130084632A1 - Multi-reactor unit for dynamic cell culture," pat., 2013.

[332] A. Legendre, R. Baudoin, G. Alberto, *et al.*, "Metabolic Characterization of Primary Rat Hepatocytes Cultivated in Parallel Microfluidic Biochips," *Journal of Pharmaceutical Sciences*, vol. 102, no. 9, pp. 3264–3276, Sep. 2013, ISSN: 00223549. DOI: 10.1002/jps.23466.

[333] T. Bricks, P. Paullier, A. Legendre, *et al.*, "Development of a new microfluidic platform integrating co-cultures of intestinal and liver cell lines," *Toxicology in Vitro*, vol. 28, no. 5, pp. 885–895, Aug. 2014, ISSN: 08872333. DOI: 10.1016/j.tiv.2014.02.005.

[334] B. K. Rubin, "Physiology of airway mucus clearance.," *Respiratory care*, vol. 47, no. 7, pp. 761–768, 2002, ISSN: 00201324.

[335] A. Dvorak, A. E. Tilley, R. Shaykhiev, R. Wang, and R. G. Crystal, "Do Airway Epithelium Air–Liquid Cultures Represent the In Vivo Airway Epithelium Transcriptome?" *https://doi.org/10.1165/rcmb.2009-0453OC*, vol. 44, no. 4, pp. 465–473, Dec. 2012, Publisher: American Thoracic Society, ISSN: 10441549. DOI: 10.1165/RCMB.2009-0453OC.

[336] P. M. de Jong, M. A. van Sterkenburg, S. C. Hesseling, *et al.*, "Ciliogenesis in human bronchial epithelial cells cultured at the air-liquid interface.," *American journal of respiratory cell and molecular biology*, vol. 10, no. 3, pp. 271–277, 1994, ISSN: 10441549. DOI: 10.1165/ajrcmb.10.3.8117445.

[337] National Center for Biotechnology Information, *PubChem Compound Summary for CID 1983, Acetaminophen*, en.

[338] S. S. Olmsted, J. L. Padgett, A. I. Yudin, K. J. Whaley, T. R. Moench, and R. A. Cone, "Diffusion of macromolecules and virus-like particles in human cervical mucus," eng, *Biophysical Journal*, vol. 81, no. 4, pp. 1930–1937, Oct. 2001, ISSN: 0006-3495. DOI: 10.1016/S0006-3495(01)75844-4.

[339] R. A. Cone, "Barrier properties of mucus," eng, *Advanced Drug Delivery Reviews*, vol. 61, no. 2, pp. 75–85, Feb. 2009, ISSN: 1872-8294. DOI: 10.1016/j.addr.2008.09.008.

[340] J. Seagrave, H. H. Albrecht, D. B. Hill, D. F. Rogers, and G. Solomon, "Effects of guaifenesin, N-acetylcysteine, and ambroxol on MUC5AC and mucociliary transport in primary differentiated human tracheal-bronchial cells," *Respiratory Research*, vol. 13, no. 1, p. 98, Oct. 2012, ISSN: 1465-993X. DOI: 10.1186/1465-9921-13-98.

[341] T. M. McKeever, S. A. Lewis, H. A. Smit, P. Burney, J. R. Britton, and P. A. Cassano, "The association of acetaminophen, aspirin, and ibuprofen with respiratory disease and lung function," eng, *American Journal of Respiratory and Critical Care Medicine*, vol. 171, no. 9, pp. 966–971, May 2005, ISSN: 1073-449X. DOI: 10.1164/rccm.200409-1269OC.

[342] A. D. Roth, P. Lama, S. Dunn, S. Hong, and M.-Y. Lee, "Polymer coating on a micropillar chip for robust attachment of PuraMatrix peptide hydrogel for 3D hepatic cell culture.," *Materials science & engineering. C, Materials for biological applications*, vol. 90, pp. 634–644, Sep. 2018, ISSN: 1873-0191. DOI: 10.1016/j.msec.2018.04.092.

[343] T. Bricks, Leclerc, U. d. T. d. Compiègne, and S. p. l. École doctorale 71, "Développement d'un dispositif microfluidique ayant pour objectif l'étude des effets de premiers passages intestinaux et hépatiques," français, Ph.D. dissertation, Université de Technologie de Compiègne, 2014.

[344] B. R. Wiggs, C. A. Hrousis, J. M. Drazen, and R. D. Kamm, "On the mechanism of mucosal folding in normal and asthmatic airways," en, *Journal of Applied Physiology*, vol. 83, no. 6, pp. 1814–1821, Dec. 1997, ISSN: 8750-7587, 1522-1601. DOI: 10.1152/jappl.1997.83.6.1814.

[345] K. Matter and M. S. Balda, "Signalling to and from tight junctions," eng, *Nature Reviews. Molecular Cell Biology*, vol. 4, no. 3, pp. 225–236, Mar. 2003, ISSN: 1471-0072. DOI: 10.1038/nrm1055.

[346] National Center for Biotechnology Information, *PubChem Compound Summary for CID 39763, Acetimidoquinone*, en.

[347] D. Raeburn and S. Webber, "Proinflammatory potential of the airway epithelium in bronchial asthma," *European Respiratory Journal*, vol. 7, no. 12, pp. 2226–2233, Dec. 1994, ISSN: 00000000, 09031936. DOI: 10.1183/09031936.94.07122226.

[348] P. Chandorkar, W. Posch, V. Zaderer, *et al.*, "Fast-track development of an in vitro 3D lung/immune cell model to study Aspergillus infections," eng, *Scientific Reports*, vol. 7, no. 1, p. 11 644, Sep. 2017, ISSN: 2045-2322. DOI: 10.1038/s41598-017-11271-4.

[349] A. V. Singh, A. Romeo, K. Scott, *et al.*, "Emerging Technologies for In Vitro Inhalation Toxicology," *Advanced Healthcare Materials*, vol. 10, no. 18, Sep. 2021, Publisher: John Wiley and Sons Inc, ISSN: 21922659. DOI: 10.1002/ADHM.202100633.

[350] I. Fizeșan, S. Cambier, E. Moschini, *et al.*, "In Vitro Cellular Models, a Resourceful Tool in Respiratory Toxicology," *Farmacia*, vol. 66, no. 4, pp. 573–580, 2018, Publisher: Romanian Society for Pharmaceutical Sciences, ISSN: 00148237. DOI: 10.31925/FARMACIA.2018.4.2.

[351] C. Francoz, H. Mal, and F. Durand, "Pulmonary abnormalities associated with liver diseases," *EMC - Pneumologie*, vol. 2, no. 1, pp. 49–60, 2005, Publisher: Elsevier Masson SAS, ISSN: 17624223. DOI: 10.1016/j.emcpn.2004.10.003.

[352] C. Oleaga, C. Bernabini, A. S. Smith, *et al.*, "Multi-Organ toxicity demonstration in a functional human in vitro system composed of four organs," *Scientific Reports 2016 6:1*, vol. 6, no. 1, pp. 1–17, Feb. 2016, Publisher: Nature Publishing Group, ISSN: 2045-2322. DOI: 10.1038/srep20030.

[353] U. Marx, T. B. Andersson, A. Bahinski, *et al.*, "Biology-inspired Microphysiological System Approaches to Solve the Prediction Dilemma of Substance Testing," *ALTEX*, vol. 33, no. 3, p. 272, 2016, Publisher: NIH Public Access, ISSN: 18688551. DOI: 10.14573/ALTEX.1603161.

[354] A. M. Larson, "Acetaminophen hepatotoxicity," *Clinics in liver disease*, vol. 11, no. 3, pp. 525–548, Aug. 2007, Publisher: Clin Liver Dis, ISSN: 1089-3261. DOI: 10.1016/J.CLD.2007.06.006.

[355] C. F. Cowell, I. K. Yan, T. Eiseler, A. C. Leightner, H. Döppler, and P. Storz, "Loss of cell-cell contacts induces NF-B via RhoA-mediated activation of protein kinase D1," en, *Journal of Cellular Biochemistry*, vol. 106, no. 4, pp. 714–728, Mar. 2009, ISSN: 07302312, 10974644. DOI: 10.1002/jcb.22067.

[356] S. Diabaté, L. Armand, S. Murugadoss, *et al.*, "Air–Liquid Interface Exposure of Lung Epithelial Cells to Low Doses of Nanoparticles to Assess Pulmonary Adverse Effects," en, *Nanomaterials*, vol. 11, no. 1, p. 65, Dec. 2020, ISSN: 2079-4991. DOI: 10.3390/nano11010065.

[357] A. Panas, A. Comouth, H. Saathoff, *et al.*, "Silica nanoparticles are less toxic to human lung cells when deposited at the air–liquid interface compared to conventional submerged exposure," en, *Beilstein Journal of Nanotechnology*, vol. 5, pp. 1590–1602, Sep. 2014, ISSN: 2190-4286. DOI: 10.3762/bjnano.5.171.

[358] J. R. Coppeta, M. J. Mescher, B. C. Isenberg, *et al.*, "A portable and reconfigurable multi-organ platform for drug development with onboard microfluidic flow control," en, *Lab on a Chip*, vol. 17, no. 1, pp. 134–144, 2017, ISSN: 1473-0197, 1473-0189. DOI: 10.1039/C6LC01236A.

[359] T. Loret, F. Rogerieux, B. Trouiller, A. Braun, C. Egles, and G. Lacroix, "Predicting the in vivo pulmonary toxicity induced by acute exposure to poorly soluble nanomaterials by using advanced in vitro methods," en, *Particle and Fibre Toxicology*, vol. 15, no. 1, p. 25, Dec. 2018, ISSN: 1743-8977. DOI: 10.1186/s12989-018-0260-6.

[360] H. Harrington, P. Cato, F. Salazar, *et al.*, "Immunocompetent 3D Model of Human Upper Airway for Disease Modeling and In Vitro Drug Evaluation," en, *Molecular Pharmaceutics*, vol. 11, no. 7, pp. 2082–2091, Jul. 2014, ISSN: 1543-8384, 1543-8392. DOI: 10.1021/mp5000295.

[361] A. Legendre, S. Jacques, F. Dumont, *et al.*, "Investigation of the hepatotoxicity of flutamide: Pro-survival/apoptotic and necrotic switch in primary rat hepatocytes characterized by metabolic and transcriptomic profiles in microfluidic liver biochips," en, *Toxicology in Vitro*, vol. 28, no. 5, pp. 1075–1087, Aug. 2014, ISSN: 08872333. DOI: 10.1016/j.tiv.2014.04.008.

[362] R. Baudoin, J. M. Prot, G. Nicolas, *et al.*, "Evaluation of seven drug metabolisms and clearances by cryopreserved human primary hepatocytes cultivated in microfluidic biochips," en, *Xenobiotica*, vol. 43, no. 2, pp. 140–152, Feb. 2013, ISSN: 0049-8254, 1366-5928. DOI: 10.3109/00498254.2012.706725.

[363] M. Danoy, Y. Tauran, S. Poulain, *et al.*, "Investigation of the hepatic development in the coculture of hiPSCs-derived LSECs and HLCs in a fluidic microenvironment," en, *APL Bioengineering*, vol. 5, no. 2, p. 026 104, Jun. 2021, ISSN: 2473-2877. DOI: 10.1063/5.0041227.